Identifying Antifungal Resistance Mechanisms and Modes of Action using SAturated Transposon Analysis in Yeast (SATAY)

Matthew Karadzas

Linacre College
University of Oxford



Thesis submitted for the degree of
Doctor of Philosophy

Trinity Term 2024

Word Count: 45,712

Declaration

I confirm that the work presented in this thesis is my own, except where explicitly stated in the text. Contributions to this work by others have been duly acknowledged.

Abstract

Fungal pathogens are a serious burden for public health and global food security. This problem is exacerbated by the rapid emergence of resistance to our limited armamentarium of antifungal compounds. The future control of fungal diseases therefore depends on the discovery of antifungals with novel modes of action and the development of robust resistance management strategies. These strategies require a comprehensive understanding of the molecular mechanisms governing antifungal resistance, yet our knowledge is incomplete.

Recently, a powerful transposon sequencing method was developed in *Saccharomyces cerevisiae*, called SAturated Transposon Analysis in Yeast (SATAY). SATAY couples saturated transposon mutagenesis to next-generation sequencing, allowing the genome-wide identification of growth-affecting loci in a straightforward and time-efficient manner. Importantly, SATAY can identify loss- and gain-of-function mutations conferring antifungal resistance, as well as the direct targets of antifungal compounds.

This thesis applies SATAY to uncover novel antifungal resistance mechanisms and to examine the modes of action of nine antifungal compounds. These screens reveal antifungal drug targets, transporters responsible for drug uptake or efflux, as well as metabolic, signalling and trafficking pathways affecting antifungal susceptibility. The most novel and interesting findings in these screens are characterised further. This includes the discovery of Hol1 as the transporter that concentrates the potent antifungal ATI-2307 within yeast, a finding that unveils a straightforward evolutionary path to ATI-

2307 resistance with minimal fitness cost. SATAY is also performed in drug-sensitive strains to examine antifungals that lack activity against conventional laboratory strains. This approach is utilised to test a previously proposed model for the mode of action of Fludioxonil, and identifies cell wall mannosylphosphate as the target for the natural antifungal Chitosan. Together, this thesis improves our understanding of several antifungal modes of action and unveils a diverse array of resistance mechanisms, supporting efforts to address the increasing threats posed by multidrug-resistant fungal pathogens.

Acknowledgements

First, I would like to express my gratitude to my supervisors Benoît Kornmann and Agnès Michel. Their unwavering support, guidance and encouragement were invaluable throughout my PhD. Benoît's ideas greatly influenced the direction of my research, and our thought-provoking discussions were a constant source of inspiration. Agnès was a brilliant mentor and role model in the laboratory. I am hugely grateful to her for training me in a multitude of experimental techniques and for helping to advance my problem-solving and critical thinking skills, which were vital for my development as a research scientist.

I am also enormously grateful to my supervisor Gabriel Scalliet at Syngenta. Gabriel was highly influential for generating ideas that shaped my research, and his encouragement and expertise were always motivating. I owe Gabriel a great deal of gratitude for making my industrial placements at Syngenta possible. I thank Gabriel for his help with organising my placement in Stein, Switzerland, and for allowing me to work in his laboratory.

I would like to thank all members of the Kornmann lab for all their support and encouragement. Thank you to Christian, Jean, Anitha and Yaan for making the Kornmann lab a positive, collaborative and fun environment for completing my PhD. I feel fortunate to have had the opportunity to work with you all. Thank you also for tolerating my music choices in the laboratory over these past 3.5 years!

I am also grateful to several research scientists at Syngenta who supported me during my industrial placements. Thank you to Andreas for your supervision during my placement in Stein, and for generating the mutant strains of *Botrytis cinerea* that I worked with during this placement. Thank you to George and Jack for your help during my placement in Jealott's Hill.

I would like to thank the BBSRC Doctoral Training Programme and Syngenta for funding.

I am really grateful for the support and encouragement I received from my close friends, particularly Sophie, Stella and Scott.

Last but not least, I am profoundly grateful to my family. Thank you for your endless support.

Contents

Abstract **1**

Acknowledgements **3**

List of Figures **13**

List of Tables **16**

Published work **18**

Nomenclature for genes, proteins and mutants of *Saccharomyces cerevisiae* **19**

Nomenclature for genes, proteins and mutants of *Botrytis cinerea* **20**

Abbreviations **21**

Chapter 1: Introduction **24**

1.1. Fungal pathogens are a significant threat to public health and global food security **24**

1.2. The control of fungal pathogens depends on a limited number of antifungal compounds **26**

1.2.1. Clinical antifungals 26

1.2.2. Agrochemical fungicides 28

1.3. The emergence of antifungal resistance is undermining the efficacy of antifungal compounds **31**

1.3.1. Target-site resistance mechanisms 32

1.3.2. Non-target site resistance mechanisms 33

1.4. Strategies for reducing the emergence and spread of antifungal resistance **38**

1.4.1. Elucidating the molecular mechanisms underpinning antifungal resistance 38

1.4.2. Discovering antifungal compounds with novel modes of action 39

1.4.3. Preserving the efficacy of existing antifungal compounds: stewardship and combination therapies 39

1.5. Chemogenomic screening approaches in *Saccharomyces cerevisiae* can accelerate the discovery of antifungal resistance mechanisms and modes of action **40**

1.5.1. *S. cerevisiae* is a powerful model for fungal research 40

1.5.2. Conventional chemogenomic screening approaches in *S. cerevisiae* 41

1.5.3. Limitations of conventional chemogenomic screening approaches in *S. cerevisiae* 44
1.6. Transposon sequencing 46
1.6.1. Principle of transposon sequencing 46
1.6.2. Transposon sequencing for chemogenomic screening 48
1.7. SAturated Transposon Analysis in Yeast (SATAY) 52
1.7.1. SATAY: overview of library generation **..... 52**
1.7.2. Advantages of SATAY 53
1.7.3. SATAY for chemogenomic screening 58
1.8. Thesis aims 62
Chapter 2 - Materials and Methods 64
2.1. Yeast strain handling 64
2.1.1. Yeast strains, storage and revival 64
2.1.2. Overnight cultures 66
2.1.3. Optical density measurements 66
2.2. Molecular Biology 67
2.2.1. Primers and Polymerase Chain Reaction 67
2.2.2. Restriction digestions and ligations 67
2.2.3. Gel electrophoresis 68
2.3. Plasmids 68
2.3.1. Plasmids used in this thesis 68
2.3.2. *Escherichia coli* plasmid transformation and plasmid preparation 70
2.3.3. Construction of plasmid p405-*TEF1*pr-*BdDRK1* (pBK864) 70
2.3.4. Construction of plasmids encoding kinase-defective *BdDRK1* genes..... 71
2.3.5. Construction of plasmid encoding the *Candida albicans HOL1* (pBK994) 71
2.4. Construction of yeast strains 72
2.4.1. Yeast transformation 72
2.4.2. Yeast deletion strains 72
2.4.3. Colony PCR genotyping 73
2.4.4. Tetrad dissections 73

2.5. Media 74
2.5.1. Yeast peptone dextrose (YPD) medium 74
2.5.2. YPA medium for sporulation 74
2.5.3. Synthetic Complete (SC) medium 74
2.6. Antifungal compounds 76
2.6.1. Compound stocks and storage 76
2.6.2. Preparation of Chitosan stock solutions 76
2.7. Antifungal susceptibility tests 78
2.7.1. Bioscreen C 78
2.7.2. ATI-2307, Pentamidine and Iminoctadine susceptibility tests in liquid medium 78
2.7.3. Fludioxonil sensitivity tests in YP 3% ethanol 0.1% galactose medium . 79
2.8. SAturated Transposon Analysis in Yeast (SATAY) 79
2.8.1. Summary of transposon libraries generated in this thesis 79
2.8.2. Transposon library generation on SC -ADE 2% galactose plates 80
2.8.3. Transposon library generation in SC -URA 2% galactose liquid medium 81
2.8.4. Antifungal treatments of transposon libraries 85
2.8.5. Transposon library sequencing and analysis 86
2.9. Gene Ontology Term Analysis 88
2.10. Quantification of Hol1 uptake of ATI-2307, Pentamidine and Iminoctadine 89
2.10.1. Cell lysate generation 89
2.10.2. Cell lysate treatments 90
2.10.3. Liquid Chromatography – Mass Spectrometry analysis 91
2.11. Screening for separation-of-function mutations in *ScHOL1* 92
2.11.1. Construction of plasmid library bearing *ScHOL1* alleles 92
2.11.2. Screening for ATI-2307 resistance 93
2.11.3. Plasmid rescue 93
2.11.4. Disc diffusion assays to validate separation-of-function mutations in *ScHOL1* 94
2.12. Pairwise sequence alignments of Hol1 protein sequences from *S. cerevisiae* and *Candida* species 94

2.13. Alcian blue staining assay 95

2.14. Live imaging of yeast 95

2.15. Experiments with *Botrytis cinerea* 96

2.15.1. BLASTp search to identify homologs of *Sc*Mnn4 in *Botrytis cinerea* 96

2.15.2. Strains of Botrytis cinerea 96

2.15.3. Construction of *Botrytis cinerea* deletion strains 97

2.15.4. Growth media and culture conditions 98

2.15.5. Conidia harvesting 98

2.15.6. Chitosan sensitivity assays of *B. cinerea* strains 99

2.15.7. Live imaging and quantification of germ tube lengths of *Botrytis cinerea* germlings 100

2.16. Viability tests of *SLN1*+ strains expressing kinase-defective *BdDRK1* alleles 101

2.17. Statistical analysis 101

2.18. AlphaFold 102

Chapter 3 – Overview of the SATAY screens performed in this thesis 103

3.1. Set-up of SATAY screens 103

3.2. Generation and treatment of transposon libraries for SATAY-based chemogenomic screening 107

Chapter 4 – Proof-of-principle SATAY screens demonstrate the utility of SATAY for chemogenomic screening 111

4.1. Introduction 111

4.2. Results 113

4.2.1. Amphotericin B sensitivity was affected by ergosterol homeostasis, TORC1 and the plasma membrane protein Pmp3 113

4.2.2. Caspofungin resistance was conferred by transposons disrupting genes involved with sphingolipid biosynthesis and membrane homeostasis 116

4.2.3. Myriocin resistance was conferred by transposons disrupting cellular trafficking and phospholipid translocation, and *SLI1* overexpression 119

4.2.4. Tavaborole susceptibility was reduced by transposons inactivating genes associated with tRNA wobble uridine modifications 122

4.2.5. Prochloraz resistance was conferred by *ERG11* and *PDR5* overexpression in a PDR-proficient transposon library, but by altered Golgi vesicle trafficking in a PDR-attenuated transposon library 125

4.3. Discussion 132

4.3.1. SATAY is a robust approach for chemogenomic screening 132

4.3.2. SATAY can identify antifungal tolerance mechanisms 132

4.3.3. SATAY could facilitate the identification of new combination therapies 134

4.3.4. SATAY can be performed in a PDR-attenuated strain of *S. cerevisiae* 134

Chapter 5 – Hol1 concentrates ATI-2307, Pentamidine and Iminoctadine in *S. cerevisiae* 136

5.1. Introduction 136

5.2. Results 138

5.2.1. ATI-2307 negatively selected transposons in genes regulating gluconeogenesis, and positively selected transposons in *HOL1* and regulators of the plasma membrane proton-motive force 138

5.2.2. *HOL1* is a major determinant of ATI-2307 susceptibility in *S. cerevisiae* and *C. albicans* 149

5.2.3. Hol1 concentrates ATI-2307 within *S. cerevisiae* 152

5.2.4. Hol1 imports Pentamidine into *S. cerevisiae* 159

5.2.5. Hol1 imports Iminoctadine into *S. cerevisiae* 165

5.2.6. Polyamine and ATI-2307 uptake by Hol1 can be functionally separated 171

5.3. Discussion 177

5.3.1. Hol1 imports ATI-2307, Pentamidine and Iminoctadine sensitivity into *S. cerevisiae* 177

5.3.2. Identifying broad-spectrum nutrient permeases in fungal pathogens could inform the design of novel antifungal compounds 179

5.3.3. The identification of separation-of-function mutations in Hol1 suggests that ATI-2307 resistance can emerge with minimal fitness cost 179

5.3.4. The intracellular target(s) of ATI-2307 were not revealed by the SATAY screen 181

5.3.5. The connection between the GID complex and ATI-2307 susceptibility is an interesting question for future research 182

Chapter 6 – Investigating the direct target and mode of action of Fludioxonil 185

6.1. Introduction 185

6.2. Results 193

6.2.1. *BdDRK1* complements *sln1Δ* in *S. cerevisiae* 193

6.2.2. *BdDRK1* expression engenders Fludioxonil and Iprodione sensitivity in *S. cerevisiae*, and this sensitivity is dominant 195

6.2.3. Fludioxonil and Iprodione positively selected transposons that suppress the HOG pathway 197

6.2.4. Fludioxonil toxicity is unlikely to be elicited by aldehydic stress in *S. cerevisiae* 203

6.2.5. An attempt to determine whether *Bd*Drk1 sequesters Ypd1 away from Sln1 208

6.3. Discussion 214

6.3.1. SATAY indicates that Fludioxonil directly targets *Bd*Drk1 214

6.3.2. The mechanism underpinning the dominance of Fludioxonil sensitivity remains enigmatic 215

Chapter 7 – Chitosan electrostatically interacts with cell wall mannosylphosphate 219

7.1. Introduction 219

7.2. Results 222

7.2.1. A yeast strain called AD1-8 was sensitive to Chitosan 222

7.2.2. Chitosan positively selected transposons in genes involved in the mannosylation of N-linked glycans or intra-Golgi retrograde transport 223

7.2.3. Chitosan susceptibility correlated with the amount of cell wall mannosylphosphate 230

7.2.4. Chitosan binds to mannosylphosphate groups on the cell wall of AD1-8 234

7.2.5. Chitosan resistance in the S288C-derived strain ByK352 is a polygenic trait 237

7.2.6. It remains unclear whether Chitosan binds to mannosylphosphate on the surface of *Botrytis cinerea* 242

7.2.6.1. Bcin05p04770 and Bcin15p02200 are putative homologs of *Sc*Mnn4 242

7.2.6.2. Deletion of *Bcin15g02200* caused a slight reduction in Chitosan susceptibility 246

7.2.6.3. It was not clear whether putative *MNN4* homologs mediate Chitosan sensitivity in *Botrytis cinerea* over the first ten hours of growth 249

7.3. Discussion 254

7.3.1. Chitosan electrostatically interacts with mannosylphosphate on the cell wall 254

7.3.2. SATAY in non-conventional strains of *S. cerevisiae* can unveil antifungal modes of action 255

7.3.3. Multiple mutations are responsible for the lack of mannosylphosphate on the surface of S288C-derived strains 256

7.3.4. It remains unclear whether Chitosan binds mannosylphosphate on the surface of *Botrytis cinerea* 257

Chapter 8 - General Discussion..... 260

8.1. Overview 260

8.2. SATAY is a powerful approach for chemogenomic screening in *S. cerevisiae* 260

8.2.1. SATAY can identify a diverse array of antifungal resistance mechanisms 260

8.2.2. SATAY can be used to screen compounds that lack activity against conventional laboratory strains of *S. cerevisiae*..... 261

8.2.3. Transposon libraries can be grown in non-fermentative conditions.... 264

8.2.4. SATAY can be used to identify novel combination therapies..... 265

8.3. Limitations of using SATAY for chemogenomic screening 266

8.3.1. Technical challenges with using SATAY for chemogenomic screening.. 266

8.3.2. Inherent limitations with using SATAY for chemogenomic screening .. 267

8.4. Additional applications of SATAY for chemogenomic screening 269

8.4.1. Fluorescence-based selection approaches..... 269

8.4.2. Identifying conditionally essential genes in drug-resistant strains 270

8.5. Developing Tn-seq approaches in fungal phytopathogens is a worthwhile pursuit 271

Appendix 1 – Primers used in this thesis 273

Appendix 2 – Calculations of intracellular concentrations of ATI-2307, Pentamidine and Iminoctadine 276

Appendix 2A – Calculations for intracellular concentration of ATI-2307..... 276

Appendix 2B – Calculations for intracellular concentration of Pentamidine 277

Appendix 2C – Calculations for intracellular concentration of Iminoctadine 278

References 279

List of Figures

Figure 1.1	Bar chart showing the main classes of antifungal compounds	30
Figure 1.2	Transposon insertion maps illustrating how Tn-seq can identify essential loci	47
Figure 1.3	Schematic depiction of using Tn-seq for chemogenomic screening	50
Figure 1.4	Transposon insertion maps illustrating how SATAY can interrogate the genome at sub-gene resolution	57
Figure 1.5	Transposon insertion maps and scatter plots illustrating that SATAY can identify antifungal drug targets	59
Figure 1.6	Transposon insertion maps illustrating that SATAY can identify drug efflux pumps that export specific compounds	61
Figure 2.1	Flow charts summarising the key stages for generating transposon libraries on SC -ADE 2% galactose plates and SC -URA 2% galactose medium.	84
Figure 2.2	Flow chart summarising the key stages for challenging transposon libraries with antifungal compounds.	86
Figure 2.3	Flow chart summarising the key stages for processing cell pellets for sequencing and analysis.	88
Figure 3.1	Schematic depiction of the protocol for treating transposon libraries with antifungal compounds	109
Figure 4.1	Scatter plot displaying SATAY screen results for Amphotericin B - number of sequencing reads in CDS	114
Figure 4.2	Scatter plot displaying SATAY screen results for Amphotericin B - number of sequencing reads in promoters	115
Figure 4.3	Scatter plot displaying SATAY screen results for Caspofungin - number of sequencing reads in CDS	118
Figure 4.4	Scatter plot displaying SATAY screen results for Myriocin - number of sequencing reads in CDS	120
Figure 4.5	Scatter plot displaying SATAY screen results for Myriocin - number of sequencing reads in promoters	121
Figure 4.6	Scatter plot displaying SATAY screen results for Tavaborole - number of sequencing reads in CDS	123
Figure 4.7	SATAY screen results for Prochloraz-treated ByK352 transposon library - number of sequencing reads in promoter	126
Figure 4.8	Scatter plot displaying SATAY screen results for Prochloraz-treated ByK352 transposon library - number of sequencing reads in CDS	127
Figure 4.9	Transposon insertion maps for *PDR5* in Prochloraz-treated ByK352 transposon library	128
Figure 4.10	SATAY screen results for Prochloraz-treated 12geneΔ0HSR transposon library - number of sequencing reads in CDS	130

Figure 5.1	Scatter plot displaying SATAY screen results for ATI-2307 - number of transposons in CDS	139
Figure 5.2	Scatter plot displaying SATAY screen results for ATI-2307 - number of sequencing reads in CDS	143
Figure 5.3	Protein sequence alignments for Rmd1, Rmd8 and Mrx10	145
Figure 5.4	AlphaFold3 models of Rmd1, Rmd8 and Mrx10	146
Figure 5.5	Scatter plot displaying SATAY screen results for ATI-2307 - number of sequencing reads in promoter	148
Figure 5.6	Growth inhibition curves for WT, *hol1Δ* and *hol1Δ CaHOL1* strains treated with ATI-2307	150
Figure 5.7	Growth inhibition curves for WT and *hol1Δ* strains treated with lysate derived from ATI-2307-treated- WT and *hol1Δ* cells	154
Figure 5.8	Calibration curve for quantifying ATI-2307 in cell lysates using LC-MS	155
Figure 5.9	Examples of chromatograms and mass spectra for cell lysate samples containing ATI-2307	156
Figure 5.10	Bar chart summarising ATI-2307 uptake by WT, *hol1Δ* and *hol1Δ CaHOL1* strains	158
Figure 5.11	ATI-2307 and Pentamidine chemical structures	160
Figure 5.12	Growth inhibition curves for WT, *hol1Δ* and *hol1Δ CaHOL1* strains treated with Pentamidine	161
Figure 5.13	Examples of chromatograms and mass spectra for cell lysate samples containing Pentamidine	162
Figure 5.14	Calibration curve for quantifying Pentamidine in cell lysates using LC-MS	163
Figure 5.15	Bar chart summarising Pentamidine uptake by WT and *hol1Δ* strains	164
Figure 5.16	Spermidine and Iminoctadine chemical structures	166
Figure 5.17	Growth inhibition curves for WT, *hol1Δ* and *hol1Δ CaHOL1* strains treated with Iminoctadine	166
Figure 5.18	Examples of chromatograms and mass spectra for Iminoctadine lysate samples	167
Figure 5.19	Calibration curve for quantifying Iminoctadine in WT cell lysates using LC-MS	168
Figure 5.20	Calibration curve for quantifying Iminoctadine in *hol1Δ* cell lysates using LC-MS	169
Figure 5.21	Bar chart summarising Iminoctadine uptake by WT and *hol1Δ* strains	170
Figure 5.22	Streaks of *spe1Δ* and *spe1Δ hol1Δ* strains on SC 2% ethanol medium supplemented with 1 µM spermidine	173
Figure 5.23	Disc diffusion assays testing ATI-2307, Pentamidine and Iminoctadine sensitivity for Hol1 separation-of-function alleles	174

Figure 5.24	AlphaFold2 model of Hol1 displaying separation-of-function mutations	176
Figure 5.25	Cartoon depiction of major ATI-2307 resistance mechanisms	184
Figure 6.1	Chemical structures of Pyrrolnitrin, Fludioxonil and Iprodione	186
Figure 6.2	Cartoon depiction of the HOG signal transduction pathway in *S. cerevisiae*	189
Figure 6.3	Cartoon depiction of the model of Fludioxonil activity proposed by Brandhorst et al., (2019)	192
Figure 6.4	Image of progeny from tetrad dissection of *SLN1+/- BdDRK1+/-* heterozygote	194
Figure 6.5	Growth inhibition curves of *BdDRK1*-expressing cells treated with Fludioxonil and Iprodione	196
Figure 6.6	Scatter plot displaying SATAY screen results for Fludioxonil and Iprodione - number of sequencing reads in CDS	199
Figure 6.7	Transposon insertions maps for *BdDRK1* and HOG pathway components in Fludioxonil- and Iprodione-treated transposon library	201
Figure 6.8	Growth inhibition curves of progeny derived *TPI1+/- BdDRK1+/-* heterozygotes treated with Fludioxonil	205
Figure 6.9	Growth inhibition curves of *Bd*Drk1-expressing *glo1Δ* mutants treated with Fludioxonil	206
Figure 6.10	Cartoon depiction of the Ypd1 sequestration model for Fludioxonil's mechanism of activity	209
Figure 6.11	Schematic representation of the internal phosphorylation reactions in *Bd*Drk1	212
Figure 6.12	Viability tests of *SLN1+* strains expressing kinase-defective *Bd*Drk1	213
Figure 7.1	Chemical structure of Chitosan	220
Figure 7.2	Scatter plot displaying SATAY screen results for Chitosan - number of sequencing reads in CDS	224
Figure 7.3	Scatter plot displaying SATAY screen results for Chitosan - number of sequencing reads in promoters	229
Figure 7.4	Growth inhibition curves for ByK352, AD1-8 and AD1-8 *mnn4Δ* treated with Chitosan	231
Figure 7.5	Alcian blue staining of ByK352, AD1-8 and AD1-8 *mnn4Δ* cells	232
Figure 7.6	Model for Chitosan binding to the yeast cell wall	233
Figure 7.7	Fluorescent microscopy images of ByK352, AD1-8 and AD1-8 *mnn4Δ* cells treated with fluorescein-labelled Chitosan	235
Figure 7.8	Growth inhibition curves for progeny from eight tetrads treated with Chitosan	238
Figure 7.9	Growth inhibition curves for ByK352, AD1-8 and the AD1-8 x ByK352 diploid	241

Figure 7.10	Multiple sequence alignment of ScMnn4, Bcin05p04770 and Bcin15p02200 proteins	244
Figure 7.11	Protein structure alignment for ScMnn4, Bcin05p04770 and Bcin15p02200	245
Figure 7.12	Growth inhibition curves of *Botrytis cinerea* WT and putative *MNN4* deletion mutants treated with Chitosan	247
Figure 7.13	Images of *Botrytis cinerea* germlings treated with Chitosan or acetic acid	250
Figure 7.14	Images of *Botrytis cinerea* germlings treated with Chitosan or acetic acid for ten hours	251
Figure 7.15	Boxplots comparing germling lengths of WT and putative *MNN4* mutants after ten hours	252

List of Tables

Table 1.1	Summary of the major resistance mechanisms for each class of clinical antifungal	37
Table 1.2	Summary of the major resistance mechanisms for each class of agrochemical fungicide	37
Table 2.1	Yeast strains used in this thesis	64
Table 2.2	Plasmids used in this thesis	68
Table 2.3	Antifungal compounds used in this thesis	77
Table 2.4	Summary of transposon libraries used in this thesis	79
Table 2.5	Summary of conditions for generating transposon libraries on solid medium	81
Table 2.6	Summary of conditions for generating transposon libraries in liquid medium	83
Table 2.7	Growth conditions for antifungal treatments of transposon libraries	86
Table 2.8	Strains of *Botrytis cinerea* used in this thesis	96
Table 2.9	Primers for constructing and genotyping *B. cinerea* deletion strains	97
Table 3.1	IC_{30} values of fourteen antifungal compounds against five *S. cerevisiae* strains	105
Table 3.2	Characteristics of the transposon libraries analysed in this thesis	110
Table 4.1	Gene Ontology term analysis of Tavaborole SATAY screen results	124
Table 4.2	Gene Ontology term analysis of Prochloraz-treated ByK352 transposon libraries	128
Table 4.3	Gene Ontology term analysis of Prochloraz-treated 12geneΔ0HSR transposon libraries	131
Table 5.1	Gene Ontology term analysis of ATI-2307 SATAY screen results	140
Table 5.2	Sequence identity matrix of Hol1 protein sequences from *Candida spp*. and *S. cerevisiae*	151
Table 5.3	Separation-of-function mutations identified in Hol1	175

Table 6.1	Total number of sequencing reads mapping to HOG pathway genes in a *sln1Δ BdDRK1* transposon library treated with Fludioxonil and Iprodione	202
Table 7.1	MIC of Chitosan for five strains of *S. cerevisiae*	222
Table 7.2	Gene Ontology term analysis of Chitosan SATAY screen results	226

Published work

Many of the findings presented in this thesis were uploaded to *bioRXiv* and submitted to a peer-reviewed journal in September 2024:

> Karadzas MT, Michel AH, Mosbach A, Giannakopoulos G, McGettigan R, Scalliet G, Kornmann B. *SATAY-Based Chemogenomic Screening uncovers Antifungal Resistance Mechanisms and Key Determinants of ATI-2307 and Chitosan Sensitivity*. *bioRXiv* (2024). https://doi.org/10.1101/2024.09.20.614104

This publication includes the following parts of this thesis: SATAY screens for Amphotericin B, Caspofungin, Myriocin, Prochloraz, ATI-2307, Fludioxonil, Iprodione, and Chitosan. All the follow-up experiments in Chapter 5 were included, whilst only the follow-up experiments in *S. cerevisiae* were included for Chapter 7. These SATAY screens and follow-up experiments were all performed and analysed by MT Karadzas. All figures were produced by MT Karadzas. The manuscript was authored by MT Karadzas, with input from B Kornmann. The experiments were conceived by MT Karadzas, AH Michel, G Scalliet and B Kornmann. G Giannakopoulos provided supervision for the LC-MS experiments included in Chapter 5 of this thesis.

This publication additionally includes SATAY screens performed by AH Michel, with support from A Mosbach and R McGettigan. The results for these SATAY screens were not included in this thesis.

Nomenclature for genes, proteins and mutants of *Saccharomyces cerevisiae*

Genes, proteins and mutants of *Saccharomyces cerevisiae* are referred to throughout this thesis using the following nomenclature system:

- Genes are indicated by italicised uppercase letters, followed by a number.
- Proteins are indicated by non-italicised letters, with only the first in uppercase, followed by a number.
- Deletion alleles of a gene are indicated by italicised lowercase letters followed by a number and a delta (Δ) symbol.
- Where necessary, an uppercase letter for genus and a lowercase letter for the species before gene or protein names indicates which species is being referred to.

Examples:

- *HOL1* – The *HistidinOL1* gene
- Hol1 – The Histidinol1 protein
- *hol1Δ* – The deletion allele of *HOL1*
- *CaHOL1 – Candida albicans HistidinOL1* gene

Nomenclature for genes, proteins and mutants of *Botrytis cinerea*

Genes, proteins and mutants of *Botrytis cinerea* are referred to in Chapter 7 using the following nomenclature system:

- Genes are indicated by italicised accession numbers e.g. *Bcin05g04770*
- Proteins are indicated by non-italicised accession numbers e.g. e.g. Bcin05p04770
- Deletion alleles of a gene are indicated by an italicised delta (Δ) symbol followed italicised accession numbers e.g. *ΔBcin05g04770*

Abbreviations

ABC – ATP-Binding Cassette

Ac/Ds – Activator/Dissociation

ADE - Adenine

Bc - Botrytis cinerea

Bd – Blastomyces dermatitidis

BLAST – Basic Local Alignment Search Tool

Bp – Base-pairs

Ca – Candida albicans

CDS – Coding DNA Sequence

CEN – Centromeric

CNVs – Copy number variations

CWI – Cell wall integrity

DMSO – Dimethyl sulfoxide

DNA - Deoxyribonucleic acid

FITC – Fluorescein isothiocyanate

GG media – Glucose Gelatine media

GID – Glucose Induced degradation Deficient

GO – Gene Ontology

HIP – Haploinsufficiency profiling

HHK – Hybrid histidine kinase

HOG – High osmolarity glycerol

HOP – Homozygous profiling

HIS – Histidine

IFI – Invasive fungal infection

LC-MS – Liquid Chromatography Mass Spectrometry

LCB – Long-chain base

LEU – Leucine

LOH – Loss of heterozygosity

MDR – Multidrug-resistant

MFS – Major Facilitator Superfamily

MIC – Minimum Inhibitory Concentration

MoBY - Molecular Bar-coded Yeast

OD_{600} – Optical Density at 600nm

ORF – Open Reading Frame

PAE – Predicted Aligned Error

PCR – Polymerase Chain Reaction

PDR – Pleiotropic Drug Resistance

PMF – Proton-motive force

Q_OI – Quinone outside inhibitor

RNA – Ribonucleic acid

Rpm – Revolutions per minute

SATAY – SAturated Transposon Analysis in Yeast

Sc – *Saccharomyces cerevisiae*

SC media – Synthetic complete media

SDHI – Succinate dehydrogenase inhibitor

Tn-seq – Transposon sequencing

TRP – Tryptophan

URA – Uracil

UTR – Untranslated region

WT – Wild-type

v/v – Volume per volume

xg – Times gravity

YPD – Yeast Peptone Dextrose

Chapter 1: Introduction

1.1. Fungal pathogens are a significant threat to public health and global food security

Fungal pathogens are of increasing concern for both public health and global food security.

Every year, invasive fungal infections (IFIs) cause 2.5 million deaths worldwide (Denning, 2024). More than 90% of these deaths are attributable to fungal species belonging to just four genera: *Cryptococcus*, *Candida*, *Aspergillus*, and *Pneumocystis* (Brown et al., 2012). The most susceptible individuals are those with underlying health conditions or weakened immune systems (Perlin et al., 2017), where mortality rates from IFIs frequently exceed 50% (Brown et al., 2012). In recent decades, the number of immunosuppressed individuals (Bongomin et al., 2017) has risen sharply due to the spread of immunosuppressive infections such as HIV/AIDS, and modern immunosuppressive medical interventions such as chemotherapy and organ transplantations (Fisher et al., 2018). The COVID-19 pandemic was also associated with a surge in the incidence of comorbid IFIs, particularly aspergillosis, mucormycosis and candidaemia (Hoenigl et al., 2022). Despite these threats, fungal infections have been largely neglected relative to other classes of infectious disease (Fisher et al., 2018).

Meanwhile, fungal phytopathogens are a significant threat to global food security, accounting for 10-23% of worldwide crop yield losses every year, and a further 10-20% post-harvest (Fisher et al., 2012). Fungal phytopathogens cause substantial annual yield

losses to the five most important calorie crops: rice, wheat, maize, soya beans and potatoes. For instance, rice blast (*Magnaporthe oryzae*) causes global rice yield losses of 10-35% each year (Talbot, 2003), Septoria tritici blotch (STB) disease (*Zymoseptoria tritici*) can cause annual wheat yield losses of 20% in the UK (Fones et al., 2015), whilst corn smut (*Ustilago maydis*) can reduce Central and South American maize yield harvests by 20% annually (Godfray et al., 2016). Astonishingly, crop losses from just five fungal diseases (rice blast, wheat stem rust, corn smut, soybean rust and potato late blight) could otherwise feed between 0.6 and 4 billion people with 2,000 calories every day for one year (Fisher et al., 2012; Stukenbrock & Gurr, 2022). At the same time, total global food demand is expected to increase by 35 - 56% by 2050 (van Dijk et al., 2021). These yield losses also have serious economic consequences. For example, STB costs UK growers around £240 million per year in yield losses (Fones et al., 2015). Additionally, some fungal phytopathogens, such as *Fusarium* and *Penicillium*, produce mycotoxins that contaminate food supplies and have adverse effects on human and animal health (Bennett & Klich, 2003).

In recent decades, the problems posed by fungal pathogens to public health and food security have been compounded by globalised trade and transport, which have facilitated their dissemination into new regions (Bebber et al., 2013; Fones et al., 2020). Indeed, the recent outbreak of the wheat blast pathogen *Magnaporthe oryzae* in Bangladesh originated from South America and was probably introduced through infected wheat imported from Brazil (Islam et al., 2016). Meanwhile, *Candida auris*, a fungal pathogen of humans, was first identified in Japan in 2009 and has now spread to

more than 40 countries across six continents (Keighley et al., 2021). Moreover, fungal pathogens are moving polewards as the climate warms (Bebber et al., 2013), with Europe and China likely to experience the greatest influx of novel fungal pathogens over the course of this century (Chaloner et al., 2021). Monoculture cropping practises have also exacerbated yield losses to fungal disease, since large areas of genetically uniform crops provide ideal breeding and feeding grounds for fungal phytopathogens (Steinberg & Gurr, 2020).

1.2. The control of fungal pathogens depends on a limited number of antifungal compounds

The control of fungal pathogens in clinical and agricultural settings depends on a limited number of antifungal compounds. In this thesis, the terms “clinical antifungals” and “agrochemical fungicides” are used to distinguish between compounds used to control fungal diseases in humans and plants, respectively. The term “antifungal compounds” is used to refer to these compounds collectively.

1.2.1. Clinical antifungals

The development of clinical antifungals has been constrained by the fact that fungi are evolutionarily close to humans (Brown et al., 2012). Currently, there are only four classes of systemic antifungals for treating IFIs in humans: polyenes, azoles, echinocandins and pyrimidines (Perlin et al., 2017).

The polyenes are the oldest class of clinical antifungals and include Nystatin and Amphotericin B. Polyenes exert fungicidal activity by forming large extramembranous aggregates that extract ergosterol from plasma membranes (Anderson et al., 2014). Ergosterol is essential for regulating membrane permeability and membrane protein activity (Jorda & Puig, 2020). Although polyenes exhibit broad-spectrum and potent activity against fungal pathogens, these compounds are not frequently used because of their poor oral bioavailability and significant host toxicities (Perfect et al., 2017).

Azoles block ergosterol biosynthesis by inhibiting the cytochrome P450 enzyme lanosterol 14α-demethylase (Erg11 in yeasts; Cyp51 in moulds). This inhibition causes the accumulation of toxic sterol intermediates, including 14α-methyl-3,6-diol (Robbins & Cowen, 2022), which are fungistatic in yeasts but fungicidal in moulds (Perlin et al., 2017). Azoles such as Fluconazole, Voriconazole and Posaconazole possess favourable safety and oral bioavailability profiles and are widely used for the treatment of aspergillosis and candidiasis (Pappas et al., 2009). In fact, azoles account for more than half of the market for clinical antifungals (**Figure 1.1**) (Lamberth, 2022). However, the clinical lifespan of azoles is threatened by widespread emergence of resistance (Pfaller et al., 2012) (discussed in section 1.3).

Echinocandins are lipopeptides that non-competitively inhibit β-1,3-glucan synthase (Douglas et al., 1997; Johnson et al., 2011), which is responsible for producing the essential cell wall component β-1,3-glucan (Shematek et al., 1980). In this way, echinocandins impair the integrity of the cell wall, which is lethal when cells become

unable to resist intracellular osmotic pressures (Letscher-Bru & Herbrecht, 2003). The echinocandins Caspofungin and Micafungin are regularly used for treating invasive candidiasis (Pappas et al., 2009). However, these compounds lack activity against certain fungal pathogens, most notably *Cryptococcus spp*. (Perlin et al., 2017).

Finally, the pyrimidine analog 5-Flucytosine interferes with DNA and RNA metabolism. Currently, 5-Flucytosine is only used in combination with other clinical antifungals, because monotherapy is prone to the rapid development of resistance (Perfect et al., 2017).

1.2.2. Agrochemical fungicides

There are more classes of agrochemical fungicides than clinical antifungals (Fisher et al., 2018). Indeed, plants are more distantly related to fungi than humans, meaning there is a lower risk of off-target toxicity to the host. Additionally, agrochemical fungicides are subject to less stringent safety requirements, and the agrochemical market size is larger, attracting more research investment (Perfect, 2017). In spite of this, the agrochemical fungicide market is also dominated by only a few classes (Lamberth, 2022) (**Figure 1.1**) due to regulation, safety concerns and the emergence of resistance to several classes (Fisher et al., 2018; Hawkins et al., 2018) (discussed in section 1.3).

Like the clinical antifungal market, azoles are also the most widely used class of agrochemical fungicide (Price et al., 2015). This is because azoles have broad-spectrum activity and minimal host toxicity, since neither humans nor plants have ergosterol (Rodrigues, 2018). Two additional widely used classes of agrochemical fungicide,

succinate dehydrogenase inhibitors (SDHIs) and quinone-outside inhibitors (Q_OIs) (also known as strobilurins), inhibit mitochondrial respiration. SDHIs inhibit succinate dehydrogenase, which is part of the tricarboxylic acid (TCA) cycle and mitochondrial electron transport chain (complex II) (Keon et al., 1991). Their primary mode of action is blocking the TCA cycle at the level of succinate to fumarate oxidation (Sierotzki & Scalliet, 2013). Meanwhile, Q_OIs bind to cytochrome b, a component of the cytochrome bc_1 complex (complex III). This blocks electron transfer between cytochrome b and cytochrome c_1 within complex III, which in turn, disrupts the production of ATP (Bartlett et al., 2002). Together, azoles, SDHIs and Q_OIs comprise ~60% of the global agrochemical fungicide market (Fones et al., 2020), and are used to control fungal phytopathogens on cereals, fruits and vegetables (Lamberth, 2022). Other commonly applied fungicides include the Anilinopyrimidines, which interfere with methionine biosynthesis (Fritz et al., 1997), Benzimidazoles, which inhibit microtubule formation (Lacey, 1990) and multi-site inhibitors such as Chlorothalonil (Tillman et al., 1973).

The high costs of polyenes and echinocandins preclude their use as agrochemical fungicides (Neoh et al., 2014; Borba et al., 2018). Polyenes are also unlikely to be stable in field conditions as they are readily oxidised (Haro-Reyes et al., 2022). Meanwhile, Q_OIs and SDHIs are not used as clinical antifungals, likely because of safety concerns (Yanicostas et al., 2021; Huang et al., 2022).

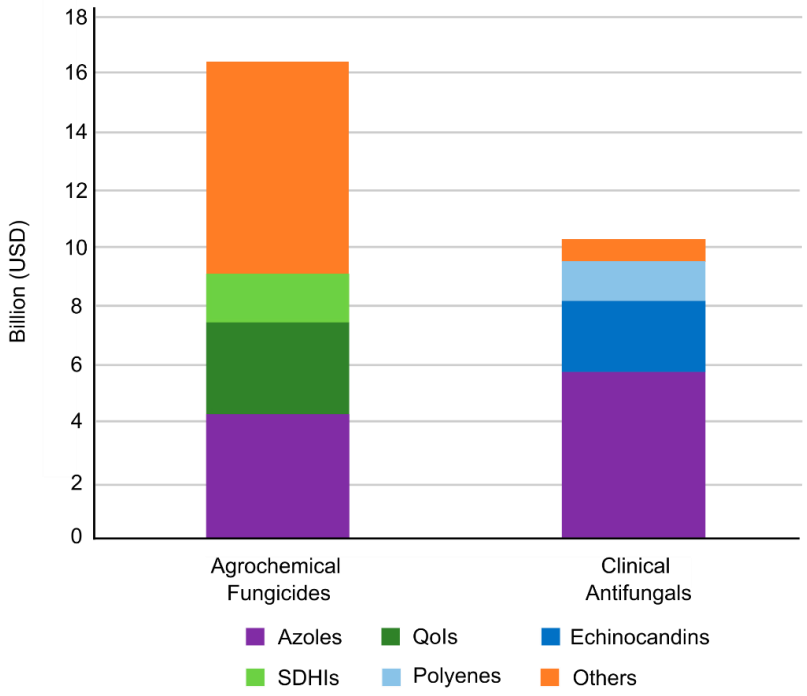

Figure 1.1 – The control of fungal pathogens depends on a limited number of antifungal modes of action. Bar charts displaying the market sizes for different classes of agrochemical fungicides and clinical antifungals in 2019. Figure adapted from Lamberth (2022).

1.3. The emergence of antifungal resistance is undermining the efficacy of antifungal compounds

Our overreliance on a limited number of antifungal compounds has led to the rapid emergence of antifungal resistance among diverse fungal pathogens (Fisher et al., 2018). Indeed, resistance to all licensed classes of clinical antifungals has emerged in most fungal species that infect humans (Robbins et al., 2017). Similarly, resistance to every main class of agrochemical fungicide has been documented in major fungal phytopathogens (Fisher et al., 2018). The emergence of resistance to any one class is a significant problem because there are limited classes available. Multidrug-resistant (MDR) isolates are increasingly reported, particularly for *Candida glabrata* (Arendrup & Patterson, 2017) and *Candida auris* (Ademe & Girma, 2020), which are challenging to eradicate from hospitals (Chowdhary et al., 2017). Infections with these isolates are associated with high morbidity and mortality (Du et al., 2020), and the main treatment option are toxic second-line antifungals such as Amphotericin B (Perlin et al., 2017). In agricultural environments, the onset of fungicide resistance is associated with total, or near total, failure of disease control, with potentially devastating consequences for food production and rural economies (Steinberg & Gurr, 2020). To date, resistance to azole fungicides has evolved in over 50 fungal phytopathogens (Hawkins & Fraaije, 2021), and resistance to benzimidazole fungicides has been documented in over 90 fungal phytopathogens (Hawkins & Fraaije, 2016). Moreover, resistance to Q_OIs was detected in downy mildew after just two years of use (Bartlett et al., 2002) and SDHI resistance was identified in 17 fungal phytopathogen species after ten years of use (Fisher et al., 2018).

There are two distinct types of antifungal resistance: intrinsic and acquired. Intrinsic resistance refers to the innate ability of a fungal species to resist antifungals without prior exposure, and is independent of specific adaptive mutations (Robbins et al., 2017). Meanwhile, acquired resistance refers to the ability of a fungal population to grow in antifungal concentrations exceeding the minimal inhibitory concentration (MIC) and is underpinned by heritable genetic mutations (Brauner et al., 2016; Berman & Krysan, 2020). Hereafter, this thesis will focus on acquired antifungal resistance, which will be referred to as "antifungal resistance".

The molecular mechanisms governing antifungal resistance can be broadly categorised into target-site and non-target site resistance mechanisms. Multiple mechanisms are often found alongside each other in resistant pathogens. In broad terms, fungal pathogens infecting humans and plants have independently evolved the same major antifungal resistance mechanisms (**Table 1.1, Table 1.2**).

1.3.1. Target-site resistance mechanisms

Target-site resistance involves point mutations in the coding region of the drug target gene which reduce drug binding and efficacy. This is the most common antifungal resistance mechanism and has been observed for nearly every antifungal class (Fisher et al., 2018). In clinical isolates of *Candida albicans*, over 140 different Erg11 amino acid substitutions conferring azole resistance have been identified (Morio et al., 2010). Moreover, echinocandin resistance in *Candida spp.* is often acquired through point mutations in *FKS* genes, which encode the catalytic subunits of the echinocandin target,

β-1,3-glucan synthase (Perlin et al., 2017). For most fungal phytopathogens in which Q_OI resistance has been reported, the major resistance mechanism is the amino acid substitution of glycine with alanine at position 143 of the cytochrome b protein (Barlett et al., 2002).

Another prevalent target-site resistance mechanism is the increased expression of the drug target. Indeed, most antifungals inhibit their targets, and therefore increased target expression prevents antifungals from inhibiting all the available target sites. For example, in *C. albicans*, gain-of-function mutations in Upc2, the transcriptional activator of *ERG11*, overexpress *ERG11* and confer azole resistance (Dunkel et al., 2008). In *Aspergillus fumigatus*, the most common azole resistance mechanism involves the L98H mutation in the target Cyp51A, in combination with tandem repeats in the *cyp51A* promoter, which increase *cyp51A* expression (Mellado et al., 2007). Similarly, in the grapevine powdery mildew *Uncinula necator*, azole resistance is conferred by *CYP51* overexpression, attributable to mutations Y136F and A1119C in *CYP51* (Frenkel et al., 2015).

1.3.2. Non-target site resistance mechanisms

The upregulation of drug efflux pumps is a ubiquitous non-target site resistance mechanism in fungal pathogens (Robbins et al., 2017; Hu & Chen, 2021). This efflux is mediated by ATP-binding cassette (ABC) and major facilitator superfamily (MFS) transporters at the plasma membrane which can export a broad-spectrum of unrelated compounds (Kolaczkowski et al., 1998; Cannon et al., 2009). The majority of these efflux

pumps are silent or weakly expressed in the absence of toxic compounds, but upon drug treatments, their expression is rapidly induced by a small number of transcription factors (Cannon et al., 2009; Hu & Chen, 2021). In *C. albicans*, the upregulation of the ABC transporters Cdr1 and Cdr2 and the MFS transporter Mdr1 are associated with azole resistance (Sanglard et al., 1995; Sanglard et al., 1997). In addition, gain-of-function mutations in *TAC1*, the transcriptional activator of *CDR1* and *CDR2*, result in the constitutive overexpression of these efflux pumps, which confers azole-resistance in clinical isolates of *C. albicans* (Coste et al., 2006). Overexpression of ABC transporters also mediates azole resistance in the clinically important pathogens *Aspergillus fumigatus* (Slaven et al., 2002) and *Cryptococcus neoformans* (Posteraro et al., 2003). Meanwhile, multidrug resistance in the fungal phytopathogen *Botrytis cinerea* is caused by gain-of-function mutations in the transcription factor Mrr1 which result in the overexpression of the ABC transporter AtrB (Kretschmer et al., 2009). Alternatively, drug efflux pumps can be upregulated by promoter mutations. For instance, a 519-bp insert in the promoter of *MFS1* is responsible for multidrug-resistance in *Z. tritici*, the causal agent of Septoria Leaf Blotch on wheat (Omrane et al., 2017). In contrast to drug efflux, antifungal detoxification by metabolic enzymes such as cytochrome P450s or glutathione transferases has only been rarely documented in fungal pathogens (Sang et al., 2018; Hu & Chen, 2021) and is considered to play a minor role in conferring antifungal resistance (Lucas et al., 2015).

Biofilm production is a clinically significant antifungal resistance mechanism. Fungal biofilms are highly structured communities of yeast and filamentous cells enclosed

within an extracellular matrix consisting of carbohydrates, proteins and nucleic acids (Ramage et al., 2012). Biofilms effectively reduce the local concentration of antifungals by sequestering them in a glucan-rich matrix (Nett et al., 2010). Drug efflux pumps are also commonly upregulated in cells residing in biofilms (Mukherjee et al., 2003). *Candida spp*. biofilms are intrinsically resistant to azoles (Ramage et al., 2012). This can cause refractory fungal infections in patients with indwelling medical devices, such as intravascular catheters, because these surfaces are often colonised with biofilm-producing *Candida spp*. (Perlin et al., 2017). Biofilm production is also an important resistance factor for *Aspergillus spp*., which form extensive extracellular matrices (Ramage et al., 2012).

Cellular stress response pathways also play integral roles in promoting resistance to antifungal compounds. A prominent example is the molecular chaperone heat-shock protein 90 (Hsp90), which regulates cellular signalling by stabilising various client proteins (Taipale et al., 2010). In *C. albicans*, Hsp90 stabilises the catalytic subunit of the protein phosphatase calcineurin (Singh et al., 2009), which is required to survive cell membrane stresses induced by azoles (Cruz et al., 2002). Hsp90 also stabilises multiple members of the cell wall integrity (CWI) pathway (LaFayette et al., 2010), which is critical for withstanding stresses induced by echinocandins (Walker et al., 2010). Indeed, in *C. albicans* and *A. fumigatus*, the CWI pathway upregulates the biogenesis of chitin, which strengthens cell walls upon exposure to echinocandins (Walker et al., 2010). Consistent with this, inhibition of Hsp90 increases susceptibility to azole and echinocandin

treatments (Robbins et al., 2017). Hsp90 has also been shown to regulate biofilm production in *C. albicans* and *A. fumigatus* (Robbins et al., 2011).

The acquisition of antifungal resistance by fungal pathogens is greatly facilitated by the plasticity of their genomes. For instance, azole exposure causes aberrant cell cycle regulation in *C. albicans*, leading to aneuploidies (Harrison et al., 2014) which can increase the expression of resistance determinants (Lee et al., 2023). Indeed, in clinical isolates of the diploid pathogen *C. albicans*, the duplication of the left arm of chromosome 5 causes azole resistance (Selmecki et al., 2006) by increasing the expression of the azole target *ERG11* and the transcriptional activator gene *TAC1* (Selmecki et al., 2008). Additionally, loss of heterozygosity (LOH) can occur for specific genomic loci harbouring azole resistance determinants (*ERG11* and *TAC1*), rendering mutations in these genes homozygous (Coste et al., 2007). In *C. albicans*, azole resistance can be conferred by a variety of LOH events, including gene conversion within the *TAC1* locus, mitotic recombination of the left arm of chromosome 5, or chromosome 5 loss and reduplication (Coste et al., 2007). Similarly, in *Candida glabrata*, azole resistance can be conferred by duplications of the chromosome harbouring the *CYP51* target gene (Marichal et al., 1997). Finally, copy number variations (CNVs) are another source of genomic diversity in fungal pathogens. CNVs refer to amplified or deleted chromosomal segments which often arise via non-allelic homologous recombination between repeat sequences (Vande Zande et al., 2023). CNVs are found throughout fungal genomes, and often contain genes associated with antifungal resistance (Todd & Selmecki, 2020). For example, recombination between transposable elements can generate CNVs in the

wheat pathogen *Z. tritici*, and stresses during the infection process can activate transposon mobilisation and drive CNV formation (Fouche et al., 2020).

	Clinical antifungals		
	Polyenes	**Azoles**	**Echinocandins**
Target-site mutations		✓	✓
Target-site overexpression		✓	
Drug efflux		✓	
Biofilms		✓	✓
Stress response pathways	✓	✓	✓
Genome plasticity		✓	

Table 1.1 – Summary of the major resistance mechanisms for each class of clinical antifungal.

	Agrochemical fungicides			
	Azoles	**QoIs**	**SDHIs**	**Benzimidazoles**
Target-site mutations	✓	✓	✓	✓
Target-site overexpression	✓			✓
Drug efflux	✓	✓	✓	
Genome plasticity	✓			

Table 1.2 – Summary of the major resistance mechanisms for each class of agrochemical fungicide.

1.4. Strategies for reducing the emergence and spread of antifungal resistance

1.4.1. Elucidating the molecular mechanisms underpinning antifungal resistance

Although significant progress has been made in identifying various antifungal resistance mechanisms, our understanding of the full range of resistance mechanisms remains incomplete (Lee et al., 2023). Indeed, the complexity of fungal biology, the diversity of resistance mechanisms, and the ability of fungi to adapt rapidly to different stresses mean that new resistance mechanisms and drug-resistant pathogens continue to emerge, with therapeutic failure increasingly common (Fisher et al., 2018). Yet a comprehensive understanding of the molecular mechanisms governing antifungal resistance is critical for developing more effective therapeutics and designing resistance management strategies (Robbins et al., 2017). To raise awareness of the rising threats posed by drug-resistant fungal infections, the World Health Organisation (WHO) recently published the first Fungal Priority Pathogens List (FPPL) (World Health Organisation, 2022). This list includes fungal pathogens that cause systemic invasive infections for which drug resistance and other management challenges exist. In this report, the WHO states that understanding the mechanisms of antifungal resistance is a top priority for fungal research and development investment.

1.4.2. Discovering antifungal compounds with novel modes of action

The current rate of antifungal discovery is outstripped by the emergence of antifungal resistance (Fisher et al., 2018). Furthermore, the dearth of antifungals available makes the problem of resistance increasingly serious (Perlin et al., 2017). Thus, concerted action is required to discover antifungal compounds with novel modes of action. Antifungals targeting new cellular processes are especially required, because they are less likely to be affected by cross-resistance to pre-existing antifungal classes. These new antifungals should exhibit rapid fungicidal activity, broad-spectrum efficacy and improved patient tolerability (Perfect et al., 2017). The development of new multi-site fungicides would also be beneficial, because resistance is unlikely to arise through target-site resistance mechanisms (Grimmer et al., 2014). Currently, there are several antifungal therapeutics in pre-clinical and clinical development stages, which include new members of existing antifungal classes as well as compounds belonging to novel classes (Puumala et al., 2024).

1.4.3. Preserving the efficacy of existing antifungal compounds: stewardship and combination therapies

Antifungal stewardship is essential for preserving the efficacy of existing antifungal compounds (Perlin et al., 2017). This encompasses selecting the optimal antifungal regimen, dose and duration of treatment (Perlin et al., 2017). For agrochemical fungicides, stewardship also involves restricting the number of treatments applied per growing season and rotating between compounds with different modes of action (Brent & Hollomon, 2007). Combination therapies can also prolong the lifespan of existing

antifungals. Indeed, the probability that a fungal pathogen simultaneously acquires resistance to two or more drugs is substantially lower than the probability of evolving resistance to a single drug alone (Anderson et al., 2005). Moreover, synergistic interactions occur when the combined effect of two drugs is greater than the sum of each drug's individual activity (Cokol et al., 2011). This allows a therapeutic effect to be achieved with lower doses of each drug, and enables fungistatic drugs such as azoles to become fungicidal (Onyewu et al., 2003). This enhanced killing effect increases the likelihood that the pathogen population will be eliminated (Anderson et al., 2005). For example, combinations of Amphotericin B, Fluconazole and 5-Flucytosine are more effective at treating cryptococcal meningitis than either drug alone (Molefi et al., 2015; Schwarz et al., 2006). For these reasons, many agrochemical fungicides are only available as mixed products (Brent & Hollomon, 2007).

1.5. Chemogenomic screening approaches in *Saccharomyces cerevisiae* can accelerate the discovery of antifungal resistance mechanisms and modes of action

1.5.1. *S. cerevisiae* is a powerful model for fungal research

Identifying antifungal resistance mechanisms and modes of action is more straightforward with the model yeast *Saccharomyces cerevisiae* than with fungal pathogens (Demuyser & Van Dijck, 2019; Ross & Santiago-Tirado, 2024). Indeed, *S. cerevisiae* has a smaller, more highly annotated genome that is easier to manipulate (Duina et al., 2014; Moller & Stukenbrock, 2017; Wang et al., 2023). The genetic manipulation of *S. cerevisiae* is also facilitated by its normal sexual cycle, with haploid

and diploid cells readily obtained. Conversely, no sexual cycle has been observed in *Candida glabrata*, whilst *Candida albicans* has a parasexual cycle, whereby tetraploid cells undergo chromosome loss to form diploid cells, without meiosis (Forche et al., 2008). Meanwhile, many fungal pathogens harbour multinucleate cells, creating challenges for generating mutants with genetically identical nuclei (Strom & Bushley, 2016). Additionally, unlike most fungal pathogens, there are a vast array of tools available for genetically manipulating *S. cerevisiae*, including plasmid libraries and mutant collections (Duina et al., 2014). *S. cerevisiae* can also be easily cultured in simple, inexpensive media and has a short generation time, allowing for rapid experimentation. In contrast, many fungal phytopathogens are difficult to cultivate in the laboratory, particularly obligate biotrophs such as *Phakopsora pachyrhizi* (Hossain et al., 2023) and rust fungi (Pucciniales) (Lorrain et al., 2019). Lastly, *S. cerevisiae* shares many antifungal resistance mechanisms with fungal pathogens (Demuyser et al., 2019). Together, these characteristics of *S. cerevisiae* make it a powerful model for identifying how resistance may emerge in fungal pathogens.

1.5.2. Conventional chemogenomic screening approaches in *S. cerevisiae*

The aforementioned characteristics of *S. cerevisiae* enabled the development and application of chemogenomic screening approaches using this yeast. Chemogenomic screening involves the genome-wide analysis of chemical-genetic interactions and is a powerful approach for elucidating antifungal modes of action and resistance mechanisms (Giaever et al., 1999, 2004). Conventional chemogenomic screening approaches with *S. cerevisiae* take advantage of yeast deletion collections (Giaever et al.,

1999, 2004). In each strain in these collections, a single open reading frame (ORF) has been replaced with a kanMX drug-resistance marker. Together, across the entire collection, all ~6,000 known and suspected ORFs have been replaced. The heterozygous deletion collection consists of ~6,000 strains, and because there are ~1,000 essential genes in *S. cerevisiae*, the haploid and homozygous diploid deletion collections comprise of ~5,000 strains each (Winzeler et al., 1999; Giaever et al., 2002). For chemogenomic screening, a deletion collection is pooled and grown competitively in the presence of antifungal compounds. The relative abundance, and hence fitness, of each strain in the treated population is then determined by sequencing the unique molecular barcodes flanking the kanMX marker in each strain (Winzeler et al., 1999; Giaever et al., 2002). In this way, yeast deletion collections can be used to systemically identify chemical-genetic interactions in an unbiased fashion (Giaever et al., 1999, 2004).

Heterozygous deletion collections have been extensively used in a chemogenomic screening approach called haploinsufficiency profiling (HIP) (Giaever et al., 1999, 2004, Hillenmeyer et al., 2008; Lee et al., 2014; Hoepfner et al., 2014). Haploinsufficiency is a dominant phenotype in diploid organisms that are heterozygous for loss-of-function alleles. It arises when reducing the dosage of a gene from two copies to one results in a growth phenotype (Deutschbauer et al., 2005). HIP operates under the assumption that the decreased expression of a drug target gene in a heterozygous mutant can confer drug hypersensitivity, causing a quantifiable growth defect (Giaever et al., 1999). In this way, HIP has been used to identify antifungal drug targets and genes acting in closely related

signalling or metabolic pathways (Giaever et al., 2004; Hillenmeyer et al., 2008; Lee et al., 2014; Hoepfner et al., 2014).

Homozygous profiling (HOP) and haploid deletion profiling (HAP) are similar to HIP but examine the full deletion of non-essential genes in either diploid or haploid strains, respectively. HOP and HAP allow the identification of genes in target-related pathways and detoxification processes which buffer cells against chemical stresses (Parsons et al., 2004, 2006; Hillenmeyer et al., 2008; Lee et al., 2014; Hoepfner et al., 2014). The complementary application of HIP and HOP/HAP has therefore accelerated the discovery of drug modes of action and resistance mechanisms.

Multicopy suppression profiling (MSP) is an analogous approach for discovering genes and pathways targeted by antifungal compounds (Xue et al., 2021). MSP relies on the assumption that the overexpression of a target gene or components of a target pathway confers antifungal resistance (Xue et al., 2021). The Molecular Bar-coded Yeast (MoBY) ORF collection is a library of centromere-based plasmids where each gene is tagged with unique barcodes (Ho et al., 2009). This collection can be transformed into any strain before pools of transformants are grown in the presence of antifungals of interest. Resistant strains are then identified by amplifying the strain-specific barcodes and using microarrays or high-throughput sequencing (Ho et al., 2009).

1.5.3. Limitations of conventional chemogenomic screening approaches in *S. cerevisiae*

Although chemogenomic screening approaches utilising yeast deletion collections (HIP, HOP, HAP) have greatly improved our understanding of antifungal modes of action and resistance (Hillenmeyer et al., 2008; Lee et al., 2014; Hoepfner et al., 2014; Ho et al., 2009), these approaches have important limitations.

Firstly, these approaches are not readily applicable to different genetic backgrounds of *S. cerevisiae*. This is because yeast deletion collections are extremely labour-intensive and time-consuming to generate. Indeed, the existing deletion collections took an international consortium of 16 laboratories over 4 years to produce (Giaever et al., 2002). As such, deletion collections are only available in a limited number of conventional laboratory strains of *S. cerevisiae* (Giaever et al., 2002). Since genetic background affects the penetrance and expression of genetic traits, this complicates the connection between genotype to phenotype (Chen et al., 2022). Moreover, conventional laboratory strains lack sensitivity to several antifungal compounds. This is partly attributed to the "Pleiotropic Drug Resistance" (PDR) network of ABC and MFS transporters that collectively export diverse antifungals from the cytoplasm (Kolaczkowski et al., 1998). As a consequence, several compounds are better studied in strains deficient for the PDR response (Coorey et al., 2015). Another limitation of using conventional laboratory strains is that the targets of several antifungal compounds are not found in *S. cerevisiae*. Analysing these compounds using yeast deletion collections

requires robotics to cross the corresponding target into ~5,000 strains. This requirement for specialist equipment limits the accessibility of this approach.

Secondly, yeast deletion collections have accumulated secondary mutations. Indeed, 56% of the strains in deletion collections are estimated to contain secondary mutations (Teng et al., 2013). This can complicate the connection from genotype to phenotype. For instance, Hoepfner et al., (2014) identified that hypersensitivity in numerous HIP strains was due to secondary mutations and not the deletion mutations.

Thirdly, regarding HIP, the deletion of one copy of a target gene does not always lead to the expected drug hypersensitivity. Additionally, gene expression in some heterozygous deletion mutants does not always manifest in the expected 50% reduction due to transcriptional feedback loops (Hoon et al., 2008). Similarly, in relation to MoBY, the overexpression of a target gene might not always confer drug resistance. This might be because the encoded protein resides within a complex with distinct stoichiometric requirements (Roemer et al., 2012), or because overexpression is toxic (Sopko et al., 2006).

Thus, these caveats can constrain the utility of conventional chemogenomic screens in *S. cerevisiae* for identifying antifungal resistance mechanisms and modes of action. Alternative chemogenomic screening approaches that overcome these limitations would therefore facilitate research efforts aiming to tackle drug-resistant fungal infections.

1.6. Transposon sequencing

1.6.1. Principle of transposon sequencing

Transposon sequencing (Tn-seq) is an innovative genome-wide screening approach with tremendous potential for chemogenomics. Tn-seq has been developed in a range of bacteria (van Opijnen et al., 2009; Christen et al., 2011; Girgis et al., 2007) and fungi, including *Saccharomyces cerevisiae* (Gangadharan et al., 2010; Michel et al., 2017; Edskes et al., 2018), *Saccharomyces uvarum* (Sanchez et al., 2019), *Schizosaccharomyces pombe* (Guo et al., 2013), *Rhodosporidium toruloides* (Coradetti et al., 2018), *Pichia pastoris* (Zhu et al., 2018), *Yarrowia lipolytica* (Patterson et al., 2018), *Candida albicans* (Segal et al., 2018; Gao et al., 2018; Mielich et al., 2018) and *Candida glabrata* (Gale et al., 2020).

Tn-seq utilises large-scale transposon mutagenesis to generate dense libraries containing millions of transposon mutants, each containing a single transposon insertion (van Opijnen et al., 2009; Michel et al., 2017; Cain et al., 2020). Across the entire library, every gene is interrupted by multiple independent transposon insertions. Upon generation, a transposon library is pooled and grown competitively under a test condition of interest. The library is then harvested, before the transposon-genome junctions are amplified and sequenced *en masse* using next-generation sequencing. The positions of the insertions are then aligned to the respective reference genome, and the number of sequencing reads for each transposon reflects the abundance of the corresponding mutants in the library population. Mutants with insertions in essential loci are inviable and lost from the

pool. Hence, transposon insertions are not detected in essential loci (**Figure 1.2**). By growing a library in different test conditions, it is possible to identify conditionally essential genes (**Figure 1.2**), and the change in the number of sequencing reads for each insertion reveals the effect of the insertions on fitness (van Opijnen et al., 2009). In this way, Tn-seq allows the direct linkage of phenotype to genotype in a high-throughput, straightforward and time-efficient manner.

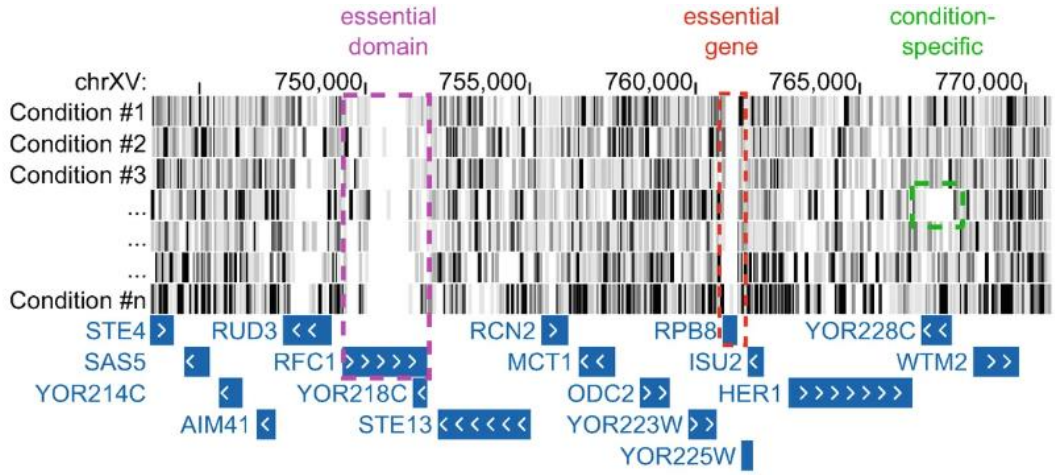

Figure 1.2 – Transposon libraries can identify essential genes, essential protein domains, and conditionally essential genes. Figure displays a section of chromosome 15 for a transposon library after seven treatment conditions. Grey lines correspond to transposon insertions. The grey level is proportional to the number of sequencing reads. Blue rectangles correspond to open reading frames. Essential genes (red dashed box), essential protein domains (pink dashed box) and conditionally essential gene (green dashed box) appear devoid of transposon insertions. Note that this figure displays transposon libraries generated using SATAY (see section 1.7). Essential protein domains are discussed in section 1.7.2. Figure source: Michel & Kornmann 2022.

1.6.2. Transposon sequencing for chemogenomic screening

Tn-seq is a powerful technique for chemogenomic screening because it can simultaneously assess the fitness contribution of all genetic loci in the presence of antimicrobial compounds (Cain et al., 2020). In these experiments, transposon insertions causing drug resistance are positively selected and have a higher number of reads. Such insertions identify loci that otherwise engender drug sensitivity. Meanwhile, transposon insertions causing drug sensitivity are negatively selected and have a lower number of reads. Such insertions identify loci that otherwise protect cells during chemical stresses (**Figure 1.3**). These chemical-genetic interactions reveal how antimicrobial resistance can emerge and can be used to link antimicrobial compounds to their modes of actions.

Tn-seq has been successfully applied in a number of bacterial pathogens to identify genes regulating antibiotic resistance: Daptomycin resistance in *Staphylococcus aureus* (Coe et al., 2019), Ciprofloxacin resistance in *Acinetobacter baumannii* (Geisinger et al., 2019), Norfloxacin resistance in *Streptococcus pneumoniae* (van Opijnen & Camilli, 2012) and resistance to range of antibiotics in *Pseudomonas aeruginosa* (Gallagher et al., 2011; Murray et al., 2015).

Recently, Tn-seq has been utilised in fungal pathogens to reveal genes affecting antifungal susceptibility. For example, Tn-seq was performed in a haploid strain of *Candida albicans* to identify genes affecting Fluconazole susceptibility (Gao et al., 2018). In addition to finding known regulators of Fluconazole susceptibility, this screen discovered that Fluconazole resistance can be conferred by the upregulation of

sphingolipid biosynthesis. Similarly, Tn-seq has been applied to reveal the genetic basis of Fluconazole susceptibility in *Candida glabrata* (Gale et al., 2020). This study uncovered a novel association between alpha-ketoglutarate production in the mitochondria and Fluconazole sensitivity. Additionally, Tn-seq has been performed in *C. glabrata* to unveil the genetic determinants of Micafungin resistance (Nickels et al., 2024) and FK506 resistance (Pavesic et al., 2024). These studies have demonstrated that Tn-seq is a robust approach for advancing our understanding of antifungal resistance and modes of action.

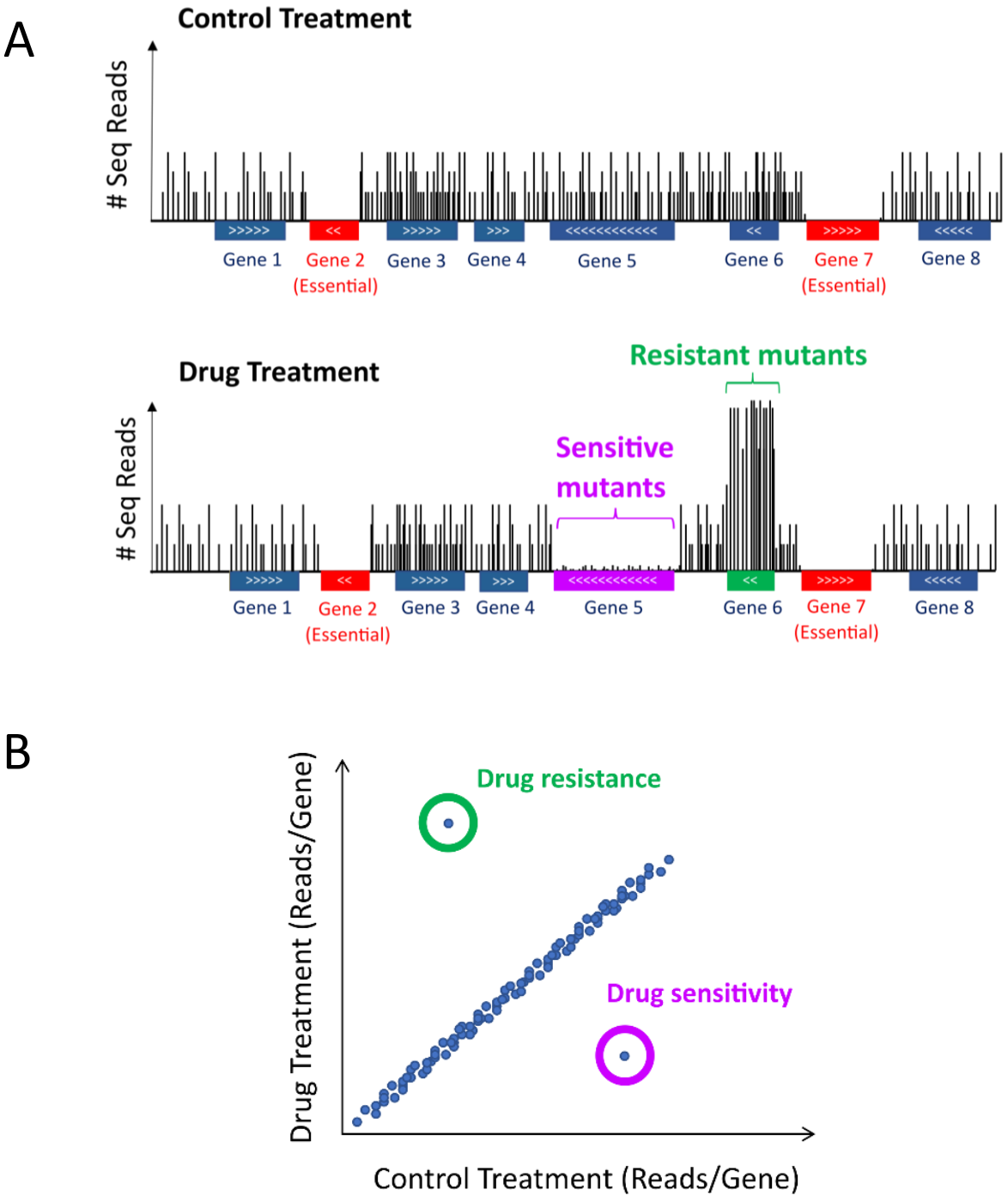

Figure 1.3 – Schematic depiction of using Tn-seq for chemogenomic screening. Full figure legend is on next page.

Figure 1.3 – Schematic depiction of using Tn-seq for chemogenomic screening

A) Schematic depiction of transposon insertion maps for a genomic region after a control treatment or drug treatment. Transposon insertions are represented by vertical black lines. The heights of the lines correspond to the number of sequencing reads. Genes are represented by coloured rectangles. Transposons conferring drug sensitivity are negatively selected and have a lower number of reads (gene 5, magenta). Transposon insertions conferring drug resistance are positively selected and have a higher number of reads (gene 6, green). Gene 2 and gene 7, shown in red, are essential for viability in both growth conditions.

B) Scatter plot comparing the number of sequencing reads mapping to each gene in a transposon library following a control treatment or a drug treatment. Most genes fall on the y = x diagonal because they are equally tolerant of transposon insertions in each treatment. However, genes engendering drug sensitivity have more reads in the drug treatment condition, whereas genes involved in drug resistance have fewer reads in the drug treatment condition.

1.7. SAturated Transposon Analysis in Yeast (SATAY)

1.7.1. SATAY: overview of library generation

SAturated Transposon Analysis in Yeast (SATAY) is a powerful Tn-seq protocol developed in the budding yeast *Saccharomyces cerevisiae* (Michel et al., 2017; Michel et al., 2019; Michel & Kornmann, 2022). In SATAY, transposon libraries are generated using a plasmid that contains a modified non-autonomous maize transposon, known as mini*Ds*, interrupting the *ADE2* gene (Weil & Kunze, 2000), and a galactose-inducible hyperactive *Ac* transposase (Lazarow et al., 2012). Strains transformed with this plasmid are subsequently selected on galactose-containing, adenine-deficient medium. Transposase-induced mini*Ds* excision is followed by the homology-directed repair of the *ADE2* gene (Michel et al., 2019), conferring adenine prototrophy to the transposed cells. The excised mini*Ds* transposon then re-inserts at random locations in the yeast genome. This protocol routinely generates libraries containing over two million transposon mutants, of which ~300,000 – 500,000 transposon insertions are detected by Illumina sequencing (Michel & Kornmann, 2022), corresponding to an average density of one insertion for every 20-40 base-pairs. This high density of insertions allows the identification of essential genes and essential protein domains (discussed below). Transposon libraries can also be generated using a plasmid in which mini*Ds* is originally interrupting the *TRP1* gene (Agnès Michel, unpublished). For these libraries, transposition is induced on galactose-containing medium lacking uracil (**Chapter 2, Section 2.8**).

1.7.2. Advantages of SATAY

SATAY has numerous advantages over alternative genome-wide screening techniques in *S. cerevisiae*.

First, SATAY can be performed in different genetic backgrounds of *S. cerevisiae* in a labour- and time-efficient manner. Indeed, SATAY has been applied to investigate gene essentiality in 16 wild strains from diverse ecological and geographical origins (Chen et al., 2022). SATAY was also recently performed in 12 different genetically engineered strains with rewired lipid biosynthesis pathways (John Peter et al., 2022). SATAY is therefore significantly more versatile than yeast deletion collections, which are limited to very few conventional laboratory strain backgrounds.

Second, in contrast to yeast deletion collections, SATAY data interpretation is not confounded by secondary mutations arising during screening because every gene is disrupted by multiple independent transposon insertions (Michel et al., 2017; Michel & Kornmann, 2022).

Third, transposon libraries generated using SATAY harbour both loss- and gain-of-function alleles. Loss-of-function mutations are generated when transposons disrupt the coding DNA sequence (CDS) of a gene, preventing the production of a functional protein. Meanwhile, gain-of-functions mutations can be generated because the mini*Ds* transposon contains promoter sequences (Yu et al., 2004). Consequently, insertions mapping in promoters can increase the expression of downstream genes (Michel et al., 2019; Serbyn et al., 2020). For example, transposons mapping in the promoter of the

aspartic protease gene *DDI1* were positively selected in a strain with defects in processing Topoisomerase1-DNA adducts (Serbyn et al., 2020). It was subsequently validated that the overexpression of *DDI1* from a strong *ADH1* promoter is sufficient to rescue the growth of the same mutant (Serbyn et al., 2020).

Moreover, SATAY libraries contain alleles encoding proteins with truncated domains. This allows the genome to be interrogated at a sub-gene resolution and allows essential protein domains to be identified (Michel et al., 2017). This was previously illustrated for *GAL10* (Michel et al., 2017), which encodes a bifunctional enzyme with an N-terminal epimerase, and a C-terminal mutarotase domain (Majumdar et al., 2004). Both functions are normally required for galactose catabolism. However, since the transposon library was grown on a mixture of alpha- and beta-D-galactose (Michel et al., 2017), the mutarotase domain was not required for catalysing their interconversion (Majumdar et al., 2004). Thus, only the epimerase domain was essential for metabolising galactose. Accordingly, the 3' end of *GAL10* was permissive of transposon insertions, whereas the 5' end was devoid of transposon insertions (**Figure 1.4A**). Gain-of-function mutations can also be generated by transposons truncating inhibitory domains (Michel et al., 2019). This was observed for the *YAP1* gene in a transposon library challenged with the antifungal Cerulenin (Michel et al., 2019). *YAP1* encodes a transcription factor which harbours a C-terminal nuclear export sequence (Kuge et al., 1997). The removal of the C-terminus triggers the constitutive nuclear localisation of Yap1 (Kuge et al., 1997). Cerulenin positively selected transposons truncating the C-terminus of Yap1 (**Figure 1.4B**). This is because Yap1 upregulates the expression of *FLR1* (Alarco et al., 1997),

which encodes an MFS transporter that exports Cerulenin (Oskouian & Saba, 1999). Additionally, the promoter sequences in mini*Ds* enable insertions in essential genes to be tolerated if they occur upstream of sequences encoding the essential domains. For example, for the essential gene *TFC7*, transposons were tolerated in the phosphatase domain situated upstream of the essential TFIIIC domain (**Figure 1.4C**) (Michel et al., 2017).

Other widely used transposons for Tn-seq in yeast, *Hermes* and *piggyBac* (Gangadharan et al., 2010; Edskes et al., 2018; Li et al., 2011), do not harbour promoter sequences and therefore cannot identify such gain-of-function mutations. Moreover, yeast deletion collections cannot be used to identify essential protein domains, since entire open reading frames have been deleted (Winzeler et al., 1999; Giaever et al., 2002).

Fourth, the mini*Ds* transposon does not preferentially insert into specific nucleotide sequences (Lazarow et al., 2012; Michel et al., 2017). In contrast, the *Hermes* and *piggyBac* transposons have strong insertion site sequence preferences: Hermes prefers to insert at genomic locations with the target sequence TnnnnA (Gangadharan et al., 2010), whilst piggyBac has a strong preference for inserting at TTAA sequences (Li et al., 2011). This allows SATAY to generate libraries with a higher density of insertions, enabling genetic loci to be interrogated at a higher resolution. Notably, mini*Ds*, *Hermes* and *piggyBac* all exhibit insertion site preferences for inter-nucleosomal regions of the genome (Michel et al., 2017; Gangadharan et al., 2010; Yoshida et al., 2017). This is presumably because transposase enzymes have greater access to nucleosome-free DNA.

However, this bias has a negligible impact because nucleosome-free DNA is found every ~160 base-pairs, and the same bias is found across all libraries. Therefore, interpreting Tn-seq data by directly comparing two or more transposon libraries effectively corrects for this bias.

Fifth, SATAY has no specific equipment requirements besides a next-generation sequencing service, which are increasingly available and inexpensive. In contrast, the handling of yeast deletion collections requires non-standard equipment, such as arraying robotics, limiting accessibility.

In summary, SATAY has multiple advantages over the use of yeast deletion collections and other fungal Tn-seq approaches. As such, recent studies have taken advantage of SATAY to functionally explore diverse cellular processes including lipid transport and metabolism, signalling, transcriptional regulation and DNA-protein crosslink repair (Michel et al., 2017; Haribowo et al., 2019; Jorgensen et al., 2020; John Peter et al., 2022; Serbyn et al., 2020; Serbyn et al., 2021).

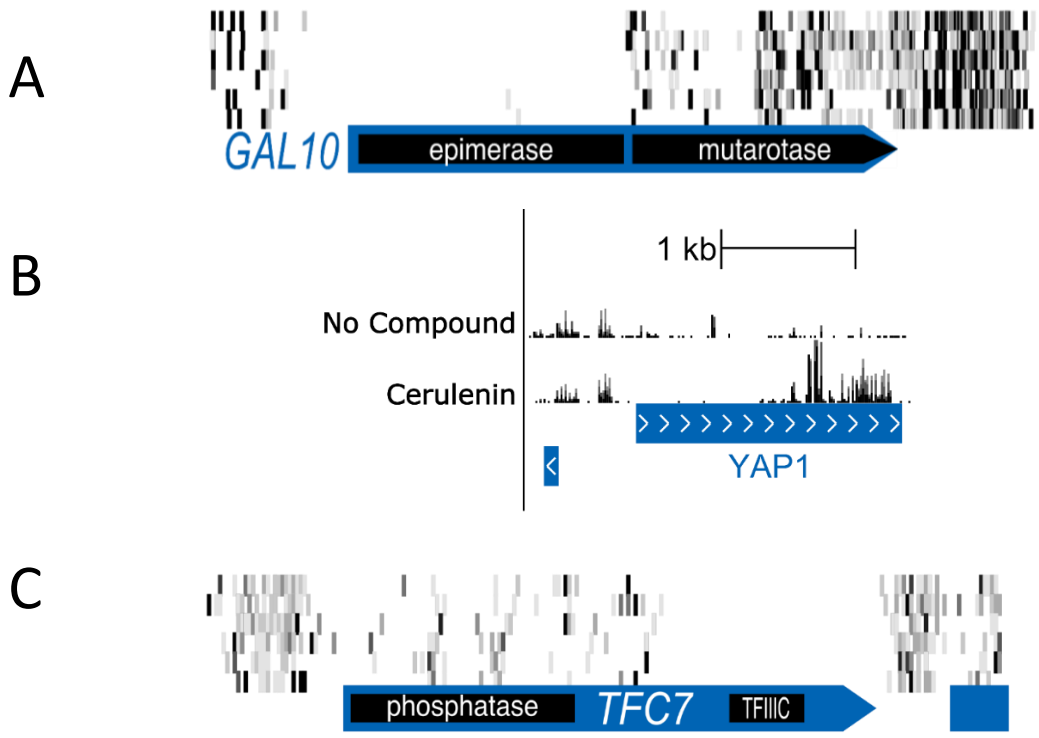

Figure 1.4 – SATAY can interrogate the genome at sub-gene resolution.

A) Transposon insertion maps for *GAL10* for six libraries, illustrating that SATAY can generate alleles with C-terminal truncations. The N-terminal epimerase- and C-terminal mutarotase -encoding domains are indicated. Grey lines represent transposons, with the grey level corresponding to the number of reads. The mutarotase domain was dispensable. Figure adapted from Michel et al., (2017).

B) Cerulenin positively selected for transposons in the 3'-end of *YAP1*. Each black bar corresponds to a transposon insertion. The height of the bars corresponds to the number of reads. capped at 500. Figure adapted from Michel et al., (2019).

C) Transposon insertion maps for *TFC7* for six libraries, illustrating that transposons can be tolerated in essential genes if they map upstream of essential domains. The non-essential 5' phosphatase domain and the essential 3' TFIIIC domain of *TFC7* are indicated. Figure adapted from Michel et al., (2017).

1.7.3. SATAY for chemogenomic screening

A recent proof-of-principle study has demonstrated that SATAY has significant potential for chemogenomic screening (Michel et al., 2019). Here, a transposon library was challenged with nine well-characterised antifungal compounds in parallel, identifying hundreds of loss- and gain-of-function mutations conferring resistance. This included gain-of-function mutations overexpressing drug targets. Indeed, for transposon libraries separately treated with Cerulenin, Fenpropimorph, or Tunicamycin, the promoters containing the most enriched transposons were precisely those upstream of the genes encoding the corresponding targets: *FAS1* for Cerulenin (Johansson et al., 2008), *ERG2* and *ERG24* for Fenpropimorph (Marcireau et al., 1990), and *ALG7* for Tunicamycin (Tkacz & Lampen, 1975) (**Figure 1.5A-D**). This demonstrated that SATAY can identify the direct targets of antifungal compounds. Furthermore, this study revealed that SATAY can identify the specific drug efflux pumps that detoxify different antifungal compounds (Michel et al., 2019). For example, transposons in the promoter of *PDR5*, which encodes an ABC transporter (Meyers et al., 1992) were strongly selected by Cerulenin, Fluconazole and Soraphen A (**Figure 1.6, red arrowheads**). Consistently, these three compounds are known Pdr5 substrates. Cerulenin also positively selected insertions in the promoter of the MFS transporter *FLR1* (**Figure 1.6, red arrowheads**) consistent with Flr1 exporting Cerulenin (Oskouian & Saba, 1999). Similarly, SATAY revealed that the ABC transporters Snq2 and Yor1 mediate Fluazinam and Soraphen A efflux, respectively (**Figure 1.6, red arrowheads**). Taken together, this proof-of-principle study demonstrated that SATAY can be utilised to accelerate our understanding of antifungal modes of action and resistance mechanisms.

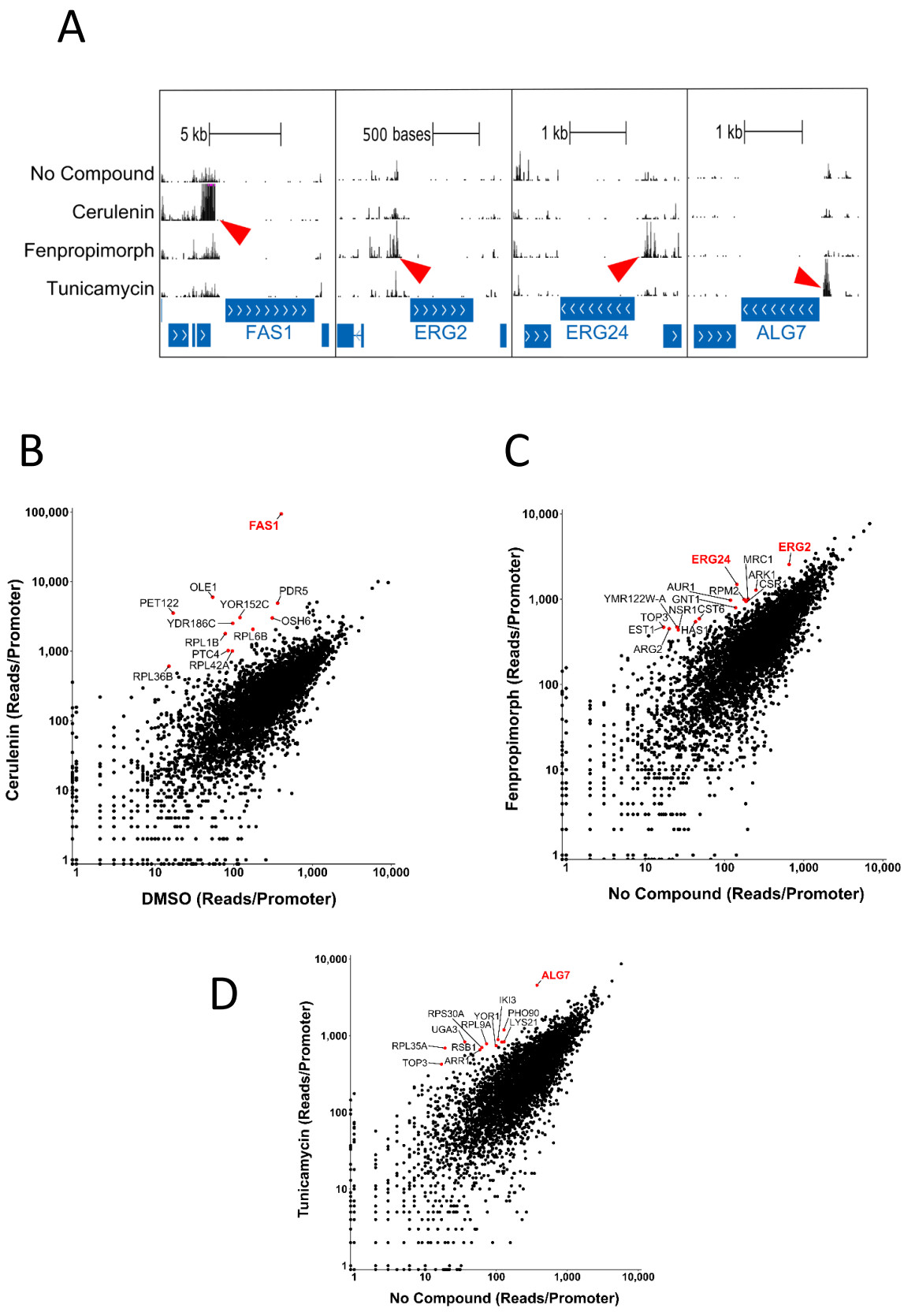

Figure 1.5 – SATAY can identify antifungal drug targets. Full figure legend is on next page.

Figure 1.5 – SATAY can identify antifungal drug targets.

A) Transposon insertion maps for four genomic regions encompassing *FAS1*, *ERG2*, *ERG24* and *ALG7*, which encode the targets for Cerulenin, Fenpropimorph and Tunicamycin, respectively. The height of the bars corresponds to the number of sequencing reads per transposon, capped at 500. Blue bars represent CDSs. Red arrowheads indicate positively selected transposons in the promoters of genes encoding drug targets. Figure adapted from Michel et al., 2019.

B-D) Scatter plots comparing the number of sequencing reads mapping to each of the 6603 yeast coding DNA sequences (CDSs) in a transposon library treated with DMSO versus **B)** Cerulenin **C)** Fenpropimorph **D)** Tunicamycin. Each dot represents a single gene. The targets for each compound (*FAS1*, *ERG2*, *ERG24* and *ALG7*) are shown in red. Figure adapted from Michel et al., 2019.

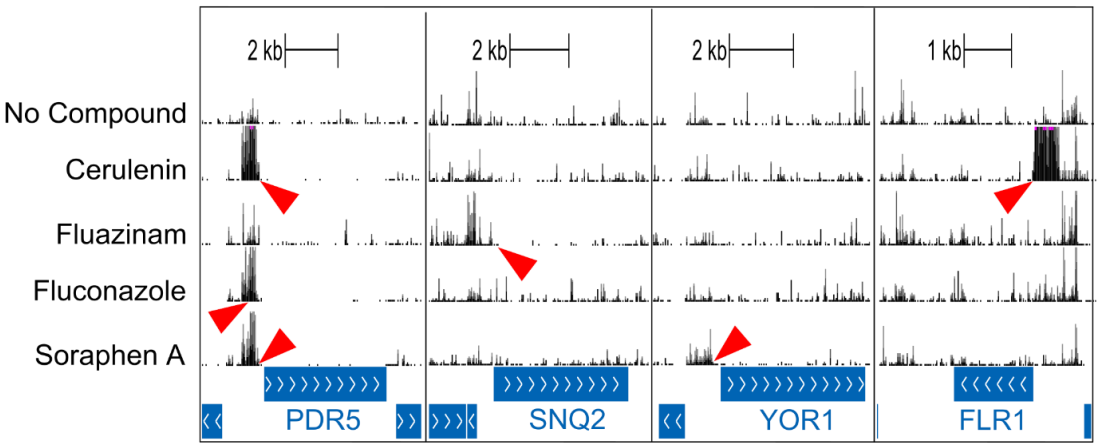

Figure 1.6 – SATAY can identify drug efflux pumps that export specific compounds. Transposon insertion maps for four genomic regions encompassing the genes for the drug efflux pumps *PDR5*, *SNQ2*, *YOR1* and *FLR1*. The height of the bars corresponds to the number of sequencing reads per transposon, capped at 500. Blue bars represent CDSs. Red arrowheads indicate positively selected transposons in the promoters. Figure adapted from Michel et al., 2019.

1.8. Thesis aims

The rapid emergence of multidrug-resistant fungal pathogens is undermining our ability to control fungal infections. This problem is exacerbated by our incomplete understanding of the molecular mechanisms governing antifungal resistance and our limited armamentarium of antifungal compounds. It is therefore critical that we improve our understanding of antifungal resistance and identify antifungals with novel modes of action. These efforts could be accelerated by SATAY, which has multiple advantages over conventional chemogenomic screening approaches in *S. cerevisiae*.

This thesis, therefore, aimed to apply SATAY to discover novel antifungal resistance mechanisms, and unveil the modes of action for several antifungal compounds. After the Materials and Methods in Chapter 2, Chapter 3 provides an overview of the SATAY screens performed in this thesis. Chapter 4 briefly discusses proof-of-principle screens further demonstrating that SATAY can identify a diverse range of resistance mechanisms. In Chapter 5, new discoveries are made about how resistance emerges against a novel antifungal compound called ATI-2307. This includes the identification of the transporter that mediates the selective accumulation of ATI-2307 inside *S. cerevisiae*. This transporter is subsequently shown to play a significant role in driving the potency of this compound. Chapter 6 focussed on Fludioxonil, a widely used fungicide with a disputed mode of action. Although it is well-established that Fludioxonil activity depends on the presence of a specific type of histidine kinase, it remains unclear whether Fludioxonil directly targets these kinases. Here, SATAY was performed to shed light on this question. Moreover, because *S. cerevisiae* lacks this specific type of histidine kinase and thus lacks

sensitivity to Fludioxonil, this SATAY screen was performed in an engineered strain heterologously expressing a histidine kinase derived from a Fludioxonil-sensitive fungal pathogen. Chapter 7 revealed a mode of action for the natural antifungal Chitosan. Since Chitosan lacks activity against conventional laboratory strains of *S. cerevisiae*, this discovery was enabled by performing SATAY in a non-conventional strain. Finally, Chapter 8 provides an evaluation of the utility of SATAY for chemogenomic screening.

Chapter 2 - Materials and Methods

2.1. Yeast strain handling

2.1.1. Yeast strains, storage and revival

Yeast strains used in this thesis are listed in **Table 2.1**. Strains were stored in 30% (v/v) glycerol (Sigma-Aldrich, G5516) cryo-stocks at -80°C (ByK database). Strains were revived by streaking cells from cryo-stocks onto the most appropriate agar media and incubating for 48hrs at 30°C.

Table 2.1 – Yeast strains used in this thesis.

#	Strain ID	Parent	Genotype	Reference
1	ByK352	BY4741	*MATa his3Δ1 leu2Δ0 met15Δ0 ura3Δ0 ade2Δ::His3MX6*	Michel et al., 2017
2	ByK831, ByK2117, ByK2118, ByK2119	W303-1B	*MATα {leu2-3,112 trp1-1 can1-100 ura3-1 ade2-1 his3-11,15}.* Four independent biological replicates.	Rothstein et al., 1977
3	ByK1151	12geneΔ0HSR	*MATα his3Δ1 leu2Δ0 met15Δ0 ura3Δ0 pdr1Δ0 pdr3Δ0 pdr8Δ0 yrr1Δ0 aus1Δ0 pdr5Δ0 pdr10Δ0 pdr11Δ0 pdr12Δ0 pdr15Δ0 snq2Δ0 yor1Δ0 RME1(ins308A)*	Chinen et al., 2011. Gift from Prof F. Strutz, University of Geneva
4	ByK1261	ByK1151	*MATα his3Δ1 leu2Δ0 met15Δ0 ura3Δ0 pdr1Δ0 pdr3Δ0 pdr8Δ0 yrr1Δ0 aus1Δ0 pdr5Δ0 pdr10Δ0 pdr11Δ0 pdr12Δ0 pdr15Δ0 snq2Δ0 yor1Δ0 RME1(ins308A) ade2Δ::His3MX6*	This study
5	ByK1174	AD12345678	*MATα Δyor1::hisG, Δsnq2::hisG, Δpdr5::hisG, Δpdr10::hisG, Δpdr11::hisG, Δycf1::hisG, Δpdr3::hisG, Δpdr15::hisG*	Decottignies et al., 1998. Gift from Prof M. Gupta, University of Iowa
6	ByK1230	BY4743Δ8a	*MATa/α, his3Δ1 leu2Δ0, his3Δ1, lys2Δ0 snq2::KanMX4 pdr3::KanMX4 pdr5::KanMX4 pdr1::NAT1 yap1::NAT1 pdr2Δ0 yrm1Δ0; yor1Δ0*	Hoepfner et al., 2014. Gift from Prof M. Spiess, University of Basel

7	ByK1262	ByK1174	*MATα Δyor1::hisG, Δsnq2::hisG, Δpdr5::hisG, Δpdr10::hisG, Δpdr11::hisG, Δycf1::hisG, Δpdr3::hisG, Δpdr15::hisG ade2Δ::kanMX6*	This study
8	ByK1266	ABC16 Monster	*MATα adp1Δ snq2Δ ycf1Δ pdr15Δ yor1Δ vmr1Δ pdr11Δ nft1Δ bpt1Δ ybt1Δ ynr070wΔ yol075cΔ aus1Δ pdr5Δ pdr10Δ pdr12Δ can1Δ::GMToolkit-α his3Δ1 leu2Δ0 ura3Δ0 met15Δ0*	Suzuki et al., 2011. Gift from Prof F. Roth, University of Toronto
9	ByK1868	ByK831	*MATa/α {leu2-3,112 trp1-1 can1-100 ura3-1 ade2-1 his3-11,15}*	This study
10	ByK1900, ByK1902	ByK1868	*MATa/α {leu2-3,112 trp1-1 can1-100 ura3-1 ade2-1 his3-11,15}* containing *p405-TEF1pr-BdDRK1* (pBK864) at one of the two *LEU2* loci. Two independent biological replicates.	This study
11	ByK1916	ByK1900	*MATa/α {leu2-3,112 trp1-1 can1-100 ura3-1 ade2-1 his3-11,15} sln1Δ::His3MX6 / SLN1* containing *p405-TEF1pr-BdDRK1* (pBK864) at one of two *LEU2* loci.	This study
12	ByK1921	ByK1902	*MATa/α {leu2-3,112 trp1-1 can1-100 ura3-1 ade2-1 his3-11,15} sln1Δ::His3MX6 / SLN1* containing *p405-TEF1pr-BdDRK1* (pBK864) at one of two *LEU2* loci.	This study
13	ByK1925, ByK1926, ByK1927	ByK1916	*MATa {leu2-3,112 trp1-1 can1-100 ura3-1 ade2-1 his3-11,15} sln1Δ::His3MX6* containing *p405-TEF1pr-BdDRK1* (pBK864) at *LEU2* locus. Three independent biological replicates.	This study
14	ByK1936, ByK1937, ByK1938	ByK1916	*MATa {leu2-3,112 trp1-1 can1-100 ura3-1 ade2-1 his3-11,15}* containing *p405-TEF1pr-BdDRK1* (pBK864) at *LEU2* locus. Three independent biological replicates.	This study
15	ByK1947, ByK1951, ByK1952	ByK1921	*MATa {leu2-3,112 trp1-1 can1-100 ura3-1 ade2-1 his3-11,15} sln1Δ::His3MX6* containing *p405-TEF1pr-BdDRK1* (pBK864) at *LEU2* locus. Three independent biological replicates.	This study
16	ByK2012, ByK2013, ByK2014	ByK1900	*MATa/α {leu2-3,112 trp1-1 can1-100 ura3-1 ade2-1 his3-11,15} tpi1Δ::kanMX6 / TPI1* with *p405-TEF1pr-BdDRK1* (pBK864) at one of two *LEU2* loci. Three biological replicates.	This study
17	ByK2018, ByK2160, ByK2161	ByK1937	*MATa {leu2-3,112 trp1-1 can1-100 ura3-1 ade2-1 his3-11,15} glo1Δ::kanMX6* transformed with the plasmid *p405-*	This study

			TEF1pr-BdDRK1 (pBK864). Three independent biological replicates.	
18	ByK2023, ByK2024	ByK1174	*MATα Δyor1::hisG, Δsnq2::hisG, Δpdr5::hisG, Δpdr10::hisG, Δpdr11::hisG, Δycf1::hisG, Δpdr3::hisG, Δpdr15::hisG mnn4Δ::kanMX6.* Two independent biological replicates.	This study
19	ByK2026	ByK352 x ByK1174	Diploid generated by crossing ByK352 and ByK1174	This study
20	ByK2032, ByK2033, ByK2034	ByK831	*MATα {leu2-3,112 trp1-1 can1-100 ura3-1 ade2-1 his3-11,15} hol1Δ::kanMX6.* Three independent biological replicates.	This study
21	ByK2036	ByK831	*MATα {leu2-3,112 trp1-1 can1-100 ura3-1 ade2-1 his3-11,15} spe1Δ::natNT2*	This study
22	ByK2037	ByK2032	*MATα {leu2-3,112 trp1-1 can1-100 ura3-1 ade2-1 his3-11,15} spe1Δ::natNT2 hol1Δ::kanMX6*	This study
23	ByK2114, ByK2115, ByK2116	ByK2032	*MATα {leu2-3,112 trp1-1 can1-100 ura3-1 ade2-1 his3-11,15} hol1Δ::kanMX6* transformed with the plasmid pBK994. Three independent biological replicates.	This study

2.1.2. Overnight cultures

Overnight cultures of 5-10mL rich or synthetic complete media were inoculated with isolated colonies. Unless stated otherwise, cultures were incubated at 30°C for approximately 16 hours with 200rpm orbital shaking.

2.1.3. Optical density measurements

Optical density measurements at 600 nm (OD_{600}) were made using a WPA CO8000 Cell Density Meter (Scientific Laboratory Supplies) in 1.5mL semi-micro cuvettes for visible wavelengths (VWR). On this instrument, OD_{600} of 1 corresponded to approximately 7,500,000 cells/mL.

2.2. Molecular Biology

2.2.1. Primers and Polymerase Chain Reaction

A full list of primers and their use in this study can be found in **Appendix 1**. Most primers were designed with Tm 57-63°C and length 18-24nt.

Unless indicated otherwise, amplification of DNA was performed using *Taq* DNA Polymerase (NEB #M0273) following the manufacturer's instructions. Briefly, 50µL PCR reactions were assembled containing 1x *Taq* buffer, 200µM dNTPs, 0.5µM of both forward and reverse primer, plasmid template (1-100ng per reaction) or genomic DNA (1ng-1µg per reaction), 1.25U of *Taq* DNA Polymerase, made up to 50µL with nuclease-free water. The PCR program consisted of an initial denaturing step of 5 minutes at 95°C, 35 cycles of: 30 seconds at 95°C, 30 seconds at 45-68°C (temperature depending on primers), 1 minute at 68°C per kilobase of expected product, followed by final extension of 10 minutes at 68°C. PCR products were analysed by gel electrophoresis (section 2.2.3).

2.2.2. Restriction digestions and ligations

Restriction enzymes were purchased from New England Biolab (NEB). Restriction digestions were performed following NEB's instructions and visualised by gel electrophoresis (section 2.2.3).

Ligation reactions were performed with T4 DNA ligase (Thermo Fisher Scientific #EL0011) following the manufacturer's instructions.

2.2.3. Gel electrophoresis

Agarose gels (1-2% w/v for PCR products depending on the size of the expected amplicon, 1% w/v for restriction digestion fragments) were prepared using 1x Tris-Borate-EDTA (TBE) buffer (89mM Tris-Borate, 2mM EDTA, pH 8.2-8.4) with ethidium bromide added to a final concentration of 0.3µg/mL. Gels were run at 100V for the required time and imaged using an iBright™ CL1500 Imaging System (Thermo Fisher Scientific, A44114).

2.3. Plasmids

2.3.1. Plasmids used in this thesis

Plasmids used in this study are listed in **Table 2.2**.

Table 2.2 – Plasmids used in this thesis.

#	Plasmid ID	Parent	Description	Reference
1	pBK507	pFA6a-*kanMX6*	pFA6a backbone carrying *kanMX6* cassette. Used for gene deletions	Longtine et al., (1998)
2	pBK508	pFA6a-*natNT2*	pFA6a backbone carrying *natNT2* cassette. Used for gene deletions	Janke et al., (2004)
3	pBK549	pBK257	CEN/*URA3*, Mini*Ds* within *ADE2*, hyperactive Ac transposase under *GAL1* promoter, 600bp repair template. Used for transposition induction on SC -ADE 2% galactose plates	Michel et al., 2019
4	pBK626	-	CEN/*URA3*, Mini*Ds* within *TRP1*, hyperactive Ac transposase under *GAL1* promoter, 600bp repair template. Used for transposition induction in SC -URA 2% galactose liquid media	John Peter et al., (2022)
5	pBK737	pFA6a-*His3MX6*	pFA6a backbone carrying *His3MX6* cassette. Used for gene deletions	Longtine et al., (1998)
6	pBK853	p405-*TEF1*pr	*LEU2*, *TEF1* promoter	Addgene plasmid #15968

7	pBK864	pBK853	*LEU2*, *TEF1*pr-*BdDRK1*. *BdDRK1* has been codon-optimised for *S. cerevisiae*, and is derived from *Blastomyces dermatitidis*	This study
8	pBK900	pBK905	pBK905 containing *BdDRK1* mutation CAC>GCA (H716A)	This study
9	pBK901	pBK905	pBK905 containing *BdDRK1* mutation CAC>CAG (H716Q)	This study
10	pBK902	pBK905	pBK905 containing *BdDRK1* mutation GAT>AAC (D1140N)	This study
11	pBK905	pYES2	2µ/*URA3*. *BdDRK1* under *GAL1* promoter. *BdDRK1* codon-optimised for *S. cerevisiae*, and is derived from *Blastomyces dermatitidis*	Gift from Dr Gabriel Scalliet (Syngenta)
12	pBK958	pC6464	CEN/*URA3*. Sc*HOL1* CDS in addition to sequences 1 kb upstream and 500 bp downstream of Sc*HOL1* CDS cloned into vector YCplac33.	Vindu et al., (2021)
13	pBK959	pRS316	CEN/*URA3*, empty vector	Sikorski & Hieter, 1989
14	pBK994	pBK958	*CaHOL1* CDS inserted in place of *ScHOL1* in pBK958	This study
15	pBK995	pBK958	pBK958 with *HOL1* mutations 1003A>G (R335G) and 1608T>C (A536A).	This study
16	pBK996	pBK958	pBK958 with *HOL1* mutations 854A>G (K285R) and 980A>G (E327G).	This study
17	pBK997	pBK958	pBK958 with *HOL1* mutations 169A>G (N57D) and 1002A>G (K334K).	This study
18	pBK998	pBK958	pBK958 with *HOL1* mutations 513A>G (E171E) and 995A>G (Y332C).	This study
19	pBK999	pBK958	pBK958 with HOL1 mutations 199T>C (F67L), 413A>G (T138A), 426T>C (F142F), 979G>A (E327K).	This study
20	pBK1000	pBK958	pBK958 with HOL1 mutations 152C>T (S51L) and 751A>G (Y250C).	This study
21	pBK1001	pBK958	pBK958 with HOL1 mutations 169A>T (N57Y), 444T>C (A148A), 1415G>A (R472K)	This study
22	pBK1002	pBK958	pBK958 with HOL1 mutations 169A>G (N57D), 202G>A (G68S)	This study
23	pBK1003	pBK958	pBK958 with HOL1 mutations 722A>G (E241G)	This study
24	pBK1004	pBK958	pBK958 with HOL1 mutations 1034T>C (L345S)	This study
25	pBK1005	pBK958	pBK958 with HOL1 mutations 1003A>G (R335G)	This study
26	pBK1006	pBK958	pBK958 with HOL1 mutations 980A>G (E327G), 1685A>T (Y562F)	This study
27	pBK1007	pBK958	pBK958 with HOL1 mutations 547T>C (F183L), 560T>G (L187W), 1437A>T (I479I)	This study
28	pBK1008	pBK958	pBK958 with HOL1 mutations 1034T>C (L345S)	This study
29	pBK1009	pBK958	pBK958 with HOL1 mutations 968A>G (D323G), 1251A>G (A417A), 1608T>C (A536A)	This study
30	pBK1010	pBK958	pBK958 with HOL1 mutations 170A>G (N57D)	This study

2.3.2. *Escherichia coli* plasmid transformation and plasmid preparation

For amplification, plasmids were transformed by heat-shock into the *Escherichia coli* strain DH5α. DH5α competent cells were prepared according to the protocol of Inoue et al., (1990) by Anitha Nair. For heat-shock transformation, 100µL DH5α was thawed on ice before ~100ng plasmid was added and left on ice for 30 minutes. Cell and plasmid mixtures were then heated to 42°C for 50 seconds, before being returned to ice for 3 minutes. Cells were then spread on Lysogeny Broth (LB) agar media containing Ampicillin (Sigma-Aldrich, 59349) for growth overnight at 37°C. Single colonies were used to inoculate 5mL LB media containing 50µg/mL Ampicillin and grown for a further 24hrs at 37°C, 200rpm. Transformed cells were stored in 30% (v/v) glycerol cryo-stocks at -80°C (pBK database). Plasmid DNA was prepared from liquid cultures using a GeneJET Plasmid Miniprep Kit according to manufacturer's instructions (Thermo Fisher Scientific).

2.3.3. Construction of plasmid p405-*TEF1*pr-*BdDRK1* (pBK864)

The *DRK1* coding DNA sequence (CDS) from *Blastomyces dermatitidis* (NCBI Reference Sequence: EGE84246.1) was commercially synthesised (Biomatik, Canada) with yeast codon optimisation, 5' restriction site for *Spe*I and a 3' restriction site for *Pst*I, and cloned into the vector pBluescript II SK (+). *BdDRK1* was then sub-cloned into p405-*TEF1*pr (Addgene plasmid #15968) using *Spe*I and *Pst*I and then T4 DNA ligase. The recombinant plasmid p405-*TEF*pr-*BdDRK1* was confirmed by restriction enzyme digestion.

2.3.4. Construction of plasmids encoding kinase-defective *BdDRK1* genes

The 2µ/*URA3* pYES2 plasmid (pBK905) bearing *GAL1*pr-*BdDRK1* was received as a kind gift from Dr Gabriel Scalliet (Syngenta, Stein). To generate kinase-defective *BdDRK1* alleles, the following mutations were introduced into *BdDRK1* on pBK905 by site-directed mutagenesis: CAC>GCA (H716A), CAC>CAG (H716Q), GAT>AAC (D1140N). Primers were designed so that nucleotide changes were in the middle of the primer. PCR amplification of pBK905 was performed using iProof™ High-Fidelity DNA polymerase (Bio-Rad Laboratories, 1725302). The PCR program consisted of an initial denaturing step of 30 seconds at 98°C, 18 cycles of: 10 seconds at 98°C, 25 seconds at 60°C, 5 minutes at 72°C, followed by final extension of 10 minutes at 72°C. Following PCR, the parent template plasmids were then digested using 30 units of *Dpn*I in 40µL reaction. Plasmids were then transformed in DH5α, colonies picked, miniprepped and verified by sequencing.

2.3.5. Construction of plasmid encoding the *Candida albicans HOL1* (pBK994)

The plasmid bearing the *HOL1* CDS from *Candida albicans* (pBK994) was generated by yeast gap-repair cloning. Briefly, the *CaHOL1* CDS was PCR-amplified from genomic DNA derived from *Candida albicans* strain ATCC MYA-2876 using primers #15 and #16. The 5' and 3' ends of the resulting *CaHOL1* PCR product were homologous to the *ScHOL1* 5' UTR and 3' UTR sequences on pBK958. The *ScHOL1* CDS was excised from pBK958 using *Bsu36*I and *Nru*I. The linearised pBK958 backbone was co-transformed with the *CaHOL1*

PCR product into the *hol1Δ* strain of *S. cerevisiae* ByK2032. The recombinant plasmid pBK994 was verified by colony PCR genotyping.

2.4. Construction of yeast strains

2.4.1. Yeast transformation

Yeast strains were transformed with ~1µg PCR product or 100ng plasmid using the lithium acetate protocol described previously (Gietz & Schiestl, 2007). Transformants were plated on selective medium and incubated at 30°C for 2-3 days.

2.4.2. Yeast deletion strains

Yeast deletion strains were generated by PCR-mediated gene disruption with selectable markers using the Longtine and Janke toolboxes (Longtine et al, 1998; Janke et al, 2004). Forward and reverse primers were designed with 5'-ends (45 nucleotides) that were homologous to the first and last 45bp of target gene sequence, respectively. PCR-amplification of deletion cassettes was performed using iProof™ High-Fidelity DNA polymerase (Bio-Rad Laboratories) and the PCR program consisted of an initial denaturing step of 30 seconds at 98°C, 35 cycles of: 10 seconds at 98°C, 25 seconds at 60°C, 2 minutes at 72°C (2 minutes 40 sec for *NAT1* cassette), followed by final extension of 10 minutes at 72°C. Gene deletions were verified by colony PCR genotyping (section 2.4.3).

2.4.3. Colony PCR genotyping

Colony PCR genotyping was performed to validate yeast deletion strains. Primers were designed to ensure that PCR product sizes did not exceed 500bp. A needle-head (< 1mm diameter) of fresh, isolated colonies (< 3 days old) was transferred into separate PCR tubes. The PCR tubes were then microwaved for four cycles of: 15 second microwave at 800W followed by 10 second pause. Microwaved cells were mixed with 20µL PCR reaction mixture by pipetting. PCR amplification was performed using *Taq* DNA Polymerase.

2.4.4. Tetrad dissections

Diploid strains were patched on YPA medium and incubated at 30°C for 5-7 days to induce sporulation. A needle-head of a sporulating colony was then inoculated into 50µL sterile water, and treated with 1mg/mL Zymolyase (AMSBio, 120491-1) for 8 minutes at 30°C. The suspension was then diluted by adding 700µL sterile water. Tetrad dissections were performed using a 10x objective on a microscope (Zeiss) fitted with a micromanipulator and a dissection needle (Singer Instruments, NDL-010). All tetrads were dissected on YPD plates, except for tetrads derived from *TPI1*+/- *BdDRK1*+/- diploids, which were dissected on YP 3% (v/v) ethanol 0.1% (v/v) galactose plates.

2.5. Media

2.5.1. Yeast peptone dextrose (YPD) medium

11g/L yeast extract (Appleton Woods Ltd, DM832), 22g/L peptone (BD Difco™, 211677), 55mg/L adenine hemisulfate salt (Sigma-Aldrich, A9126). For solid YPD medium, 22g/L agar (BD Difco™, 214030) was additionally included. After sterilisation by autoclaving, 10x filter-sterilised glucose (Sigma-Aldrich, G8270) was added to a final concentration of 2% (w/v).

For selective YPD medium, the following antibiotics were added after autoclaving: Geneticin (Fisher Scientific, 15444999) at 0.2mg/mL or Nourseothricin (Melford, N51200-0.1) at 0.1mg/mL.

2.5.2. YPA medium for sporulation

10g/L yeast extract (Appleton Woods Ltd, DM832), 20g/L peptone (BD Difco™, 211677), 10g/L Potassium acetate (Sigma-Aldrich, W292001).

2.5.3. Synthetic Complete (SC) medium

Amino Acid Mixes

Recipe A (Department of Biochemistry, University of Oxford)

Prepared as 100x stocks. 6g/L L-Isoleucine (Sigma-Aldrich, W527602), 5.5g/L Adenine Hemisulfate salt (Sigma-Aldrich, A9126), 2g/L L-Arginine (Thermo Fisher Scientific, A15738), 1g/L L-Histidine monohydrochloride monohydrate (Sigma-Aldrich, H8000),

6g/L L-Leucine (Sigma-Aldrich, L8000), 4g/L L-Lysine monohydrochloride (Sigma-Aldrich, L8662), 1g/L L-Methionine (Sigma-Aldrich, M9625), 6g/L L-Phenylalanine (Sigma-Aldrich, P2126), 5g/L L-Threonine (Sigma-Aldrich, 89179), 4g/L L-Tryptophan (Sigma Aldrich, T0254), 5.5g/L L-Tyrosine (Sigma-Aldrich, 93829), 5.5g/L Uracil (Sigma-Aldrich, U1128). 100x stocks were filter sterilised and stored at 4°C.

Recipe B (Institute for Biochemistry, ETH Zurich-like):

Prepared as 10x stocks. 0.3g/L L-Isoleucine (Sigma-Aldrich, W527602), 1.5g/L L-Valine (Sigma-Aldrich, V0500), 0.4g/L Adenine Hemisulfate salt (Sigma-Aldrich, A9126), 0.2g/L L-Arginine (Thermo Fisher Scientific, A15738), 0.2g/L L-Histidine (Sigma-Aldrich, H8000), 1g/L L-Leucine (Sigma-Aldrich, L8000), 0.3g/L L-Lysine monohydrochloride (Sigma-Aldrich, L8662), 0.2g/L L-Methionine (Sigma-Aldrich, M9625), 0.5g/L L-Phenylalanine (Sigma-Aldrich, P2126), 2g/L L-Threonine (Sigma-Aldrich, 89179), 0.4g/L L-Tryptophan (Sigma Aldrich, T0254), 0.3g/L L-Tyrosine (Sigma-Aldrich, 93829), 0.2g/L Uracil (Sigma-Aldrich, U1128), 1g/L L-Glutamic Acid (Sigma-Aldrich, G1251), 1g/L L-Aspartic Acid (Thermo Fisher Scientific, A13520). 10x stocks were sterilised by autoclaving and stored at 4°C.

Yeast nitrogen base (YNB): 4x stock solutions of YNB were prepared by dissolving 27.2g/L of YNB containing ammonium sulfate without amino acids (BD Difco™, 291920) in Milli-Q water. 4x stocks were sterilised by autoclaving.

***Synthetic Complete (SC) medium*:** 1x amino acid mix, 1x YNB, 2% (w/v) of filter-sterilised carbon source (glucose, galactose, raffinose or ethanol). Unless stated otherwise, all SC medium was prepared using the amino acid mix according to Recipe A.

SC -ADE, SC -HIS, SC -LEU, SC -TRP and SC -URA media were prepared by excluding the following amino acids from the amino acid mixes, respectively: Adenine Hemisulfate salt, L-Histidine, L-Leucine, L-Tryptophan or Uracil.

2.6. Antifungal compounds

2.6.1. Compound stocks and storage

Antifungal compounds used in this thesis are listed in **Table 2.3**. Compounds were stored at the manufacturer's recommended temperature. Stocks were prepared using dimethyl sulfoxide (DMSO) (Fisher Scientific, 10103483), Milli-Q® or acetic acid (Sigma, A6283) and stored at -20°C for maximally 18 months.

2.6.2. Preparation of Chitosan stock solutions

Chitosan stock solutions were prepared by performing a nitrous deamination reaction on medium molecular weight Chitosan (190-310kDa, 75-85% deacetylated, shrimp shells), as described previously (Zakrzewska *et al.,* 2005). Briefly, 10g Chitosan was dissolved in 200mL 10% (v/v) acetic acid (Sigma-Aldrich, A6283) and incubated with 200mg sodium nitrite (Sigma-Aldrich, 237213) in the dark at room temperature for 17hrs. The reaction was terminated by adjusting to pH 5.5 with 5M NaOH at room temperature.

Table 2.3 – Antifungal compounds used in this thesis

Compound	CAS Number	Supplier, SKU	Stock (mg/mL)	Solvent
Amphotericin B	1397-89-3	Sigma-Aldrich, 1032007-125MG	30	DMSO
ATI-2307	873546-31-7	Syngenta	10	Milli-Q®
Caspofungin	179463-17-3	Sigma-Aldrich, SML0425-25MG	5	Milli-Q®
Cerulenin	17397-89-6	Sigma-Aldrich, C2389-50MG	20	DMSO
Chitosan (Medium Molecular Weight)	9012-76-4	Sigma-Aldrich, 448877-50G	50	10% (v/v) Acetic Acid
Chlorothalonil	1897-45-6	Sigma-Aldrich, 36791-250MG	20	DMSO
Dodine		Sigma-Aldrich, 45466-250MG	25	100% (v/v) Ethanol
Fenpropimorph	67564-91-4	Sigma-Aldrich, 36772-100MG-R	5	DMSO
Fludioxonil	131341-86-1	Sigma-Aldrich, 46102-100MG-R	25	DMSO
Guazatine trifluoroacetate (Iminoctadine)	57520-17-9	Biosynth, FG180000	25	Milli-Q®
Iprodione	36734-19-7	Sigma-Aldrich, 36132-100MG	25	DMSO
Myriocin	35891-70-4	Sigma-Aldrich, M1177-5MG	5	DMSO
Pentamidine isethionate salt	140-64-7	Sigma-Aldrich, P0547-25MG	25	Milli-Q®
Prochloraz	67747-09-5	Sigma-Aldrich, 45631-250MG	25	DMSO
Tavaborole	174671-46-6	Sigma-Aldrich, SML1227-10MG	20	DMSO
Terbinafine Hydrochloride	78628-80-5	Sigma-Aldrich, T8826-100MG	10	DMSO

2.7. Antifungal susceptibility tests

2.7.1. Bioscreen C

Antifungal susceptibility tests for all compounds (except ATI-2307, Pentamidine and Iminoctadine – see section 2.7.2) were performed using a Bioscreen C™ instrument (Oy Growth Curves Ab Ltd, Helsinki, Finland). Cells were cultured from OD_{600} 0.2 in 250µL SC 2% glucose medium containing antifungal compounds at 30°C for 24hrs with continuous shaking, and OD_{600} readings were recorded every 20 minutes. Final DMSO concentrations never exceeded 1% (v/v).

2.7.2. ATI-2307, Pentamidine and Iminoctadine susceptibility tests in liquid medium

Wild-type yeast strains were first transformed with an empty CEN/*URA*3 plasmid (pBK959) (Sikorski & Hieter, 1989) whilst *hol1Δ* strains were transformed with pBK959 or the plasmid pBK994, which encodes the *HOL1* gene from *Candida albicans*. Transformants were then grown to saturation in 10mL SC -URA 2% (v/v) glucose. To facilitate a smooth transition during the diauxic shift from glucose to ethanol, transformants were reseeded at OD_{600} 0.2 in 10mL SC -URA 2% (v/v) ethanol 0.2% (v/v) glucose. Transformants were then reseeded at OD_{600} 0.2 in 10mL SC -URA 2% (v/v) ethanol containing ATI-2307, Pentamidine or Iminoctadine. SC -URA media was prepared using Amino Acid Recipe B (see section 2.5.3).

2.7.3. Fludioxonil sensitivity tests in YP 3% ethanol 0.1% galactose medium

To determine whether Fludioxonil interferes with Tpi1, Fludioxonil sensitivity tests were performed with progeny derived from *TPI1*+/- *BdDRK1*+/- diploids. Spores germinated on YP 3% (v/v) ethanol 0.1% (v/v) galactose plates were inoculated into 5mL YP 3% (v/v) ethanol 0.1% (v/v) galactose medium with or without Fludioxonil at OD_{600} 0.05. Cultures were incubated at 30°C, 200rpm, until end-point OD_{600} measurements were recorded after 40 hours. Three independent spores were tested for each genotype in each growth condition.

2.8. SAturated Transposon Analysis in Yeast (SATAY)

2.8.1. Summary of transposon libraries generated in this thesis

Two methods were used to generate transposon libraries in this thesis: 1) using the plasmid pBK549 on SC -ADE 2% galactose solid medium (see section 2.8.2) or 2) using the plasmid pBK626 in SC -URA 2% galactose liquid medium (see section 2.8.3). The method used to generate each transposon library is summarised in **Table 2.4**.

Table 2.4 – Summary of transposon libraries generated in this thesis

Treatment	Transposon library background	Plasmid	Transposition Medium (Solid/Liquid)
DMSO	ByK352	pBK549	SC -ADE 2% galactose (Solid)
Amphotericin B	ByK352	pBK549	SC -ADE 2% galactose (Solid)
Caspofungin	ByK352	pBK549	SC -ADE 2% galactose (Solid)
Myriocin	ByK352	pBK549	SC -ADE 2% galactose (Solid)
Prochloraz	ByK352	pBK549	SC -ADE 2% galactose (Solid)
DMSO	ByK1261 (12geneΔ0HSR)	pBK549	SC -ADE 2% galactose (Solid)

Prochloraz	ByK1261 (12geneΔ0HSR)	pBK549	SC -ADE 2% galactose (Solid)
No compound control for ATI-2307	ByK831	pBK626	SC -URA 2% galactose (Liquid)
ATI-2307	ByK831	pBK626	SC -URA 2% galactose (Liquid)
Acetic Acid	ByK1262 (AD1-8)	pBK549	SC -ADE 2% galactose (Solid)
Chitosan	ByK1262 (AD1-8)	pBK549	SC -ADE 2% galactose (Solid)
DMSO	ByK1925	pBK626	SC -URA 2% galactose (Liquid)
Fludioxonil	ByK1925	pBK626	SC -URA 2% galactose (Liquid)
Iprodione	ByK1925	pBK626	SC -URA 2% galactose (Liquid)

2.8.2. Transposon library generation on SC -ADE 2% galactose plates

Transposon libraries were generated on SC -ADE 2% galactose plates using previously described protocols (Michel et al., 2017; Michel & Kornmann 2022). The conditions specific to each transposon library generated using these protocols are summarised in **Table 2.5**. The key steps for generating libraries on SC -ADE 2% galactose plates are summarised in **Figure 2.1A**. Briefly, *ade2Δ ura3Δ* yeast strains were transformed with plasmid pBK549 and selected on SC -URA 2% glucose. Isolated colonies of pBK549 transformants were streaked on SC -URA 2% glucose and SC -ADE 2% glucose plates and incubated at 30°C for three days. For transformants that showed full growth on SC -URA while producing only a few (2-6) colonies on SC -ADE, cells were scraped from the SC -URA plates and used to inoculate pre-cultures of SC -URA 2% raffinose 0.2% glucose at OD_{600} 0.2 and grown to saturation. Saturated precultures were then concentrated to an OD_{600} of at least 40 (**Table 2.5**), before 200µL suspension was spread on each SC -ADE 2% galactose plate. The number of plates used was strain-specific (**Table 2.5**). Plates were incubated at 30°C for 10-14 days to induce transposition, before transposed colonies were harvested using previously described protocols (Michel et al., 2017;

Michel & Kornmann 2022). Harvested libraries were directly inoculated into 200mL SC -ADE 2% glucose at OD_{600} 0.2 for antifungal compound treatments (see section 2.8.4).

Table 2.5 – Summary of conditions for generating transposon libraries on solid medium

	ByK352 (BY4741) Transposon library	ByK1261 (12geneΔ0HSR) Transposon Library	ByK1262 (AD1-8) Transposon Library
Precultures			
Culture volume (mL)	70	300	1000
Number of precultures	3	1	1
Number of independent transformants cultured	3	6	6
Transposition Induction			
OD_{600} for plating	40	70	160
Number of SC -ADE 2% galactose plates	72	55	55
Length of induction (days)	14	14	10

2.8.3. Transposon library generation in SC -URA 2% galactose liquid medium

Transposon libraries were generated in SC -URA 2% galactose liquid medium using previously described protocols (Michel et al., 2019; John Peter et al., 2022). The growth conditions specific to each transposon library are summarised in **Table 2.6**. The key steps for generating libraries in SC -URA 2% galactose medium are summarised in **Figure 2.1B**. Briefly, *trp1- ura3-* yeast strains were transformed with the plasmid pBK626 and selected on SC -URA 2% glucose. Isolated colonies of pBK626 transformants were streaked on SC -URA 2% glucose and SC -TRP 2% glucose plates and incubated at 30°C

for three days. For transformants that showed full growth on SC -URA while producing only a few (2-6) colonies on SC -TRP, cells were scraped from the SC -URA plates and used to inoculate pre-cultures of SC -URA 2% raffinose 0.2% glucose at OD_{600} 0.2 and grown to saturation. To induce transposition, saturated pre-cultures were diluted to OD_{600} 0.2 in SC -URA 2% galactose and grown for ~50 hrs at 30°C, 200 rpm. The media for transposition induction was prepared using amino acid recipe B (see section 2.5.3). The efficiency of transposition was monitored by plating samples of the liquid induction cultures on SC, SC -URA, and SC -TRP at T_0, T_{20} and at the end of induction, and then scoring the number of colonies on these plates after three days of incubation at 30°C. After ~50 hrs of induction, the saturated transposon libraries were diluted in SC -TRP 2% glucose at OD_{600} 1 and grown to saturation. The estimated number of transposed cells reseeded at the start of the first expansion is shown in **Table 2.6**. The saturated cultures were then reseeded for a second expansion in SC -TRP 2% glucose from OD_{600} 0.3 to saturation. As each independent transposed cell is represented by a single cell at the end of induction (Agnès Michel, personal communication), these expansion steps were necessary to increase the number of copies of each transposition event. The expanded libraries were then harvested by centrifugation at 600x *g* and washed using Milli-Q. The ByK1925 transposon library was then directly inoculated into medium for the antifungal treatment whereas the ByK831 transposon library was stored in 30% (v/v) glycerol at -80°C.

The ByK831 transposon library was prepared previously by Dr Agnès Michel and Ruairi McGettigan (University of Oxford). In this thesis, prior to the treatment with ATI-2307,

an aliquot of ByK831 library was thawed in SC -TRP 2% glucose medium, re-seeded at OD_{600} 0.25 in 1.2L of SC -TRP 2% glucose and grown to saturation. The viability of the thawed library was verified by plating dilutions of the SC -TRP 2% glucose culture at T_0 on SC 2% glucose plates, and comparing the number of cells per OD_{600} to the number of cells per OD_{600} before freezing.

Table 2.6 – Summary of culture conditions for generating transposon libraries in liquid medium

	ByK1925 (*sln1Δ BdDRK1*) Transposon library	**ByK831 (W303) Transposon Library**
Precultures		
Culture volume (mL)	10mL	20mL
Number of precultures	6	6
Transposition Induction		
Culture volume (mL)	100	20
Number of cultures	6	6
First library expansion		
Number of transposed cells at start of expansion	63,000,000	12,000,000
Culture volume (L)	2.5	1.25
Number of cultures	2	2
Starting OD_{600}	1	1
Final OD_{600}	6	5
Second library expansion		
Culture volume (mL)	2.5	1
Number of cultures	2	2
Starting OD_{600}	0.3	0.3
Final OD_{600}	6	4.5

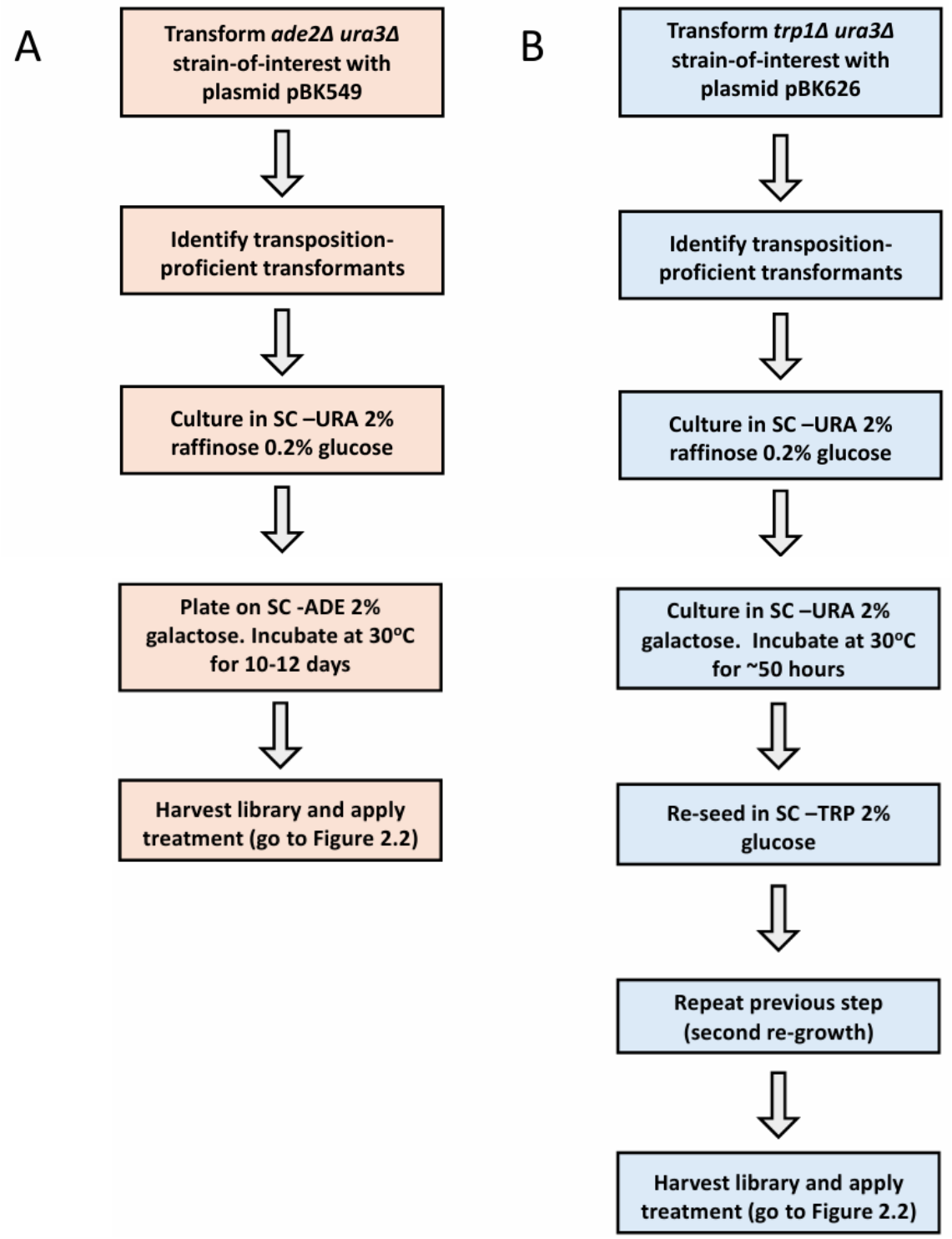

Figure 2.1 – Flow charts summarising the key stages for generating transposon libraries on A) SC -ADE 2% galactose plates and B) SC -URA 2% galactose medium.

2.8.4. Antifungal treatments of transposon libraries

Transposon libraries were treated with sub-lethal concentrations of antifungal compounds for two successive growth rounds from OD_{600} 0.2 to saturation (OD_{600} ~5) at 30°C, 200rpm. The sub-lethal concentrations were at or close to the inhibitory concentration of 30% (IC_{30}) and are summarised in **Table 3.1**, **Chapter 3**. The culture volumes for all treatments was 200mL, and media for the treatments are summarised in **Table 2.7**. The treated libraries were harvested for cell pellets of 500mg using previously described protocols (Michel et al., 2017; Michel & Kornmann 2022) and stored at -80°C. A flow chart summarising the key stages for antifungal treatments of transposon libraries is shown in **Figure 2.2**.

The Amphotericin B (0.75µg/mL) and Caspofungin (0.03µg/mL) treatments initially prevented the growth of the ByK352 transposon library. After 24hrs, the concentrations of these two compounds were diluted two-fold by the addition of 200mL SC -ADE 2% glucose medium into each culture.

Prior to the ATI-2307 treatment, the ByK831 transposon library was grown to saturation in 500mL SC -TRP 2% ethanol 0.2% glucose to facilitate the diauxic shift from glucose to ethanol. The library was then re-seeded into 200mL SC -TRP 2% ethanol at OD_{600} 0.2 for the ATI-2307 treatment.

Table 2.7 – Growth conditions for antifungal treatments of transposon libraries

Antifungal Drug	Transposon Library Background	Sub-lethal concentration (µg/mL)	Medium for Treatment
Amphotericin B	ByK352	0.375 (0.75 initially)	SC -ADE 2% glucose
ATI-2307	ByK831	0.000175	SC -TRP 2% ethanol
Caspofungin	ByK352	0.015 (0.03 initially)	SC -ADE 2% glucose
Chitosan	AD1-8 (ByK1262)	2	SC -ADE 2% glucose
Fludioxonil	ByK1925 (*sln1Δ BdDRK1*)	0.1	SC -LEU 2% glucose
Iprodione	ByK1925 (*sln1Δ BdDRK1*)	3	SC -LEU 2% glucose
Myriocin	ByK352	0.2	SC -ADE 2% glucose
Prochloraz	ByK352	10	SC -ADE 2% glucose
Prochloraz	12geneΔ0HSR	0.4	SC -ADE 2% glucose

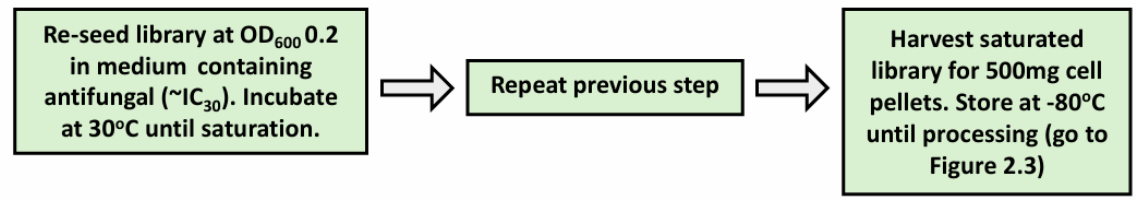

Figure 2.2 – Flow chart summarising the key stages for challenging transposon libraries with antifungal compounds.

2.8.5. Transposon library sequencing and analysis

Cell pellets were processed for sequencing by following previously described protocols (Michel et al., 2017; Michel & Kornmann 2022) and the key steps are summarised in **Figure 2.3**. Briefly, genomic DNA was extracted from cell pellets using

Phenol:Chloroform:Isoamyl Alcohol 25:24:1 (Sigma-Aldrich, P2069) and quantified on a 0.6% agarose gel using 1kb GeneRuler™ (ThermoFisher Scientific, SM0311) as a reference. For each gDNA sample, 2µg was digested in parallel with 50 units of *Dpn*II or *NIa*III and then circularised with 25 Weiss units of T4 DNA ligase. Circularised DNA was then precipitated using 100% ethanol, 0.3M sodium acetate pH 5.2 and 3.5ng/µL linear acrylamide (Invitrogen, AM9520) and placed at -20°C for 24hrs. Precipitated DNA was pelleted by centrifugation at 16,100x*g* and washed with 70% ethanol before dried pellets were resuspended in water and used as a template for PCR amplification of the transposon-genome junctions. PCR was performed following the protocol in (Michel et al., 2017; Michel & Kornmann 2022), except the extension time was modified to 1 minute to improve the reaction efficiency. The reverse primers contained distinct 8bp Illumina® barcode sequences, enabling the samples to be demultiplexed upon sequencing. PCR amplified samples were purified using a NucleoSpin Gel and PCR clean-up kit (Macherey-Nagel). PCR products were quantified using a NanoDrop™ 2000 Spectrophotometer (Thermo Scientific, ND-2000). For each sample, equal amounts of purified PCR product derived from the corresponding *Dpn*II- and *NIa*III-digests were pooled and sequenced using NextSeq™ 500/550 High Output Kits v2.5 (75 cycles) (Illumina, 20024906) and NextSeq™ 500 Sequencing System (Illumina, SY-415-1001) following (Michel & Kornmann, 2022) and the manufacturer's guidelines.

SATAY sequencing data processing and alignment was performed as described previously (Michel & Kornmann, 2022), using the web server at https://kornmann.bioch.ox.ac.uk/satay/. This web server was used to generate *.bed*,

.wig, *pergene.txt* and *perpromoter.txt* files. The *.bed* and *.wig* files were uploaded to UCSC Genome Browser to visualise transposition events and read counts per transposon, respectively. The *pergene.txt* and *perpromoter.txt* output files were used to construct scatter plots comparing the number of sequencing reads mapping to coding DNA sequences and promoters, respectively. Scatter plots were constructed in R (v4.2.0) using the packages ggplot2 (Wickham, 2016), ggrepel (Slowikowski et al., 2024) and cowplot (Wilke et al., 2024).

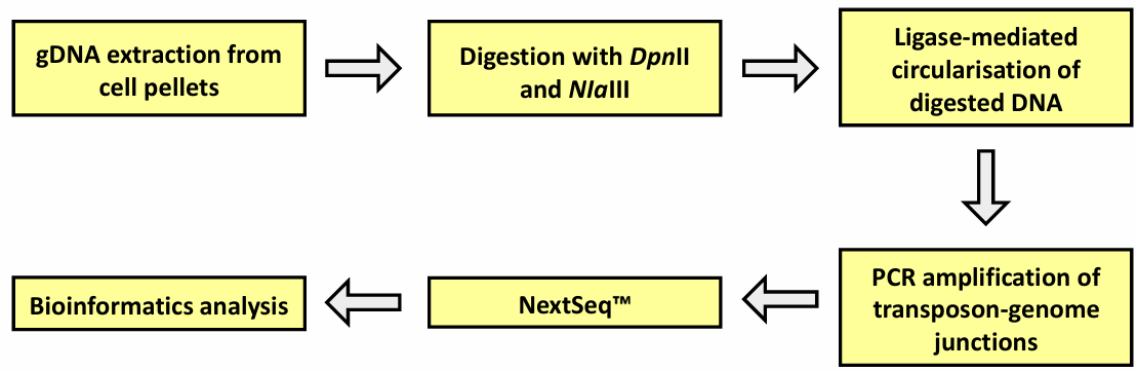

Figure 2.3 - Flow chart summarising the key stages for processing cell pellets for sequencing and analysis.

2.9. Gene Ontology Term Analysis

Gene Ontology term analyses were performed using GO Term Finder (v0.86) (https://www.yeastgenome.org/). For each transposon library, analyses were performed for the "Process" Ontology aspect for the 25-50 genes with the highest read counts in the compound treatment relative to the control treatment. The background set of genes

consisted of all the genes listed in the *pergene.txt* output file. Only terms with a Holm-Bonferroni-corrected *p*-value below 0.05 were considered significant.

2.10. Quantification of Hol1 uptake of ATI-2307, Pentamidine and Iminoctadine

2.10.1. Cell lysate generation

Wild-type and *hol1Δ* strains were grown to saturation in 100mL SC 2% ethanol 0.2% glucose. Cells were then reseeded at OD_{600} 0.5 in SC 2% ethanol (1L for obtaining cell lysate for subsequent yeast growth assays; 200mL for subsequent LC-MS experiments). Upon reaching OD_{600} ~1, the cells were treated with ATI-2307 (0.003µg/mL), Pentamidine (1µg/mL) or Iminoctadine (1µg/mL) for 2 hrs at 30°C, 200rpm. Cultures were harvested for cell pellets by centrifugation at 2,000x *g* for 10 minutes, room temperature, before cell pellets were washed three times in 40mL SC 2% ethanol. Experiments involving *hol1Δ* strains transformed with *CaHOL1* (pBK994) were performed with SC -URA medium (Amino Acid Recipe B) + carbon source. All media was prepared according to Amino Acid Recipe B (see section 2.5.3).

For subsequent yeast growth assays, 500mg cell pellets were resuspended in 500µL Cell Breaking Buffer (2% Triton X-100, 1% SDS, 100mM NaCl, 100mM Tris–HCl, pH 8.0, 1mM EDTA). Cell suspensions were distributed into 280µL aliquots, to which 400µL SC 2% ethanol and 200µL 0.5 mm Glass Mill Beads (BioSpec Products, 11079105) were added, before vortexing at 2850rpm for 10 minutes, 4°C, using a Disruptor Genie (Scientific

Industries, SI-DD38). Aliquots were centrifuged at 16,100x *g* for 5 minutes before the lysate was pooled for each condition and stored at -20°C.

For LC-MS, ~250mg cell pellets were resuspended in 500µL of 80% (v/v) acetonitrile (HPLC-grade, VWR) 20% (v/v) Milli-Q® and stored at -20°C for ~24 hours. Cell suspensions were then transferred to 2mL tubes (Precellys® MK28-R Hard Tissue Grinding Kit, Bertin Technologies), from which the steel beads were replaced with 200µL 0.5 mm Glass Mill Beads (BioSpec Products, 11079105). Bead-beating was performed using a Precellys® Evolution homogeniser (Bertin Technologies, P002511-PEVT0-A.0) at 6,000 rpm for 10 cycles of: 1 minute beating, 30 second pause, 1 minute beating. Cycles were spaced by 2-minute intervals, during which the samples were kept on ice. Samples centrifuged at 13,000x *g* for 5 minutes before the lysate was pooled for each condition and stored at -20°C until LC-MS analysis.

2.10.2. Cell lysate treatments

Wild-type (ByK831) and *hol1Δ* (ByK2032) strains were first grown to saturation in 10mL SC 2% ethanol 0.2% glucose medium. The strains were reseeded at OD_{600} 0.2 in seven 10mL SC 2% ethanol cultures and inoculated with a total of 64µL cell lysate derived from wild-type or *hol1Δ* cultures. Of the 64µL, the lysate volume derived from ATI-2307-treated cells was: 0µL, 2µL, 4µL, 8µL, 16µL, 32µL or 64µL. The remaining lysate volume was derived from untreated wild-type or *hol1Δ* cultures. OD_{600} measurements were recorded after 40 hours. All SC media was prepared according to amino acid Recipe B (see section 2.5.3).

2.10.3. Liquid Chromatography – Mass Spectrometry analysis

LC-MS analysis was performed using a Vanquish™ Flex™ Tandem UHPLC system (Thermo Fisher Scientific, UK) connected to a Q-Exactive™ Hybrid Quadrupole-Orbitrap™ Mass Spectrometer (Thermo Fisher Scientific, UK).

Cell lysate samples were injected at a volume of 5µL and separated using one of two, ACQUITY Premier BEH C18 Columns with VanGuard FIT, 1.7µm, 2.1 x 50mm (Waters, 186009455) at a column temperature of 40°C and a flow rate of 700µL min^{-1}. Samples were analysed using a six-minute gradient method using water with 0.2% (v/v) formic acid (Optima™ LC/MS-grade, Thermo Fisher Scientific, UK) and acetonitrile (HPLC-grade, VWR) as the A and B mobile phases, respectively. Starting with 95% mobile phase A, 5% mobile phase B, the LC gradient was as follows:

Time (min)	%A	%B
0.0	95.0	5.0
1.0	95.0	5.0
2.0	5.0	95.0
5.0	5.0	95.0
5.1	95.0	5.0
6.0	95.0	5.0

Flow from the column was sent to the mass spectrometer in a window set to between 0.5 and 4.5 minutes. Three consecutive injections of acetonitrile/water (80/20 (v/v)) were performed after each sample injection to prevent carry-over.

Mass spectrometry analysis was performed with electrospray ionisation in positive ionisation mode using the following source conditions: source gas flow = 55 arb. units;

auxiliary gas flow = 10 arb. units; auxiliary gas heater; temperature = 310°C; spray voltage = 3.2 kV; capillary temperature = 320°C; S-lens RF level = 55.0 arb. units. Analysis was performed using a full scan MS method with 35,000 mass resolution at 200 *m/z*, and a scan window from 100-900 *m/z*. Target peaks were as follows: ATI-2307 *m/z* = 219.6468 $[M+2H]^{2+}$, Pentamidine *m/z* = 171.1022 $[M+2H]^{2+}$, Iminoctadine *m/z* = 178.6784 $[M+2H]^{2+}$.

Quantifications of ATI-2307, Pentamidine and Iminoctadine were performed using matrix-matched calibration curves with R^2 values greater than 0.997. Calibration curves were prepared using serial dilutions of compound stock solutions in yeast lysate extracts. Calibration curves were calculated using Xcalibur™ (v4.6) (Thermo Fisher Scientific), and the *m/z* of the peaks for each calibration point were verified using Quan Browser software (v4.6) (Thermo Fisher Scientific).

2.11. Screening for separation-of-function mutations in *ScHOL1*

2.11.1. Construction of plasmid library bearing *ScHOL1* alleles

To identify separation-of-function mutations in *S. cerevisiae HOL1* (*ScHOL1*), a plasmid library bearing *ScHOL1* alleles was generated by gap-repair cloning. This library was constructed using a CEN/*URA3* plasmid bearing *S. cerevisiae HOL1* (pBK958), which was a kind gift from Dr Thomas Dever (NIH, Bethesda, Maryland, USA). The *ScHOL1* CDS and flanking UTR sequences were PCR-amplified from pBK958 using primers #17 and #18 and *Taq* DNA Polymerase (NEB #M0273), generating a product that contained 5' and 3'

sequences homologous to the pBK958 backbone. Meanwhile, the backbone for gap-repair cloning was generated by excising the *ScHOL1* CDS from pBK958 using *Bsu36*I and *Age*I. The resulting backbone and PCR product bearing *ScHOL1* alleles were co-transformed into the *spe1Δ hol1Δ* strain (ByK2037), where the plasmid was reconstituted. Transformants were selected on SC -URA 2% glucose for three days at 30°C.

2.11.2. Screening for ATI-2307 resistance

Ura+ transformants were replica plated onto SC -URA 2% ethanol medium containing 1µM spermidine (Sigma-Aldrich, S2626) and 0.01µg/mL ATI-2307 and incubated at 30°C for six days. ATI-2307-resistant isolated colonies were then streaked onto SC -URA 2% ethanol medium containing 1µM spermidine and 0.01µg/mL ATI-2307 for a second round of selection at 30°C for an additional six days.

2.11.3. Plasmid rescue

Isolated colonies of ATI-2307-resistant strains were grown to saturation in 5mL SC -URA 2% glucose supplemented with 1mM spermidine and 100nM pantothenic acid (Sigma-Aldrich, 21210). 1.5mL saturated culture was centrifuged at 13,000x *g* for 5 minutes and pellets were resuspended in 250µL Resuspension Solution (Thermo Fisher Scientific, 10242490). 300µL glass beads were added and samples were vortexed using a Disruptor Genie (Scientific Industries, SI-DD38) for 5 minutes at 2850 rpm, 4°C. Plasmids were then prepared using the GeneJET Plasmid Miniprep Kit (Thermo Fisher Scientific, 10242490) following the manufacturer's instructions. The *ScHOL1* alleles on the

rescued plasmids were sequenced by Sanger Sequencing (Source BioScience) using primers #19, #20 and #21.

2.11.4. Disc diffusion assays to validate separation-of-function mutations in *ScHOL1*

Disc diffusion assays were used to validate the separation-of-function mutations in *ScHOL1*. The *spe1Δ hol1Δ* mutant (ByK2037) was first transformed with each rescued plasmid bearing the *ScHOL1* alleles and selected on SC -URA 2% glucose. Transformants were then grown to saturation in 5mL SC -URA 2% ethanol 0.2% glucose medium supplemented with 1mM spermidine and 100nM pantothenic acid. 175 µL of each saturated culture was then plated on SC 2% ethanol supplemented with 1µM spermidine. Discs (ThermoFisher Scientific, 10066142) were wetted with 17µL of 0.4µg/mL ATI-2307, 80µg/mL Pentamidine or 30µg/mL Iminoctadine and placed on the agar surface. Plates were incubated at 30°C for five days and imaged using an iBright™ CL1500 System (ThermoFisher Scientific, A44114).

2.12. Pairwise sequence alignments of Hol1 protein sequences from *S. cerevisiae* and *Candida* species

Pairwise sequence alignments of Hol1 protein sequences from *S. cerevisiae* and *Candida* species were performed using EMBOSS Needle. Hol1 protein sequences for each species were obtained from UniProt with the following identifiers: *Candida albicans* Q5AP74; *Candida auris* A0A890CZK8; *Candida parapsilosis* G8BA41; *Candida tropicalis* C5MB76; *Saccharomyces cerevisiae* P53389.

2.13. Alcian blue staining assay

Yeast were grown to saturation in SC 2% glucose and then adjusted to OD_{600} 4. 10µg/mL alcian blue solution (Sigma-Aldrich, 1016470500) was added to 1mL of each adjusted culture and after brief vortexing, cells were left at room temperature for three minutes. Cells were then centrifuged at 13,000x *g* for three minutes before the pellets were imaged.

2.14. Live imaging of yeast

Yeast grown to saturation in 5mL SC 2% glucose medium were treated with 25µg/mL Chitosan Fluorescein (CD Bioparticles, CDHA061) for 2 hours. Chitosan Fluorescein stocks were prepared at 5mg/mL using 30% (v/v) acetic acid (Sigma-Aldrich, A6283). For the last 30 minutes of the Chitosan Fluorescein treatment, cells were optionally treated with 0.1µM MitoTracker™ Orange CMTMRos (Thermo Fisher Scientific, M7510). Cells were then washed twice with SC 2% glucose medium. Washed cells were mixed pairwise in the same 1.5mL microtube, ensuring that a similar number of cells were mixed from each strain. Mixed cells were transferred to a microscope slide and imaged with a 100× oil objective (NA = 1.4) on an IX81 Olympus® inverted spinning disk microscope fitted with an EM-CCD camera (Hamamatsu Photonics). Images were analysed in ImageJ (v1.53c) (www.imagej.nih.gov).

2.15. Experiments with *Botrytis cinerea*

2.15.1. BLASTp search to identify homologs of *Sc*Mnn4 in *Botrytis cinerea*

To identify homologs of *Sc*Mnn4 in *Botrytis cinerea*, the amino acid sequence of the *S. cerevisiae* Mnn4 protein (reference strain S288C) was obtained from the *Saccharomyces* Genome Database (SGD) (https://www.yeastgenome.org/) and used as a query in a BLASTp search against the *Botrytis cinerea* B05.10 protein database on EnsemblFungi (https://fungi.ensembl.org/index.html). The BLASTp search used a BLOSUM62 scoring matrix and E-value threshold of 1e-1. The two hits with the highest homology to *Sc*Mnn4 (*Bcin05g04770* and *Bcin15g02200*) were subsequently deleted (see section 2.15.3).

2.15.2. Strains of Botrytis cinerea

The strains of *B. cinerea* used in this thesis are listed in **Table 2.8**. All strains were derived from *B. cinerea* reference strain B05.10 (Büttner et al. 1994).

Table 2.8 – Strains of *Botrytis cinerea* used in this thesis

Name	Genotype	Reference
Wild-type (WT)	B05.10	Büttner et al. 1994
ΔBcin05g04770-1	B05.10, *ΔBcin05g04770::hph*; homokaryon	This study
ΔBcin05g04770-5	B05.10, *ΔBcin05g04770::hph*; homokaryon	This study
ΔBcin15g02200-2	B05.10, *ΔBcin15g02200::nat1*; homokaryon	This study
ΔBcin15g02200-6	B05.10, *ΔBcin15g02200::nat1*; homokaryon	This study
ΔBcin05g04770_ ΔBcin15g02200-4	B05.10, *ΔBcin05g04770::hph*, *ΔBcin15g02200::nat1*; homokaryon	This study
ΔBcin05g04770_ ΔBcin15g02200-8	B05.10, *ΔBcin05g04770::hph*, *ΔBcin15g02200::nat1*; homokaryon	This study

2.15.3. Construction of *Botrytis cinerea* deletion strains

B. cinerea strains deleted in putative *Sc*Mnn4 homologs were constructed by Dr Andreas Mosbach (Syngenta, Stein). *Bcin05g04770* and *Bcin15g02200* were replaced by hygromycin and nourseothricin resistance cassettes, respectively. Resistance cassettes were PCR-amplified using primers (**Table 2.9**) with 5' ends that are homologous to 500bp upstream of the start codon and 500bp downstream of the stop codon for each gene.

B. cinerea protoplasts were transformed using a PEG-based protocol described at Mosbach *et al*., (2017). The *ΔBcin05g04770::hph ΔBcin15g02200::nat1* double-mutant strains were generated using a co-transformation approach. Putative transformants were subsequently validated by PCR amplification of genomic regions encompassing homologous recombination sites, using primers listed in **Table 2.9**. Transformed strains were selected on Difco™ Malt Extract Agar (Becton, Dickinson and Company, 211220) containing either hygromycin B (Thermo Fisher Scientific, Gibco™ 10687010) and/or nourseothricin (Jena Bioscience, AB-102XL) and incubated at 20°C, 16 hr, white light, 60% relative humidity, for up to 14 days.

Table 2.9 – Primers for constructing and genotyping *B. cinerea* deletion strains

Primer Name	Sequence (5' to 3')	Use
Bcin05g04770-for1	TTTCCTTTCATTCTCTCCAGGCG	Amplification of hygromycin resistance cassette for *Bcin05g04770* deletion
Bcin05g04770-rev1	TCTAGCAGCTGTGACATTGAACC	Amplification of hygromycin resistance cassette for *Bcin05g04770* deletion
Bcin05g04770-for2	GATGCCAGCTTCTCATGTCCCTC	Screening of putative transformants
Bcin05g04770-rev2	ATGGCCCAATCTAGTTCCAGTCC	Screening of putative transformants
Bcin05g04770-for3	TGGATCATCACTTTGCCTGGAC	Screening for WT CDS (WT contamination)

Bcin05g04770-rev3	GTTTGCTTACGGGTGGTGTGTC	Screening for WT CDS (WT contamination)
Bcin15g02200-for1	CCCTTTACGTTGGCTTCTATCGC	Amplification of nourseothricin resistance cassette for *Bcin15g02200* deletion
Bcin15g02200-rev1	CCGTTTCCATTCACCTAGCCATTC	Amplification of nourseothricin resistance cassette for *Bcin15g02200* deletion
Bcin15g02200-for2	CCTGCATCCCAACCCATCTAATC	Screening of putative transformants
Bcin15g02200-rev2	ATACAAGCCCACGAGACACAGTC	Screening of putative transformants
Bcin15g02200-for3	CGCCACCATATCCATTCTCCTTG	Screening for WT CDS (WT contamination)
Bcin15g02200-rev3	AAAGCTCTCGGACTATACTCATCC	Screening for WT CDS (WT contamination)

2.15.4. Growth media and culture conditions

Media recipes were as follows:

GG: 1.5g/L KH_2PO_4, 0.75g/L $MgSO_4 \cdot 7H_2O$, 4g/L gelatine from porcine skin (Sigma-Aldrich, 48722), 4g/L glucose.

GEA: 160g/L frozen peas mixed homogeneously in a blender, 5g/L sucrose, 20g/L agar. pH 6.0 with 1M HCl.

For non-selective propagation of *B. cinerea* strains, GEA plates were inoculated with spores from stock suspensions and incubated at 20°C, 16 hr white light, 60% relative humidity, for up to 14 days. Stocks were prepared in a mixture of skim milk (8.5% (w/v), Magermilchpulver medium heat, Emmi AG) and glycerol (10% (v/v), Sigma-Aldrich, G2025) and stored at -80 °C.

2.15.5. Conidia harvesting

Conidia were harvested from 7-10 days old sporulating mycelium grown on GEA plates. Conidia were dislodged from mycelium using a plastic T-spatula, gentle pressure and

10-15mL sterile water. The conidia were filtered through glass wool, and centrifuged at 3,000x *g* for 3 minutes. The pellet was then washed with sterile water five times, before being re-suspended in 10mL sterile water. Concentrations of harvested conidia were determined photometrically using a Moxi™ Z automated cell counter (Orflo, MXZ001). Conidia were first diluted 100-fold in 1x PBS before 75µL was added to a Moxi™ Type S Cassette (Orflo, MXC002-3). Cassettes were then loaded, and conidia concentrations were measured using the Coulter Principle (spores passing a detector result in a voltage change directly proportional to particle volume). Conidia suspensions were stored in sterile water at 4°C for up to 14 days.

2.15.6. Chitosan sensitivity assays of *B. cinerea* strains

Harvested conidia were adjusted to a starting density of 10^5/mL in GG medium and 198µL of conidia suspension was distributed into each well of a 96-well microplate (Corning®, 3370). Wells were pre-loaded with 2µL 100x concentrated Chitosan or acetic acid (pH adjusted to 5.5) solutions, resulting in final solvent concentrations of 1% (v/v). Chitosan and acetic acid dilution series were prepared in ten 1:2x dilution steps in sterile water. Microplates were then incubated at 20°C for 3 days in the dark, 60% relative humidity. OD_{600} measurements were recorded using an EnVision™ XCite Multimode Plate Reader (Revvity, 2105-0020). OD_{600} readings at 0hrs were subtracted from the readings at 72hrs and the mean OD_{600} reading was calculated for 4 technical replicates at each concentration. Dose response curves were fitted using the mean OD_{600} readings in GraphPad Prism 10.0, and IC_{50} values were calculated using the function: Dose-response-inhibition, log(inhibitor) vs. response – Variable slope (four parameters).

2.15.7. Live imaging and quantification of germ tube lengths of *Botrytis cinerea* germlings

Harvested conidia were adjusted to a starting density of 10^4/mL in GG medium and 198µL of conidia suspension was distributed into the wells of a CellCarrier 96 Ultra microplate (Revvity, 50-209-9831). Wells were pre-loaded with 2µL 100x concentrated Chitosan or acetic acid (pH adjusted to 5.5 with NaOH) solutions in sterile water, resulting in final solvent concentrations of 1% (v/v). The final concentrations of Chitosan and acetic acid were 20µg/mL and 0.004% (v/v), respectively. Microplates were then incubated at 20°C for 10 hours in the dark, 60% relative humidity. Ten minutes before imaging, germlings were treated with 3µL 100µM FM4-64 (Invitrogen, T13320) (final concentration 1.5µM) at room temperature, and the suspension was gently stirred using a pipette tip. Germlings were imaged using an Opera Phenix™ Plus High-Content Screening System (Revvity, HH14001000) using a 10x air objective (NA = 0.3) in confocal imaging mode. Brightfield images were captured with an exposure time of 100ms at 100% laser power. Fluorescent images were captured with an exposure time of 800ms at 100% laser power, excitation wavelength of 488nm, and emission filter set to 650-760nm. Nine fields of view were captured per well for Brightfield and Fluorescent images.

Fluorescence thresholding was performed on images of FM4-64-stained *B. cinerea* germlings using a Python script written by Dr Pouria Sadeghi-Tehran (Syngenta, Stein). Upon thresholding, germling lengths were determined using an ImageJ macro and the "Skeletonize (2D/3D)" plugin.

2.16. Viability tests of *SLN1*+ strains expressing kinase-defective *BdDRK1* alleles

The *SLN1*+ strain ByK831 was individually transformed with plasmids harbouring WT (pBK905) or kinase-defective (pBK900-902) alleles of *BdDRK1* (see section 2.3.3) and selected on SC -URA. Ura+ transformants were then streaked onto SC -URA 2% glucose, SC -URA 2% galactose or SC -URA 2% galactose containing 25µg/mL Fludioxonil. Plates were incubated at 30°C for three days before imaged using an iBright™ CL1500 Imaging System (Thermo Fisher Scientific, A44114).

2.17. Statistical analysis

Growth curves show the mean OD_{600} of three independent biological replicates for each genotype ± either standard deviation (SD) or standard error of the mean (SEM). SD was computed when one technical replicate was examined per biological replicate. SEM was computed when three technical replicates were examined per biological replicate (thereby showing the variability of the sample mean from the population mean).

Statistical significance was determined using GraphPad Prism software (v10.2.3) or R (v4.2.0). Normality was assessed using the Shapiro-Wilk test. For normal data, statistical significance was determined using a Student's t-test or ANOVA with a Tukey or Dunnett's post-hoc test, respectively. For non-parametric data, the Mann Whitney-U test or Kruskall-Wallis test were used.

2.18. AlphaFold

AlphaFold2 (Jumper et al., 2021) and AlphaFold3 (Abramson et al., 2024) models were analysed using ChimeraX (v1.7.1) (Pettersen et al., 2021). AlphaFold models of homologous proteins were superimposed using the matchmaker command in ChimeraX (v1.7.1).

Chapter 3 – Overview of the SATAY screens performed in this thesis

3.1. Set-up of SATAY screens

Prior to utilising SATAY for chemogenomic screening, it was necessary to 1) select antifungal compounds of interest, 2) identify *S. cerevisiae* strains sensitive to these compounds, and 3) determine the optimal concentrations of these compounds for SATAY.

1. Selection of antifungal compounds of interest

This selection included clinical antifungals (Amphotericin B, Caspofungin, Tavaborole, Terbinafine), widely used agrochemical fungicides (Chlorothalonil, Chitosan, Dodine, Fenpropimorph, Fludioxonil, Iprodione, Prochloraz), experimental agents for biochemical research (Cerulenin, Myriocin) and a novel antifungal currently in clinical trials (ATI-2307). Several of these compounds have well-characterised modes of action, whereas others have unclear modes of action that require resolving.

2. Identification of *S. cerevisiae* strains sensitive to the selection of antifungals

The *S. cerevisiae* strains that were screened for compound sensitivities included one conventional laboratory strain (BY4741), and four PDR-attenuated strains, namely 12geneΔ0HSR (Chinen et al., 2011), AD12345678 (AD1-8) (Decottignies et al., 1998), BY4743Δ8a (Hoepfner et al., 2014) and ABC16 Monster (Ottilie et al., 2022). These PDR-attenuated strains contain deletions in multiple drug efflux pumps of the “Pleiotropic

Drug Resistance" (PDR) network. Together, these pumps export a broad-spectrum of compounds from the cytoplasm (Kolaczkowski et al., 1998; Rogers et al., 2001), which is often problematic for chemogenomic screening approaches in *S. cerevisiae* (Coorey et al., 2015). Since SATAY is not tied to a specific genetic background (Michel et al., 2017; Chen et al., 2022), these PDR-attenuated strains presented an opportunity for screening PDR substrates at lower concentrations, improving the physiological and agricultural relevance of the screens, and potentially allowing the identification of resistance mechanisms other than those associated with the PDR network.

3. Optimal concentration of each antifungal compound for SATAY

Previous proof-of-principle SATAY screens have demonstrated that the 30% inhibition concentration (IC_{30}) is an appropriate concentration for challenging transposon libraries with antifungal compounds (Michel et al., 2019). Indeed, this concentration permits, in the same screen, the identification of transposon insertions conferring antifungal resistance or sensitivity. For this reason, the IC_{30} values of the selected compounds were determined for each the five aforementioned *S. cerevisiae* strains. This was achieved using growth assays in liquid media, and the results are presented in **Table 3.1**.

	IC_{30} values (µg/mL)					
	BY4741 (ByK352)	**12geneΔ0HSR (ByK1151)**	**AD1-8 (ByK1174)**	**BY4743Δ8a (ByK1230)**	**ABC16 Monster (ByK1266)**	***sln1Δ BdDRK1* (ByK1925)**
Amphotericin B (see Chapter 4)	0.75	0.5	5	0.75	0.75	n.t.
ATI-2307 (see Chapter 5)	0.000175	n.t.	n.t.	n.t.	n.t.	n.t.
Caspofungin (see Chapter 4)	0.03	0.02	0.05	0.03	0.03	n.t.
Cerulenin	0.7	0.25	0.35	0.35	0.6	n.t.
Chitosan (see Chapter 7)	>500	>500	2	>500	>500	n.t.
Chlorothalonil	0.4	1	0.2	0.2	0.4	n.t.
Dodine	5	5	3.5	2.5	2.5	n.t.
Fenpropimorph	2	1	1.5	1.5	1.5	n.t.
Fludioxonil (see Chapter 6)	>10	n.t.	n.t.	n.t.	n.t.	0.1
Iprodione (see Chapter 6)	>10	n.t.	n.t.	n.t.	n.t.	3
Myriocin (see Chapter 4)	0.2	0.1	0.3	0.1	0.1	n.t.
Prochloraz (see Chapter 4)	10	0.4	0.4	0.4	0.4	n.t.
Tavaborole (see Chapter 4)	0.03	0.025	0.015	0.03	0.03	n.t.
Terbinafine	7.5	7.5	7.5	7.5	7.5	n.t.

Table 3.1 – Susceptibilities (IC_{30} values) of five strains of *S. cerevisiae* to fourteen antifungal compounds. IC_{30}'s for all compounds (except ATI-2307) were determined for SC 2% glucose cultures after 24 hours of growth using a Bioscreen C™ instrument (Chapter 2, Section 2.7.1). For ATI-2307, the IC_{30} was determined for SC 2% ethanol cultures after 48 hours of growth (Chapter 2, Section 2.7.2). IC_{30} values are the average of three technical replicates in at least two independent experiments. ByK archival names are shown for each strain. n.t. stands for not tested.

Multiple patterns emerged from the IC_{30} values shown in **Table 3.1**.

First, a couple of compounds exhibited striking differences in activity towards the strains. Most notably, Chitosan sensitivity was only observed for AD1-8. The reason for this difference is identified in Chapter 7, together with a newly discovered mode of action for Chitosan against fungi. In addition, the IC_{30} of Prochloraz was 25-fold lower for all four PDR-attenuated strains than for the BY4741 strain. Consistently, Prochloraz is a known substrate of the PDR network (Kolaczkowski et al., 1998). Chapter 4 demonstrates how SATAY can reveal different resistance mechanisms when performed a PDR-proficient versus PDR-attenuated strain.

Second, the IC_{30}'s for Amphotericin B and Caspofungin were not significantly decreased in the PDR-attenuated strains, in line with the fact that polyenes and echinocandins are not substrates of the PDR network (Niimi et al., 2004; Niimi et al., 2006). Chlorothalonil, Dodine, Myriocin and Tavaborole also exhibited similar activity towards the BY4741 and the PDR-attenuated strains. This suggests that they are not substrates of the efflux pumps deleted in the PDR-attenuated strains. Since Chlorothalonil was not more toxic towards the PDR-attenuated strains and has been previously analysed with SATAY in a PDR-proficient background (Michel et al., 2019), it was not examined further in this thesis.

Third, unexpectedly, the activity of several known substrates of the PDR network was not dramatically different between the BY4741 and PDR-attenuated strains. This was particularly notable for Fenpropimorph (Kolaczkowski et al., 1998) and Terbinafine (Rogers et al., 2001). The PDR-attenuated strains were also only marginally more

sensitive to Cerulenin. Perhaps the transporters that detoxify these compounds were only weakly expressed in the BY4741 strain (Michel et al., 2019). Alternatively, the PDR-attenuated strains might not have been deficient in all the transporters capable of exporting these compounds.

Fourth, since very low concentrations of ATI-2307 were potent against the BY4741 strain, it was not necessary to use the PDR-attenuated strains.

Finally, Fludioxonil sensitivity, and to a lesser extent, Iprodione sensitivity, were only observed in a strain engineered to express a group III hybrid histidine kinase (HHK) called *DRK1* from the fungal pathogen *Blastomyces dermatitidis*. This endeavour is described in Chapter 6.

Overall, the PDR-deficient strains only exhibited increased sensitivity towards a limited number of compounds. This unexpected finding might, however, reflect a bias in the compound selection.

3.2. Generation and treatment of transposon libraries for SATAY-based chemogenomic screening

Having identified yeast strains that were sensitive to the selection of antifungal compounds, the next step for SATAY-based chemogenomic screening was the generation of transposon libraries in these strains. The transposon libraries generated in this thesis are summarised in **Table 3.2**. The protocols followed to generate these libraries are documented in Chapter 2, Section 2.2.8.

For all the SATAY screens in this thesis, transposon libraries were challenged with antifungal compounds at the IC_{30} for two successive growth rounds from OD_{600} 0.2 to saturation i.e. approximately ten cell cycles (**Figure 3.1**). The number of insertions and reads mapped in the transposon libraries after each treatment are summarised in **Table 3.2**. The variation in the number of insertions mapped between libraries relates to the differing efficiencies of different library generation protocols, and to the fact that some antifungal treatments were more stringent than others.

Genes promoting antifungal resistance or susceptibility were identified by comparing the total number of reads mapping to each gene in the compound treatment versus that in the corresponding untreated condition. Since the annotation of promoters in *S. cerevisiae* is incomplete, three separate analyses were performed to identify promoters containing enriched transposon insertions. Specifically, analyses were performed on transposons mapping within 1) 200-bp upstream of the ATG start codon 2) 500-bp upstream of the ATG start codon and 3) 200-bp upstream of the transcription start site, where known (Xu et al., 2009).

Each library treatment and its analysis are described in their respective chapters, except for Dodine, Fenpropimorph, and Terbinafine, which did not produce significant follow-up leads, and have thus been excluded from further discussion.

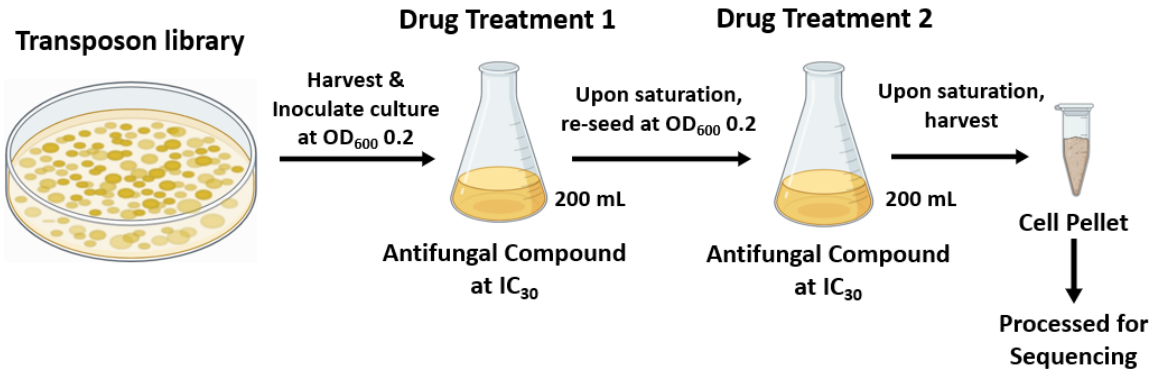

Figure 3.1 – Schematic depiction of the protocol for treating transposon libraries with antifungal compounds. Transposon libraries were harvested and inoculated into 200mL cultures containing antifungal compounds at an inhibitory concentration of 30% (IC_{30}). The cultures were then grown for two successive growth rounds from OD_{600} 0.2 to saturation. Transposon libraries were then harvested for cell pellets, which were subsequently processed for sequencing.

Treatment	Transposon library strain background	Total number of mutants in library (approx.)	Number of transposons mapped	Number of reads mapped	Mean reads per transposon	Median reads per transposon
DMSO	ByK352	1,400,000	212,231	16,321,286	76.9	7
Amphotericin B	ByK352	1,400,000	30,485	11,851,497	388.76	2
Caspofungin	ByK352	1,400,000	49,785	21,175,255	425.33	4
Myriocin	ByK352	1,400,000	125,920	8,131,846	64.58	6
Prochloraz	ByK352	1,400,000	208,732	15,671,993	75.08	8
Tavaborole	ByK352	1,400,000	123,450	7,531,475	61.01	7
DMSO	ByK1261 (12geneΔ0HSR)	1,800,000	259,501	22,355,868	86.15	11
Prochloraz	ByK1261 (12geneΔ0HSR)	1,800,000	51,915	3,672,773	70.75	3
No compound control for ATI-2307	ByK831	12,000,000	378,315	17,553,017	46.4	7
ATI-2307	ByK831	12,000,000	406,629	17,567,889	43.2	6
Acetic Acid	ByK1262 (AD1-8)	1,800,000	228,584	30,152,269	131.91	12
Chitosan	ByK1262 (AD1-8)	1,800,000	169,120	32,276,932	190.85	10
DMSO	ByK1925	63,000,000	511,498	20,494,530	40.07	6
Fludioxonil	ByK1925	63,000,000	206,595	14,680,471	71.06	5
Iprodione	ByK1925	63,000,000	397,202	18,592,934	46.81	4

Table 3.2 – Characteristics of the transposon libraries analysed in this thesis.

Chapter 4 – Proof-of-principle SATAY screens demonstrate the utility of SATAY for chemogenomic screening

4.1. Introduction

In this chapter, proof-of-principle SATAY screens were performed with five antifungal compounds that have well-characterised modes of action: Amphotericin B, Caspofungin, Myriocin, Tavaborole and Prochloraz.

The polyene Amphotericin B is reserved for treating life-threatening invasive fungal infections (Perlin et al., 2017) and kills yeast by extracting ergosterol from the plasma membrane (Anderson et al., 2014). Caspofungin is a first-line therapy for invasive fungal infections such as candidiasis (Pappas et al., 2009) that non-competitively inhibits β-1,3-glucan synthase (Douglas et al., 1997; Johnson et al., 2011), impairing cell wall integrity. Myriocin inhibits serine palmitoyltransferase, which catalyses the first step of sphingolipid biosynthesis (Miyake et al., 1995). Since Myriocin is a potent immunosuppressant, it is primarily used as a biochemical research tool (Miyake et al., 1995). Tavaborole belongs to the oxaboroles class of antifungals and is a therapy for the fungal nail plate infection Onychomycosis (Jinna & Finch, 2015). By inhibiting leucyl-tRNA synthetase, Tavaborole prevents the synthesis of leucine-charged tRNAs (Rock et al., 2007) and blocks protein synthesis. Lastly, Prochloraz is widely used to protect wheat and barley from fungal phytopathogens. Like all azoles, Prochloraz inhibits sterol 14α-demethylase of the ergosterol biosynthesis pathway (Becher & Wirsel, 2012).

All five compounds were examined using the same transposon library, generated in a BY4741 strain of *S. cerevisiae* (ByK352). Because Prochloraz exhibits limited activity against ByK352 (**Chapter 3, Table 3.1**), this compound was additionally analysed using a transposon library generated in the Prochloraz sensitive strain 12geneΔ0HSR (**Chapter 3, Table 3.1**). Overall, these proof-of-principle SATAY screens recapitulate known or expected chemical-genetic interactions, further demonstrating that SATAY is a powerful approach for chemogenomic screening.

4.2. Results

4.2.1. Amphotericin B sensitivity was affected by ergosterol homeostasis, TORC1 and the plasma membrane protein Pmp3

Upon treating a transposon library with Amphotericin B, transposon insertions were positively selected in the ergosterol biosynthesis gene *ERG5* (Skaggs et al., 1996) and ergosterol transport gene *OSH2* (Beh et al., 2001; Beh & Rine, 2004) (**Figure 4.1**). Consistently, *erg5Δ* and *osh2Δ* mutants are resistant to Amphotericin B (Bojsen et al., 2016; Daum et al., 1999; Martel et al., 2010). Given that *erg5Δ* and *osh2Δ* mutants have altered membrane ergosterol compositions (Skaggs et al., 1996; Martel et al., 2010; Daum et al., 1999), these mutations likely interfered with Amphotericin B's ability to extract ergosterol from the plasma membrane.

Furthermore, Amphotericin B positively selected transposons in subunits of the Target Of Rapamycin Complex 1 (TORC1) (*TOR1* and *TCO89*) (Loewith & Hall, 2011) and in subunits of the TORC1-activating EGO complex (*GTR1*, *MEH1* and *SLM4*) (Binda et al., 2009) (**Figure 4.1**). Consistently, a previous study has showed that TORC1 inactivation increases Amphotericin B tolerance in *S. cerevisiae* (Bojsen et al., 2016).

There was also a striking enrichment of reads in the promoter of *PMP3* (**Figure 4.2**). *PMP3* overexpression is known to confer Amphotericin B resistance (Huang et al., 2013; Bari et al., 2015; Balkan et al., 2019), yet the precise mechanism underpinning this effect remains to be elucidated. Given that *PMP3* encodes a small protein embedded in the

plasma membrane (Navarre & Goffeau, 2000), it is possible that increased Pmp3 levels interfered with Amphotericin B-ergosterol interactions.

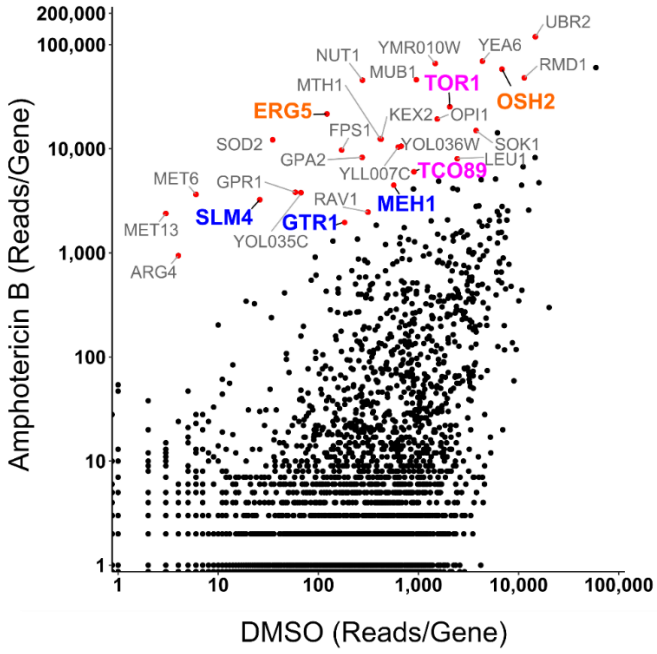

Figure 4.1 - Amphotericin B positively selected transposons in ergosterol homeostasis genes, and genes encoding subunits of TORC1 and EGO. Scatter plot comparing the number of sequencing reads mapping to each of the 6603 yeast coding DNA sequences (CDSs) in a ByK352 transposon library treated with DMSO versus Amphotericin B (0.75 µg/mL for initial 24 hours, 0.375 µg/mL for remaining 96 hrs of treatment) in SC -ADE 2% glucose medium. Each dot represents a single gene. Gene names are colour-coded by biological process: orange - ergosterol homeostasis, pink - TORC1 complex subunits, blue – EGO complex subunits. Additional genes with significantly enriched insertions in the Amphotericin B-treated library are labelled in grey. Genes with a comparable number of reads in each treatment, and thus lying close to the y = x diagonal, are not labelled.

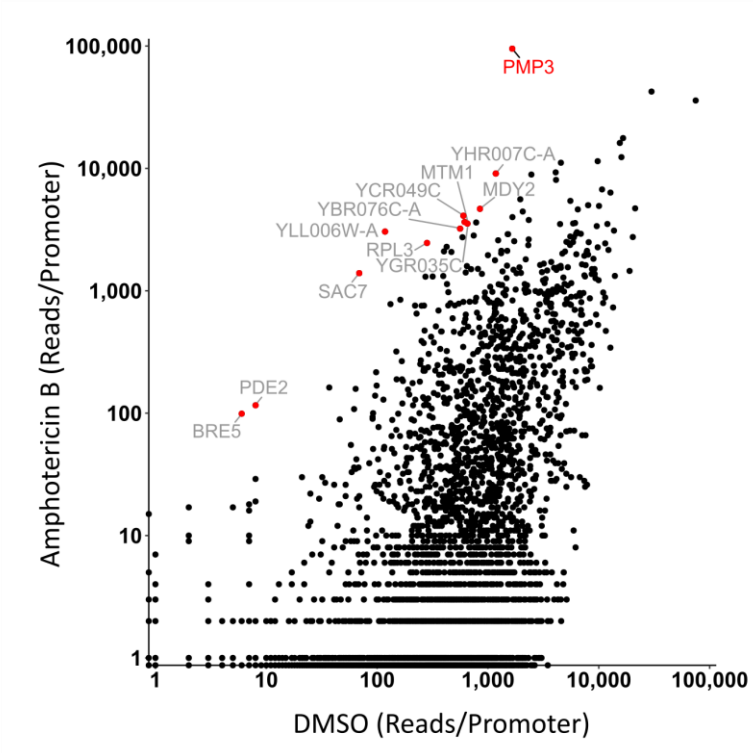

Figure 4.2 – Amphotericin B positively selected transposons in the promoter of *PMP3*. Scatter plot comparing the number of sequencing reads mapping to every promoter in a ByK352 transposon library treated with DMSO versus Amphotericin B (0.75 µg/mL for initial 24 hours, 0.375 µg/mL for remaining 96 hrs of treatment) in SC -ADE 2% glucose medium. Promoters were defined as the 500bp upstream of the translation start sites. *PMP3* is coloured red. Additional genes with significantly enriched promoter insertions in the Amphotericin B-treated library are labelled in grey. Genes with a comparable number of reads in their promoters in each treatment, and thus lying close to the y = x diagonal, are not labelled.

4.2.2. Caspofungin resistance was conferred by transposons disrupting genes involved with sphingolipid biosynthesis and membrane homeostasis

Following Caspofungin treatment, there was a significant enrichment of reads in sphingolipid biosynthesis genes, namely *ELO2*, *ELO3*, *SUR1*, *CSG2*, *CKA2*, *IPT1* and *FLC2* (**Figure 4.3**) (Dickson et al., 2006). These genes have been previously implicated in Caspofungin sensitivity (García et al., 2015; Healey et al., 2012) and their loss causes an accumulation of long-chain base (LCB) intermediates of sphingolipid biosynthesis within the plasma membrane (Oh et al., 1997; Abe et al., 2001; Kobayashi & Nagiec, 2003). LCB accumulation is thought to weaken the interaction between Caspofungin and its target β-1,3-glucan synthase in the plasma membrane (Healey et al., 2012), and *in vitro* evidence supporting this model has recently been obtained in *Aspergillus fumigatus* (Satish et al., 2019). These findings suggest that an inhibitor of LCB biosynthesis, such as Myriocin could enhance Caspofungin therapy.

Additionally, Caspofungin positively selected transposons in *ERG3*, *LEM3*, *CRZ1*, and *GSC2* (**Figure 4.3**), aligning with reports that strains deleted in these genes are resistant to Caspofungin (García et al., 2015; Lesage et al., 2004; Markovich et al., 2004). Erg3 is involved in ergosterol biosynthesis (Arthington et al., 1991) and Lem3 is required for phospholipid translocation across the plasma membrane (Kato et al., 2002). As such, mutations in these genes may alter the lipid microenvironment of β-1,3-glucan synthase, reducing accessibility to Caspofungin. Meanwhile, *GSC2* encodes one of two catalytic subunits of β-1,3-glucan synthase (Douglas et al., 1994; Mazur et al., 1995), and *crz1Δ* mutants are defective in *GSC2* expression (Stathopoulos & Cyert, 1997). Interestingly,

Candida albicans mutants lacking *FKS2*, the homolog of *GSC2*, have higher levels of cell wall β-1,3-glucan (Suwunnakorn et al., 2018). It is therefore possible that transposons disrupting *GSC2* triggered compensatory pathways that increased β-1,3-glucan levels, thereby reducing Caspofungin toxicity.

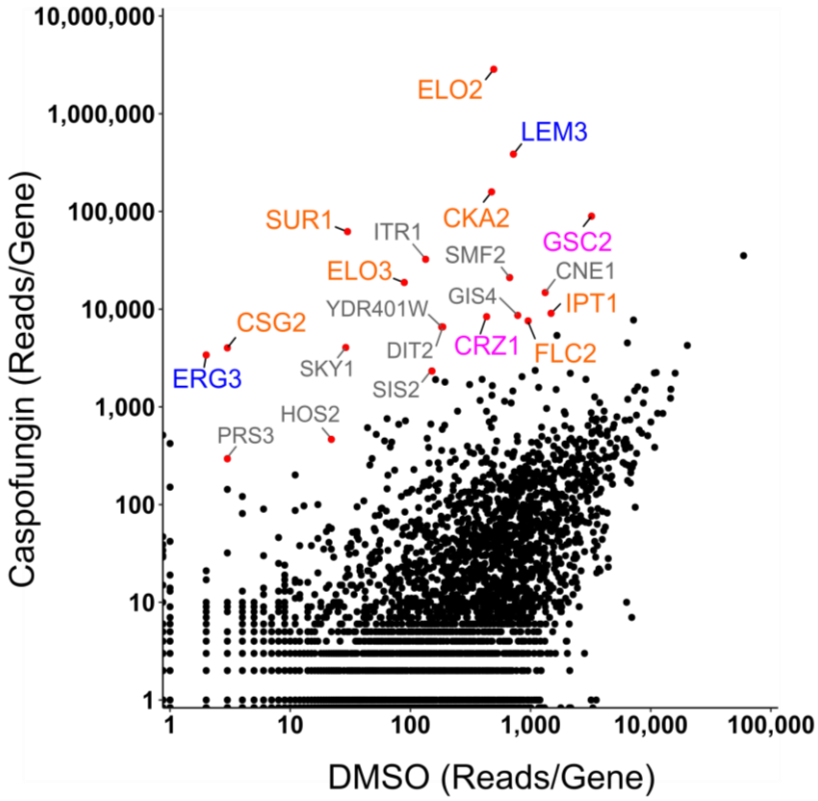

Figure 4.3 - Caspofungin positively selected transposons in genes involved with sphingolipid biosynthesis, membrane homeostasis and β-1,3-glucan biosynthesis. Scatter plot comparing the number of reads mapping to each of the 6603 yeast CDSs in a ByK352 transposon library treated with DMSO versus Caspofungin (0.015 µg/mL) in SC -ADE 2% glucose medium. Gene names are colour-coded by biological process: orange – sphingolipid biosynthesis, blue – membrane lipid homeostasis, pink – β-1,3-glucan biosynthesis. Additional genes with significantly enriched insertions in the Caspofungin-treated library are labelled in grey. Genes with a comparable number of reads in each treatment, and thus lying close to the y = x diagonal, are not labelled.

4.2.3. Myriocin resistance was conferred by transposons disrupting cellular trafficking and phospholipid translocation, and *SLI1* overexpression

Myriocin caused a significant enrichment of reads in genes encoding subunits of the Golgi-Associated Retrograde Protein (GARP) complex (*VPS51*, *VPS53*, *VPS54*) (Fröhlich et al., 2015) and retromer (*PEP8*, *VPS29*) (Seaman et al., 1997, 1998) (**Figure 4.4**). GARP and retromer function in endosome-to-Golgi retrograde trafficking, which regulates sphingolipid homeostasis (Fröhlich et al., 2015). Meanwhile, transposons were also selected in genes involved with vesicular transport (*ARF1*, *ERV14*, *TLG2*) (Holthuis et al., 1998), phospholipid translocation across the plasma membrane (*DNF1*, *DNF2*, *LEM3*, *FPK1*) (Hua et al., 2002; Kato et al., 2002) and chromatin remodelling (*CHD1*) (Woodage et al., 1997) (**Figure 4.4**). Consistently, yeast strains harbouring deletions in each of these genes were previously shown to exhibit reduced Myriocin susceptibility (Fröhlich et al., 2015). These mutations likely restored membrane homeostasis in the absence of sphingolipids through compensatory mechanisms. Furthermore, Myriocin positively selected transposons in the promoter of *SLI1* (**Figure 4.5**). *SLI1* overexpression is known to suppress Myriocin toxicity (Momoi et al., 2004). Indeed, *SLI1* encodes an N-acetyltransferase that inactivates Myriocin by converting it into N-acetyl-Myriocin (Momoi et al., 2004). This example demonstrates that SATAY can also identify antifungal detoxification pathways.

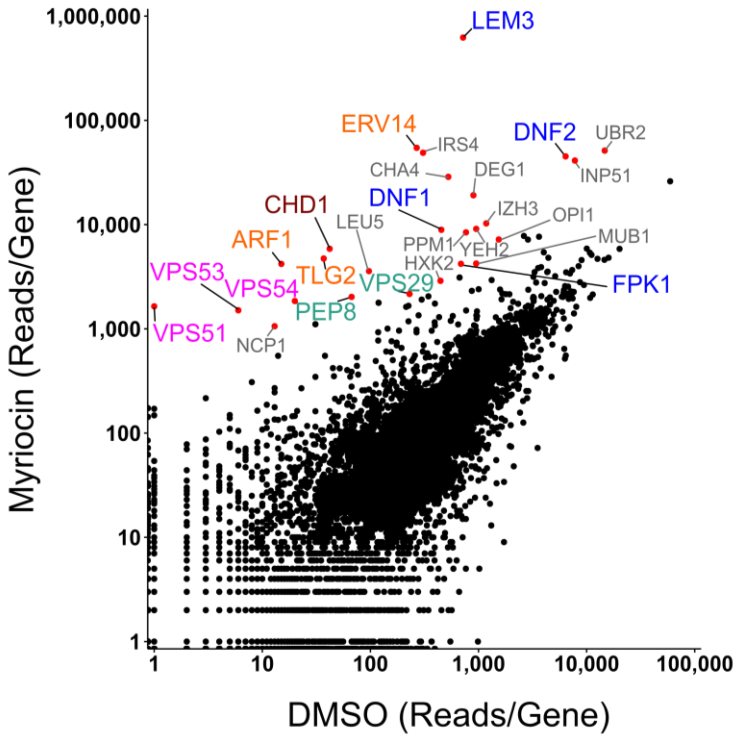

Figure 4.4 - Myriocin positively selected transposons in genes involved with membrane homeostasis. Scatter plot comparing the number of sequencing reads mapping to each of the 6603 yeast CDSs in a ByK352 transposon library treated with DMSO versus Myriocin (0.2 µg/mL) in SC -ADE 2% glucose medium. Gene names are colour-coded by biological process: orange – vesicular-mediated transport, pink – GARP complex subunits, blue – phospholipid translocation, teal – retromer subunits, maroon – chromatin remodelling. Additional genes with significantly enriched insertions in the Myriocin-treated library are labelled in grey. Genes with a comparable number of reads in each treatment, and thus lying close to the y = x diagonal, are not labelled.

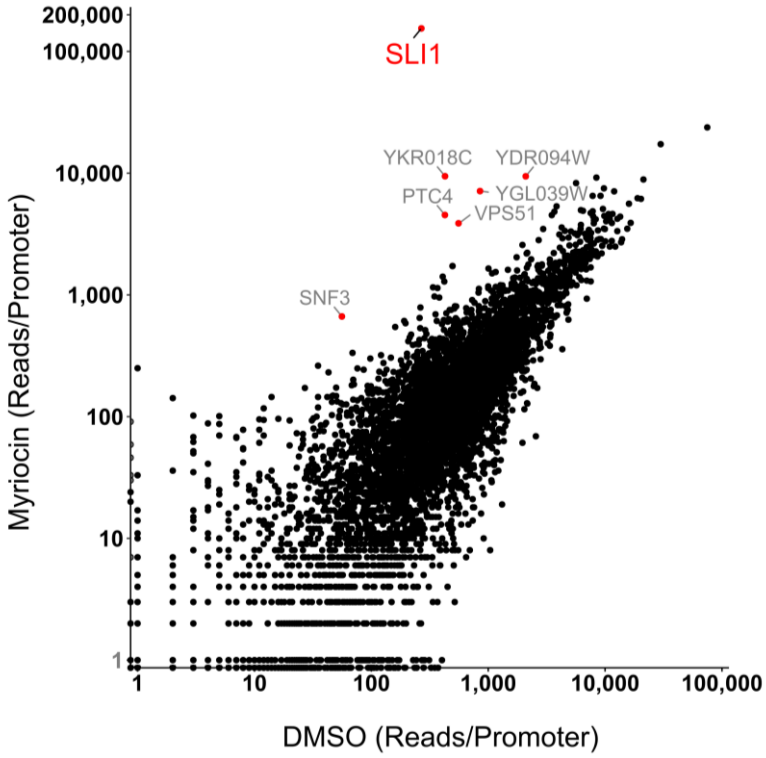

Figure 4.5 – Myriocin positively selected transposons in the promoter of *SLI1*. Scatter plot comparing the number of sequencing reads mapping to promoters in a ByK352 transposon library treated with DMSO versus Myriocin (0.2 µg/mL) in SC -ADE 2% glucose medium. Promoters were defined as the 500 bp upstream of the translation start sites. *SLI1* is coloured red. Additional genes with significantly enriched promoter insertions in the Myriocin-treated library are labelled in grey. Genes with a comparable number of reads in their promoters in each treatment, and thus lying close to the y = x diagonal, are not labelled.

4.2.4. Tavaborole susceptibility was reduced by transposons inactivating genes associated with tRNA wobble uridine modifications

Tavaborole positively selected transposons in genes associated with the Gene Ontology (GO) terms “RNA metabolic process”, “tRNA wobble uridine modification” and “tRNA modification” (**Figure 4.6, Table 4.1**). This includes genes encoding core and accessory subunits of the Elongator Complex, namely *IKI3*, *ELP2*, *ELP4*, *IKI1*, *ELP6* and *KTI12* (Karlsborn et al., 2014; Krutyholowa et al., 2019). Elongator promotes post-transcriptional modifications on uridines in the wobble position (U_{34}) of tRNAs (Johansson et al., 2018), and all Elongator subunits are required for this activity (Huang et al., 2005). Similarly, the SATAY screen identified *URM1* (**Figure 4.6**), which serves as the sulphur donor for the thiolation of U_{34} on tRNAs (Leidel et al., 2009), and *DEG1*, which introduces pseudouridines at position 38 and 39 in tRNAs (Lecointe et al., 1998). These post-transcriptional tRNA modifications promote accurate and efficient decoding during translation (El-Yacoubi et al., 2012). Given that Tavaborole inhibits leucyl-tRNA synthetase (Rock et al., 2007), the enrichment of genes involved with tRNA modifications highlights the specificity of SATAY for chemogenomic screening, and strongly suggests that tRNA modifications promote Tavaborole susceptibility. However, there are no straightforward explanations for these observations. Indeed, the inactivation of Elongator causes pleiotropic phenotypes, including defects in mitochondrial function and protein homeostasis (Xu et al., 2020). Tavaborole sensitivity assays with *elp2Δ*, *iki3Δ*, and *kti12Δ* mutants of *S. cerevisiae* revealed that these mutations only caused a modest reduction in Tavaborole sensitivity (data not shown). For this reason, the hits in this screen were not pursued further in this thesis.

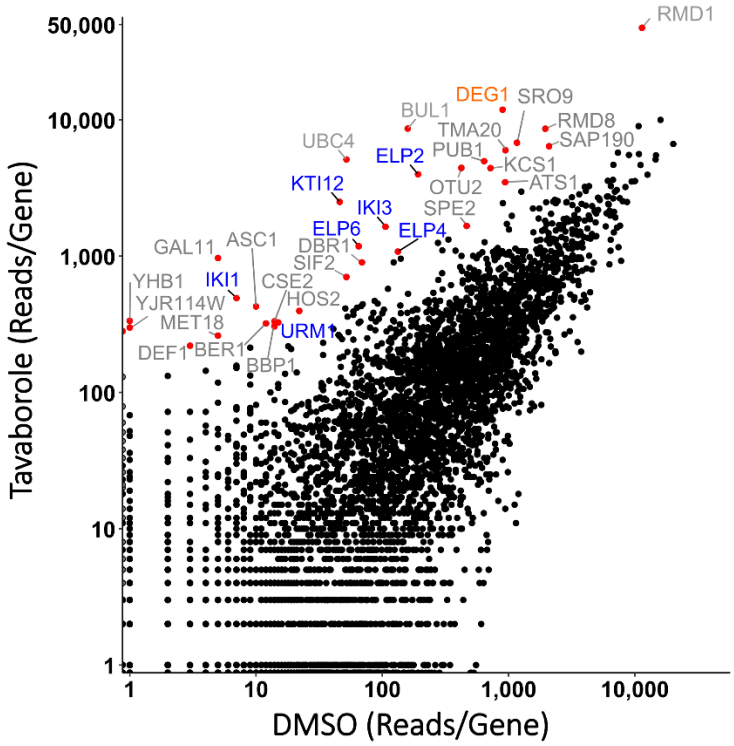

Figure 4.6 – Tavaborole positively selected transposons in genes associated with tRNA modifications. Scatter plot comparing the number of sequencing reads mapping to every gene in a ByK352 transposon library treated with DMSO versus Tavaborole (0.03 µg/mL) in SC -ADE 2% glucose medium. Genes involved with tRNA wobble uridine modifications are coloured blue. *DEG1*, which introduces tRNA pseudouridine modifications, is coloured orange. Additional genes containing significantly enriched insertions in the Tavaborole-treated library are labelled in grey. Genes with a comparable number of reads in each treatment, and thus lying close to the y = x diagonal, are not labelled.

GO term	GO ID	Cluster frequency	Corrected *p*-value	Genes annotated to the term
RNA metabolic process	GO:0016070	24 of 42 genes, 57.1%	3.61E-06	*TMA20, CSE2, MSL1, ASC1, HAP3, ELP2, IKI1, DEG1, ELP6, GAL11, URM1, IKI3, HCR1, TYE7, PUB1, DRS1, SIF2, ELP4, IST3, DBR1, DEF1, HOS2, SFP1, KTI12*
tRNA wobble uridine modification	GO:0002098	6 of 42 genes, 14.3%	4.12E-06	*URM1, ELP2, IKI3, ELP6, ELP4, KTI12*
tRNA modification	GO:0006400	8 of 42 genes, 19.0%	6.62E-06	*IKI3, URM1, ELP6, IKI1, DEG1, ELP4, KTI12, ELP2*

Table 4.1 – Gene Ontology term analysis of the 42 genes containing the highest number of reads in the ByK352 transposon library following Tavaborole treatment. Only the most significantly enriched GO Terms is displayed. *p*-values were corrected using the Holm-Bonferroni method.

4.2.5. Prochloraz resistance was conferred by *ERG11* and *PDR5* overexpression in a PDR-proficient transposon library, but by altered Golgi vesicle trafficking in a PDR-attenuated transposon library

Prochloraz strongly selected transposons in the promoter of its direct molecular target, *ERG11* (**Figure 4.7A-B**). Consistently, the overexpression of *ERG11* is a major azole resistance mechanism (Dunkel et al., 2008; Flowers et al., 2012). This example further demonstrates that SATAY can identify the direct targets of antifungal compounds.

In the ByK352 transposon library, Prochloraz also positively selected transposons in genes associated with the GO terms "mitochondrial gene expression" and "mitochondrial translation" (**Figure 4.8, Table 4.2**). This result is likely explained by the fact that mutations disrupting mitochondrial functions trigger a signalling pathway that increases the expression of the ABC transporter Pdr5 (Hallstrom & Moye-Rowley, 2000; Zhang & Moye-Rowley, 2001). Indeed, Prochloraz is a known substrate of Pdr5 (Kolaczkowski et al., 1998), and Prochloraz also positively selected for transposons in the promoter of *PDR5* (**Figure 4.9, red arrowhead**). Although these results show that SATAY can uncover major antifungal resistance pathways, this PDR-dependent resistance mechanism was associated with almost all the top-hits in this transposon library, obscuring other mechanisms of Prochloraz resistance.

The PDR-attenuated strain 12geneΔ0HSR is more sensitive to Prochloraz than the BY4741 strain ByK352, with a 25-fold lower IC_{30} (0.4 vs. 10µg/mL) (**Chapter 3, Table 3.1**). 12geneΔ0HSR is also derived from BY4741, but lacks eight major ABC transporters

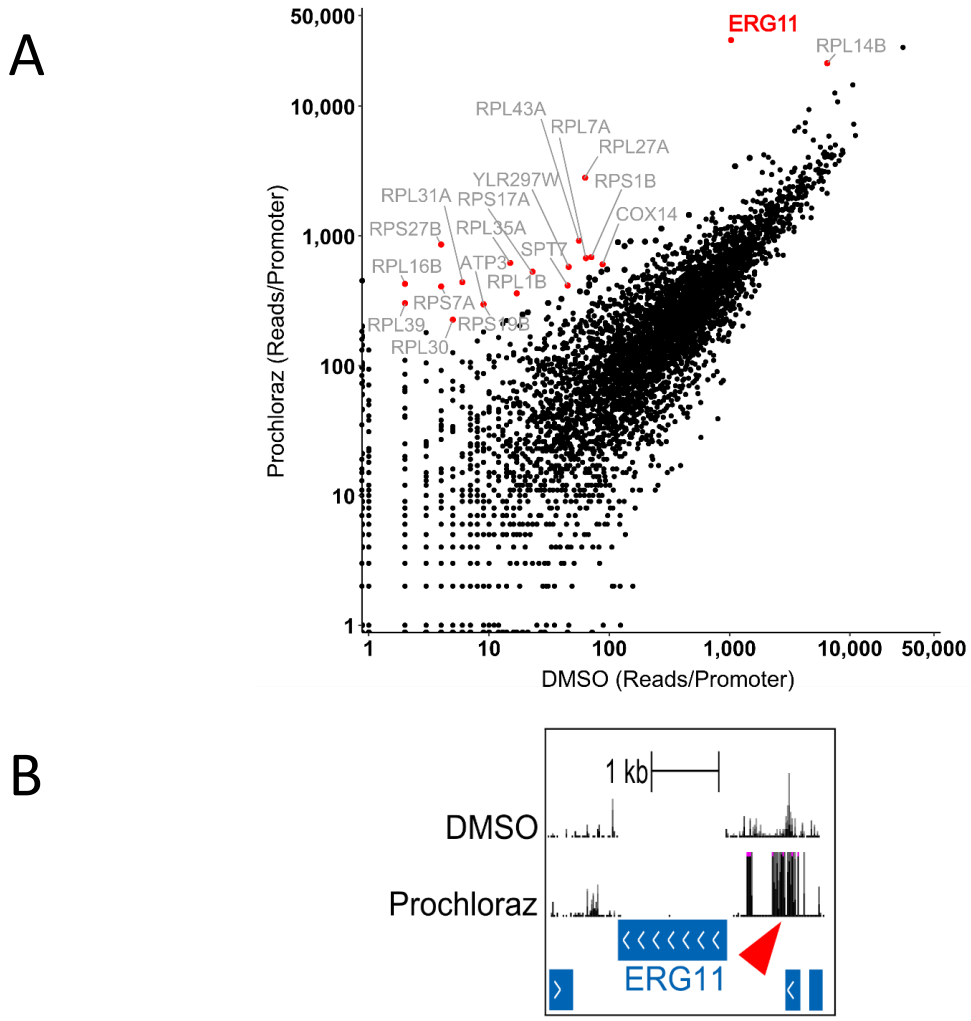

Figure 4.7 – Prochloraz positively selected transposons in the promoter of *ERG11*. A) Scatter plot comparing the number of sequencing reads mapping to promoters in a ByK352 transposon library treated with DMSO versus Prochloraz (10 µg/mL) in SC -ADE 2% glucose medium. Promoters were defined as the 200 bp upstream of the transcription start sites, where known (Xu et al., 2009). *ERG11* is coloured red. Additional genes with significantly enriched promoter insertions in the Prochloraz-treated library are labelled in grey. **B)** Transposon insertion maps for *ERG11* in a ByK352 transposon library after a DMSO treatment or Prochloraz treatment (10 µg/mL). The heights of the bars correspond to the number of sequencing reads and are capped at 500 reads. Red arrowhead indicates positively selected transposons in the promoter region of *ERG11*.

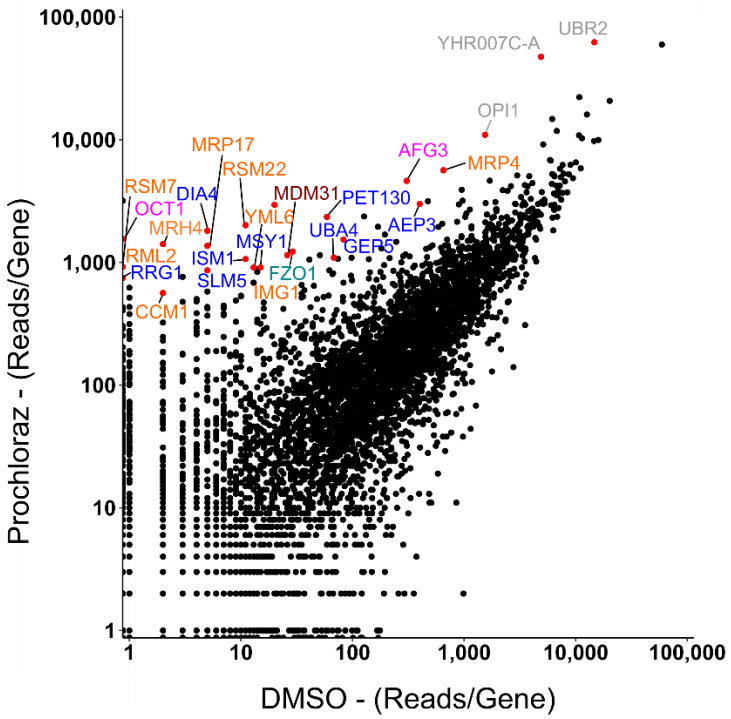

Figure 4.8 – Prochloraz positively selected transposons in genes involved with mitochondrial functions. Scatter plot comparing the number of reads mapping to each of the 6603 yeast CDSs in a ByK352 transposon library treated with DMSO versus Prochloraz (10 µg/mL) in SC -ADE 2% glucose medium. Gene names are colour-coded by biological process: orange – mitochondrial gene expression, blue – mitochondrial translation, pink – mitochondrial protein processing, teal – mitochondrial genome maintenance, maroon – mitochondrial phospholipid homeostasis. Additional genes containing significantly enriched insertions in the Prochloraz-treated library are labelled in grey. Genes with a comparable number of reads in each treatment, and thus lying close to the y = x diagonal, are not labelled.

GO term	GO ID	Cluster frequency	Corrected *p*-value	Genes annotated to the term
Mitochondrial gene expression	GO:0140053	15 of 40 genes, 37.5%	3.94E-18	*YML6, MRP1, DIA4, MRPL8, RPO41, PET130, RML2, SLM5, RSM22, RSM7, MRP17, RRG1, MRPL9, SOV1, MST1, IMG1, MRP4, IMG2, CCM1, GEP5*
Mitochondrial translation	GO:0032543	10 of 40 genes, 25.0%	3E-12	*SOV1, MRPL9, MST1, MRP17, IMG1, MRP4, IMG2, MRPL8, YML6, MRP1, DIA4, SLM5, RML2, RSM22, RSM7*

Table 4.2 – GO term analysis of the 40 genes containing the highest number of reads in the ByK352 transposon library following Prochloraz treatment. Only the two most significantly enriched GO terms are displayed. *p*-values were corrected using the Holm-Bonferroni method.

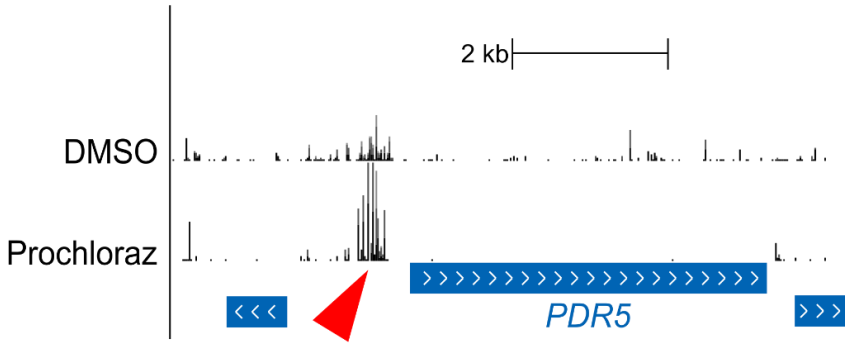

Figure 4.9 – Prochloraz positively selected transposons in the promoter of *PDR5*. Transposon insertion maps for *PDR5* in a ByK352 transposon library after a DMSO treatment or Prochloraz treatment (10 µg/mL). The heights of the bars correspond to the number of sequencing reads and are capped at 500 reads. Red arrowhead indicates positively selected transposons in the promoter region of *PDR5*.

(including Pdr5) and four transcriptional regulators of the PDR network (Chinen et al., 2011) **(Chapter 2, Table 2.1).** 12geneΔ0HSR therefore presented an opportunity for using SATAY to identify PDR-independent mechanisms of Prochloraz resistance.

Compared to the ByK352 transposon library, Prochloraz positively selected insertions in an entirely different set of genes in the 12geneΔ0HSR transposon library (**Figure 4.10**). Indeed, the most enriched transposons were in genes associated with the GO term "vesicle-mediated transport" (**Table 4.3**). Five of the most enriched genes (*MAK3*, *MAK10*, *ARL3*, *SYS1, ARL1*) all act in the same signalling pathway that culminates in the Golgi recruitment of Arl1. Arl1 is a small GTPase that promotes selective vesicle transport from the trans-Golgi network (TGN) to the plasma membrane, and from endosomes to the TGN (Yu & Lee, 2017). Given that the Golgi plays an important role in lipid homeostasis (Daum et al., 1999), it is possible that these mutations re-routed Golgi trafficking pathways in a way that restored membrane homeostasis when ergosterol was depleted by Prochloraz, akin to what was observed for Myriocin (section 4.2.3). Interestingly, a recent Tn-seq study in a PDR-attenuated (*pdr1Δ*) strain of *Candida glabrata* observed that transposon insertions in genes with roles at the Golgi, including *MAK3* and *MAK10*, conferred Fluconazole resistance (Gale et al., 2023). This suggests that vesicle trafficking to/from the Golgi might also engender azole susceptibility in *C. glabrata*. Thus, this example demonstrates that SATAY can be performed in a PDR-attenuated strain to unveil PDR-independent mechanisms of antifungal resistance.

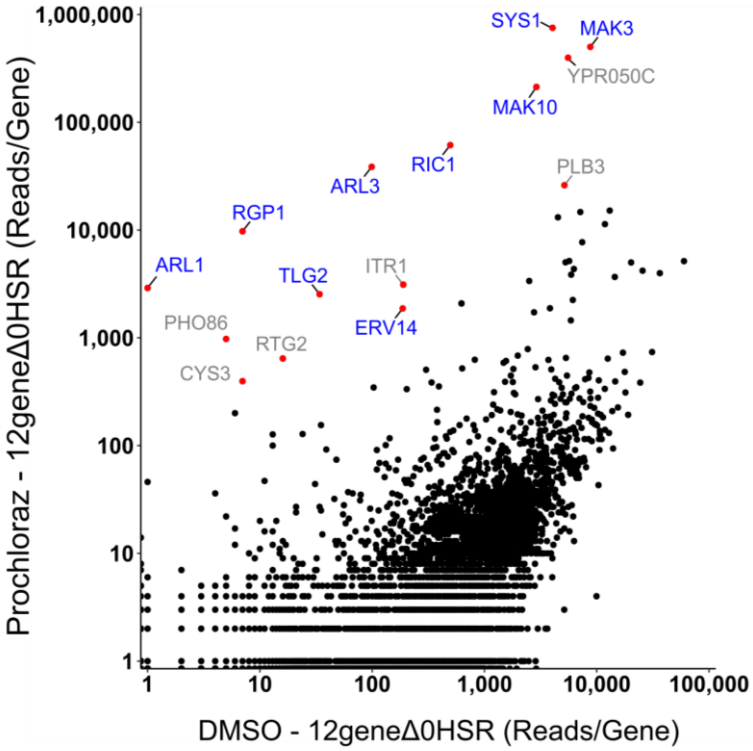

Figure 4.10 – Prochloraz resistance in the 12geneΔ0HSR was conferred by transposons disrupting vesicle trafficking. Scatter plot comparing the number of sequencing reads mapping to each of the 6603 yeast CDSs in the 12geneΔ0HSR transposon library treated with DMSO versus Prochloraz (0.4 µg/mL). Genes involved with vesicle-mediated transport are coloured blue. Additional genes containing significantly enriched insertions in the Prochloraz-treated library are labelled in grey. Genes with a comparable number of reads in each treatment, and thus lying close to the y = x diagonal, are not labelled.

GO term	GO ID	Cluster frequency	Corrected *p*-value	Genes annotated to the term
Vesicle-mediated transport	GO:0016192	10 of 24 genes, 41.7%	9.90E-05	*ERV14, RIC1, ARL3, RGP1, SWH1, TLG2, ARL1, PHO86, TDA3, SYS1*

Table 4.3 – GO term analysis of the 24 genes containing the highest number of reads in the 12geneΔ0HSR transposon library following Prochloraz treatment. Only the most significantly enriched GO term is displayed. *p*-value was corrected using the Holm-Bonferroni method.

4.3. Discussion

4.3.1. SATAY is a robust approach for chemogenomic screening

This chapter further demonstrates that SATAY is a robust approach for chemogenomic screening in *S. cerevisiae*. The screens presented here show that SATAY can identify both loss- and gain-of-function mutations conferring resistance to antifungals with different modes of action. These mutations occurred in genes involved a variety of cellular processes, including lipid metabolism, membrane homeostasis, vesicle trafficking, translation and mitochondrial gene expression, showing that SATAY can reveal a range of resistance mechanisms. Furthermore, transposons mapping to promoter regions revealed antifungal detoxification pathways. This encompassed drug efflux, such as Pdr5 driving Prochloraz export, and metabolic detoxification, such as Sli1 inactivating Myriocin. These screens therefore show that SATAY has significant potential for improving our understanding of antifungals with unclear modes of action, which is the focus of the remaining chapters of this thesis.

4.3.2. SATAY can identify antifungal tolerance mechanisms

The SATAY screen with Amphotericin B illustrates that SATAY can also reveal mechanisms of antifungal tolerance. Tolerance refers to the ability of drug-susceptible strains to survive transient exposure to inhibitory drug concentrations, which is often achieved by slow growth (Brauner et al., 2016). Transposons inactivating TORC1 were enriched by Amphotericin B, and consistently, a previous study has reported that TORC1 inactivation

increases Amphotericin B tolerance in *S. cerevisiae* (Bojsen et al., 2016). Indeed, Bojsen et al., (2016) reported that although *tor1Δ* mutants had significantly higher survival rates on Amphotericin B compared to wild-type cells, this increase was not caused by a change in the MIC value. Therefore, TORC1 inactivation increases tolerance, but not resistance to Amphotericin.

TORC1 regulates cell growth in response to nutrient availability and cellular stresses (Loewith & Hall, 2011), and the EGO complex (Dubouloz et al., 2005) couples TORC1 activation to the availability of amino acids (Peli-Guilli et al., 2015; Binda et al., 2009). The inactivation of TORC1 triggers a quiescent-like state (Barbet et al., 1996).

The enrichment of insertions in TORC1 and EGO subunits by Amphotericin B might be an unintentional consequence of the applied selection regime. Indeed, the transposon library was inadvertently challenged with an inhibitory concentration of Amphotericin B for the first 24 hours of treatment (**Chapter 2, section 2.8.4**), during which TORC1 inactivation might have promoted survival. Then, upon diluting the Amphotericin B concentration in the culture to a sub-lethal level (**Chapter 2, section 2.8.4**), the surviving TORC1 mutants resumed growth, and became increasingly represented in the library population. Thus, in this screen, TORC1 inactivation likely promoted survival until the growth conditions became more favourable. This accidental treatment might demonstrate how SATAY can be used to study antifungal tolerance mechanisms i.e. by initially challenging the library with an inhibitory drug concentration, before diluting the

antifungal compound. Future experiments could replicate this selection regime to identify a greater range of antifungal tolerance mechanisms.

4.3.3. SATAY could facilitate the identification of new combination therapies

The SATAY screen with Caspofungin suggests that Caspofungin therapy could be potentiated by co-administration with an inhibitor of LCB biosynthesis, such as Myriocin. Consistently, a previous study has shown that Myriocin enhances susceptibility to Caspofungin in *Candida glabrata* (Healey et al., 2012). This screen therefore demonstrates how SATAY could support efforts to identify potential new combination therapies, which are necessary for preserving the efficacy of our existing antifungal compounds (Cui et al., 2015).

4.3.4. SATAY can be performed in a PDR-attenuated strain of *S. cerevisiae*

One problem with using *S. cerevisiae* for chemogenomic screening is that the PDR network might in some cases reduce compound sensitivities and mask biological responses relevant to a compound's mode of action. This was illustrated by the SATAY screen with a PDR-proficient transposon library treated with Prochloraz, in which most of the top-hits were associated with a single Pdr5-dependent resistance pathway. This study demonstrates that these problems can be overcome by performing SATAY in a PDR-attenuated strain. Indeed, the 12geneΔ0HSR transposon library revealed that Prochloraz resistance can instead be conferred by mutations disrupting Golgi-plasma membrane and endosome-Golgi vesicle trafficking pathways. Vesicle trafficking may

therefore play an important role in Prochloraz sensitivity, and further studies are required to understand this association. Thus, SATAY screens in PDR-attenuated strains can unveil new resistance mechanisms for PDR-substrates, increase the specificity of chemogenomic profiles, and permit PDR substrates to be studied at lower concentrations.

Chapter 5 – Hol1 concentrates ATI-2307, Pentamidine and Iminoctadine in *S. cerevisiae*

5.1. Introduction

ATI-2307 (formerly T-2307) is a novel arylamidine with significant potential to become a new clinical antifungal (Wiederhold, 2021). ATI-2307 exhibits broad-spectrum *in vitro* and *in vivo* activity against many clinically important fungal pathogens, including *Aspergillus spp.*, *Candida spp.* and *Cryptococcus spp.* (Mitsuyama et al., 2008; Nishikawa et al., 2017; Wiederhold et al., 2020). Furthermore, ATI-2307 has potent activity against Fluconazole-resistant strains of *C. albicans* (Mitsuyama et al., 2008) and Echinocandin-resistant *Candida spp.* (Wiederhold et al., 2015, 2016). ATI-2307 has completed phase I clinical trials and is currently under evaluation as a treatment for cryptococcal meningitis and drug-resistant *Candida* infections (Appili Therapeutics, 2019).

Currently, little is known about ATI-2307's mode of action. ATI-2307 is considered to target mitochondrial respiration, because it only inhibits *S. cerevisiae* and *C. albicans* under non-fermentative growth conditions and causes the collapse of their mitochondrial membrane potentials (Shibata et al., 2012). More recently, ATI-2307 was found to inhibit respiratory chain complexes III and IV *in vitro*, albeit at high concentrations (Yamashita et al., 2019). ATI-2307 treatment also reduced ATP levels in *S. cerevisiae* (Yamashita et al., 2019). Thus, further research is required to elucidate the mode of action of this novel compound. Moreover, very little is known about how ATI-

2307 resistance arises, yet this is important for informing the potential clinical use of this compound.

ATI-2307 exhibits potent activity against *S. cerevisiae* and *C. albicans* in non-fermentative growth conditions, with minimal inhibitory concentrations (MIC) ranging from 0.001 to 0.002 µg/mL (Mitsuyama et al., 2008; Shibata et al., 2012). This potency is attributed to an energy-dependent, high-affinity transporter that concentrates ATI-2307 from the extracellular medium, generating toxic intracellular concentrations (Nishikawa et al., 2010, 2016). The identity of this transporter is currently unknown, but because ATI-2307 import is competitively inhibited by spermine and spermidine, it is thought that ATI-2307 is imported by a polyamine transporter (Nishikawa et al., 2016).

The aim of this chapter was to identify genes affecting ATI-2307 susceptibility in *S. cerevisiae*. This was achieved by challenging a transposon library with a sub-lethal concentration of ATI-2307 in non-fermentative growth conditions. The gene with the most strongly selected transposons upon ATI-2307 treatment, *HOL1*, was subsequently shown to encode the high-affinity transporter mediating the uptake and accumulation of ATI-2307. Hol1 was also found to import two additional antimicrobial compounds that have similar chemical structures to ATI-2307, namely Pentamidine and Iminoctadine. Finally, this chapter identifies separation-of-function mutations in Hol1 that diminish ATI-2307 uptake whilst preserving spermidine import, thereby revealing a straightforward pathway for ATI-2307 resistance to emerge with minimal fitness cost.

5.2. Results

5.2.1. ATI-2307 negatively selected transposons in genes regulating gluconeogenesis, and positively selected transposons in *HOL1* and regulators of the plasma membrane proton-motive force

To identify genes affecting ATI-2307 susceptibility in *S. cerevisiae*, a wild-type (ByK831) transposon library (**Chapter 3, Table 3.2**) was grown in non-fermentative medium containing a sub-lethal concentration of ATI-2307. Genes causing ATI-2307 hypersensitivity when disrupted by transposons were significantly associated with the GO term "Regulation of Gluconeogenesis" (**Figure 5.1, Table 5.1**). This includes subunits of the GID (Glucose Induced degradation Deficient) complex, namely *GID7*, *GID8*, *VID28* and *VID30*. GID is an E3 ligase that polyubiquitylates the gluconeogenic enzyme fructose-1,6-bisphosphatase when non-fermenting cells encounter glucose (Regelmann et al., 2003), the preferred carbon source of *S. cerevisiae* (Kayikci & Nielsen, 2015). *UBC8* was also identified, which encodes a ubiquitin-conjugating enzyme that regulates the activity of the GID complex (Regelmann et al., 2003; Schule et al., 2000). Moreover, transcription factors regulating the expression of gluconeogenic genes were essential on ATI-2307, namely *RDS2* (Soontorngun et al., 2007) and *ERT1* (Gasmi et al., 2014) (**Figure 5.1**). The connection between gluconeogenesis and ATI-2307 susceptibility is unclear, but this enrichment of these functionally related hits underlines the specificity and comprehensiveness of the screen. Furthermore, multiple stress response genes were conditionally essential on ATI-2307. This included *PSR1* and *WHI2* (**Figure 5.1**), which form a complex required for the full activation of the general stress response (Kaida et

al., 2002), and the paralogs *WHI3* and *WHI4*, which also regulate stress response genes (Holmes et al., 2013). These general stress responses likely mitigated ATI-2307 toxicity.

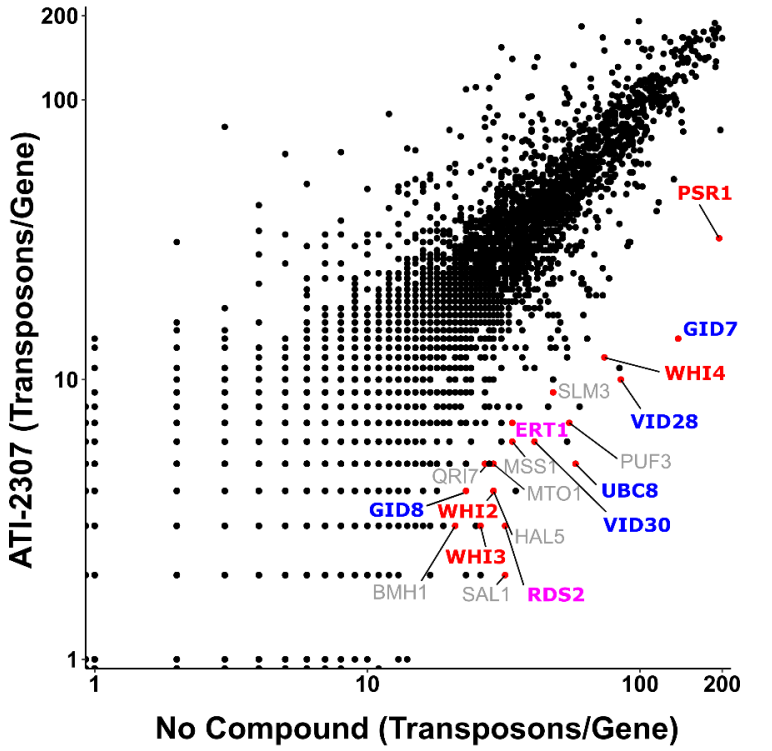

Figure 5.1 – ATI-2307 negatively selected transposons in genes encoding GID complex subunits and regulators of the general stress response. Scatter plot comparing the number of transposons mapping to each of the 6603 yeast CDSs in a wild-type (ByK831) transposon library after a control treatment versus ATI-2307 treatment (0.000175 µg/mL). For both treatments, the transposon library was cultured in SC -TRP 2% ethanol. Genes encoding subunits of the GID complex, and its regulators, are coloured blue. Transcription factors that regulate the expression of gluconeogenic genes are coloured pink. Stress response regulators are coloured red.

Gene Ontology term	GO ID	Cluster frequency	Corrected *p*-value	Genes annotated to the term
Regulation of Gluconeogenesis	GO:0006111	7 of 38 genes, 18.42%	1.31E-07	*GID7, GID8, VID28, VID30, UBC8, ERT1, RDS2*

Table 5.1 – ATI-2307 negatively selected transposons in genes regulating gluconeogenesis. Gene Ontology (GO) term analysis of the 38 genes with the lowest number of transposons on ATI-2307 relative to the control-treated library. Only the most significantly enriched GO term is displayed. *p*-values were corrected using the Holm-Bonferroni method.

Among the genes causing ATI-2307 resistance when disrupted by transposons were the paralogs *RMD1* and *RMD8* (**Figure 5.2A**). Very little is known about the biological functions of these genes, which were originally identified in a screen for mutants defective in meiosis and sporulation (Enyenihi & Saunders, 2003). Rmd1 and Rmd8 are targeted to the vacuole (Eising et al., 2022). Interestingly, Rmd1 and Rmd8 are homologous to the inner mitochondrial protein, Mrx10 (**Figure 5.3, Figure 5.4A**). Mrx10 is a component of MIOREX complexes, which are large assemblies that spatially organise mitochondrial protein synthesis (Kehrein et al., 2015). Although Mrx10 was not identified by the SATAY screen, the homology to Rmd1 and Rmd8 is notable because mitochondrial protein synthesis is required for the biogenesis of respiratory complexes, which were previously implicated as targets for ATI-2307 (Yamashita et al., 2019). Phobius (https://phobius.sbc.su.se/) predicts that Rmd1, Rmd8 and Mrx10 have a transmembrane domain at their C-terminus (data not shown). Moreover, AlphaFold3 predicts that Rmd1, Rmd8 and Mrx10 interact (**Figure 5.4B**). Given this prediction, one can speculate that Rmd1 and/or Rmd8 might sequester Mrx10 at vacuole. In such a scenario, mutations disrupting Rmd1 or Rmd8 might increase the mitochondrial localisation of Mrx10, which may alleviate ATI-2307 toxicity by facilitating the biogenesis of respiratory complexes.

Transposon insertions in *HOL1* were the most strongly selected by ATI-2307 (**Figure 5.2A**). Hol1 was recently identified as the high-affinity polyamine transporter in *S. cerevisiae* that localises to the plasma membrane (Vindu et al., 2021). Strikingly, a high-affinity polyamine transporter of unknown identity is implicated in ATI-2307 uptake in *C.*

albicans (Nishikawa et al., 2010; 2016). Together, this suggested that Hol1 might be the transporter responsible for ATI-2307 uptake in *S. cerevisiae*. Additional findings in the SATAY screen support this hypothesis. First, transposons mapping upstream of *HOL1*, in a region that negatively regulates *HOL1* expression in a post-transcriptional manner (Vindu et al., 2021), were negatively selected by ATI-2307 (**Figure 5.2B, red arrowhead**). This suggests that *HOL1* expression was detrimental during ATI-2307 treatment. Second, Hol1 transport is predicted to be driven by the proton-motive force (PMF) across the plasma membrane (Vindu et al., 2021), and transposon insertions that weakened this PMF and likely thwarted Hol1 activity were positively selected by ATI-2307. This included transposon insertions in *PTK2* and *PSG1* (**Figure 5.2A**), both of which positively regulate the H^+-ATPase Pma1 (Eraso et al., 2006; Geva et al., 2017; Goossens et al., 2000) that generates the PMF in *S. cerevisiae* (Serrano et al., 1986). Additionally, ATI-2307 positively selected transposons inserted into the extreme 3'-end of *TRK1* (**Figure 5.2B, pink arrowhead**). The deletion of the last 35 amino acids of Trk1 increases the stability of the Trk1-Trk2 potassium ion transporter (Pérez-Valle et al., 2007) and potassium ion influx via Trk1-Trk2 dissipates the PMF (Gaber et al., 1988; Ko et al., 1990; Madrid et al., 1998). Consistently, ATI-2307 also positively selected transposons in the promoter regions of *HAL4* and *HAL5* (**Figure 5.5A,B**) (Mulet et al., 1999), two partially redundant positive regulators of Trk1-Trk2 (Pérez-Valle et al., 2007), and in the CDS of *SKY1* (**Figure 5.2A**), a negative regulator of Trk1-Trk2. Like *ptk2Δ* mutants, *sky1Δ* mutants are resistant to toxic concentrations of polyamines (Erez & Kahana, 2001; Forment et al., 2002; Kaouass et al., 1997) and ATI-2307 (Nishikawa et al., 2016). Taken together, I hypothesised that Hol1 is

the high-affinity transporter that mediates ATI-2307 uptake and accumulation in *S. cerevisiae*. This hypothesis is tested in the remaining sections of this chapter.

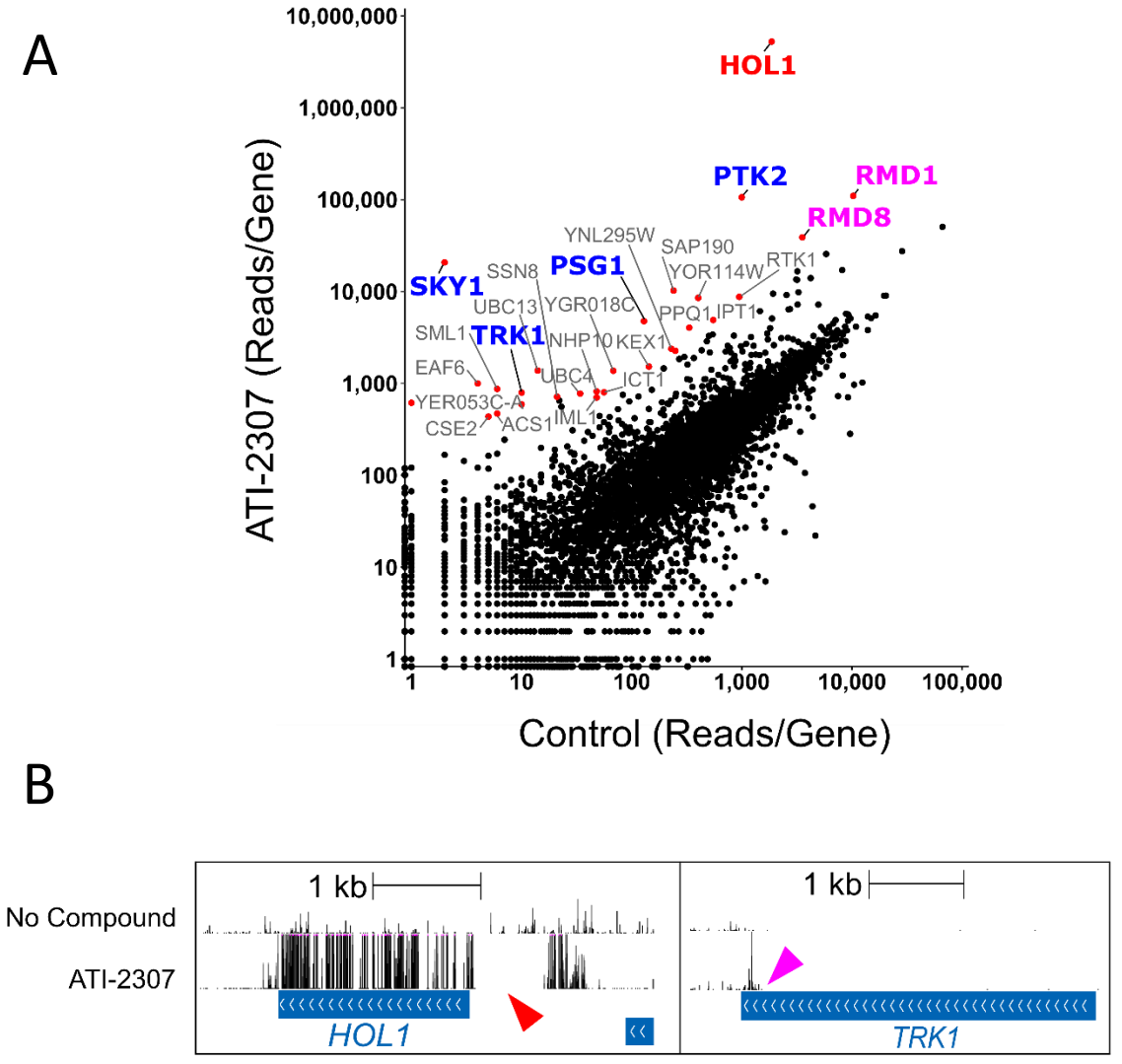

Figure 5.2 – ATI-2307 positively selected transposons in the CDS of *HOL1* and regulators of the proton-motive force. Full figure legend is on the next page.

Figure 5.2 – ATI-2307 positively selected transposons in the CDS of *HOL1* and regulators of the proton-motive force.

A) Scatter plot comparing the number of sequencing reads mapping to each of the 6603 yeast CDSs in a wild-type (ByK831) transposon library after a control treatment versus ATI-2307 treatment (0.000175 µg/mL). For both treatments, the transposon library was cultured in SC -TRP 2% ethanol. *HOL1* is labelled in red. Genes that regulate the proton-motive force across the plasma membrane are coloured blue. *RMD1* and *RMD8* are coloured pink. Additional genes containing significantly enriched insertions in the ATI-2307-treated library are labelled in grey. Genes with a comparable number of reads in each treatment, and thus lying close to the y = x diagonal, are not labelled.

B) Transposon insertion maps for *HOL1* and *TRK1* after the control and ATI-2307 treatments. The heights of the bars correspond to the number of sequencing reads and are capped at 500 reads. Red arrowhead indicates the locus upstream of *HOL1* where transposons were negatively selected by ATI-2307. Pink arrowhead indicates positively selected insertions in the 3'-end of *TRK1*.

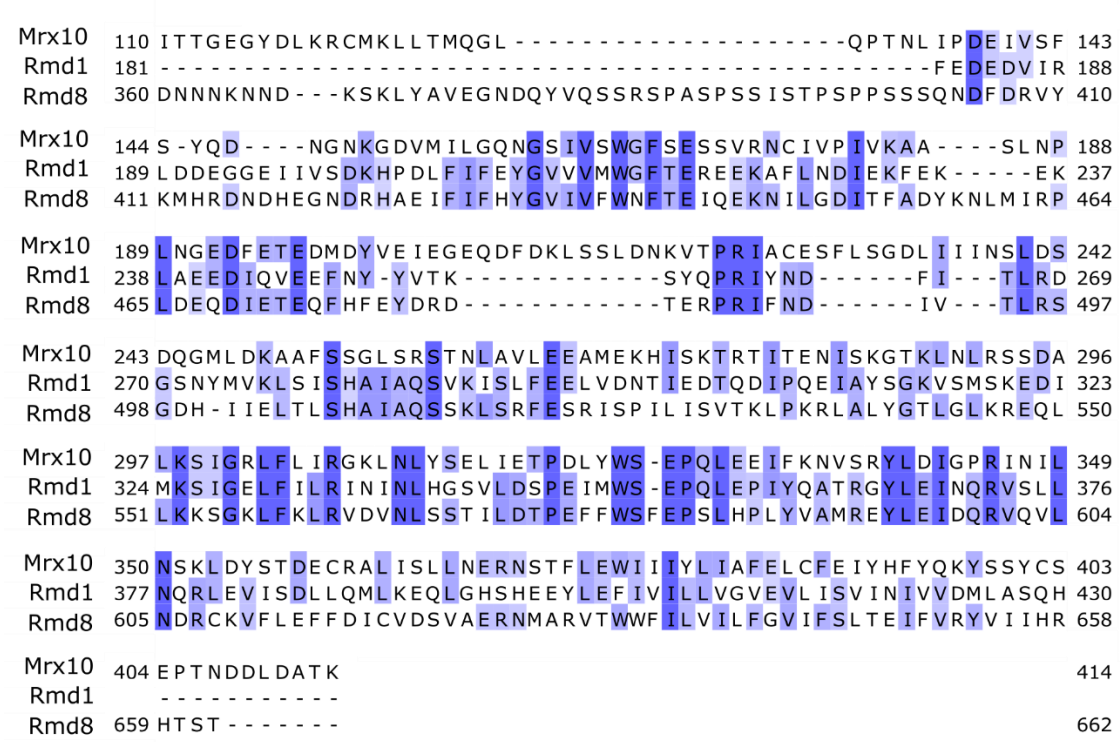

Figure 5.3 – Rmd1, Rmd8 and Mrx10 are homologous. Amino acid sequence alignment of Rmd1, Rmd8 and Mrx10 was performed using Clustal Omega. Sequence identity is indicated by blue highlighting. The alignment is only shown for last 250-300 amino acids at the C-terminus of each protein. The N-terminal sequences exhibited no homology. Alignment was visualised using Jalview (v 2.11.3.3).

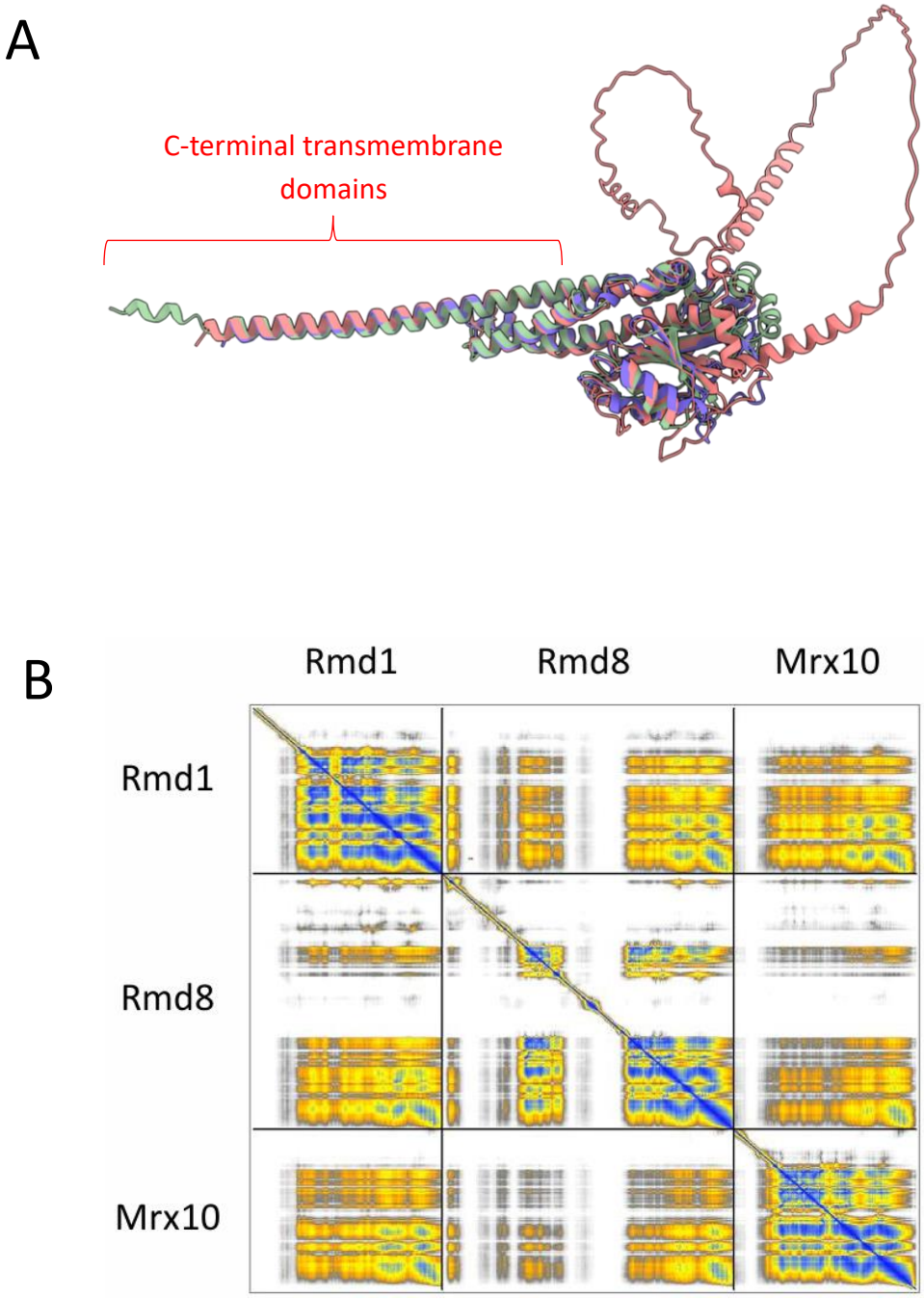

Figure 5.4 – AlphaFold3 predicts that Rmd1, Rmd8 and Mrx10 have similar structures, and likely interact at their C-terminal domains. Full figure legend is on the next page.

Figure 5.4 – AlphaFold3 predicts that Rmd1, Rmd8 and Mrx10 have similar structures, and likely interact at their C-terminal domains.

A) Superimposition of AlphaFold3 models of Rmd1 (purple) (UniProt Identifier Q03441), Rmd8 (peach) (UniProt Identifier P43620) and Mrx10 (green) (UniProt Identifier Q05648). Models were superimposed using the matchmaker command in ChimeraX (v.1.7.1) (Pettersen et al., 2021). The models are structurally similar, particularly in their C-terminal transmembrane domains, as indicated by the red bracket.

B) Predicted Aligned Error (PAE) matrix for the AlphaFold3 models of Rmd1, Rmd8 and Mrx10. The matrices on the diagonal show the intra-protein confidences, whereas the matrices positioned away from the diagonal show the inter-protein confidences. The predicted positional error for each residue (x, y) is indicated by the colour scheme. For the intra-protein matrices, blue patches (corresponding to low PAE values) indicate that AlphaFold3 has high confidence in the relative positions of two residues within a protein, whereas yellow, orange or white patches indicate residues that are positioned with lower confidence. For the inter-protein matrices, blue patches indicate that AlphaFold3 has high confidence in the relative positions of two residues on two different proteins, suggesting a shared interaction interface, whereas yellow, orange or white patches indicate residues that are positioned with lower confidence. The blue patches in the bottom-right corners of the inter-protein matrices suggest that the C-terminal transmembrane domains of Rmd1, Rmd8 and Mrx10 interact with each other.

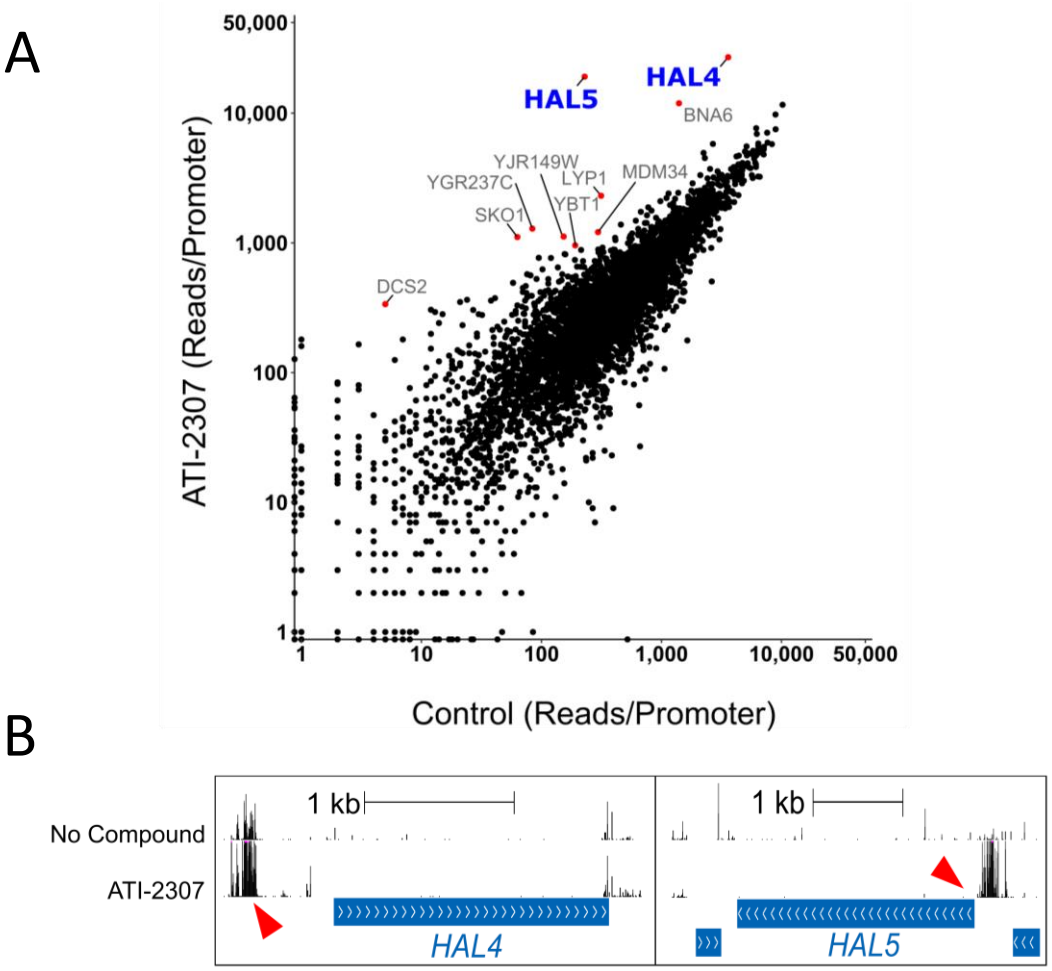

Figure 5.5 – ATI-2307 positively selected transposons in the promoters of *HAL4 and HAL5*.

A) Scatter plot comparing the number of sequencing reads mapping to promoter regions in a wild-type (ByK831) transposon library after a control treatment versus ATI-2307 treatment (0.000175 µg/mL). Promoters were defined as the 200 bp upstream of the transcription start sites, as assessed by Xu *et al*., (2009). For both treatments, the transposon library was cultured in SC -TRP 2% ethanol. *HAL4* and *HAL5* are coloured blue.

B) Transposon insertion maps for *HAL4* and *HAL5* after the control and ATI-2307 treatments. The heights of the bars correspond to the number of sequencing reads and are capped at 500 reads. Red arrowheads indicate positively selected insertions in the promoter regions of *HAL4* and *HAL5*.

5.2.2. *HOL1* is a major determinant of ATI-2307 susceptibility in *S. cerevisiae* and *C. albicans*

To verify that *HOL1* mediates ATI-2307 susceptibility in *S. cerevisiae*, the sensitivity of *HOL1* deletion mutants to ATI-2307 was assessed in non-fermentative medium. Consistent with the SATAY screen results, the *hol1Δ* mutants were resistant to ATI-2307 (**Figure 5.6**). Indeed, the MIC of ATI-2307 for the *hol1Δ* mutants (~1 µg/mL) was approximately 1000-fold higher than the MIC for the *HOL1* wild-type (WT) strains (~0.001 µg/mL). Since the *hol1Δ* mutants were still inhibited by ATI-2307, this shift in the MIC is consistent with the hypothesis that Hol1 concentrates ATI-2307 inside *S. cerevisiae*, generating toxic intracellular concentrations.

A previous study has reported that ATI-2307 uptake by *C. albicans* is driven by an unknown high-affinity polyamine transporter (Nishikawa et al., 2016). Given that Hol1 from *S. cerevisiae* shares over 50% sequence identity with Hol1 from *C. albicans* (*Ca*Hol1) (**Table 5.2**), it seemed likely that *Ca*Hol1 may mediate ATI-2307 uptake. To test this prediction, ATI-2307 sensitivity was assessed in *hol1Δ* mutants of *S. cerevisiae* that were heterologously expressing *CaHOL1*. As shown in **Figure 5.6**, *CaHOL1* expression partially restored ATI-2307 sensitivity to the *hol1Δ* mutants. This suggests that Hol1 from *C. albicans* can also import ATI-2307. ATI-2307 is known to exhibit potent activity against additional *Candida spp*. including *C. parapsilosis*, *C. tropicalis* and *C. auris* (Mitsuyama et al., 2008; Wiederhold et al., 2020). Since *Ca*Hol1 shows a high level of homology to Hol1 in these additional *Candida spp*. (**Table 5.2**) it is plausible that Hol1 mediates ATI-2307 susceptibility in these *Candida* species too.

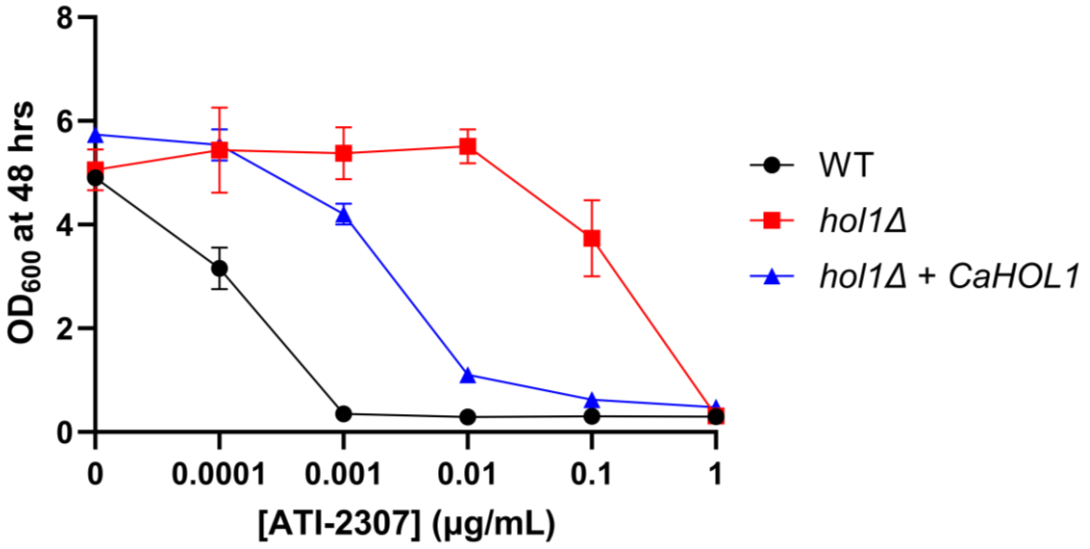

Figure 5.6 – *HOL1* is a major determinant of ATI-2307 sensitivity in *S. cerevisiae*, and may mediate ATI-2307 uptake in *C. albicans*. Growth inhibition curves for wild-type, *hol1Δ* and *hol1Δ CaHOL1* strains treated with ATI-2307. Strains were cultured in SC -URA 2% ethanol medium. WT strains were transformed with pRS316 (CEN/*URA3*) empty vector. *hol1Δ* strains were transformed with pRS316 empty vector or pBK994 (CEN/*URA3* vector encoding *CaHOL1*). Each data point is the mean OD_{600} measurement for three independent biological replicates. Error bars show standard deviation (SD). Error bars for some measurements were too small to be displayed.

	Candida albicans	*Candida auris*	*Candida parapsilosis*	*Candida tropicalis*
Candida albicans				
Candida auris	0.658			
Candida parapsilosis	0.719	0.656		
Candida tropicalis	0.778	0.638	0.698	
Saccharomyces cerevisiae	0.539	0.532	0.521	0.533

Table 5.2 – Hol1 protein sequences from *S. cerevisiae* and several *Candida* species show a high-level of conservation. Sequence identity matrix for pairwise alignments of Hol1 protein sequences from several *Candida* species and *S. cerevisiae*. Pairwise sequence alignments were performed using EMBOSS Needle. Hol1 protein sequences for each species were obtained from UniProt with the following identifiers: *Candida albicans* Q5AP74; *Candida auris* A0A890CZK8; *Candida parapsilosis* G8BA41; *Candida tropicalis* C5MB76; *Saccharomyces cerevisiae* P53389.

5.2.3. Hol1 concentrates ATI-2307 within *S. cerevisiae*

ATI-2307 accumulates to high concentrations in *C. albicans* (Nishikawa et al., 2010). To determine whether Hol1 mediates the selective accumulation of ATI-2307 within *S. cerevisiae*, growth assays were performed with WT and *hol1Δ* strains treated with lysates from ATI-2307-treated WT and *hol1Δ* cells. The rationale was that only lysate from ATI-2307-treated WT cells would contain sufficient ATI-2307 to inhibit the growth of WT cultures of *S. cerevisiae*. To this end, non-fermentative, log-phase cultures of WT and *hol1Δ* cells were treated with 0.003 µg/mL ATI-2307 for 2 hours. This concentration was selected because it is inhibitory to WT cells but not to *hol1Δ* mutants (**Figure 5.6**), suggesting that Hol1 is primarily responsible for ATI-2307 uptake. Cells were then harvested, washed three times with medium, and homogenised to obtain lysate. As predicted, only lysate from ATI-2307-treated WT cells inhibited the growth of non-fermentative WT cultures (**Figure 5.7A**). This lysate did not inhibit *hol1Δ* cultures, indicating that growth inhibition was due to ATI-2307. In contrast, lysate from ATI-2307-treated *hol1Δ* cells lacked inhibitory activity (**Figure 5.7B**), consistent with Hol1-dependent ATI-2307 accumulation in *S. cerevisiae*.

To measure Hol1-dependent ATI-2307 accumulation in *S. cerevisiae*, lysates from ATI-2307-treated WT and *hol1Δ* cells were analysed by Liquid Chromatography – Mass Spectrometry (LC-MS). As before, lysates were obtained from non-fermentative WT and *hol1Δ* cells following a two-hour treatment with 0.003 µg/mL ATI-2307. The concentration of ATI-2307 in the resulting lysates were determined using matrix-matched calibration curves with R^2 values >0.997 (**Figure 5.8A,B**), and subsequently

normalised to cell pellet weights. In the WT lysate, ATI-2307 was detected as a doubly charged ion ($[M+2H]^{2+}$) at *m/z* = 219.6472 (**Figure 5.9A,B**). Whilst an average of ~0.1 µg ATI-2307 was detected per gram of WT pellet (**Figure 5.10**), the concentration of ATI-2307 in *hol1Δ* lysate was below the detection limit i.e. less than 0.005 µg/mL (**Figure 5.8B**). To determine the intracellular concentration of ATI-2307, an approximation of the cell pellet volume attributable to yeast cells vs. intercellular spaces was made. This volume was estimated as 52%, since an inscribed sphere (a yeast cell) occupies 52% of the volume of the surrounding cube. Under this assumption, the average concentration of ATI-2307 in the WT cells was estimated as 0.178 µg/mL (**calculations in Appendix 2A**), which was 58 times higher than the concentration of ATI-2307 applied to the medium (0.003 µg/mL). These results show that Hol1 mediates the selective accumulation of ATI-2307 in *S. cerevisiae*, and thus plays a central role in driving this compound's potency. Moreover, the heterologous expression of *HOL1* from *Candida albicans* (*CaHOL1*) partially restored ATI-2307 uptake in *hol1Δ* mutants of *S. cerevisiae* (**Figure 5.10**). This demonstrates that *Ca*Hol1 can also import ATI-2307, and therefore likely mediates ATI-2307 accumulation in this fungal pathogen.

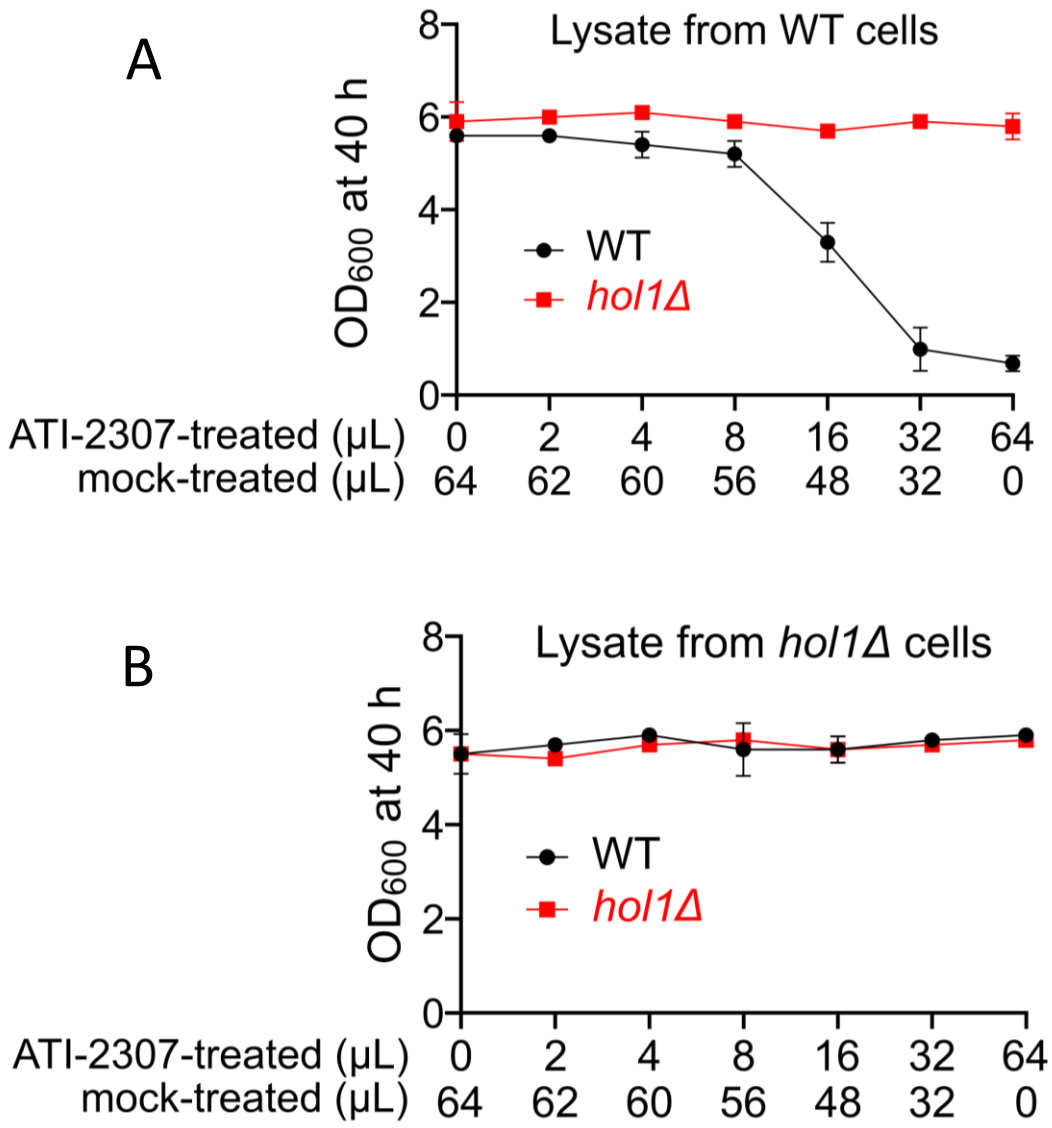

Figure 5.7 – Hol1 concentrates ATI-2307 inside *S. cerevisiae*. Growth inhibition curves for WT and *hol1Δ* strains treated with lysate derived from ATI-2307-treated- WT **(A)** or ATI-2307-treated- *hol1Δ* **(B)** cells. SC 2% ethanol cultures were inoculated with a total of 64 µL lysate derived from WT or *hol1Δ* cells. The volume of lysate from ATI-2307-treated versus mock-treated cells is indicated on the x-axis. Each data point is the mean of three independent biological replicates. Error bars show standard deviation (SD).

A

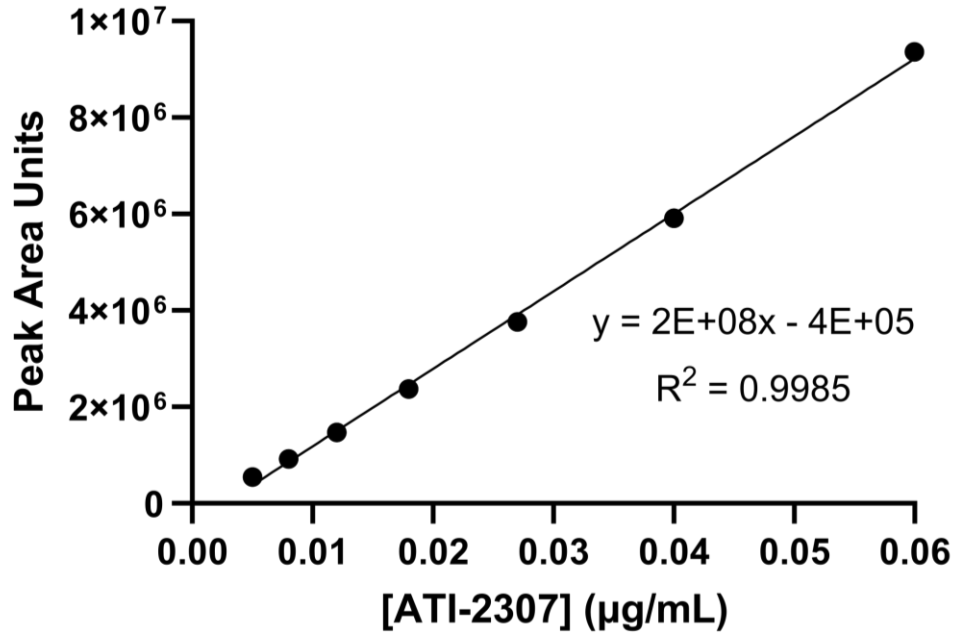

B

	WT			*hol1Δ*			*hol1Δ + CaHOL1*		
[ATI-2307] detected in lysate (µg/mL)	0.045	0.031	0.015	<0.005	<0.005	<0.005	0.0062	0.0068	0.0079

Figure 5.8 – Quantification of ATI-2307 in cell lysate samples using matrix-matched calibration curves.

A) Calibration curve for quantifying ATI-2307 in cell lysate samples. Calibration points (0.005, 0.008, 0.012, 0.018, 0.027, 0.04, 0.06 µg/mL) were prepared by serially diluting ATI-2307 in yeast lysate.

B) ATI-2307 concentrations detected in cell lysates derived from WT, *hol1Δ* and *hol1Δ CaHOL1* strains. Three independent biological replicates are shown for each strain. Concentrations were determined using the calibration curve shown in **A)**.

A

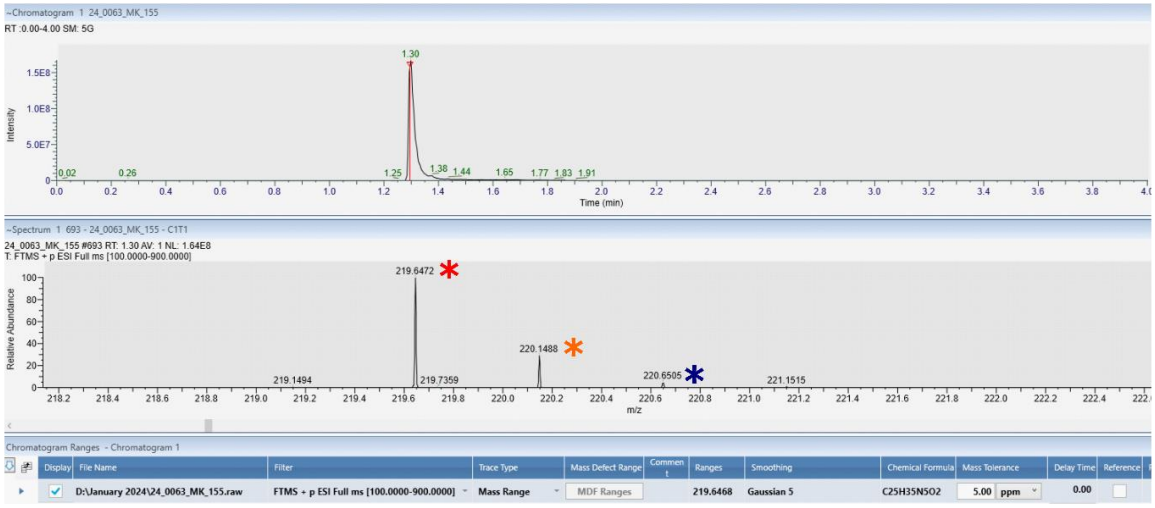

B



C



Figure 5.9 – ATI-2307 uptake was dependent on Hol1. Full figure legend is on next page.

Figure 5.9 – ATI-2307 uptake was dependent on Hol1. Chromatograms and mass spectra for **A)** yeast lysate spiked with 1.25 µg/mL ATI-2307 (control sample) **B)** lysate sample from ATI-2307-treated WT cells **C)** lysate sample from ATI-2307-treated *hol1Δ* cells. In **A)** and **B)**, ATI-2307 was identified with a retention time of 1.30-minutes (using a six-minute gradient method). Red asterisks denote molecular ion peak ($[M + 2H]^{2+}$) at *m/z* = 219.6472. Orange and dark blue asterisks denote isotope peaks at M+0.5 and M+1. ATI-2307 was not detected in the lysate from the *hol1Δ* samples, exemplified by **C)**.

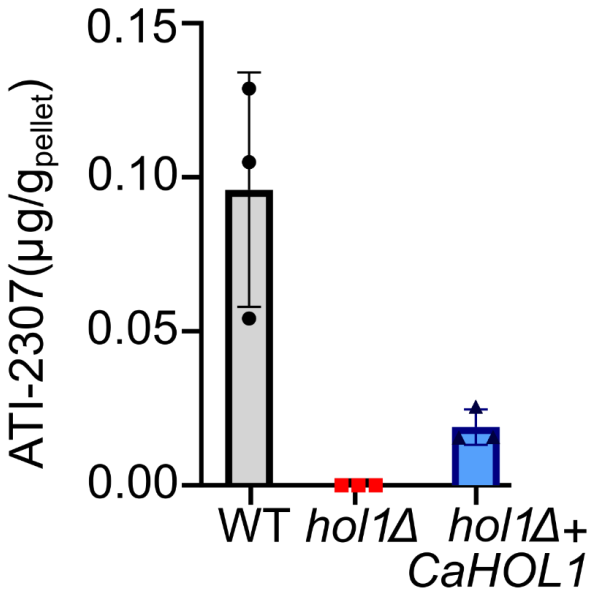

Figure 5.10 – ATI-2307 uptake was dependent on Hol1. Bar chart summarising the uptake of ATI-2307 by WT, *hol1Δ* and *hol1Δ* + *CaHOL1* cells. Log-phase cells were treated for 2 hrs with 0.003 µg/mL ATI-2307 in SC 2% ethanol (or SC -URA 2% ethanol medium for the *hol1Δ* cells expressing *CaHOL1*). The amount of ATI-2307 has been normalised to the cell pellet weight in grams. Each bar plots the mean of three independent biological replicates (n = 3). Error bars show the standard deviation.

5.2.4. Hol1 imports Pentamidine into *S. cerevisiae*

Pentamidine, an antiprotozoal drug, competitively inhibits the uptake of polyamines and ATI-2307 by *C. albicans* (Nishikawa et al., 2010, 2016), suggesting that Pentamidine shares the same transporter as polyamines and ATI-2307. Additionally, given that Pentamidine and ATI-2307 are both aromatic diamidines with similar chemical structures (**Figure 5.11**), I hypothesised that Hol1 imports Pentamidine in *S. cerevisiae* and *C. albicans*. Consistent with this, *hol1Δ* mutants were less susceptible to Pentamidine than WT cells of *S. cerevisiae* (**Figure 5.12**). Furthermore, the heterologous expression of *CaHOL1* partially restored Pentamidine sensitivity in the *hol1Δ* mutants (**Figure 5.12**), implying that *Ca*Hol1 can also import Pentamidine. Pentamidine was notably less potent towards WT cells than ATI-2307 (MIC of Pentamidine was ~1 µg/mL; MIC of ATI-2307 was ~0.001 µg/mL).

LC-MS was used to test whether Hol1 imports Pentamidine into *S. cerevisiae*. Cell lysates were obtained from WT and *hol1Δ* cells treated with 1 µg/mL Pentamidine for two hours in non-fermentative conditions. Pentamidine was detected in WT and *hol1Δ* lysate as a doubly charged ion ($[M+2H]^{2+}$) at *m/z* = 171.1027 (**Figure 5.13**) and quantified using a matrix-matched calibration curve (**Figure 5.14**). On average, 25.7 µg Pentamidine was detected per gram of WT pellet, whereas 1.02 µg was detected per gram of *hol1Δ* pellet (**Figure 5.15**). Using these results, the average intracellular concentration of Pentamidine in the WT cells was estimated to be 49-fold higher than the concentration applied to the medium (**Calculations in Appendix 2B**). This demonstrates that Hol1 also imports

Pentamidine into *S. cerevisiae*, consistent with reports that ATI-2307 and Pentamidine share the same transporter (Nishikawa et al., 2016).

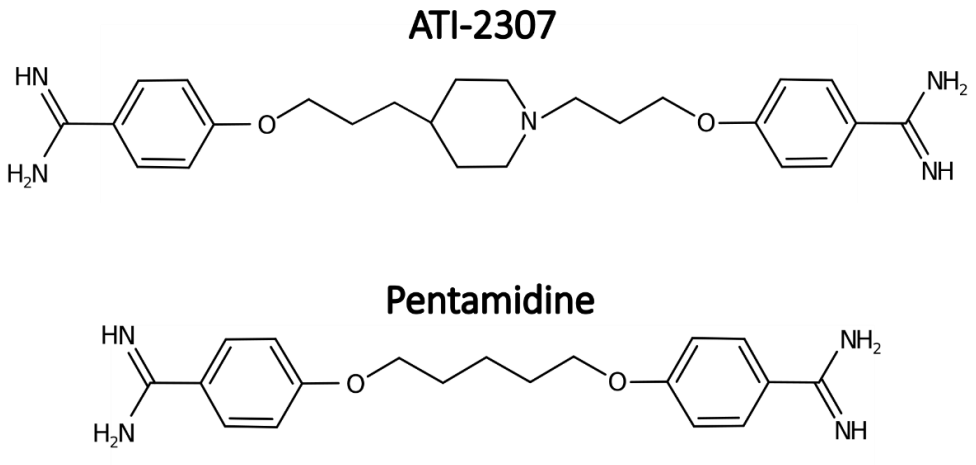

Figure 5.11 – ATI-2307 and Pentamidine have similar chemical structures.

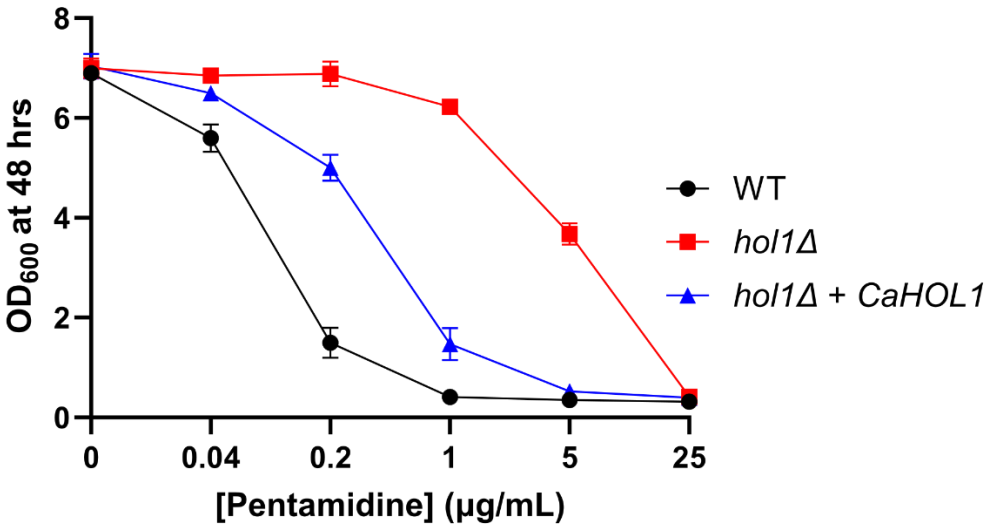

Figure 5.12 - *HOL1* is a major determinant of Pentamidine sensitivity in *S. cerevisiae* and may mediate Pentamidine uptake in *C. albicans*. Growth inhibition curves for wild-type, *hol1Δ* and *hol1Δ* + *CaHOL1* cells treated with Pentamidine. Strains were cultured in SC -URA 2% ethanol medium. WT strains were transformed with pRS316 (CEN/*URA3*) empty vector. *hol1Δ* strains were transformed with pRS316 empty vector or pBK994 (CEN/*URA3* vector encoding *CaHOL1*). Each data point is the mean OD_{600} measurement for three independent biological replicates. Error bars show the standard deviation (SD).

A



B

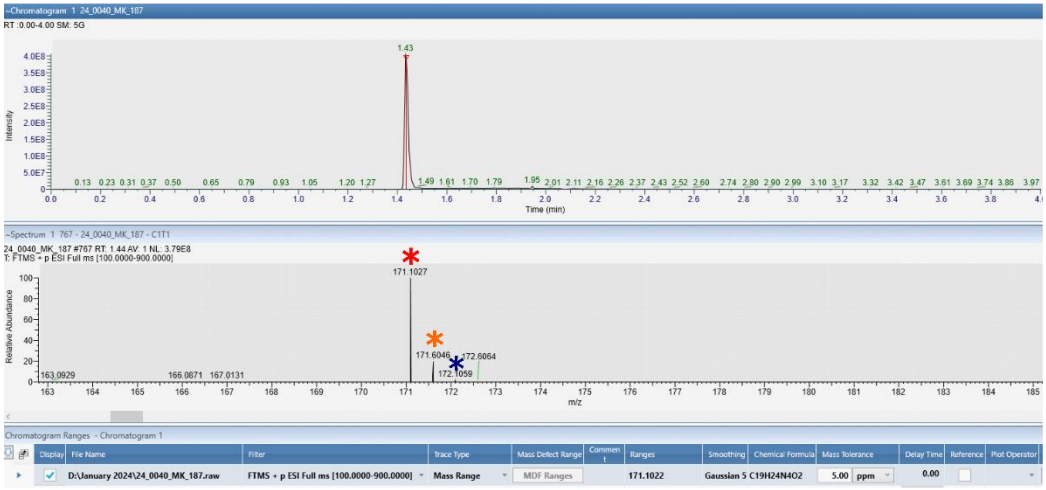

C



Figure 5.13 - Pentamidine uptake was dependent on Hol1. Full figure legend is on next page.

Figure 5.13 - Pentamidine uptake was dependent on Hol1. Chromatograms and mass spectra for **A)** yeast lysate spiked with 1.25 µg/mL Pentamidine **B)** lysate from Pentamidine-treated WT cells (diluted 1/10 in yeast lysate) **C)** lysate from Pentamidine-treated *hol1Δ* cells. Pentamidine was identified with a retention time of 1.43-minutes (using a six-minute method). Red asterisks denote molecular ion peak ($[M + 2H]^{2+}$) at *m/z* = 171.1027. Orange and dark blue asterisks denote isotope peaks at M+0.5 and M+1.

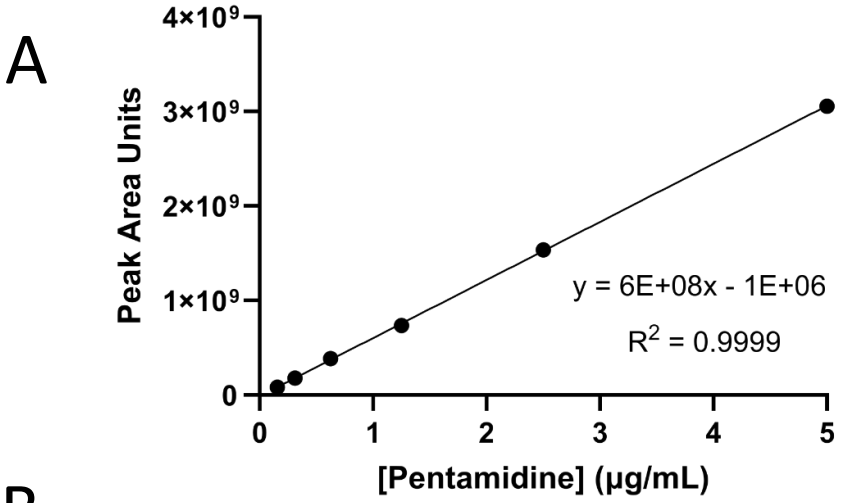

	WT (1/10 dilution)			*hol1Δ*		
[Pentamidine] detected in lysate (µg/mL)	0.713	0.933	0.876	0.262	0.516	0.275

Figure 5.14 – Matrix-matched calibration curve for quantifying Pentamidine in cell lysate samples. A) Calibration curve for quantifying Pentamidine in cell lysate samples. Calibration points (0.156, 0.3125, 0.625, 1.25, 2.5, 5 µg/mL) were prepared by serially diluting Pentamidine in yeast lysate. **B)** Pentamidine concentrations detected in cell lysates derived WT and *hol1Δ*. Three independent biological replicates are shown for each strain. Concentrations were determined using the calibration curve shown in **A)**. The WT lysate samples were diluted ten-fold in yeast lysate prior to the LC-MS analysis.

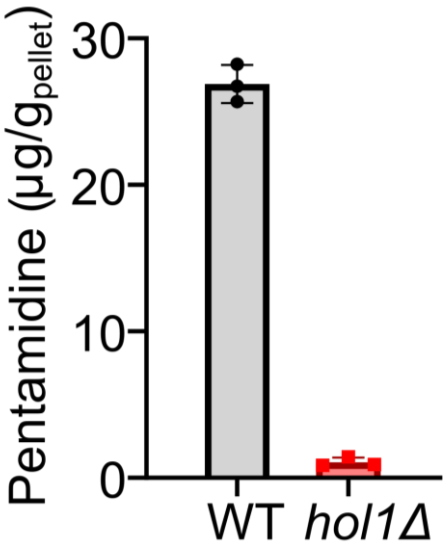

Figure 5.15 – Pentamidine uptake was dependent on Hol1. Bar chart summarising the uptake of Pentamidine by WT and *hol1Δ* cells. Log-phase cells were treated for 2 hrs with 1 µg/mL Pentamidine in SC 2% ethanol. The amount of Pentamidine has been normalised to the cell pellet weight in grams. Each bar plots the mean for independent biological replicates (n = 3). Error bars show the standard deviation.

5.2.5. Hol1 imports Iminoctadine into *S. cerevisiae*

Hol1 is the high-affinity polyamine transporter in *S. cerevisiae* (Vindu et al., 2021). As such, it was hypothesised that Hol1 might import the polyamine Iminoctadine (**Figure 5.16**), which is found within mixtures of the fungicide Guazatine (Raffi et al., 2007; Castagnolo et al., 2011). Iminoctadine has activity against multiple fungal phytopathogens (Ryu et al., 2014; Zhu et al., 2019) and fluconazole-resistant *Candida spp*. (Castagnolo et al., 2011). Consistent with Hol1 mediating Iminoctadine uptake, the deletion of *HOL1* reduced Iminoctadine susceptibility in *S. cerevisiae* (**Figure 5.17**). Moreover, the heterologous expression of *CaHOL1* restored Iminoctadine sensitivity in the *hol1Δ* mutants, indicating that *Ca*Hol1 may also import Iminoctadine (**Figure 5.17**).

LC-MS analysis was also utilised to assess whether Hol1 imports Iminoctadine into *S. cerevisiae*. Cell lysates were obtained from WT and *hol1Δ* cells treated with 1 µg/mL Iminoctadine for 2 hours in non-fermentative conditions. Iminoctadine was detected in WT and *hol1Δ* lysates as a doubly charged ion ($[M+2H]^{2+}$) at *m/z* = 178.6790 (**Figure 5.18**). The WT and *hol1Δ* lysates were quantified using separate calibration curves (**Figure 5.19, 5.20**) because they contained significantly different concentrations of Iminoctadine. Indeed, compared to the average of 52.5 µg detected per gram of WT pellet, only 0.015 µg was detected per gram of *hol1Δ* pellet, representing a 3,500-fold difference (**Figure 5.21**). This clearly demonstrates that Hol1 also imports Iminoctadine. The propensity of Hol1 to accumulate Iminoctadine was further illustrated by the fact that the average intracellular concentration of Iminoctadine in WT cells was estimated at 103.5 µg/mL (**Calculations in Appendix 2C**): 100-fold higher than that in the medium.

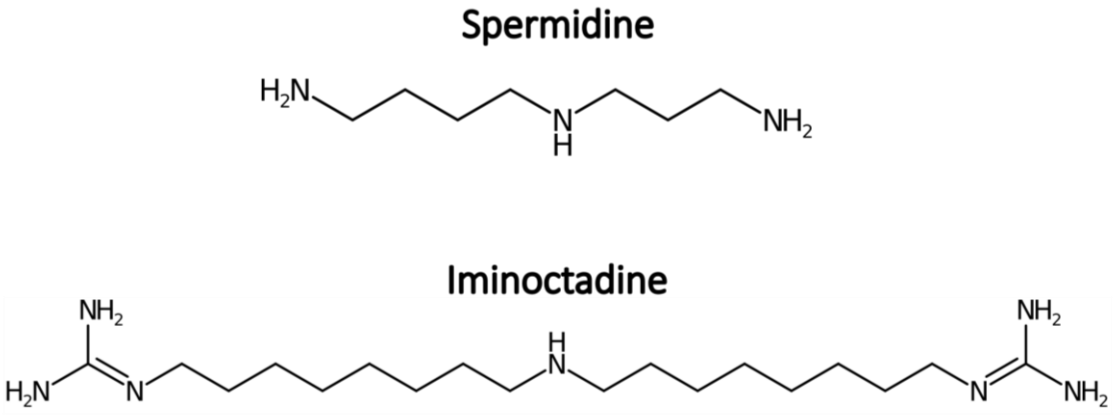

Figure 5.16 – Spermidine and Iminoctadine have similar chemical structures.

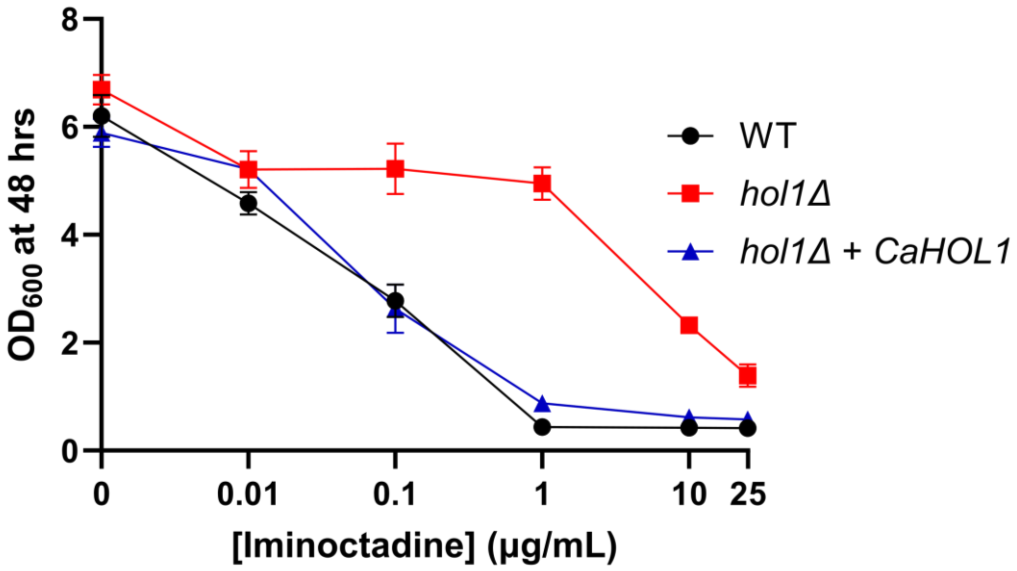

Figure 5.17 – *HOL1* is a major determinant of Iminoctadine sensitivity in *S. cerevisiae*, and may mediate Iminoctadine uptake in *C. albicans*. Growth inhibition curves for wild-type, *hol1Δ* and *hol1Δ* + *CaHOL1* strains treated with Iminoctadine. Strains were cultured in SC -URA 2% ethanol medium. WT strains were transformed with pRS316 (CEN/*URA3*) empty vector. *hol1Δ* strains were transformed with pRS316 empty vector or pBK994 (CEN/*URA3* vector encoding *CaHOL1*). Each data point is the mean OD_{600} measurement for three independent biological replicates. Error bars show standard deviation (SD).

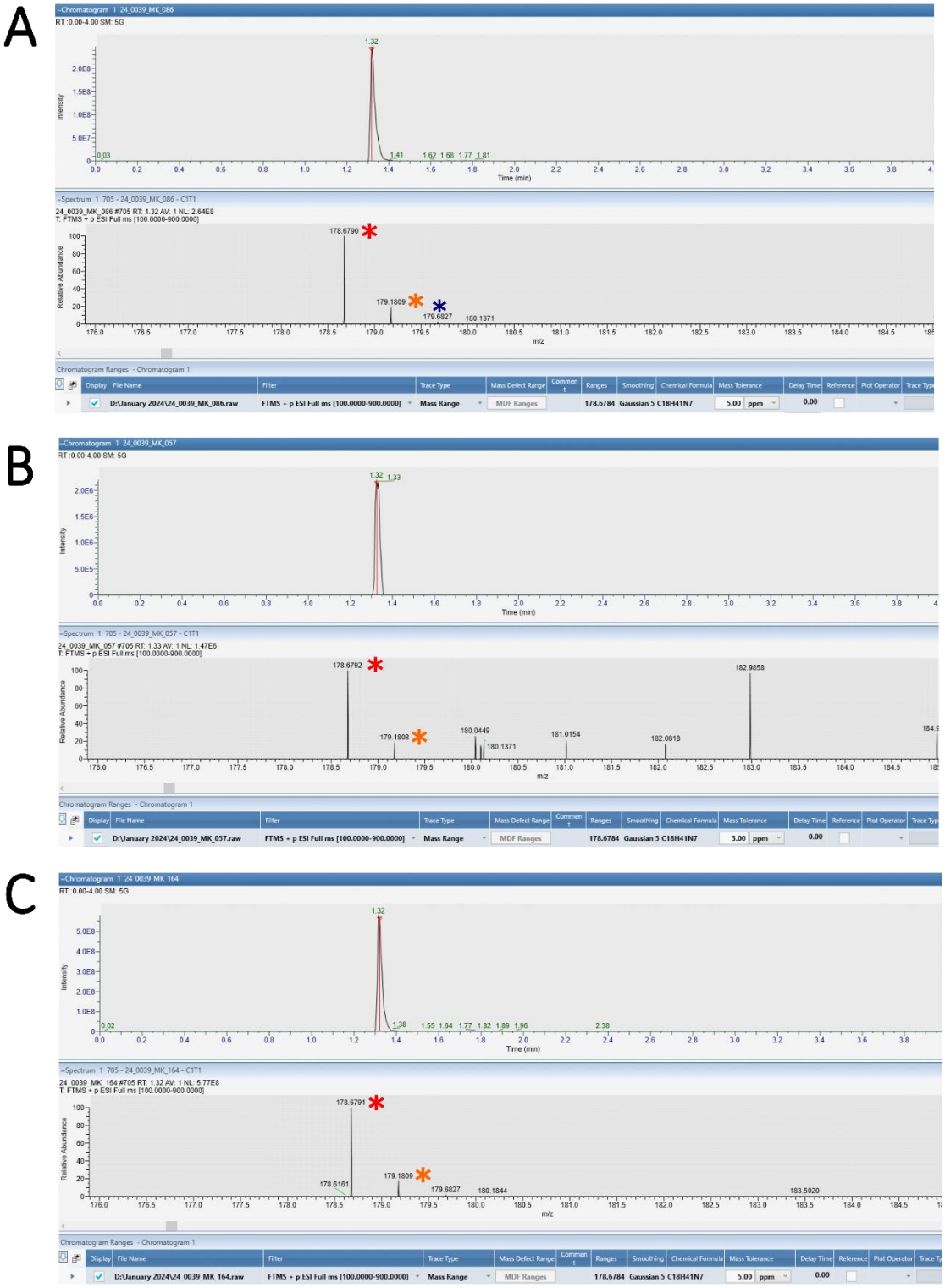

Figure 5.18 – Iminoctadine uptake was dependent on Hol1. Full figure legend is on next page.

Figure 5.18 – Iminoctadine uptake was dependent on Hol1. Chromatograms and mass spectra for **A)** yeast lysate spiked with 1.25 µg/mL Iminoctadine (control sample) **B)** lysate sample from Iminoctadine-treated WT cells (diluted 1/10 in yeast lysate) **C)** lysate sample from Iminoctadine-treated *hol1Δ* cells. Iminoctadine was identified with a retention time of 1.32-minutes (using a six-minute method). Red asterisks denote molecular ion peak ($[M + 2H]^{2+}$) at m/z = 178.6790. Orange and dark blue asterisks denote isotope peaks at M+0.5 and M+1.

A

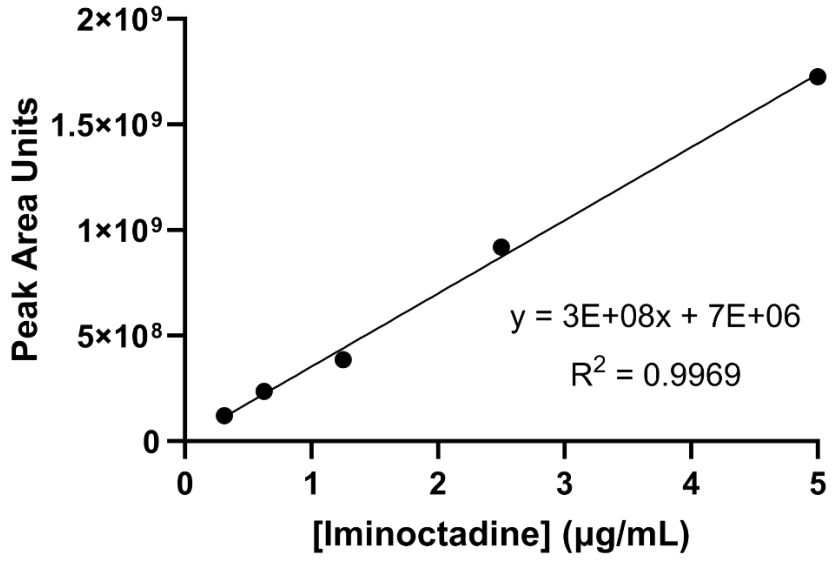

B

	WT (1/10 dilution)		
[Iminoctadine] detected in lysate (µg/mL)	0.864	2.438	2.935

Figure 5.19 – Matrix-matched calibration curve for quantifying Iminoctadine in WT lysate. A) Calibration curve for quantifying Iminoctadine in WT lysate samples. Calibration points (0.3125, 0.625, 1.25, 2.5, 5 µg/mL) were prepared by serially diluting Iminoctadine in yeast lysate. **B)** Iminoctadine concentrations detected in WT lysates. Three independent biological replicates are shown. Concentrations were determined using the calibration curve shown in **A)**. Lysate samples were diluted ten-fold in yeast lysate prior to the LC-MS analysis.

A

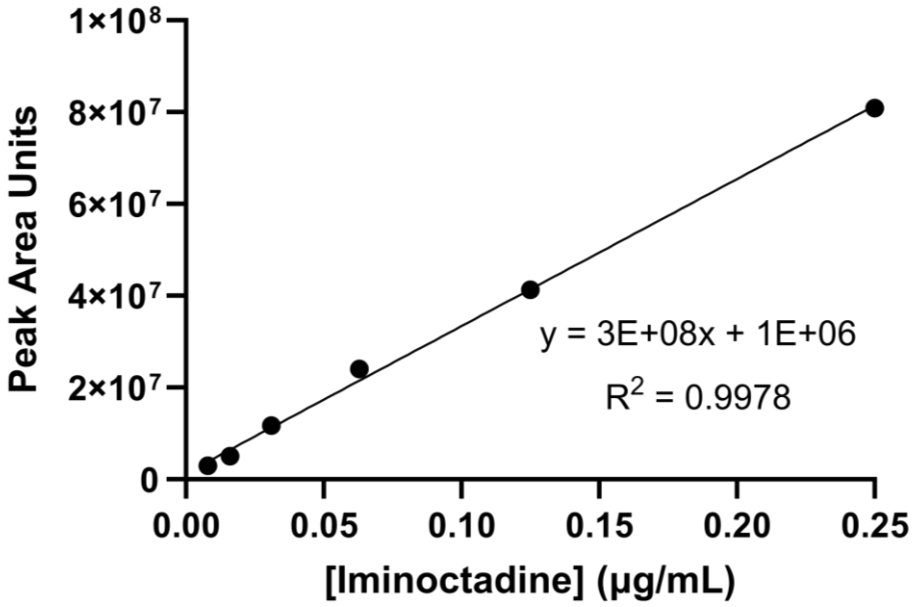

B

	hol1Δ		
[Iminoctadine] detected in lysate (µg/mL)	<0.008	0.0084	0.0086

Figure 5.20 – Matrix-matched calibration curve for quantifying Iminoctadine in *hol1Δ* lysate samples. A) Calibration curve for quantifying Iminoctadine in *hol1Δ* lysate samples. Calibration points (0.008, 0.016, 0.031, 0.063, 0.125, 0.25 µg/mL) were prepared by serially diluting Iminoctadine in yeast lysate. **B)** Iminoctadine concentrations detected in *hol1Δ* lysates. Three independent biological replicates are shown. Concentrations were determined using the calibration curve shown in **A)**.

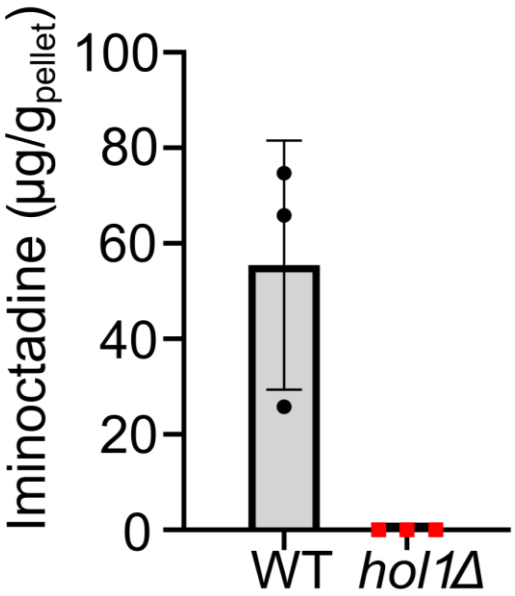

Figure 5.21 – Iminoctadine uptake is driven by Hol1 in *S. cerevisiae*. Bar chart summarising the uptake of Iminoctadine by WT and *hol1Δ* cells. Log-phase cells were treated for 2 hrs with 1 µg/mL Iminoctadine in SC 2% ethanol. The amount of Iminoctadine has been normalised to the cell pellet weight in grams. Each bar plots the mean of three independent biological replicates (n = 3). Error bars show the standard deviation.

5.2.6. Polyamine and ATI-2307 uptake by Hol1 can be functionally separated

Loss-of-function mutations in *HOL1* confer ATI-2307 resistance in *S. cerevisiae* (**Figure 5.6**). This resistance mechanism, however, is likely to carry a fitness cost in low-nitrogen conditions, in which Hol1 is required for growth (Vindu et al., 2021). This cost might be circumvented by point mutations in Hol1 that disrupt ATI-2307 uptake without sacrificing polyamine import. The occurrence of such separation-of-function mutations could present a caveat for the continued therapeutic development of ATI-2307.

To determine whether separation-of-function mutations in Hol1 can arise, a forward genetics screen was performed that coupled random PCR mutagenesis to phenotypic selection. This screen required conditions in which Hol1 was essential for growth. In *S. cerevisiae*, the first step of polyamine biosynthesis is catalysed by Spe1 (Whitney & Morris, 1978; Fonzi, 1989), and hence, *spe1Δ* mutants are obligate polyamine auxotrophs that must acquire polyamines from exogenous sources. Hol1 is essential for the growth of *spe1Δ* mutants in low-polyamine conditions i.e. SC 2% ethanol medium containing 1µM spermidine (**Figure 5.22**). In rich medium (e.g. YPD), the *spe1Δ hol1Δ* strains can grow, presumably due to the presence of a low-affinity spermidine transporter(s) (Nishikawa et al., 2016). To initiate the screen, a plasmid library of randomly mutagenized *HOL1* genes was generated by gap-repair cloning in a *spe1Δ hol1Δ* strain. Approximately 10,000 *spe1Δ hol1Δ* transformants were then replica plated onto SC 2% ethanol medium containing 1µM spermidine and 0.01 µg/mL ATI-2307. These growth conditions selected for *HOL1* alleles that import polyamines without accumulating ATI-2307. In total, sixteen ATI-2307-resistant strains were generated, from

which the plasmids were rescued. To verify that the separation-of-function phenotypes were driven by Hol1, seven randomly selected plasmids were transformed back into the *spe1Δ hol1Δ* strain before susceptibility to ATI-2307, Pentamidine and Iminoctadine was assessed on SC 2% ethanol medium containing 1µM spermidine. All seven transformants exhibited resistance to ATI-2307, Pentamidine and Iminoctadine (**Figure 5.23**). Given that *HOL1* was essential for growth on this medium, these findings validate that the polyamine- and antifungal- transport activities of Hol1 can be functionally separated.

All sixteen rescued plasmids contained at least one non-synonymous mutation in *HOL1* (**Table 5.3**). Notably, the codons for residues N57, L325 and E327 were mutated in more than one independent plasmid, suggesting that the screen was approaching saturation. Multiple plasmids also contained synonymous mutations in *HOL1*, indicating that the screen strongly selected for Hol1 functionality. The non-synonymous mutations considered to be causal of the separation-of-function phenotype are indicated in **Table 5.3**. For plasmids bearing multiple non-synonymous mutations in *HOL1*, causality was assigned to mutations found on several independent plasmids e.g. N57 and E327. Mapping these causal residues onto the AlphaFold2 model of Hol1 revealed that they clustered on the cytoplasmic side of the transporter, near the base of the pore (**Figure 5.24**). Although it was conceivable that the selected phenotype could be obtained by a mere reduction in Hol1 activity, this clustering on the cytoplasmic side instead suggests that the screen pinpointed a specific domain that may have a critical role in mediating ATI-2307, Pentamidine and Iminoctadine, but not spermidine uptake. Taken together, these results indicate that mutations in Hol1 can disrupt ATI-2307, Pentamidine and

Iminoctadine uptake without sacrificing polyamine import. Thus, the evolution of such separation-of-function mutations in fungal pathogens could challenge the efficacy of ATI-2307 as a novel antifungal therapy.

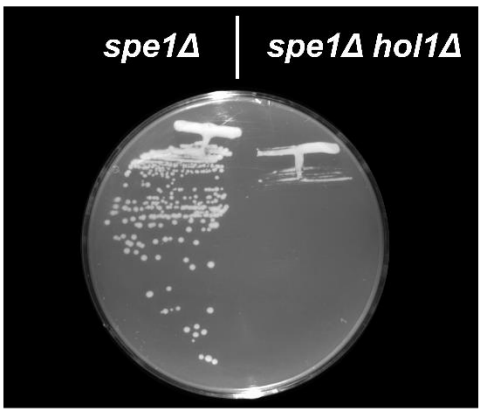

Figure 5.22 – *HOL1* was essential for the growth of *spe1Δ* mutants on SC 2% ethanol medium supplemented with 1 µM spermidine. Streaks of *spe1Δ* and *spe1Δ hol1Δ* strains on SC 2% ethanol medium supplemented with 1 µM spermidine. Image taken after 6 days of incubation.

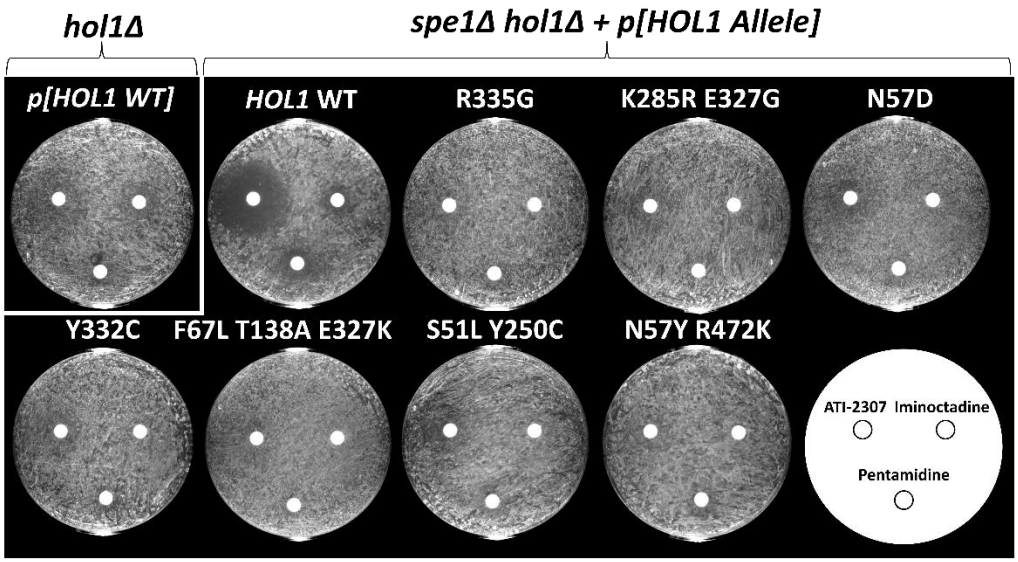

Figure 5.23 – The plasmid-borne *HOL1* alleles conferred resistance to ATI-2307, Pentamidine and Iminoctadine in low-polyamine conditions, validating the separation-of-function phenotype. Disc diffusion assays performed on SC 2% ethanol medium supplemented with 1 µM spermidine. Discs were treated with 0.4 µg/mL ATI-2307, 80 µg/mL Pentamidine or 30 µg/mL Iminoctadine. *hol1Δ* transformed with pBK958 (*HOL1* WT) (top-left). *spe1Δ hol1Δ* transformed with pBK958 (*HOL1* WT) or one of seven rescued plasmids (pBK995-pBK1001) encoding *HOL1* alleles. Non-synonymous mutations in *HOL1* for each transformant are shown above the corresponding plate. Images taken after 5 days of incubation at 30°C. The *hol1Δ* strain (top-left) did not require the plasmid-borne *HOL1* gene for viability on SC 2% ethanol + 1 µM spermidine medium, since it is *SPE1+*. Hence, this strain could lose the plasmid and grow in the presence of each compound. In contrast, the *spe1Δ hol1Δ* transformants required the plasmid-borne *HOL1* gene for growth. As such, the *spe1Δ hol1Δ* transformant encoding a WT copy of *HOL1* was susceptible to all three compounds.

	Mutation(s) in Hol1
1	S51L, Y250C
2	N57D, G68S
3	N57D
4	N57D, K334K
5	N57Y, A148A, R472K
6	F183L, L187W, I479I
7	E241G
8	D323G, A417A, A536A
9	E327G, Y562F
10	K285R, E327G
11	F67L, T138A, F142F, E327K
12	E171E, Y332C
13	R335G
14	R335G, A536A
15	L345S
16	L345S

Table 5.3 – Hol1 mutations associated with the separation-of-function phenotype. Sixteen plasmids were rescued from *spe1Δ hol1Δ p[HOL1]* strains and *HOL1* alleles were sequenced. For each strain, all the mutations identified in *HOL1* are listed, including synonymous mutations. Non-synonymous mutations shown in red were considered causal of the separation-of-function phenotype. For plasmids bearing multiple non-synonymous mutations in *HOL1*, the causal mutation was assigned to mutations identified in several independent plasmids e.g. N57 and E327.

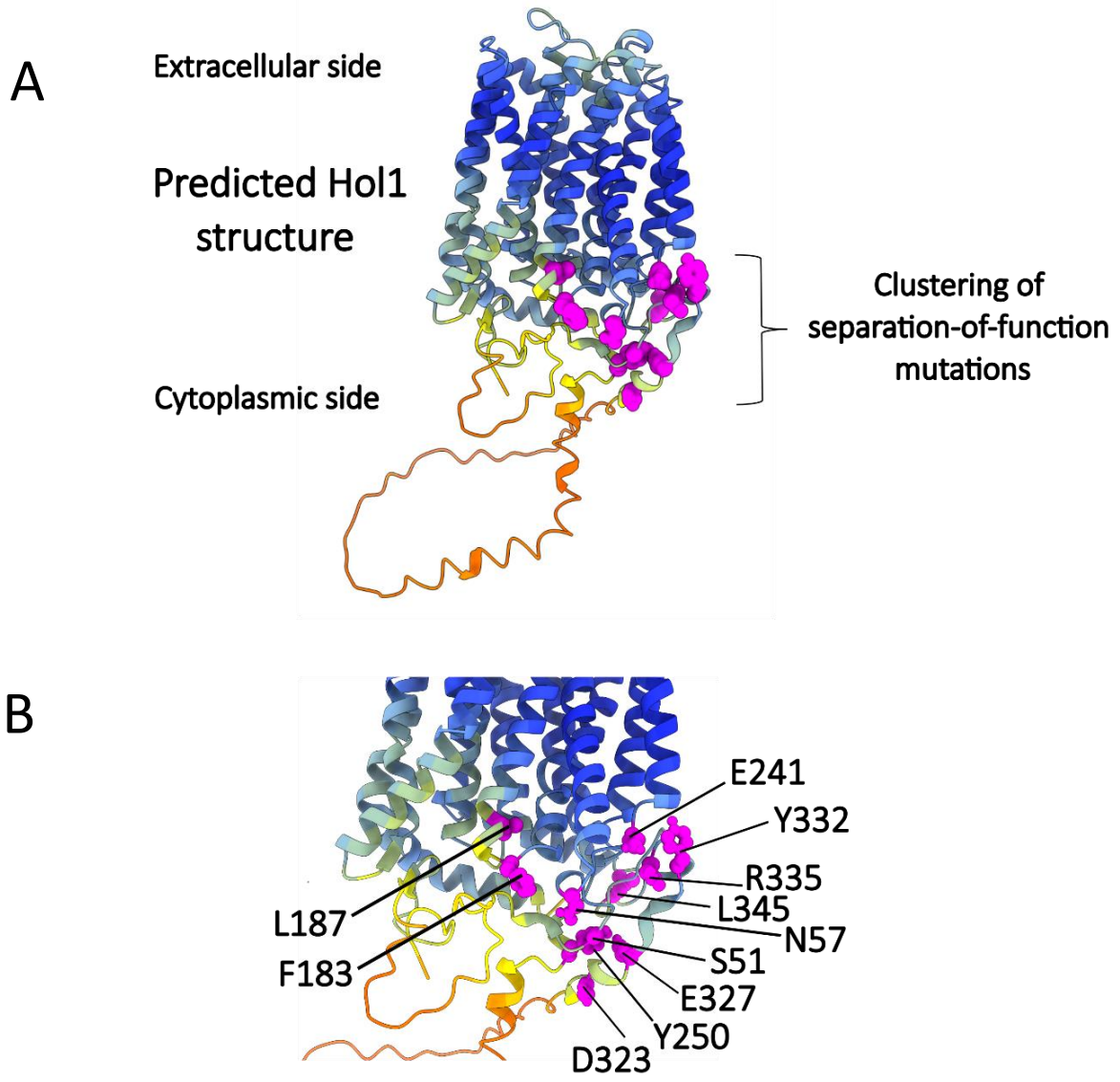

Figure 5.24 – Separation-of-function mutations clustered on the cytoplasmic side of Hol1. A) AlphaFold2 model of the *S. cerevisiae* Hol1 protein (UniProt Identifier P53389) showing the positions of the amino acid residues (in pink) that, when mutated, caused a functional separation of polyamine and ATI-2307 uptake. **B)** Zoomed in version of the AlphaFold2 model of the *S. cerevisiae* Hol1, in which the amino acids residues causing the separation-of-function phenotype when mutated are labelled.

5.3. Discussion

5.3.1. Hol1 imports ATI-2307, Pentamidine and Iminoctadine sensitivity into *S. cerevisiae*

This chapter demonstrates that the polyamine transporter Hol1 mediates the uptake and accumulation of ATI-2307 in *S. cerevisiae*. This work therefore improves our understanding of how ATI-2307 exhibits potent activity. Hol1 was also found to import Pentamidine, an aromatic diamidine like ATI-2307, and Iminoctadine, a polyamine (Vindu et al., 2021). This promiscuity suggests that Hol1 might import other structurally-related aromatic diamidines and polyamines into *S. cerevisiae*. Hol1 is therefore a promising candidate for the development of novel actively imported drugs or pro-drugs. In addition, the propensity of Hol1 to concentrate antifungal compounds, particularly ATI-2307, is unique, and could be exploited to develop a new generation of potent antifungal compounds.

Hol1 from *C. albicans* was also found to import ATI-2307, consistent with reports that ATI-2307 uptake in *C. albicans* is driven by a high-affinity polyamine transporter (Nishikawa et al., 2010, 2016). As observed for ATI-2307, the heterologous expression of *CaHOL1* only partly restored Pentamidine sensitivity in *hol1Δ* strains, but fully restored Iminoctadine sensitivity. This observation might reflect the fact ATI-2307 and Pentamidine share greater structural similarity with each other than with Iminoctadine. Given that *Sc*Hol1 and *Ca*Hol1 share over 50% sequence identity, it could be that Iminoctadine interacts more extensively with the residues that are highly conserved between these proteins than ATI-2307 and Pentamidine.

Regarding the LC-MS experiments, the fold-changes in the detected intracellular concentrations of ATI-2307, Pentamidine and Iminoctadine in WT cells relative to the concentrations applied to the medium were similar for all three compounds: 58-fold for ATI-2307, 49-fold for Pentamidine and 100-fold for Iminoctadine. The WT strains were treated with each compound under the same growth conditions (SC 2% ethanol). Given that Hol1 transport is predicted to be driven by the PMF (Vindu et al., 2021) and the PMF is sensitive to the available carbon source (Goossens et al., 2000; Eraso et al., 2006), these comparable fold-changes might reflect the possibility that Hol1 transport was limited by the PMF under these growth conditions.

Interestingly, Hol1 belongs to the 12-spanner drug:proton (H+) antiporter (DHA1) family of Major Facilitator Superfamily (MFS) transporters (Gbelska et al., 2006). Typically, proton-coupled antiporters use the energy released from the downhill translocation of protons to drive the uphill translocation of substrates in the opposite direction (Yan, 2015). Many DHA1 transporters are therefore drug efflux pumps (Sa-Correia, 2009). However, the findings presented in this study, and the results of Vindu et al., (2021), suggest that Hol1 is a proton-coupled symporter, in which ATI-2307 and polyamines are translocated into the cytoplasm down the proton gradient. This implies that proton-coupled antiporters can evolve into proton-coupled symporters. Hol1 might have made this transition under nitrogen-poor growth conditions, in which the acquisition of a high-affinity polyamine importer would have facilitated cell growth and survival.

5.3.2. Identifying broad-spectrum nutrient permeases in fungal pathogens could inform the design of novel antifungal compounds

In *S. cerevisiae*, transporter-mediated uptake of antifungals is typically mediated by nutrient permeases, through which antifungals can pass as opportunistic substrates (Galocha et al., 2020; Lanthaler et al., 2011). Few studies have investigated drug uptake in fungal pathogens (Galocha et al., 2020), yet these pathogens might harbour broad-spectrum, high-affinity nutrient permeases that could be easily hijacked by antifungal compounds. Indeed, nutrient uptake by fungal pathogens is a prerequisite for the successful colonisation of plant and animal hosts (Johns et al., 2021), and as such, fungal pathogens encode a multitude of nutrient permeases, especially during infection stages (Divon & Fluhr, 2007). Identifying and characterising such nutrient permeases could unveil transporters that might be easily hijacked by antifungal compounds, potentially informing the design of novel antifungal compounds.

5.3.3. The identification of separation-of-function mutations in Hol1 suggests that ATI-2307 resistance can emerge with minimal fitness cost

This chapter reveals a straightforward pathway for the emergence of ATI-2307 resistance. Indeed, separation-of-function mutations in Hol1, which limit ATI-2307 uptake without disrupting polyamine uptake, can confer ATI-2307 resistance with minimal fitness cost. These findings may therefore support further precautionary measures in the clinical use of ATI-2307. Given that these separation-of-function mutations also conferred resistance to Iminoctadine, this study might also reveal a mechanism by which fungal phytopathogens evolve resistance to the fungicide

Guazatine, of which Iminoctadine is a key constituent (Zhao et al., 2023; Zhang et al., 2024).

Given that ATI-2307 is a larger molecule than the natural Hol1-substrates spermidine and spermine, it was predicted that mutations narrowing the Hol1 translocation pore might specifically limit ATI-2307 transport. However, using the AlphaFold2 model of Hol1, the identified separation-of-function mutations were instead found to cluster on the cytoplasmic side of Hol1, near the base of the pore. These mutations therefore pinpoint a specific domain of Hol1 that, through an unknown mechanism, is involved in ATI-2307, Pentamidine and Iminoctadine uptake. There are no straightforward explanations for how these mutations caused the observed separation-of-function phenotype. It is notable that there are multiple lysine residues (K326, K330, K334, K334, K341 and K346) in close proximity to the separation-of-function mutations. This raises the possibility that these mutations affect the regulation of Hol1 endocytosis in the presence of these antifungals. Indeed, in *S. cerevisiae*, nutrient transporter endocytosis is mediated by ubiquitination (Nikko & Pelham, 2009). However, the mechanism for how altered Hol1 endocytosis might led to ATI-2307, Pentamidine and Iminoctadine resistance without impacting spermidine uptake remains to be elucidated.

The screen identifying these separation-of-function mutations in Hol1 only involved a single round of mutagenesis and selection. It is conceivable that additional rounds of artificial evolution might further refine the selectivity of Hol1 for polyamines over ATI-2307. This could be achieved using a directed evolution approach such as OrthoRep

(Ravikumar et al., 2014, 2018), in which an error-prone orthogonal DNA polymerase would repeatedly mutate *HOL1* in cells passaged in medium containing low-polyamines but increasing ATI-2307 concentrations. Alternatively, deep mutational scanning (Fowler & Fields, 2014) could be used to generate a vast library of Hol1 variants, which could then be grown competitively in medium containing a low concentration of polyamines and a stringent concentration of ATI-2307. The variants with the highest fitness in these conditions could identify more complete separation-of-function mutations in Hol1.

5.3.4. The intracellular target(s) of ATI-2307 were not revealed by the SATAY screen

Previous studies have shown that ATI-2307 collapses the mitochondrial membrane potential (Shibata et al., 2012) and inhibits respiratory chain complexes III and IV *in vitro*, albeit at high concentrations (Yamashita et al., 2019). Consistent with ATI-2307 targeting the mitochondria, this study observed that ATI-2307 only inhibits non-fermentative growth of *S. cerevisiae*. Whilst the SATAY screen did not yield any obvious direct molecular target(s) for ATI-2307, it remains possible that the target(s) are among the findings of this dataset. However, since Hol1 is the major determinant of ATI-2307 susceptibility, the SATAY screen strongly favoured mutants with defects in Hol1 transport, potentially obscuring hits relating to the target(s). *HOL1*-independent mechanisms of ATI-2307 resistance and sensitivity could be identified by performing a SATAY screen with a *hol1Δ* strain of *S. cerevisiae*. Indeed, *hol1Δ* strains still exhibit sensitivity to ATI-2307. In addition to potentially identifying the target(s) of ATI-2307, this screen would be helpful for determining whether *HOL1* is required for ATI-2307 hypersensitivity in mutants defective in gluconeogenesis regulation, or for ATI-2307 resistance in *RMD1* or *RMD8*

mutants. Moreover, this *hol1Δ* SATAY screen might unveil the identity of the putative low-affinity ATI-2307 transporter (Nishikawa et al., 2010).

There are additional reasons why the SATAY screen might not have identified the target(s) of ATI-2307. Indeed, the target(s) of ATI-2307 might be highly expressed, in which case insertions in the promoter of the target(s) were of little selective advantage. Furthermore, the target(s) might be encoded by the mitochondrial genome, which is inaccessible to the mini*Ds* transposon. Notably, subunits of complex III (Cytb) and complex IV (Cox1, Cox2, Cox3), which are the presumed targets for ATI-2307 (Yamashita et al., 2019), are encoded by the mitochondrial genome (Malina et al., 2018).

5.3.5. The connection between the GID complex and ATI-2307 susceptibility is an interesting question for future research

The discovery that the GID complex (hereafter GID) was essential on ATI-2307 is intriguing. When non-fermenting cells are supplied with glucose, GID plays an important role in blocking gluconeogenesis by polyubiquitylating the regulatory enzyme fructose-1,6-bisphosphatase (FBPase) (Regelmann et al., 2003), which is subsequently degraded at the proteosome (Schork et al., 1994). Since FBPase is required for gluconeogenesis (Sedivy & Fraenkel, 1985), GID should be redundant in non-fermentable growth conditions. Consistently, transposons were tolerated in GID subunits in the control-treated library in non-fermentative growth conditions, but this was not the case in ATI-2307-treated, non-fermenting cells. Gluconeogenesis therefore appears detrimental to ATI-2307-treated cells. Although this observation might be revealing an important aspect

of ATI-2307's mode of action, it is difficult to rationalise using our current understanding of GID. It is unlikely that ATI-2307 inhibits GID, because ATI-2307 is only toxic under non-fermentative conditions, under which GID is redundant. Perhaps GID has additional targets besides FBPase that elicit ATI-2307 toxicity. Alternatively, the production of glucose might be detrimental on ATI-2307. One possible explanation for this is that glucose activates the plasma membrane H^+-ATPase Pma1 via Ptk2 (Goosens et al., 2000; Eraso et al., 2006). Since the PMF likely drives Hol1 transport (Vindu et al., 2021), glucose (and hence gluconeogenesis) might indirectly stimulate ATI-2307 import. GID may therefore play a role in limiting Hol1-mediated uptake of ATI-2307 (**Figure 5.25**). The connection between ATI-2307 sensitivity and gluconeogenesis presents an interesting question for future ATI-2307 research.

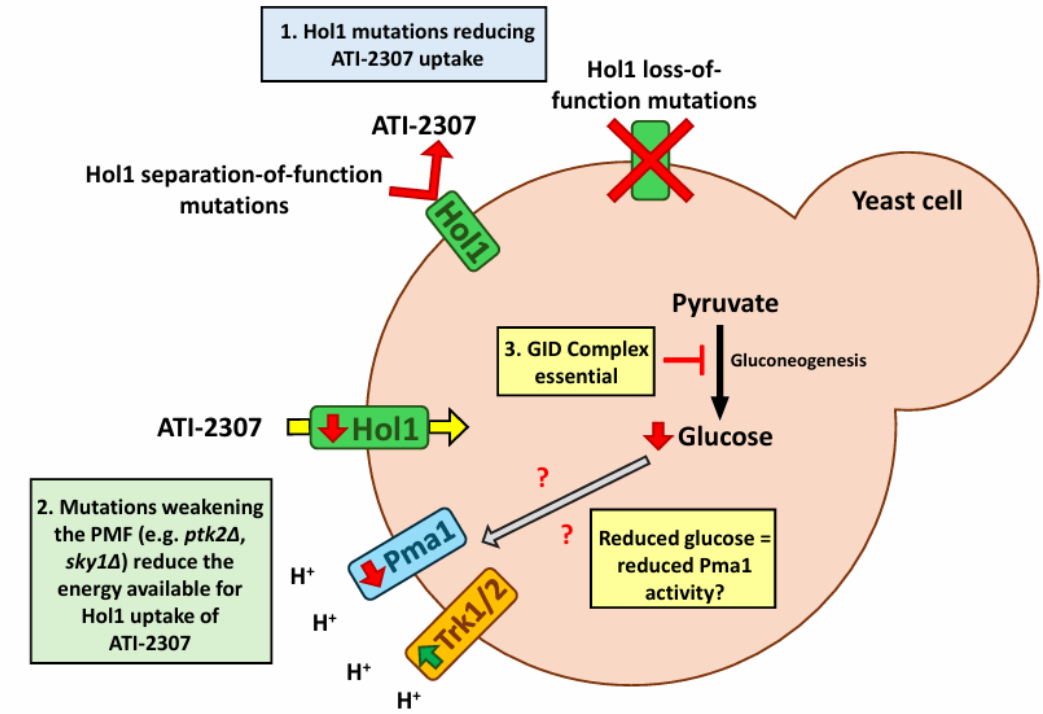

Figure 5.25 – Cartoon depiction of the major ATI-2307 resistance mechanisms identified in this chapter. Green rectangles indicate Hol1. Blue rectangle indicates Pma1, the plasma membrane H^+-ATPase that pumps protons (H^+) out of the cell, generating the proton-motive force (PMF). Orange rectangle indicates the potassium ion transporter Trk1/2, which consumes the PMF. Yellow arrow indicates Hol1 transport of ATI-2307. Green and red arrows represent increased or decreased activity, respectively. Grey arrow indicates a hypothesised connection between the GID Complex, reduced glucose levels and the PMF via Pma1.

Chapter 6 – Investigating the direct target and mode of action of Fludioxonil

6.1. Introduction

Fludioxonil belongs to the phenylpyrrole class of fungicides and is widely used for pre- and post-harvest disease control, particularly on grapes, fruit and vegetable crops (Kilani & Fillinger, 2016). Fludioxonil is effective at controlling fungal pathogens belonging to a broad range of genera, including *Botrytis*, *Fusarium*, *Magnaporthe*, *Aspergillus*, *Monilinia* and *Penicillium* (Bersching & Jacob, 2021). Fludioxonil was inspired by the natural product pyrrolnitrin (**Figure 6.1A-B**) and was commercialised by Syngenta in 1993. Despite over 30 years of intensive commercial use, very few cases of field resistance have been reported (Kilani & Fillinger, 2016). Fludioxonil is therefore a highly successful fungicide.

Fludioxonil has a distinctive mode of action involving the constitutive activation of the High Osmolarity Glycerol (HOG) signal transduction pathway (Kojima et al., 2004; Zhang et al., 2002). The HOG pathway is ubiquitous in fungi and mediates cellular adaptation to osmotic and oxidative stress (Hohmann et al., 2002). Following Fludioxonil treatment, HOG pathway activation leads to the abnormal accumulation of glycerol, cell growth arrest, hyphal swelling and subsequently cell lysis (Zhang et al., 2002; Ochiai et al., 2002). Fludioxonil is thought to share the same mode of action as dicarboximide fungicides such as Iprodione (**Figure 6.1C**) (Tanaka & Izumitsu, 2010; Fillinger et al., 2012), since these fungicides elicit the same phenotypic effects in filamentous fungi and cross-resistance

has been observed in laboratory mutants of *Botrytis cinerea* (Fillinger et al., 2012; Yin et al., 2023).

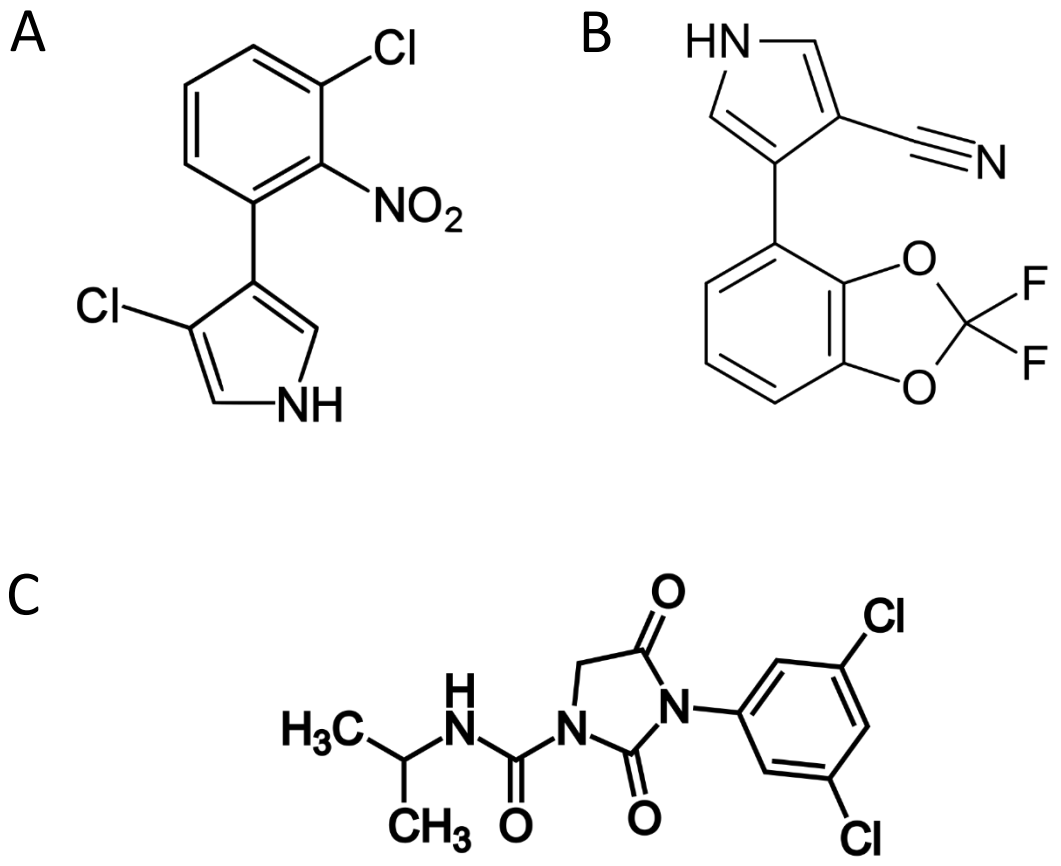

Figure 6.1 – Chemical structures of A) Pyrrolnitrin B) Fludioxonil C) Iprodione.

Fludioxonil sensitivity is dependent upon group III Hybrid Histidine Kinases (HHKs) (Fillinger et al., 2012; Furukawa et al., 2012; Motoyama et al., 2005). Indeed, Fludioxonil fails to activate the HOG pathway in filamentous fungi that are deleted in group III HHKs (Fujimura et al., 2000; Yoshimi et al., 2005). Group III HHKs are found in the majority of fungal species (Catlett et al., 2003; Defosse et al., 2015) and in addition to having roles in morphogenesis, virulence and conidiation (Defosse et al., 2015), these kinases function as sensors upstream of the HOG pathway (Yoshimi et al., 2005; Meena et al., 2010). Group III HHKs are cytoplasmic (Meena et al., 2010) and structurally diverge from other classes of HHKs because they possess N-terminal HAMP domain repeats (Defosse et al., 2015). These HAMP domains are required for sensing hyperosmolarity and Fludioxonil (Meena et al., 2010; Furukawa et al., 2012; Buschart et al., 2012), and hence, mutations conferring Fludioxonil and Iprodione resistance frequently localise to the HAMP domains (Avenot et al., 2005; Fillinger et al., 2012; Ren et al., 2016; Zhou et al., 2020). Although it is well-established that Fludioxonil activity requires group III HHKs (Fillinger et al., 2012; Furukawa et al., 2012; Motoyama et al., 2005), it is not clear whether group III HHKs are the direct target of Fludioxonil. Moreover, the precise mechanism by which Fludioxonil causes the constitutive activation of the HOG pathway is not understood.

Recent studies have sought to elucidate the mode of action of Fludioxonil using the model yeast *S. cerevisiae* (Lawry et al., 2017; Brandhorst et al., 2019; Randhawa et al., 2019). This is because *S. cerevisiae* is genetically tractable and has an extensively characterised HOG pathway (Hohmann et al., 2002, de Nadal & Posas, 2022). The HOG

pathway consists of a two-component-like phospho-relay positioned upstream of a MAPK cascade (Hohmann et al., 2002). In *S. cerevisiae*, the HOG pathway is negatively regulated by a group VI HHK called Sln1, which is located at the plasma membrane (Maeda et al., 1994; Ota & Varshavsky, 1993). Under normal osmotic conditions, Sln1 is autophosphorylated and transfers the phosphate to a cytosolic protein called Ypd1, which in turn transfers the phosphate to Ssk1 (Posas et al., 1996). Since only the unphosphorylated form of Ssk1 binds to and activates the MAPKKKs Ssk2 and Ssk22 (Horie et al., 2008), Sln1-dependent phosphotransfer to Ssk1 keeps the HOG pathway switched off (**Figure 6.2A**). As such, the deletion of *SLN1* is lethal (Maeda et al., 1994). Under osmotic stress, Sln1 does not undergo autophosphorylation and a phosphate is not transferred to Ssk1. Activated Ssk2 and Ssk22 can then phosphorylate the MAPKK Pbs2, which subsequently phosphorylates the MAPK Hog1 (Hohmann et al., 2002). Phosphorylated Hog1 then moves into the nucleus where it phosphorylates osmoresponsive transcription factors, leading to the upregulation of stress-response genes that protect the cell against osmotic stress (Posas et al., 2000) (**Figure 6.2B**).

S. cerevisiae does not harbour a group III HHK (Catlett et al., 2003) and is therefore innately insensitive to Fludioxonil (Motoyama et al., 2005). However, Fludioxonil sensitivity can be introduced by the heterologous expression of a group III HHK (Buschart et al., 2012; Furukawa et al., 2012; Lawry et al., 2017; Motoyama et al., 2005). Group III HHK expression can also complement the deletion of *SLN1* (Meena et al., 2010; Randhawa et al., 2016), implying that these kinases can repress the HOG pathway. Following Fludioxonil treatment, the HOG pathway is inappropriately activated in strains

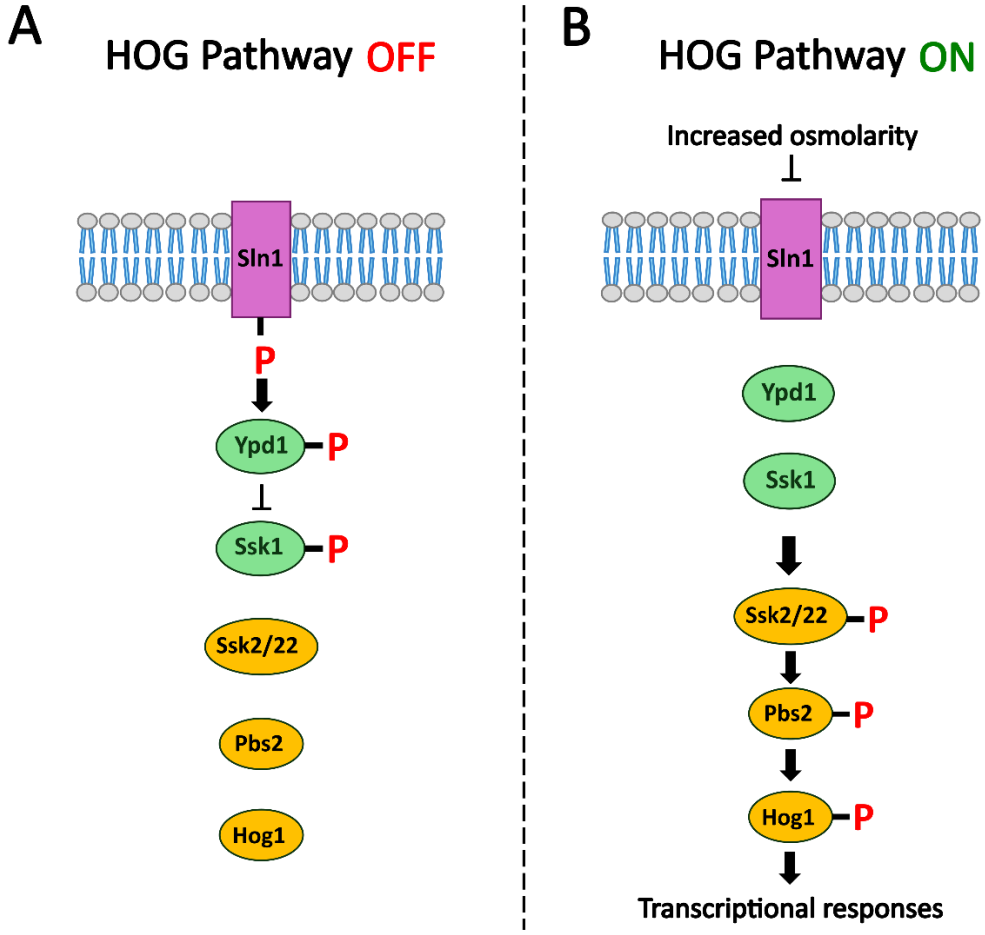

Figure 6.2 – Cartoon depictions of the HOG signal transduction pathway in *S. cerevisiae*. A) Under normal osmotic conditions, Sln1 in the plasma membrane is autophosphorylated and transfers the phosphate to the cytosolic protein Ypd1. Ypd1 then transfers the phosphate to Ssk1, preventing the activation of the downstream components of the HOG pathway. **B)** Under hyperosmotic stress, Sln1 does not undergo autophosphorylation, and the Sln1-Ypd1-Ssk1 phospho-relay is inhibited. Unphosphorylated Ssk1 can then interact with and activate the MAPKKKs Ssk2 and Ssk22, which then phosphorylate the MAPKK Pbs2. Phosphorylated Pbs2 then phosphorylates Hog1, which moves to the nucleus to phosphorylate a range of targets that initiate transcriptional changes, protecting the cell against osmotic stress. In both diagrams, coloured ovals represent proteins. Black arrows indicate the activation of a downstream component in the signalling pathway. Lines with flat ends represent the inhibition of a downstream component in the signalling pathway. Phosphate groups represented as a red letter "P".

heterologously expressing group III HHKs (Motoyama et al., 2005; Lawry et al., 2017; Randhawa et al., 2019). Interestingly, Fludioxonil can hyperactivate the HOG pathway in these strains in the presence of Sln1 (Lawry et al., 2017; Randhawa et al., 2019), meaning that Fludioxonil sensitivity is dominant. Fludioxonil toxicity cannot be explained by the inhibition of the group III HHK, since inhibition would be equivalent to not expressing a group III HHK. Moreover, Fludioxonil cannot increase group III HHK activity, since these kinases negatively regulate the HOG pathway. Instead, the dominance of Fludioxonil sensitivity could be caused by Fludioxonil altering the function of the group III HHK.

A recent study tested whether Fludioxonil converts a group III HHK from a kinase to a phosphatase in *S. cerevisiae*, prompting Ypd1 dephosphorylation and HOG pathway activation (Lawry et al., 2017). This study engendered Fludioxonil sensitivity in *S. cerevisiae* by heterologously expressing the group III HHK *DRK1* (Dimorphism-Regulating Kinase) from the fungal pathogen *Blastomyces dermatitidis* (Lawry et al., 2017). Although evidence in support of this phosphatase model was obtained *in vivo*, Fludioxonil was not found to induce *Bd*Drk1 to dephosphorylate Ypd1 *in vitro* (Lawry et al., 2017). To explain this discrepancy, Lawry et al., (2017) suggested that Fludioxonil does not act directly on *Bd*Drk1, but instead acts upon an upstream target, leading to changes in the intracellular milieu that convert *Bd*Drk1 into a phosphatase. A subsequent study using the same *Bd*Drk1-expressing *S. cerevisiae* strain claimed that this upstream target is triosephosphate isomerase (Tpi1) of the glycolysis pathway (Brandhorst et al., 2019). Fludioxonil was found to interfere with Tpi1 activity *in vitro*, causing it to convert triosephosphate into the toxic aldehyde methylglyoxal (MG), although the Fludioxonil

concentrations required for this effect were much higher than those active *in vivo*. This increase in MG is supposedly sensed by cysteine thiols in *Bd*Drk1, converting it into a phosphatase (Brandhorst et al., 2019) (**Figure 6.3**). Although this model can explain the dominance of Fludioxonil sensitivity, some of the key assumptions were either not tested directly or not supported by *in vivo* evidence. Verifying whether Fludioxonil targets Tpi1 and triggers the release of MG is crucially important, because this possibility has raised concerns about the potential toxicity of Fludioxonil to human cells (Brandhorst et al., 2019; Brandhorst & Klein, 2019).

The aim of this chapter was to identify the drug target and mode of action of Fludioxonil. SATAY was employed to achieve this because it can be readily performed in different genetic backgrounds of *S. cerevisiae* (Michel et al., 2017), and is a powerful approach for unveiling antifungal modes of action (**Chapter 4**; Michel et al., 2019). A transposon library was generated in a Fludioxonil-sensitive, *Bd*Drk1-expressing *S. cerevisiae* strain, and treated with a sub-lethal concentration of Fludioxonil. As expected, transposons disrupting HOG pathway components downstream of *Bd*Drk1 conferred Fludioxonil resistance. However, no evidence was obtained to support the claims that Fludioxonil targets a factor upstream of *Bd*Drk1 and elicits an intracellular stress. This suggests that Fludioxonil directly targets *Bd*Drk1. Following this, an attempt was made to test an alternative model for the dominance of Fludioxonil sensitivity, but ultimately no conclusions could not be drawn about this model's validity.

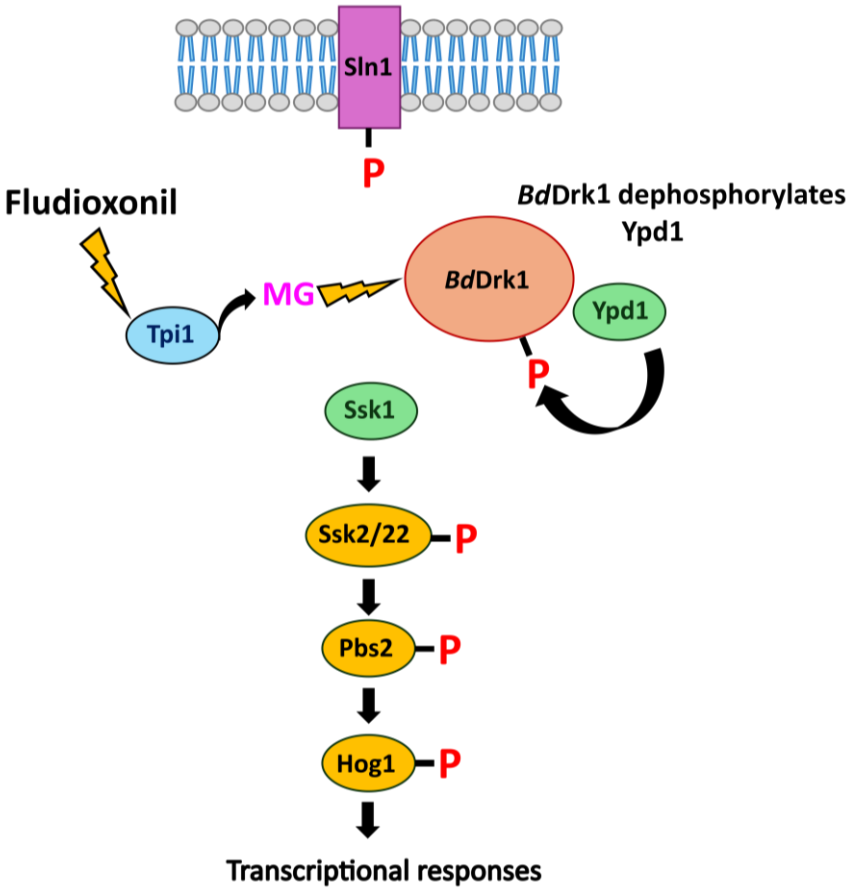

Figure 6.3 – Cartoon depiction of the model of Fludioxonil activity proposed by Brandhorst *et al.*, (2019). Fludioxonil interferes with Tpi1 activity, causing it to release the toxic aldehyde methylglyoxal (MG). MG is then sensed by *Bd*Drk1, converting it from a kinase to a phosphatase. This enables *Bd*Drk1 to dephosphorylate Ypd1, subsequently activating the HOG pathway. Coloured ovals represent proteins. Black arrows indicate the activation of a downstream component in the signalling pathway. Phosphate groups represented as red "P"s.

6.2. Results

6.2.1. *BdDRK1* complements *sln1Δ* in *S. cerevisiae*

Prior to assessing the mode of action of Fludioxonil using SATAY, it was necessary to engineer a strain of *S. cerevisiae* that was heterologously expressing a group III HHK. It was important to ensure the group III HHK was essential for viability to avoid Fludioxonil selecting for transposons disrupting the group III HHK. Previous studies have shown that group III HHKs can complement the *sln1Δ* deletion and perform the essential function of repressing the HOG pathway in normal osmotic conditions (Meena et al., 2010; Randhawa et al., 2016). As such, a strain was constructed in which *SLN1* has been functionally replaced by a group III HHK. The group III HHK *DRK1* from *Blastomyces dermatitidis* was selected because *BdDRK1* expression was previously shown to engender Fludioxonil sensitivity in *S. cerevisiae* (Lawry et al., 2017). Moreover, one of the aims of this study was to assess the model that *Bd*Drk1 activity is modified by a Fludioxonil-induced stress condition (Brandhorst et al., 2019), as opposed to direct binding by Fludioxonil. To verify whether *Bd*Drk1 complements the *sln1Δ* deletion, *BdDRK1* was integrated into the genome of a *SLN1*+/- heterozygote strain, and tetrads from the resulting *SLN1*+/- *BdDRK1*+/- heterozygotes were dissected. Progeny showed a Mendelian meiotic segregation pattern and *BdDRK1* was found to suppress the lethality of the *sln1Δ* deletion (**Figure 6.4**). The *sln1Δ BdDRK1*-expressing strain exhibited a similar growth rate to the *SLN1 BdDRK1*-expressing strain, further indicating that *Bd*Drk1 can functionally replace *SLN1*.

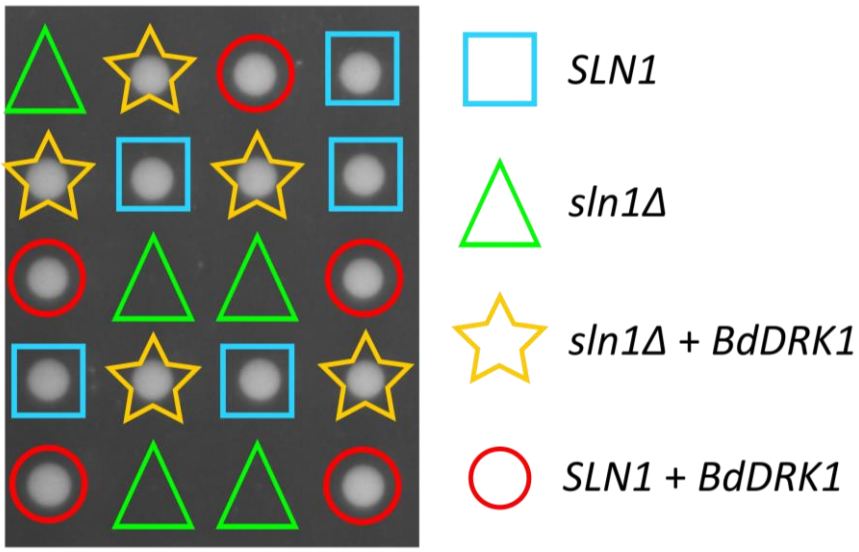

Figure 6.4 – *BdDRK1* complements *sln1Δ* in *S. cerevisiae*. Tetrad dissection of *SLN1+/- BdDRK1*+/- heterozygote on YPD medium. The genotypes of the non-growing spores have been inferred from the genotypes of the growing spores, assuming a Mendelian meiotic segregation pattern. Image was taken after three days of incubation at 30°C.

6.2.2. *BdDRK1* expression engenders Fludioxonil and Iprodione sensitivity in *S. cerevisiae*, and this sensitivity is dominant

Before generating a transposon library in the *sln1Δ BdDRK1*-expressing strain, it was important to verify whether this strain was sensitive to Fludioxonil. Given that Fludioxonil is considered to share the same mode of action as the dicarboximide fungicide Iprodione (Tanaka & Izumitsu, 2010; Fillinger et al., 2012), Iprodione was also included in these assays.

As shown in Figure 6.5, the *BdDRK1*-expressing strains were sensitive to Fludioxonil and Iprodione concentrations of at least 0.1µg/mL and 3µg/mL, respectively. *sln1Δ BdDRK1*-expressing strains exhibited the same level of sensitivity towards Fludioxonil and Iprodione as the *SLN1 BdDRK1*-expressing strains (**Figure 6.5**). Given that Sln1 represses the HOG pathway (Maeda et al., 1994) and Fludioxonil activates the HOG pathway in *SLN1 BdDRK1*-expressing cells (Lawry et al., 2017), these results are consistent with reports that Fludioxonil activates the HOG pathway in a dominant manner (Lawry et al., 2017; Randhawa et al., 2019). It is also noteworthy that the *BdDRK1*-expressing strains exhibited the same sensitivity towards 0.1µg/mL and 10µg/mL Fludioxonil (**Figure 6.5C-D**), suggesting that a maximum level of inhibition was reached at 0.1 µg/mL Fludioxonil. Similar observations could not be made for Iprodione, because this compound had reduced activity (**Figure 6.5E-F**). Nonetheless, the *sln1Δ BdDRK1*-expressing strain was sensitive to Fludioxonil and Iprodione and thus presented a suitable genetic background for the SATAY screen.

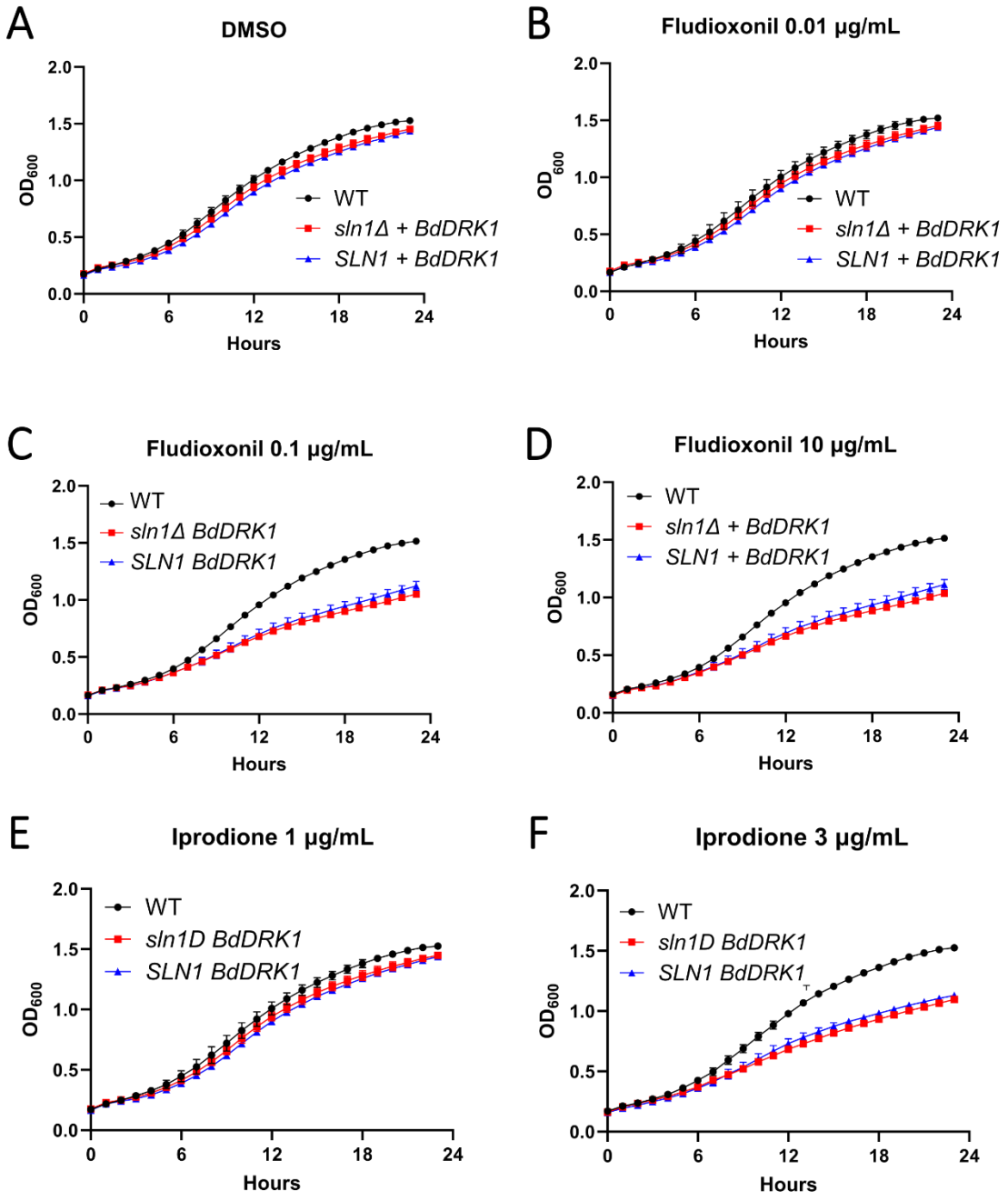

Figure 6.5 – *BdDRK1* expression confers Fludioxonil and Iprodione sensitivity in *S. cerevisiae*. Growth curves of wild-type, *sln1Δ BdDRK1* and *SLN1 BdDRK1* strains in SC 2% glucose medium containing **(A)** 1% DMSO (v/v), **(B)** 0.01 µg/mL Fludioxonil, **(C)** 0.1 µg/mL Fludioxonil, **(D)** 10 µg/mL Fludioxonil, **(E)** 1 µg/mL Iprodione, **(F)** 3 µg/mL Iprodione. OD_{600} measurements were recorded every 20 minutes using a Bioscreen C™ instrument. Each data point is the mean OD_{600} measurement for three independent biological replicates. Error bars show standard error of mean (SEM).

6.2.3. Fludioxonil and Iprodione positively selected transposons that suppress the HOG pathway

A transposon library was generated in the *sln1Δ BdDRK1*-expressing strain and challenged with 0.1µg/mL Fludioxonil or 3µg/mL Iprodione. Expectedly, Fludioxonil and Iprodione very strongly selected transposons in non-essential components of the HOG signalling pathway (**Figure 6.6, Figure 6.7**). This included *SSK1*, which encodes the response regulator of the phosphorelay (Posas et al., 1996), and all the components of the downstream MAPK signalling cascade, namely *SSK2*, *SSK22*, *PBS2* and *HOG1* (Hohmann et al., 2002). In fact, these five genes accounted for 14.3% and 17.9% of all the sequencing reads mapped in the Fludioxonil- and Iprodione-treated transposon libraries, respectively (**Table 6.1**). In contrast, these five genes only comprised 0.06% of the total reads mapped in the DMSO-treated library (**Table 6.1**). All five of these genes are required for the activation of the HOG pathway (Hohmann et al., 2002), consistent with reports that the HOG pathway is activated by Fludioxonil and Iprodione (Zhang et al., 2002; Ochiai et al., 2002). Thus, these findings validate that the screen was working. Additionally, there were no reads mapping to the essential gene *YPD1* (Maeda et al., 1994), and the few insertions mapping to *BdDRK1*, which is essential in the absence of Sln1, had a very low number of reads (**Figure 6.7A**), likely reflecting sick cells that persisted in the library population.

Fludioxonil and Iprodione also positively selected transposons that presumably disrupted the transcriptional reprogramming activities of phosphorylated Hog1. Upon phosphorylation, Hog1 upregulates stress-responsive genes (Posas et al., 2000) by

phosphorylating osmoresponsive transcription factors and recruiting RNA polymerase II, coactivators (Alepuz et al., 2003; Zapater et al., 2007) and chromatin remodelling complexes to stress-response loci (Nadal-Ribelles et al., 2012; Mas et al., 2009; de Nadal et al., 2004; Klopf et al., 2009). Consistently, Fludioxonil and Iprodione positively selected transposons in subunits of the RNA polymerase II holoenzyme (*SSN8*) and mediator complex (*SSN2*, *SRB8*) (**Figure 6.6A-B**). Additionally, there was an enrichment of transposons in subunits of the INO80 chromatin remodelling complex (*IES5*, *NHP10*) (Conaway & Conaway, 2009; Myer & Young, 1998) and in the transcriptional regulator gene *TUP1*, which recruits the SAGA histone acetylase and SWI/SNF nucleosome-remodelling complex to stress-regulated promoters following Hog1 activation (Proft & Struhl, 2002). Thus, these transposon insertions may have suppressed the deleterious downstream effects of HOG pathway hyperactivation on Fludioxonil and Iprodione. The similarity in the genes enriched by Fludioxonil and Iprodione (**Figure 6.6A-B**) also supports claims that these compounds share the same mode of action.

A

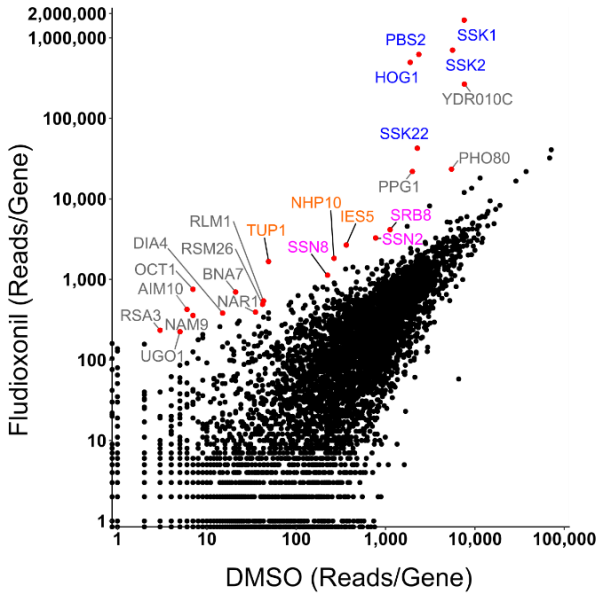

B

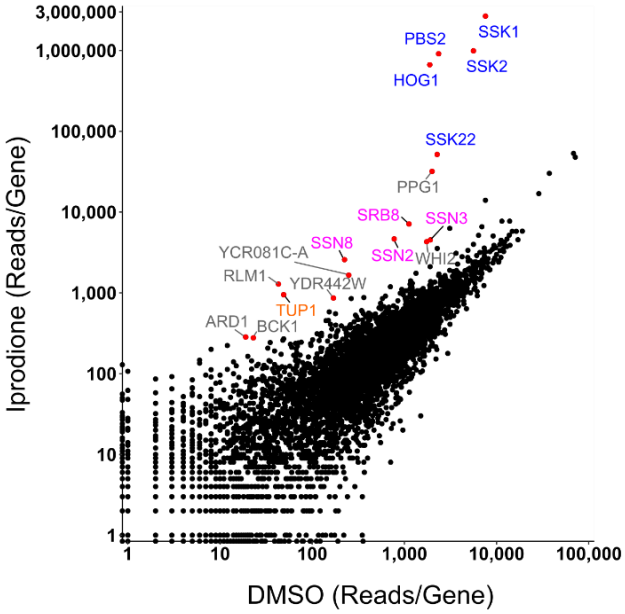

Figure 6.6 – Fludioxonil and Iprodione positively selected transposons that suppress the HOG pathway. Full figure legend is on next page.

Figure 6.6 – Fludioxonil and Iprodione positively selected transposons that suppress the HOG pathway. Scatter plot comparing the number of sequencing reads mapping to each of the 6603 yeast CDSs for a *sln1Δ BdDRK1* transposon library treated with **(A)** Fludioxonil (0.1 µg/mL) or **(B)** Iprodione (3 µg/mL) in SC -LEU 2% glucose medium. Gene names are colour-coded by biological process: blue – HOG signalling pathway, pink – RNA polymerase holoenzyme or mediator complex subunit, orange – chromatin remodelling. Note that *YDR010C* is a dubious open reading frame (ORF) located in the promoter of the drug-efflux pump *SNQ2*. Additional genes containing significantly enriched insertions in the Fludioxonil or Iprodione-treated library are labelled in grey. Genes with a comparable number of reads in each treatment, and thus lying close to the y = x diagonal, are not labelled.

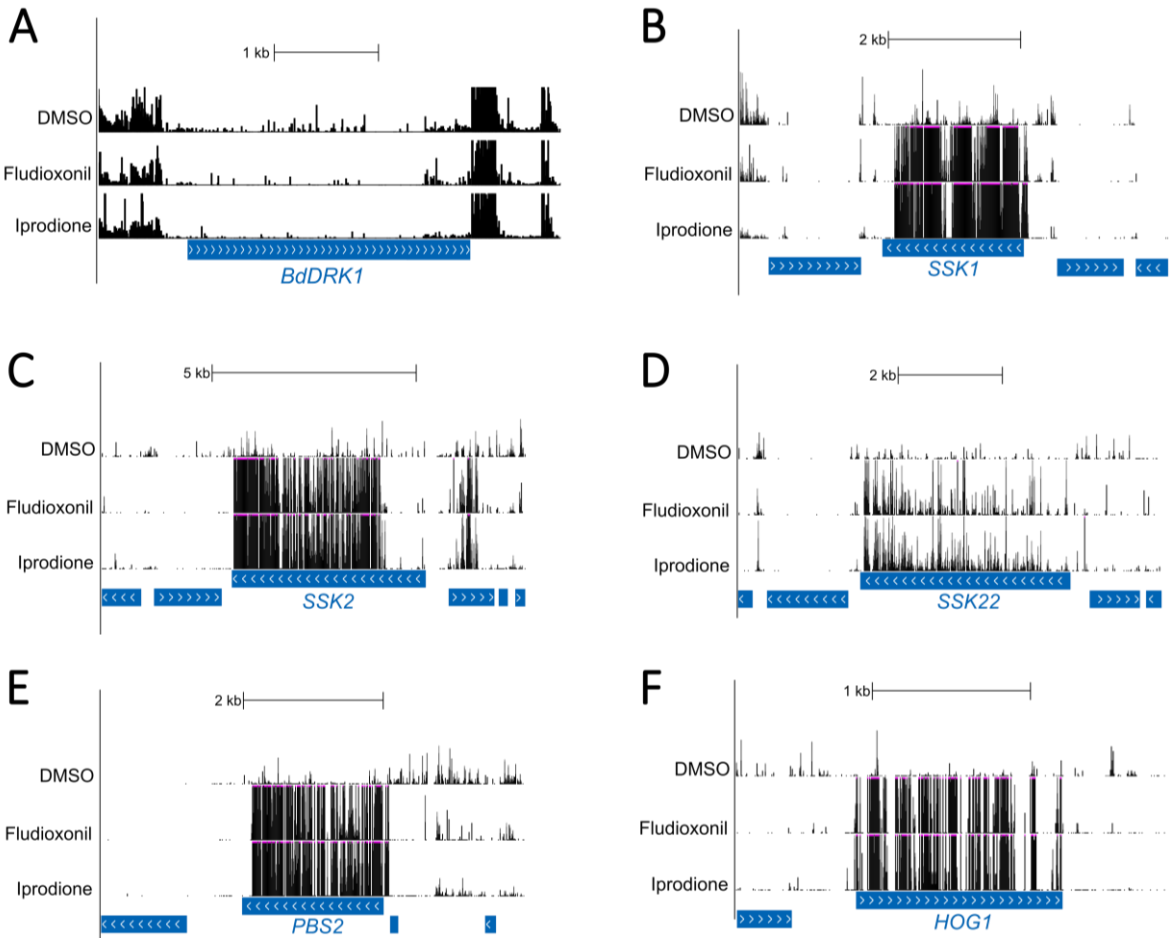

Figure 6.7 – Fludioxonil and Iprodione positively selected transposons inserted into non-essential components of the HOG pathway. Transposon insertion maps for **(A)** *BdDRK1*, **(B)** *SSK1*, **(C)** *SSK2*, **(D)** *SSK22*, **(E)** *PBS2*, **(F)** *HOG1* in the *sln1Δ BdDRK1* transposon library following treatments with 0.03% DMSO (v/v), 0.1 µg/mL Fludioxonil or 3 µg/mL Iprodione in SC -LEU 2% glucose medium. The height of the bars corresponds to the number of sequencing reads and are capped at 500. Blue bars represents CDSs.

	DMSO	Fludioxonil	Iprodione
Number of reads mapped to HOG pathway genes	19,683	3,524,247	5,276,748
Number of reads mapped to the entire genome	33,064,165	24,509,083	29,426,298
% reads mapping to HOG pathway genes	**0.06**	**14.38**	**17.93**

Table 6.1 – Transposons in HOG pathway genes were positively selected by Fludioxonil and Iprodione. Table summarising total number of sequencing reads mapping to HOG pathway genes (*SSK1*, *SSK2*, *SSK22*, *PBS2*, *HOG1*) and to the entire genome in a *sln1Δ BdDRK1* transposon library treated with DMSO (0.03% (v/v), 0.1µg/mL Fludioxonil or 3µg/mL Iprodione. The percentage of reads mapping to the HOG pathway for each treatment was calculated by dividing the total number of reads in the HOG pathway genes by the total number of reads across entire genome, and then multiplied by 100.

6.2.4. Fludioxonil toxicity is unlikely to be elicited by aldehydic stress in *S. cerevisiae*

A previous study has claimed that Fludioxonil interferes with Tpi1, generating an aldehydic stress (methylglyoxal) that triggers *Bd*Drk1 to activate the HOG pathway (Brandhorst et al., 2019). Tpi1 is a glycolytic enzyme that is essential for growth on glucose (Compagno et al., 1996; Compagno et al., 2001). Indeed, *TPI1* was essential in the *sln1Δ BdDRK1*-expressing transposon library grown on glucose (**Figure 6.8A**). Thus, the fitness effects of transposons disrupting *TPI1* on Fludioxonil could not be evaluated by this screen. As such, a reverse genetics approach was undertaken to directly test whether Fludioxonil interferes with Tpi1. To this end, Fludioxonil sensitivity was assessed in *tpi1Δ BdDRK1*-expressing strains in YP 3% ethanol 0.1% galactose medium. This medium was used to feed carbon both upstream (galactose) and downstream (ethanol) of Tpi1 in central carbon metabolism (Compagno et al., 1996; Compagno et al., 2001). Despite using this medium, the growth rates of the *tpi1Δ* deletion mutants were still considerably lower than *TPI1+* strains (**Figure 6.8B**). Nonetheless, it could still be determined that the *tpi1Δ BdDRK1*-expressing strains were sensitive to Fludioxonil (**Figure 6.8B**). This shows that Tpi1 is not required for *Bd*Drk1-mediated Fludioxonil sensitivity.

Brandhorst *et al*., (2019) reported that *Bd*Drk1 activity is altered by a spike in methylglyoxal upon Fludioxonil treatment. In *S. cerevisiae*, the major methylglyoxal detoxification pathway is catalysed by glyoxalase I, which is encoded by the non-essential gene *GLO1* (Inoue & Kimura, 1996). As such, *glo1Δ* mutants are hypersensitive to

methylglyoxal (Inoue & Kimura, 1996). If the model proposed by Brandhorst et al., (2019) was true, transposons inserted into *GLO1* should cause Fludioxonil hypersensitivity. However, transposons in *GLO1* were tolerated on Fludioxonil and Iprodione (**Figure 6.9A**). In validation of these SATAY results, *glo1Δ BdDRK1*-expressing strains were as sensitive to Fludioxonil as *BdDRK1*-expressing strains harbouring wild-type copies of *GLO1* (**Figure 6.9B-C**). This suggests that a spike in cytosolic methylglyoxal does not elicit Fludioxonil toxicity.

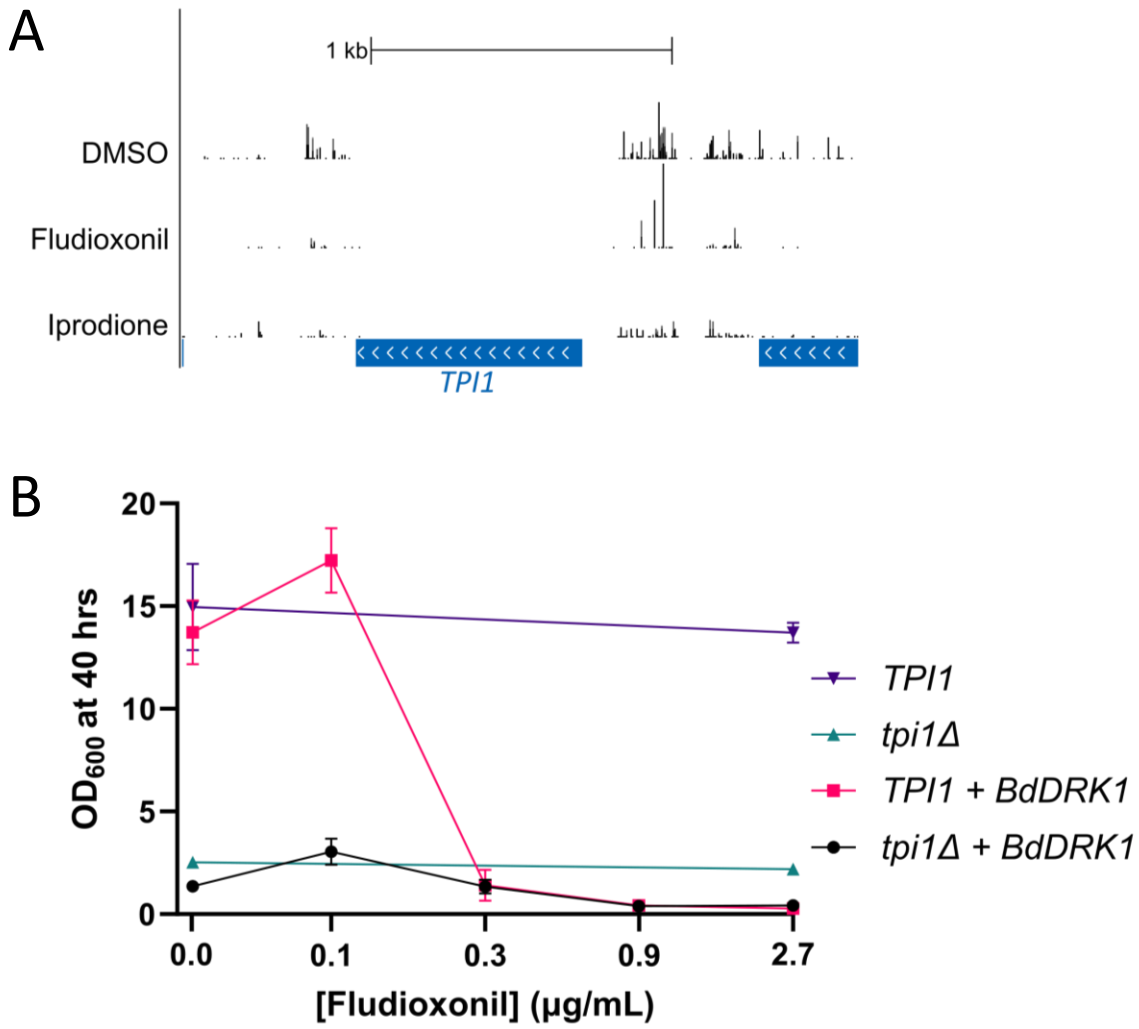

Figure 6.8 – Fludioxonil does not inhibit *BdDRK1*-expressing *S. cerevisiae* cells by interfering with *TPI1*. (A) Transposon map for *TPI1* in the *sln1Δ BdDRK1* transposon library following treatments with 0.03% DMSO (v/v), 0.1 µg/mL Fludioxonil or 3 µg/mL Iprodione in SC -LEU 2% glucose medium. *TPI1* was essential because the library was grown on glucose. The height of the bars corresponds to the number of reads and are capped at 500. Blue bars represent CDSs. **(B)** Growth inhibition curves of progeny derived from a *TPI1*+/- *BdDRK1*+/- heterozygote following treatments with Fludioxonil in YP 3% ethanol 0.1% galactose medium. The starting OD_{600} was 0.05, and end-point OD_{600} measurements were recorded after 40 hours. Each data point is the mean OD_{600} measurement for three independent biological replicates of each genotype. Error bars show SD.

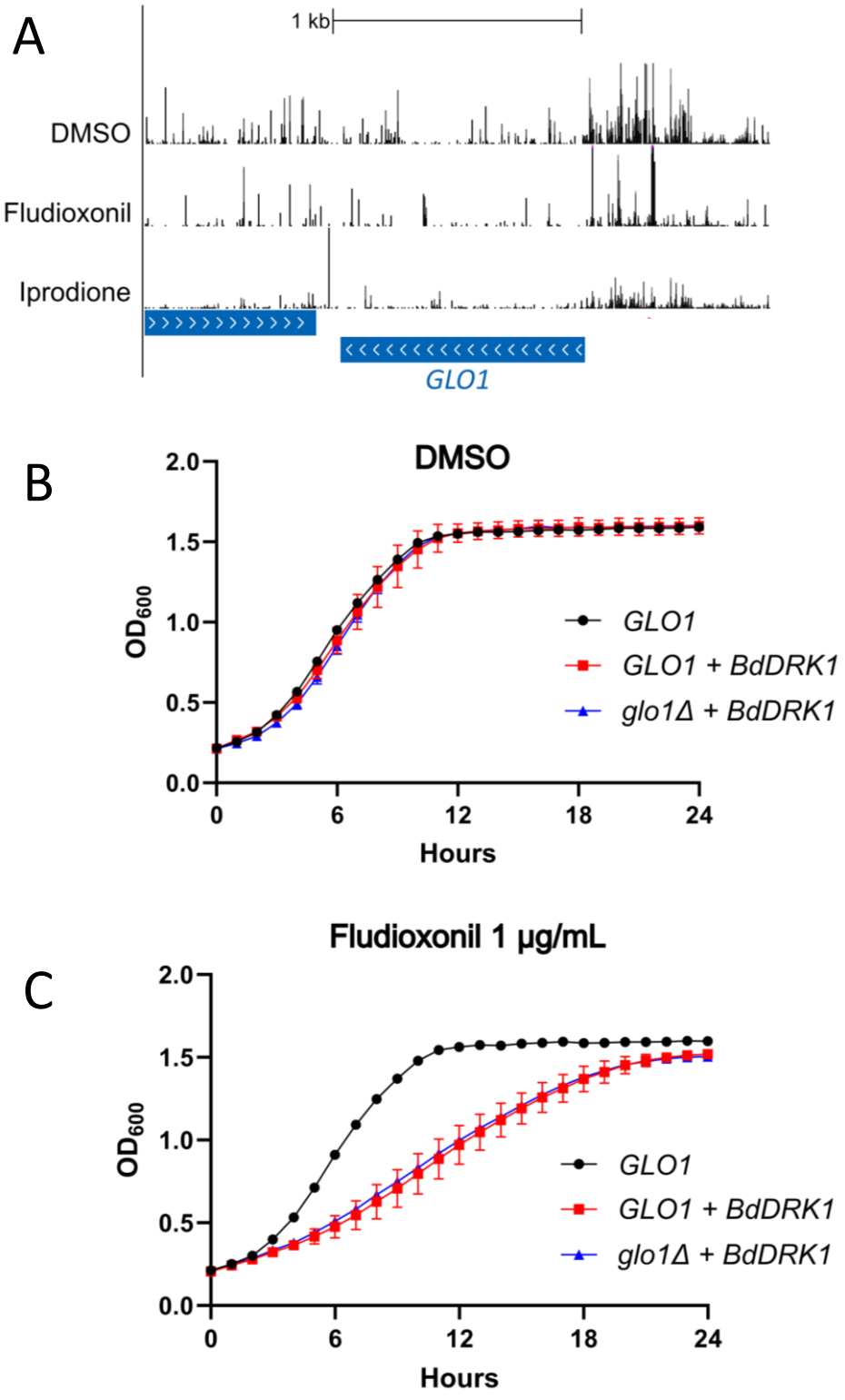

Figure 6.9 – *glo1Δ BdDRK1*-expressing mutants are not hypersensitive to Fludioxonil.

Full figure legend is on next page.

Figure 6.9 – *glo1Δ BdDRK1*-expressing mutants are not hypersensitive to Fludioxonil.

(A) Transposon map for *GLO1* in the *sln1Δ BdDRK1* transposon library following treatments with 0.03% DMSO (v/v), 0.1 µg/mL Fludioxonil or 3 µg/mL Iprodione in SC - LEU 2% glucose medium. Transposon insertions in *GLO1* were tolerated on Fludioxonil and Iprodione. The height of the bars corresponds to the number of reads and are capped at 500. Blue bars represent CDSs.

(B) Growth curves of wild-type, *glo1Δ BdDRK1* and *GLO1 BdDRK1* strains in YPD medium containing 0.004% (v/v) DMSO. OD_{600} measurements were recorded every 20 minutes using a Bioscreen C™ instrument. Each data point is the mean OD_{600} measurement for three independent biological replicates. Error bars show standard error of mean (SEM).

(C) As in **(B)** in YPD containing 1 µg/mL Fludioxonil.

6.2.5. An attempt to determine whether *Bd*Drk1 sequesters Ypd1 away from Sln1

The SATAY screen revealed that Fludioxonil susceptibility is primarily engendered by the HOG pathway in *BdDRK1*-expressing cells. Importantly, the screen did not identify any potential targets for Fludioxonil upstream of *Bd*Drk1. This suggests that Fludioxonil activates the HOG pathway by acting directly on *Bd*Drk1. In addition, this and previous studies (Lawry et al., 2017; Randhawa et al., 2019) have shown that Fludioxonil is toxic to *BdDRK1*-expressing cells containing wild-type copies of *SLN1* (**Figure 6.5**). This dominance of *Bd*Drk1-mediated Fludioxonil sensitivity is incompatible with Fludioxonil simply inhibiting *Bd*Drk1. Instead, Fludioxonil must change *Bd*Drk1 activity, leading to HOG pathway activation. For instance, Fludioxonil may directly induce *Bd*Drk1 to dephosphorylate Ypd1. This model was suggested previously (Lawry et al., 2017), but was not supported by *in vitro* experiments. Alternatively, Fludioxonil might induce *Bd*Drk1 to phosphorylate Ypd1 on a different residue besides the histidine (H64) phosphoacceptor (Posas et al., 1996). This alternative phosphorylation site could interfere with the otherwise stable interaction between Ypd1 and phosphorylated Ssk1, which is necessary for repressing the HOG pathway (Janiak-Spens et al., 2000). A third possibility is that Fludioxonil-inhibited *Bd*Drk1 fails to phosphorylate Ypd1 but remains tightly bound to it, preventing Ypd1 phosphorylation by Sln1. This model, hereafter referred to as the "Ypd1 sequestration model" (**Figure 6.10**) seemed plausible because *Bd*Drk1 is expressed from a strong heterogenous promoter, and the depletion of Ypd1 is known to inappropriately activate the HOG pathway (Dexter et al., 2015). Moreover, this

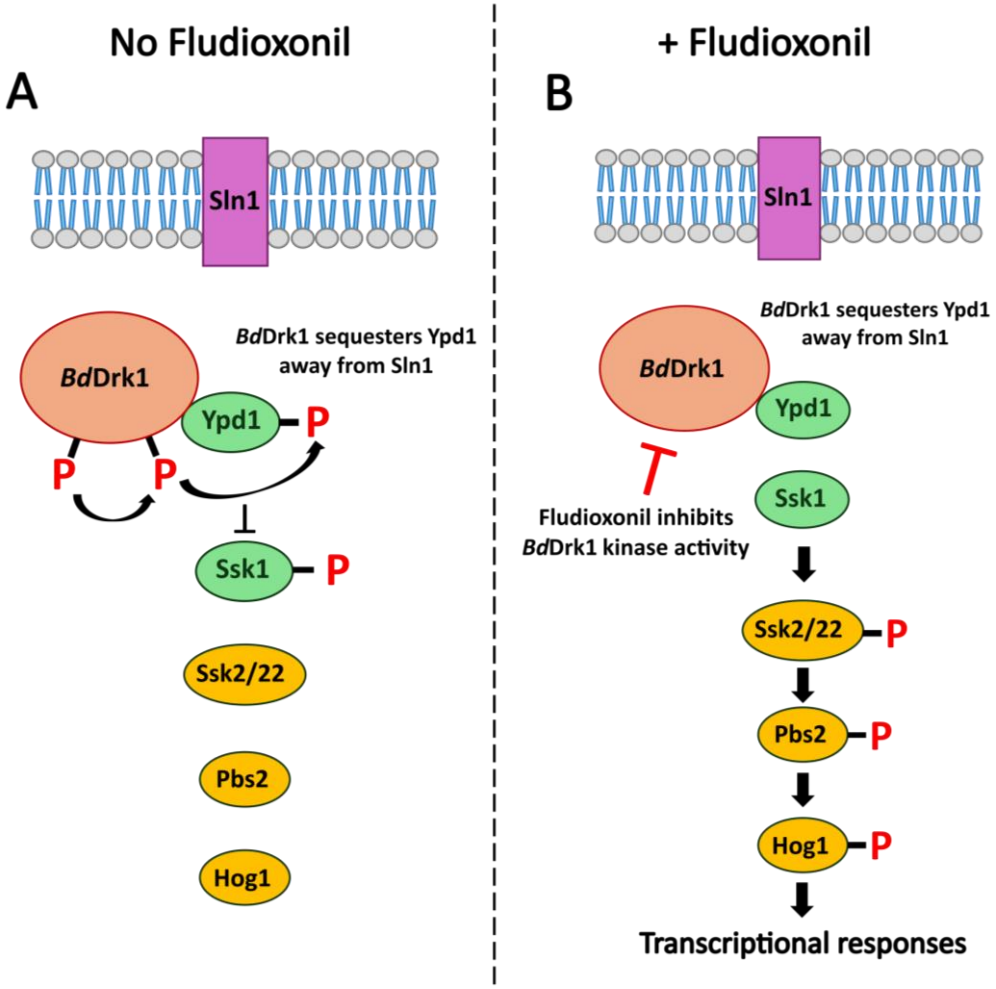

Figure 6.10 – Cartoon depiction of the Ypd1 sequestration model for Fludioxonil's mechanism of activity. A) In the absence of Fludioxonil, *Bd*Drk1 binds tightly to Ypd1, preventing it from interacting with and becoming phosphorylated by Sln1. *Bd*Drk1 still phosphorylates Ypd1, which then phosphorylates Ssk1, keeping the HOG pathway switched off. **B)** Fludioxonil directly inhibits kinase activity of *Bd*Drk1. Since *Bd*Drk1 sequesters Ypd1 away from Sln1, Ypd1 is not phosphorylated, leading to HOG pathway activation. In both diagrams, coloured ovals represent proteins. Black arrows indicate the activation of a downstream component in the signalling pathway. Lines with flat ends represent the inhibition of a downstream component in the signalling pathway. Phosphate groups represented as a red letter "P".

model appeared more straightforward to test than the other two models, because *in vitro* assays did not seem necessary.

If the Ypd1 sequestration model is correct, then the expression of kinase-defective variants of *Bd*Drk1 should be lethal, akin to inhibiting *Bd*Drk1 with Fludioxonil. The histidine kinase activity of *Bd*Drk1 is critically dependent on a conserved histidine residue at position 716 (H716) in the histidine kinase domain (Chaves et al., 2016) and a conserved aspartate residue at position 1140 (D1140) in the receiver domain (Lawry et al., 2017) (**Figure 6.11**). Thus, to ablate the kinase activity of *Bd*Drk1, the following point mutations were individually introduced into plasmid-borne copies of *BdDRK1*: H716A, H716Q, D1140A. On each plasmid, *BdDRK1* expression was under the control of a galactose-inducible promoter. A wild-type strain of *S. cerevisiae* was transformed with one of four 2μ/*URA3* plasmids bearing either *BdDRK1* WT, *BdDRK1* H716A, *BdDRK1* H716Q or *BdDRK1* D1140N. Plasmid transformants were streaked onto SC -URA medium containing glucose or galactose. All the transformants were viable on glucose (**Figure 6.12A**) and galactose (**Figure 6.12B**). The viability of the strains expressing kinase-defective *Bd*Drk1 on galactose suggests that *Bd*Drk1 does not sequester Ypd1 away from Sln1. Additionally, strains encoding kinase-defective *Bd*Drk1 were insensitive to Fludioxonil (**Figure 6.12C**). This suggests that both the histidine kinase and response receiver domains of *Bd*Drk1 are required for Fludioxonil sensitivity.

However, this experiment alone is not sufficient to falsify the Ypd1 sequestration model. Indeed, to validate these findings, it is necessary to show that the kinase-defective

*Bd*Drk1 proteins are stably expressed and can still bind Ypd1. At this point, I decided not to pursue the Ypd1 sequestration model further, because the core aim of this chapter was to use SATAY to identify the target of Fludioxonil, and I decided to prioritise more promising leads described in other chapters of this thesis.

The question of whether Fludioxonil directly targets *Bd*Drk1 now requires *in vitro* assays. These assays would allow the direct effect of Fludioxonil on *Bd*Drk1 activity to be studied in the absence of other cellular factors and metabolites such as methylglyoxal. In December 2023, my collaborators at Syngenta attempted *in vitro* kinase assays with *Bd*Drk1 recombinantly expressed in *E. coli* in the presence of Fludioxonil. These attempts failed due to the poor quality of the *Bd*Drk1 purification (Andy Corran, personal communication). Syngenta are going to repeat the assay with new purifications of *Bd*Drk1 in late 2024. These purifications will be made using yeast strains that I have engineered to express *Bd*Drk1 tagged with GFP, AviTag and 8XHIS. I have validated that this construct can functionally replace Sln1 and engender Fludioxonil sensitivity, thereby confirming that the tagged *Bd*Drk1 protein is functional. In late 2024, Syngenta will also perform Surface Plasmon Resonance (SPR) experiments with the new *Bd*Drk1 purifications to test whether Fludioxonil directly binds to *Bd*Drk1.

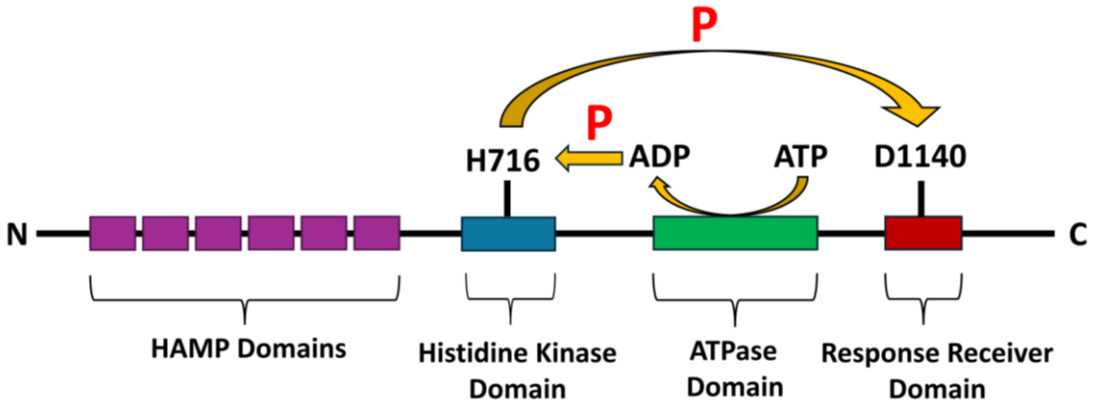

Figure 6.11 – Schematic representation of the internal phosphorylation reactions in *Bd*Drk1. In response to a stimulus, ATP is hydrolysed to ADP and P_i by the ATPase domain. The P_i then phosphorylates the conserved histidine residue (H716) in histidine kinase domain. The phosphate is then transferred to a conserved aspartate residue (D1140) in the response receiver domain prior to transfer to Ypd1.

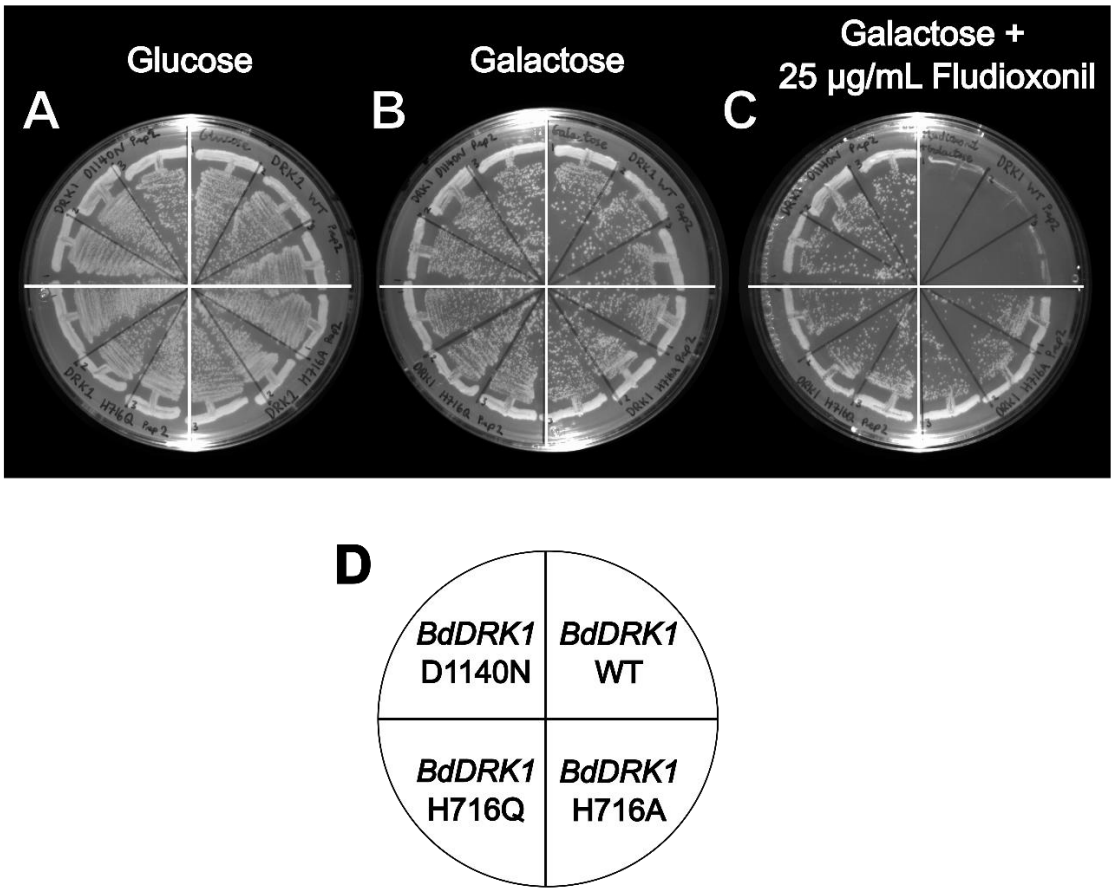

Figure 6.12 – *SLN1+* strains expressing kinase-defective *Bd*Drk1 proteins are viable. *SLN1*+ strain of *S. cerevisiae* (ByK831) transformed with CEN/*URA3* plasmids containing a galactose-inducible promoter to drive the expression of either *BdDRK1* WT, *BdDRK1* H716A, *BdDRK1* H716Q or *BdDRK1* D1140N. Three independent transformants for each plasmid were streaked onto SC -URA medium containing **(A)** 2% glucose **(B)** 2% galactose or **(C)** 2% galactose and 25 µg/mL Fludioxonil. The positions of the strains on each plate are indicated in **(D)**. Images were taken after three days of growth at 30°C.

6.3. Discussion

6.3.1. SATAY indicates that Fludioxonil directly targets *Bd*Drk1

In this chapter, SATAY was utilised to identify genes modulating Fludioxonil sensitivity. This work was undertaken because recent reports have suggested that Fludioxonil does not directly target group III HHKs, but instead acts on an upstream factor(s) (Lawry et al., 2017; Brandhorst et al., 2019). However, the SATAY screen revealed that Fludioxonil sensitivity is solely dependent on the HOG pathway, and no targets upstream of *Bd*Drk1 were identified. This suggests that Fludioxonil acts directly on *Bd*Drk1. The SATAY screen also disputed the claim that Fludioxonil causes a spike in cytosolic methylglyoxal (Brandhorst et al., 2019), because Fludioxonil did not negatively select transposons in *GLO1*, which encodes the enzyme that detoxifies methylglyoxal (Inoue et al., 1996). Moreover, a reverse genetics approach disproved the claim of Brandhorst et al., (2019) that Fludioxonil interferes with Tpi1. Indeed, *tpi1Δ BdDRK1*-expressing strains remained sensitive to Fludioxonil, showing that *TPI1* is not required for Fludioxonil sensitivity.

The SATAY screen does not, however, rule out the possibility that Fludioxonil targets an essential gene whose product acts upstream of *Bd*Drk1. Such a target could not have been directly identified using SATAY, because transposons disrupting essential genes are lethal. Having said that, if this situation does occur, transposons would likely have been positively or negatively selected in non-essential genes that act in the same pathway, or in compensatory pathways. Haploinsufficiency profiling (HIP) could be utilised to test whether Fludioxonil targets an essential gene (Giaever et al., 2004; Hoepfner et al.,

2014). To adapt this approach for screening Fludioxonil, each strain in the collection would need to be transformed with *BdDRK1*, or another group III HHK. If Fludioxonil does target an essential gene, then the corresponding heterozygote might be either resistant or sensitive, depending on how such a factor affects *Bd*Drk1.

6.3.2. The mechanism underpinning the dominance of Fludioxonil sensitivity remains enigmatic

This study confirms that Fludioxonil is toxic to *BdDRK1*-expressing cells even when they harbour wild-type copies of *SLN1*. This shows that *Bd*Drk1-mediated Fludioxonil sensitivity is dominant. Models of Fludioxonil's mode of action must reconcile this dominant activity with the observations, made using SATAY, that Fludioxonil appears to act directly upon *Bd*Drk1. Using this, three potential models for Fludioxonil's mode of action were described:

1) Fludioxonil induces *Bd*Drk1 to dephosphorylate Ypd1. This was proposed by Lawry et al., (2017), based on the observed reversibility of the phosphotransfer reaction *in vivo*, but lacks supporting *in vitro* data.
2) Fludioxonil induces *Bd*Drk1 to phosphorylate Ypd1 on a different residue besides the histidine phosphoacceptor. This unconventional model is nonetheless consistent with the fact that both H716 and D1140 on *Bd*Drk1 are necessary for Fludioxonil sensitivity.
3) The Ypd1 sequestration model: Fludioxonil-inhibited *Bd*Drk1 fails to phosphorylate Ypd1 but remains tightly bound to it, preventing Sln1-mediated Ypd1 phosphorylation. This model is consistent with the fact *Bd*Drk1 is expressed

from a strong promoter, and depletions in Ypd1 are known to inappropriately activate the Hog1 pathway.

Attempts at testing the first model using *in vitro* assays were unsuccessful. Collaborators at Syngenta have experienced significant challenges when attempting *Bd*Drk1 recombinant expression and purification (Andy Corran, personal communication). I briefly tested whether Fludioxonil induces *Bd*Drk1 to dephosphorylate Ypd1 *in vivo* by analysing protein extracts from *slnΔ BdDRK1* cells using Phos-tag gel electrophoresis, which separates proteins based on their phosphorylation pattern (O'Donoghue & Smolenski, 2022). However, no phosphorylated band for Ypd1 was detected in untreated control samples (data not shown), presumably because phosphohistidine groups are highly labile (Kalagiri et al., 2021) and were lost from Ypd1 during the protein extraction.

The second model could be assessed by analysing Ypd1 phosphorylation sites using tandem mass spectrometry (Dephoure et al., 2013). Alternatively, isoelectric focusing (IEF) could be used, which separates proteins according to their isoelectric point (Anderson et al., 2008). IEF can readily detect different phosphorylated forms of proteins, since each additional phosphate increases the negative charge on a protein. IEF may therefore allow the identification of Ypd1 proteins bearing additional phosphorylated residues in Fludioxonil-treated *Bd*Drk1-expressing cells. However, the lability of the phosphohistidine on Ypd1 will likely also pose challenges for these experiments (Dephoure et al., 2013). Additional phosphorylation events on Ypd1 might alter the conformation of this protein, interfering with its interaction with Ssk1, which is

necessary for repressing the HOG pathway (Janiak-Spens et al., 2000). It is also possible that such events might alter the subcellular localisation of this protein, which normally shuttles between the cytoplasm and the nucleus (Lu et al., 2003). If these events cause Ypd1 to accumulate in the nucleus, then this might reduce interactions with Ssk1 in the cytoplasm, and hence inappropriately activate the HOG pathway.

A brief attempt was made to test the Ypd1 sequestration model. Contrary to the predictions of this model, *SLN1+* strains expressing kinase-defective mutants of *Bd*Drk1 were viable. However, these findings alone do not invalidate the Ypd1 sequestration model, since it was unclear whether the kinase-defective *Bd*Drk1 proteins were stably expressed and could still bind Ypd1. To check for stable expression, the kinase-defective *Bd*Drk1 proteins could be tagged and quantified by western blotting. Yeast two-hybrid assays or co-immunoprecipitation could be performed to verify whether the kinase-defective *Bd*Drk1 proteins can bind Ypd1. If the Ypd1 model is indeed incorrect, then this would suggest that Fludioxonil directly alters the kinase activity of *Bd*Drk1.

There are most likely additional models that could be proposed to explain the dominance of Fludioxonil activity. It would, however, be more efficient to confirm the validity of the three aforementioned models before making detailed considerations about alternative possibilities.

Identifying the mode of action of Fludioxonil is in the fundamental interests of the fungicide research community, and to Syngenta in particular, because Fludioxonil is a highly successful fungicide (Kilani & Fillinger, 2016), and the constitutive activation of a

signalling pathway is a rare, and academically intriguing, mode of action. Understanding this mechanism could inform the design of new compounds that could replicate Fludioxonil's success. Syngenta are therefore in the process of attempting *in vitro* assays to determine whether Fludioxonil directly interacts with *Bd*Drk1. The outcome of these tests will not be known until after this thesis is submitted, but if successful, these tests would bring clarity and a renewed sense of direction to future Fludioxonil research efforts.

Chapter 7 – Chitosan electrostatically interacts with cell wall mannosylphosphate

7.1. Introduction

Chitosan is a natural polysaccharide derived from the deacetylation of chitin (Kong et al., 2010). Chitosan has garnered significant attention from the agricultural and biomedical research communities because it has broad-spectrum antimicrobial activity against bacteria and fungi, is biodegradable, biocompatible, and inexpensive to produce from readily available resources (Muzzarelli et al., 2012; Ke et al., 2021). Chitosan can control many economically important fungal phytopathogens, including *Fusarium oxysporum* (Benhamou, 1992), *Botrytis cinerea* (Ben-Shalom et al., 2003), *Rhizopus stolonifer* (El Ghaouth, 1992) and *Colletotrichum gloeosporioides* (Bautista-Banos et al., 2003). Chitosan is also an effective elicitor of plant defence reactions, which further prevent the onset of fungal infections (Bautista-Banos et al., 2006). For these reasons, Chitosan is sold commercially as an agrochemical fungicide (Sharathchandra et al., 2004). Moreover, Chitosan has potential as a clinical antifungal because it can inhibit the growth of human fungal pathogens, including *Candida spp*. (Alburquenque et al., 2010; Garcia et al., 2018) and *Cryptococcus neoformans* (Martinez et al., 2010).

The antimicrobial activity of Chitosan is pH-dependent (Ke et al., 2021). Indeed, Chitosan is only soluble in dilute aqueous acidic solutions below its pKa (~6.3), in which the amino groups are protonated (**Figure 7.1**). In this polycationic form, Chitosan interacts electrostatically with negative charges on the cell surfaces of bacteria and fungi, thereby

increasing membrane permeability and causing metabolite leakage (Helander et al., 2001; Liu et al., 2004; Mellegård et al., 2011; Palma-Guerrero et al., 2010; Palmeira-de-Oliveira et al., 2011; Raafat et al., 2008; Tayel et al., 2010; Tsai & Su, 1999). However, the exact mechanisms underlying Chitosan's antifungal activity are not fully understood (Shih et al., 2019; Li et al., 2022). For example, the specific targets for Chitosan on the surface of fungal cells have not been identified, and it is unclear how this interaction leads to membrane permeability and metabolite leakage (Ma et al., 2017). Advancing our understanding of Chitosan's mode of action is critical for optimising this compound's use and for developing effective resistance management strategies.

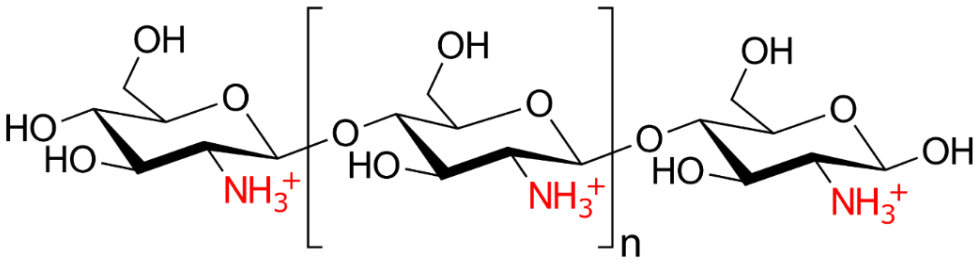

Figure 7.1 – Chemical structure of Chitosan. Protonated amino groups are shown in red.

Despite having a broad antimicrobial spectrum (Goy et al., 2009; Ke et al., 2021), Chitosan has minimal activity against widely used *S. cerevisiae* strains derived from the laboratory strain S288C (Zakrzewska et al., 2005; Zakrzewska et al., 2007; Jaime et al., 2012). As yeast deletion collections are only available in the S288C genetic background (Winzeler et al., 1999; Giaever et al., 2002), chemogenomic studies using yeast deletion

collections have evaluated Chitosan's mode of action at high concentrations (Zakrzewska et al., 2007; Jaime et al., 2012; Marquez et al., 2013), potentially limiting the physiological and agricultural relevance of these screens. Thus, our understanding of Chitosan's mode of action would be improved by a chemogenomic screen performed with a Chitosan-sensitive strain of *S. cerevisiae*.

SATAY can perform genome-wide screens in diverse genetic backgrounds of *S. cerevisiae* (Michel et al., 2017; Chen et al., 2022). This chapter takes advantage of this possibility by performing SATAY in a Chitosan-sensitive, non-conventional strain of *S. cerevisiae*. This SATAY screen led to the discovery that Chitosan electrostatically interacts with mannosylphosphate groups incorporated into mannan chains on cell wall proteins. Cell wall mannosylphosphate was thus identified as a major determinant of Chitosan sensitivity in *S. cerevisiae*. Attempts to determine whether this also applies for the fungal phytopathogen *Botrytis cinerea* were ultimately inconclusive. In summary, this chapter uncovers a mode of action for Chitosan against fungal cells and demonstrates the potential of using SATAY in non-conventional genetic backgrounds of yeast for revealing antifungal modes of action.

7.2. Results

7.2.1. A yeast strain called AD1-8 was sensitive to Chitosan

Prior to using SATAY to assess Chitosan's mode of action, it was necessary to identify a Chitosan-sensitive strain of *S. cerevisiae*. Chitosan susceptibility tests were performed on five strains, four of which were PDR-attenuated (**Table 7.1**) (**Chapter 3, Table 3.1**). Chitosan susceptibility was only observed for the PDR-attenuated strain AD1-8. AD1-8 is derived from a non-conventional strain called US50-18C and lacks seven ABC transporters and the transcription factor *PDR3* (Decottignies et al., 1998). Notably, the PDR-attenuated strains derived from S288C, which lack the same ABC transporters as AD1-8 (**Chapter 2, Table 2.1**), were resistant to Chitosan, indicating that AD1-8's Chitosan sensitivity was not attributable to the disruption of the PDR network, but to unknown characteristics of the US50-18C background. Thus, AD1-8 was selected for the SATAY screen.

Strain	Chitosan MIC (µg/mL)	Parent
BY4741 (ByK352)	**> 500**	**S288C**
AD1-8 (ByK1174)	**5**	**US50-18C**
12geneΔ0HSR (ByK1151)	**> 500**	**S288C**
BY4743Δ8a (ByK1230)	**> 500**	**S288C**
ABC16 Monster (ByK1266)	**> 500**	**S288C**

Table 7.1 – Yeast strain AD1-8 was sensitive to Chitosan. Minimal Inhibitory Concentrations (MICs) of Chitosan for five strains of *S. cerevisiae*. MICs were determined after 24 hours of growth in SC 2% glucose medium. All strains contained deletions in multiple ABC transporters, except for the BY4741 strain ByK352.

7.2.2. Chitosan positively selected transposons in genes involved in the mannosylation of N-linked glycans or intra-Golgi retrograde transport

A transposon library was generated in AD1-8 and challenged with 2 μg/mL Chitosan, and the corresponding acetic acid control (**Chapter 3, Table 3.2**). Chitosan positively selected transposons in genes involved with the mannosylation of N-linked glycans on cell wall proteins, or intra-Golgi retrograde transport (**Figure 7.2A**). Indeed, the 40 genes with the highest number of reads in the Chitosan-treated library were significantly overrepresented by the GO terms "glycoprotein biosynthetic process" and "Golgi vesicle transport" (**Table 7.2**). In *S. cerevisiae*, there are two distinct types of N-linked glycans, both of which are synthesised by Golgi-localised mannosyltransferases. One is a "core-type" structure comprising 10-14 mannose residues and is found on intracellular glycoproteins. The other consists of a large, branched polymer of approximately 200 mannose residues, and is attached to proteins destined for the cell wall and periplasmic space (Munro, 2001; Orlean, 2012). Many of the genes involved in the synthesis and modification of this latter structure contained transposons that were positively selected by Chitosan, namely *ANP1*, *HOC1*, *MNN2*, *MNN4*, *MNN5*, *MNN6* and *MNN11* (**Figure 7.2A**). Additionally, Chitosan positively selected transposons in *GDA1* and *YND1*, which encode homologous Golgi-localised nucleoside phosphatases (Berninsone et al., 1994; Gao et al., 1999). Gda1 and Ynd1 are required for the transport of GDP-mannose into the Golgi lumen, where it is utilised as the mannose donor for mannosylation (Orlean, 2012). Furthermore, Chitosan positively selected transposons in the CDS of *SMF2* (**Figure 7.2A**), which encodes a manganese ion (Mn^{2+}) transporter necessary for the delivery of Mn^{2+} to the Golgi (Luk & Culotta, 2001). Consistently, Mn^{2+} is a critical cofactor for Ynd1

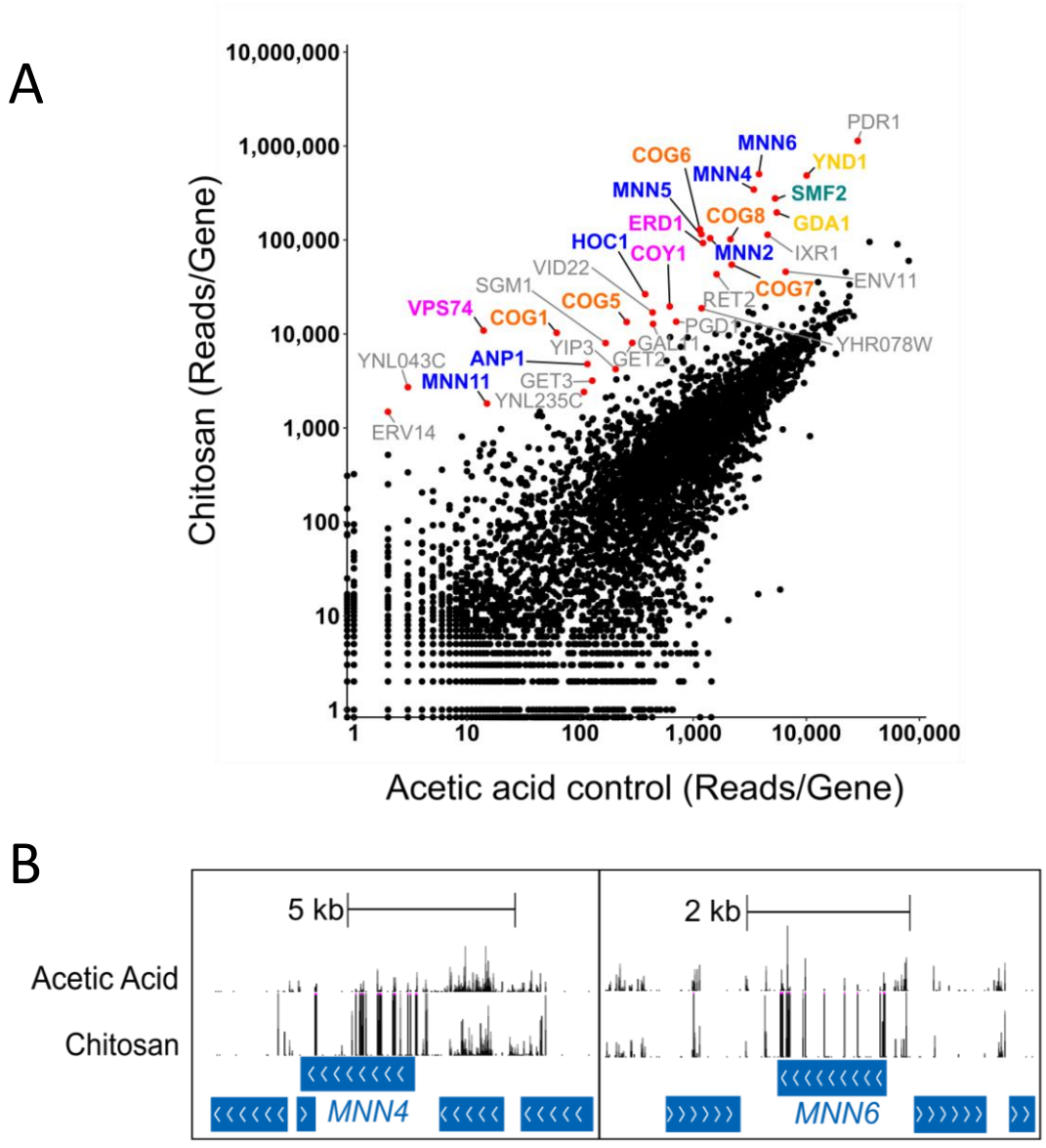

Figure 7.2 - Chitosan positively selected transposons in genes involved with the mannosylation of N-linked glycans or intra-Golgi retrograde transport. Full figure legend is on the next page.

Figure 7.2 - Chitosan positively selected transposons in genes involved with the mannosylation of N-linked glycans or intra-Golgi retrograde transport.

A) Scatter plot comparing the number of sequencing reads mapping to each of the 6603 yeast CDSs for an AD1-8 transposon library treated with acetic acid (0.0004%) versus Chitosan (2 µg/mL). An acetic acid control was required because Chitosan was solubilised in acetic acid (Methods 2.6.2). Gene names are colour-coded by biological process: blue – mannan chain elaboration on N-linked glycans of cell wall proteins; orange - COG complex subunits; pink – intra-Golgi retrograde transport; yellow – nucleoside phosphatases for Golgi import of GDP-mannose; teal - manganese transport. Additional genes containing significantly enriched insertions in the Chitosan-treated library are labelled in grey. Genes with a comparable number of reads in each treatment, and thus lying close to the y = x diagonal, are not labelled.

B) Transposon insertion maps for *MNN4* and *MNN6* in the AD1-8 transposon library following treatments with acetic acid (0.0004%) and Chitosan (2 µg/mL). The height of the bars corresponds to the number of sequencing reads and is capped at 2,000. Blue bars represent CDSs.

Gene Ontology term	GO ID	Cluster frequency	Corrected *p*-value	Genes annotated to the term
Golgi vesicle transport	GO:0048193	15 of 40 genes, 37.5%	2.47E-11	*SEC28, VPS74, COG1, COG7, GET2, COG6, YIP3, ERV14, RET2, COG5, KTR6, ERD1, GET3, COG8, COY1*
Glycoprotein biosynthetic process	GO:0009101	10 of 40 genes, 25.0%	8.57E-10	*ERD1, KTR6, HOC1, ANP1, YND1, MNN2, MNN4, MNN5, GDA1, MNN11*

Table 7.2 – Gene Ontology analysis results of the 40 genes containing the highest number of reads in the AD1-8 transposon library following Chitosan treatment. Only the two most significantly enriched Gene Ontology terms are displayed. *p*-values were corrected using the Holm-Bonferroni method.

and Golgi-localised mannosyltransferases (Gao et al., 1999; Kuhn et al., 1991). Finally, there was a significant enrichment of transposons in *VPS74*, *ERD1*, *COY1* and five of the eight subunits of the conserved oligomeric Golgi (COG) complex (**Figure 7.2A**). These genes are required for intra-Golgi retrograde transport (Schmitz et al., 2008; Smith & Lupashin, 2008; Hsu et al., 2013; Anderson et al., 2017; Sardana et al., 2021) which recycles glycosyltransferases from *trans*-Golgi to *cis/medial*-Golgi compartments, thereby maintaining their steady-state distribution. This is critical for ensuring that the distinct steps of glycosylation occur in the correct sequential order. Consequently, loss-of-function mutations impairing intra-Golgi retrograde transport are associated with glycosylation defects (Bruinsma et al., 2004; Anderson et al., 2017; Schmitz et al., 2008; Sardana et al., 2021). Thus, the SATAY screen strongly indicated that Chitosan sensitivity in AD1-8 is engendered by the mannosylation of N-linked glycans on proteins destined for the cell wall. Given that mannan chains form the outermost layer of the yeast cell wall (Osumi, 1998; Zlotnik et al., 1984), these findings were consistent with reports that Chitosan interacts with the fungal cell wall (Li et al., 2022; Tayel et al., 2010).

In *S. cerevisiae*, cell wall mannans are modified with phosphate groups. This process, called mannosylphosphorylation, confers a net negative charge to the cell wall, altering the properties and environment of the yeast cell surface (Karson & Ballou, 1978). Given that Chitosan is polycationic (Ke et al., 2021), I hypothesised that Chitosan might electrostatically interact with mannosylphosphate groups on the cell wall of AD1-8. This hypothesis was supported by multiple findings in the SATAY screen. First, the genes required for mannosylphosphate transfer, *MNN4* (Odani et al., 1996) and *MNN6* (Karson

& Ballou, 1978; Wang et al., 1997), were among the top-hits in the Chitosan-treated transposon library (**Figure 7.2A,B**). This implied that the loss of mannosylphosphate was particularly beneficial for Chitosan-treated cells. Second, Chitosan positively selected transposons in several genes that function upstream of *MNN4* and *MNN6* in the mannosylation pathway, specifically *ANP1*, *MNN11*, *HOC1*, *MNN2* and *MNN5* (**Figure 7.2A**). These upstream genes are epistatic to *MNN4* and *MNN6*, because they are essential for the synthesis of α1,2-linked mannose side branches, which are the sole substrates of Mnn4 and Mnn6 (Karson & Ballou, 1978; Orlean, 2012). As such, mutants lacking these acceptor side branches are devoid of cell wall mannosylphosphate (Karson & Ballou, 1978). Third, Chitosan positively selected transposons in the promoter region of *MNN1*, and negatively selected transposons in the CDS of this gene (**Figure 7.3A,B**). Mnn1 adds terminal α1,3-linked mannose residues to α1,2-linked mannose side chains acceptor sites (Karson & Ballou, 1978). Thus, *MNN1* overexpression could have tipped this competition in favour of α1,3-linked mannose, and conferred Chitosan resistance by reducing the density of negative charges on the surface of AD1-8. Taken together, the SATAY screen indicated that Chitosan may target mannosylphosphate groups on the cell wall of AD1-8.

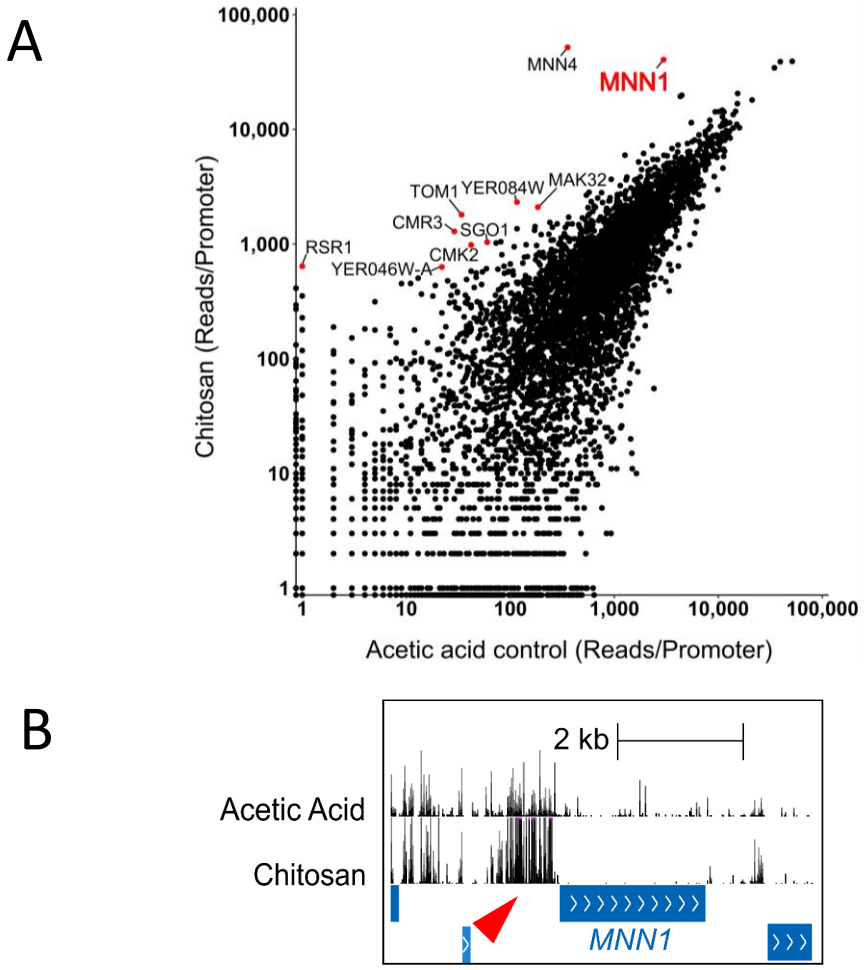

Figure 7.3 – Chitosan positively selected transposons in the promoter of *MNN1*.

A) Scatter plot comparing the number of sequencing reads mapping to promoter regions in an AD1-8 transposon library treated with acetic acid (0.0004%) versus Chitosan (2 µg/mL) in SC -ADE 2% glucose medium. Promoters were defined as the 200 bp upstream of the translation start sites. *MNN1* is coloured red. Note that positively selected insertions in the promoter of *MNN4* were likely interfering with the expression of this gene.

B) Transposon insertion maps for *MNN1* for the acetic acid- and Chitosan-treated AD1-8 libraries. Heights of the bars correspond to the number of reads and are capped at 2,000. Red arrowheads indicate positively selected insertions in the promoter of *MNN1*.

7.2.3. Chitosan susceptibility correlated with the amount of cell wall mannosylphosphate

Mnn4 positively regulates mannosylphosphorylation in *S. cerevisiae* (Odani et al., 1996). As such, *MNN4* deletion mutants have significantly lower levels of mannosylphosphate on N-linked glycans (Karson & Ballou, 1978; Odani et al., 1996). Consistent with mannosylphosphate engendering Chitosan sensitivity, AD1-8 *mnn4Δ* mutants were significantly less susceptible to Chitosan than AD1-8 WT cells (**Figure 7.4A**). Indeed, the MIC of Chitosan for AD1-8 *mnn4Δ* mutants was between 100-200 µg/mL, whereas AD1-8 WT cells were inhibited by 5 µg/mL. These strains were not sensitive to the acetic acid concentrations found within each Chitosan treatment (**Figure 7.4B**).

Alcian blue is a cationic, phthalocyanine dye that can distinguish between yeast cells with different amounts of mannosylphosphate (Ballou, 1990). I therefore tested whether Chitosan sensitivity correlated with alcian blue staining. Since mannosylphosphorylation occurs during stationary phase (Odani et al., 1997), alcian blue staining was performed on saturated cultures of AD1-8 WT, AD1-8 *mnn4Δ* and the S288C-derived strain ByK352**.** Quantifications of alcian blue staining intensity were performed on images displayed in the red channel because alcian blue strongly absorbs red light. As shown in **Figure 7.5A-B**, AD1-8 WT cells were strongly stained by alcian blue, whereas AD1-8 *mnn4Δ* mutants did not bind the dye. ByK352 also failed to bind alcian blue, despite being *MNN4+*. These findings support the hypothesis that Chitosan electrostatically interacts with cell wall mannosylphosphate (**Figure 7.6**).

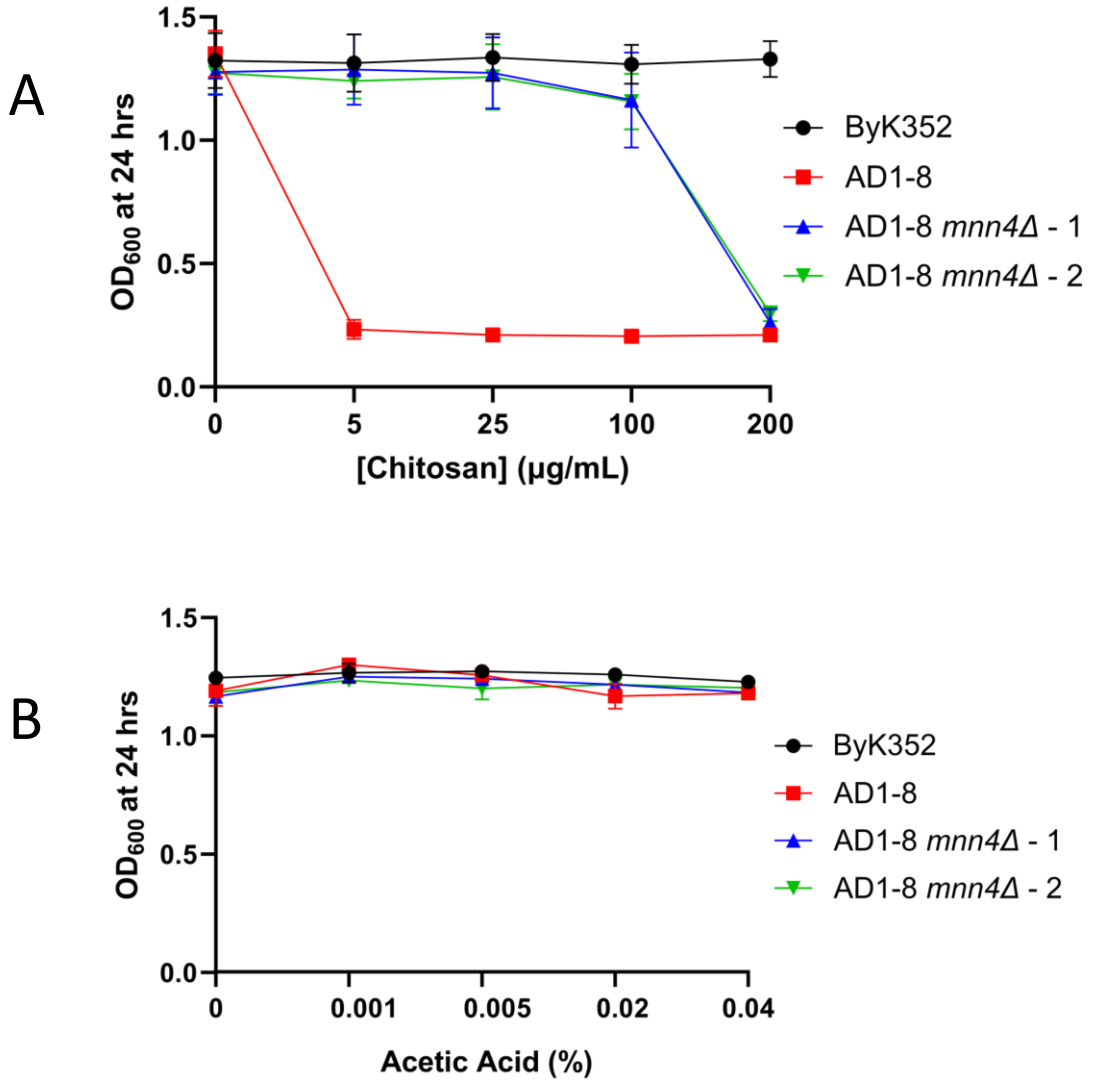

Figure 7.4 – AD1-8 *mnn4Δ* mutants were resistant to Chitosan. Growth inhibition curves of ByK352 (S288C-dervied strain), AD1-8 WT, and two independent AD1-8 *mnn4Δ* mutants treated with **(A)** Chitosan or **(B)** acetic acid in SC 2% glucose medium. Acetic acid concentrations (% v/v) correspond to those in each Chitosan treatment (i.e. 200 µg/mL Chitosan contained 0.04% acetic acid). OD_{600} measurements were recorded using a Bioscreen C™ instrument. Each data point is the mean OD_{600} measurement for three technical replicates. Error bars show standard deviation (SD). Error bars for some data points were too small to be displayed.

A

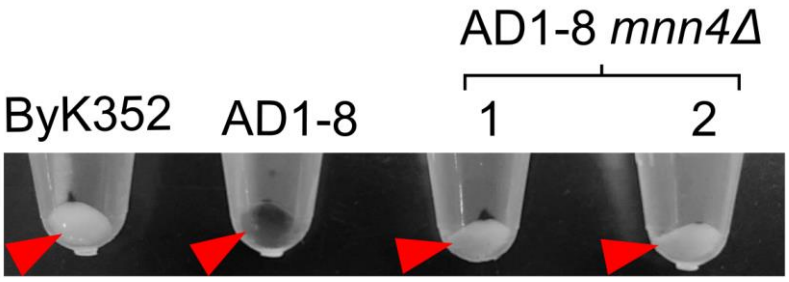

B

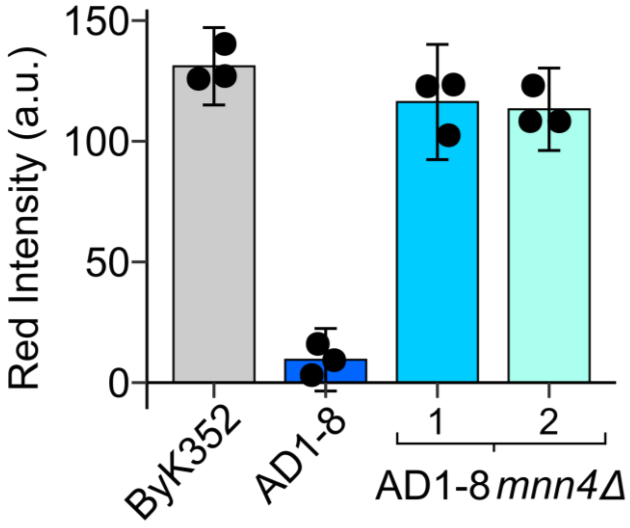

Figure 7.5 – Alcian blue staining reveals that AD1-8 has a high density of cell wall mannosylphosphate.

A) Cell pellets of ByK352, AD1-8 WT, and two independent AD1-8 *mnn4Δ* mutants stained with alcian blue. Saturated cultures were treated with 10 µg/mL alcian blue for 3 minutes in SC 2% glucose medium. Image is displayed in the red channel to highlight the staining differences, because alcian blue strongly absorbs red light. Red arrowheads indicate cell pellets.

B) Quantification of background-subtracted red channel intensity of alcian blue stained pellets of ByK352, AD1-8 WT, and two independent AD1-8 *mnn4Δ* mutants. Three technical replicates for each strain. Error bars show standard deviation.

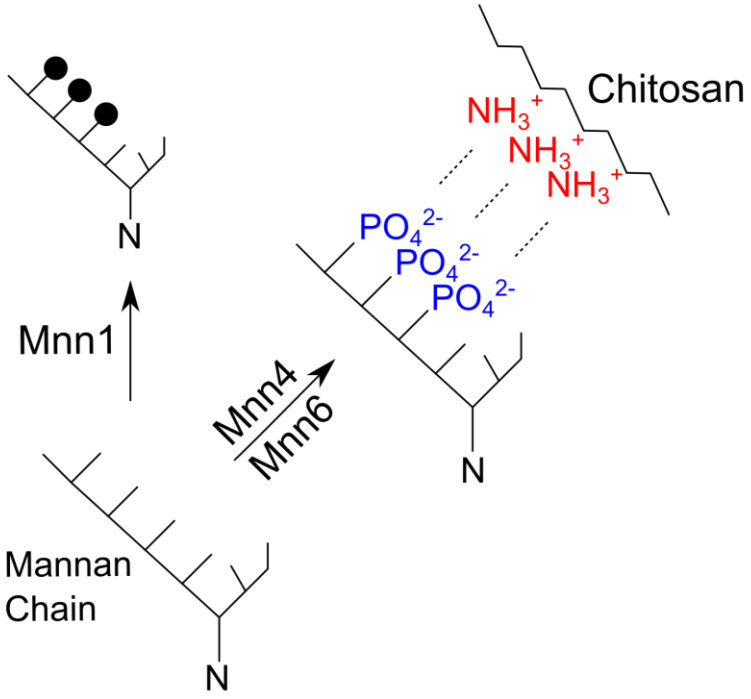

Figure 7.6 - Model for Chitosan binding to the yeast cell wall. Model depicts electrostatic interactions (black dashes) between Chitosan's positively charged amino groups (red) and negatively charged mannosylphosphate groups (blue) on an N-linked glycan chain. Mannosylphosphate groups are added onto α1,2-linked mannose side branches by the mannosylphosphate transferases Mnn4 and Mnn6. Meanwhile, Mnn1 adds terminal α1,3-linked mannose residues (black circles) to α1,2-linked mannose side chains. Terminal α1,3-linked mannose residues compete with mannosylphosphate groups for available α1,2-linked mannose acceptor sites. *MNN1* overexpression in AD1-8 likely conferred Chitosan resistance by tipping this competition towards non-phosphorylated α1,3-linked mannose residues.

7.2.4. Chitosan binds to mannosylphosphate groups on the cell wall of AD1-8

To assess whether Chitosan interacts with cell wall mannosylphosphate, live imaging experiments were performed with stationary phase AD1-8 WT, AD1-8 *mnn4Δ* and ByK352 cells treated with fluorescein-labelled Chitosan. To directly compare the fluorescence staining intensities of the strains on the same images, strains were mixed pairwise in same tube after staining and then imaged. The strains were distinguishable because only one strain received a pre-treatment with the unrelated vital stain, MitoTracker, which stains active mitochondria. Fluorescein-labelled Chitosan strongly stained the cell walls of AD1-8 WT cells but failed to bind the cell walls of either the AD1-8 *mnn4Δ* mutants (**Figure 7.7A**) or ByK352 (**Figure 7.7B**). It was verified that this failure to bind fluorescein-labelled Chitosan was not due to MitoTracker staining (**Figure 7.7A,B**). This shows that Chitosan binds to mannosylphosphate groups on the cell wall of AD1-8 WT cells. As such, Chitosan resistance in AD1-8 *mnn4Δ* and ByK352 cells can be explained by the fact Chitosan hardly binds the cell walls of these strains.

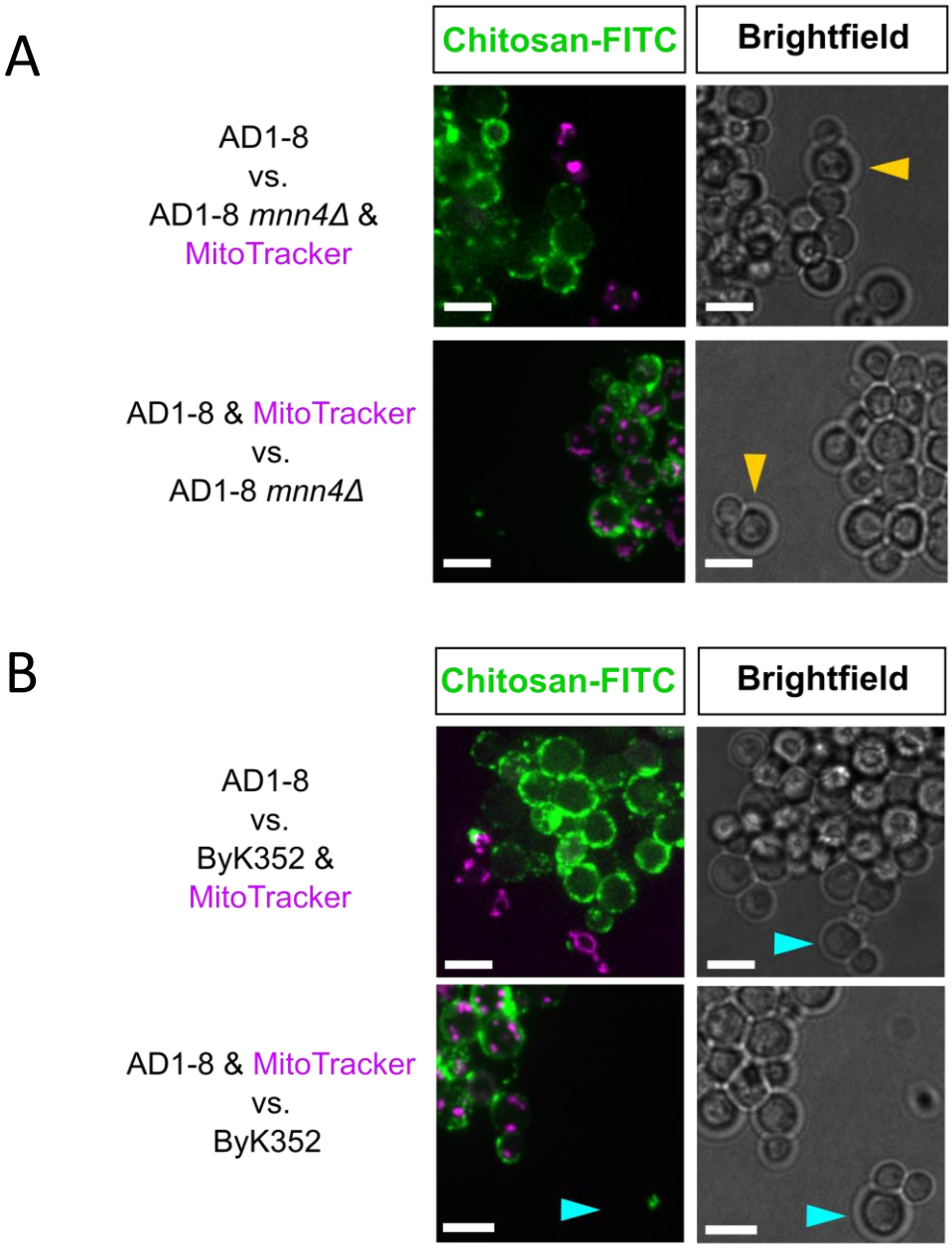

Figure 7.7 – Chitosan binds to mannosylphosphate residues on the cell wall of AD1-8. Full figure legend is on next page.

Figure 7.7 – Chitosan binds to mannosylphosphate on the cell wall of AD1-8.

A) Representative images of AD1-8 wild-type and AD1-8 *mnn4Δ* cells following treatment with 25 µg/mL Chitosan Fluorescein (green) for 2 hours in SC 2% glucose medium. Cells were treated in stationary phase. MitoTracker (magenta) was applied at 0.1 µM. Yellow arrowheads indicate representative AD1-8 *mnn4Δ* cells. Images are Z-stacks. Scale bars represent 5 µm.

B) As in **(A)**, for representative images of AD1-8 wild-type and ByK352 (S288C-derived strain) cells. Blue arrowheads indicate representative AD1-8 *mnn4Δ* cells.

7.2.5. Chitosan resistance in the S288C-derived strain ByK352 is a polygenic trait

Chitosan sensitivity in AD1-8 is underpinned by mannosylphosphorylation, which is mediated by Mnn4 (Odani et al., 1996) and Mnn6 (Karson & Ballou, 1978; Wang et al., 1997). Given that the S288C-derived strain ByK352 supposedly harbours wild-type copies of *MNN4* and *MNN6*, it was surprising that this strain lacks mannosylphosphate.

A brief attempt was made to pinpoint the gene(s) responsible for Chitosan resistance in ByK352 by crossing ByK352 to AD1-8. The resulting diploid was sporulated and the progeny from eight tetrads were individually assessed for Chitosan sensitivity and alcian blue staining. The progeny showed a direct correlation between alcian blue staining and Chitosan sensitivity, further demonstrating the importance of cell wall mannosylphosphate for Chitosan activity (**Figure 7.8**). However, the observed segregation patterns revealed that alcian blue staining and Chitosan sensitivity were inherited in a complex Mendelian polygenic fashion (**Figure 7.8**). This indicates that Chitosan resistance in ByK352 is determined by at least three genes. Moreover, the AD1-8 x ByK352 diploid was resistant to Chitosan (**Figure 7.9**), revealing that Chitosan resistance was a dominant trait. This ruled out the possibility that ByK352 contains non-functional copies of *MNN4* and/or *MNN6*, because this would be a recessive trait. Given the complex polygenic nature of Chitosan resistance in ByK352, and the core aim of this chapter of identifying the mode of action of Chitosan, the genetic basis for Chitosan resistance in this strain was not pursued further.

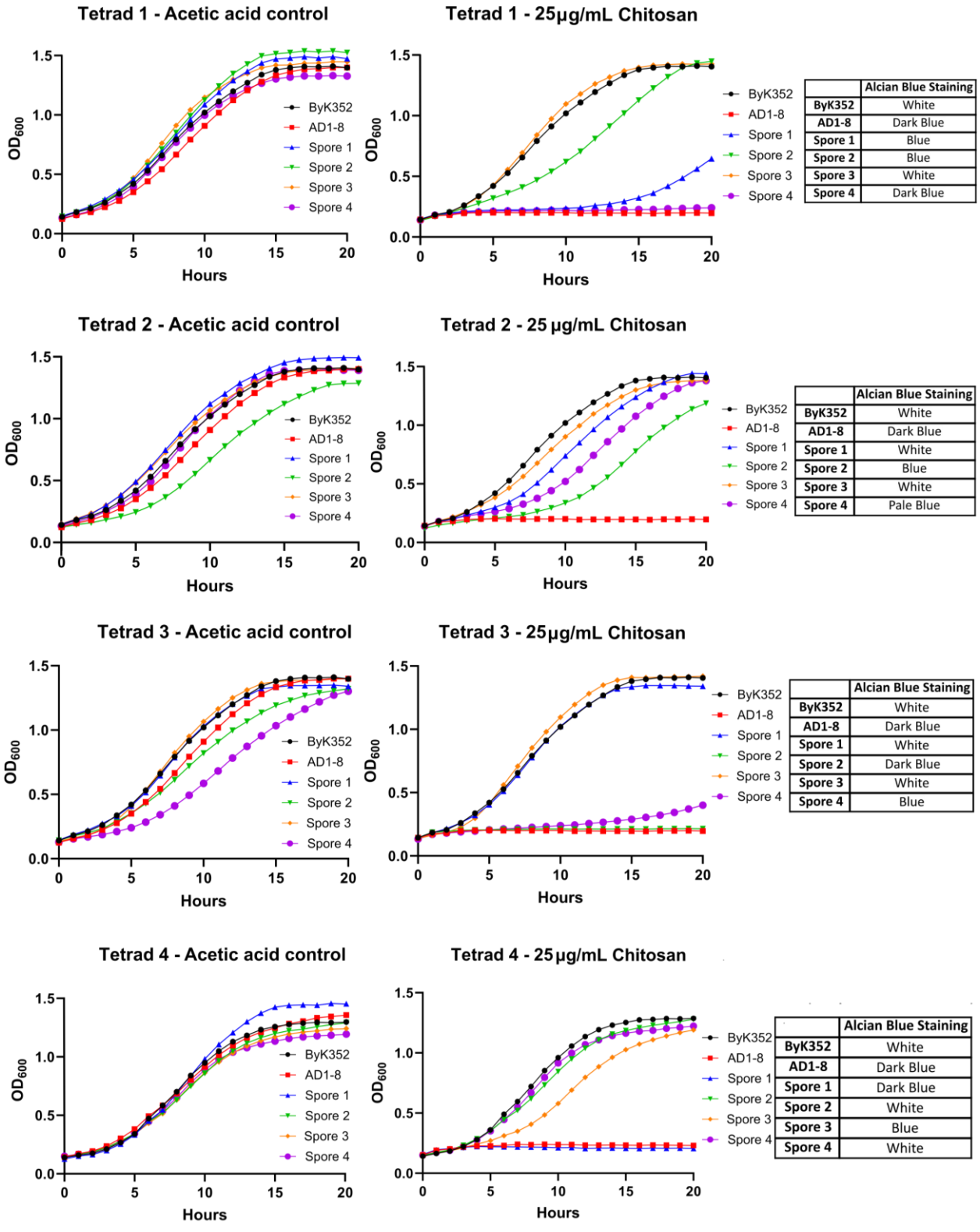

	Alcian Blue Staining
ByK352	White
AD1-8	Dark Blue
Spore 1	Blue
Spore 2	Blue
Spore 3	White
Spore 4	Dark Blue

	Alcian Blue Staining
ByK352	White
AD1-8	Dark Blue
Spore 1	White
Spore 2	Blue
Spore 3	White
Spore 4	Pale Blue

	Alcian Blue Staining
ByK352	White
AD1-8	Dark Blue
Spore 1	White
Spore 2	Dark Blue
Spore 3	White
Spore 4	Blue

	Alcian Blue Staining
ByK352	White
AD1-8	Dark Blue
Spore 1	Dark Blue
Spore 2	White
Spore 3	Blue
Spore 4	White

Figure 7.8 – Chitosan resistance in ByK352 is a polygenic trait. Full figure legend is two pages over.

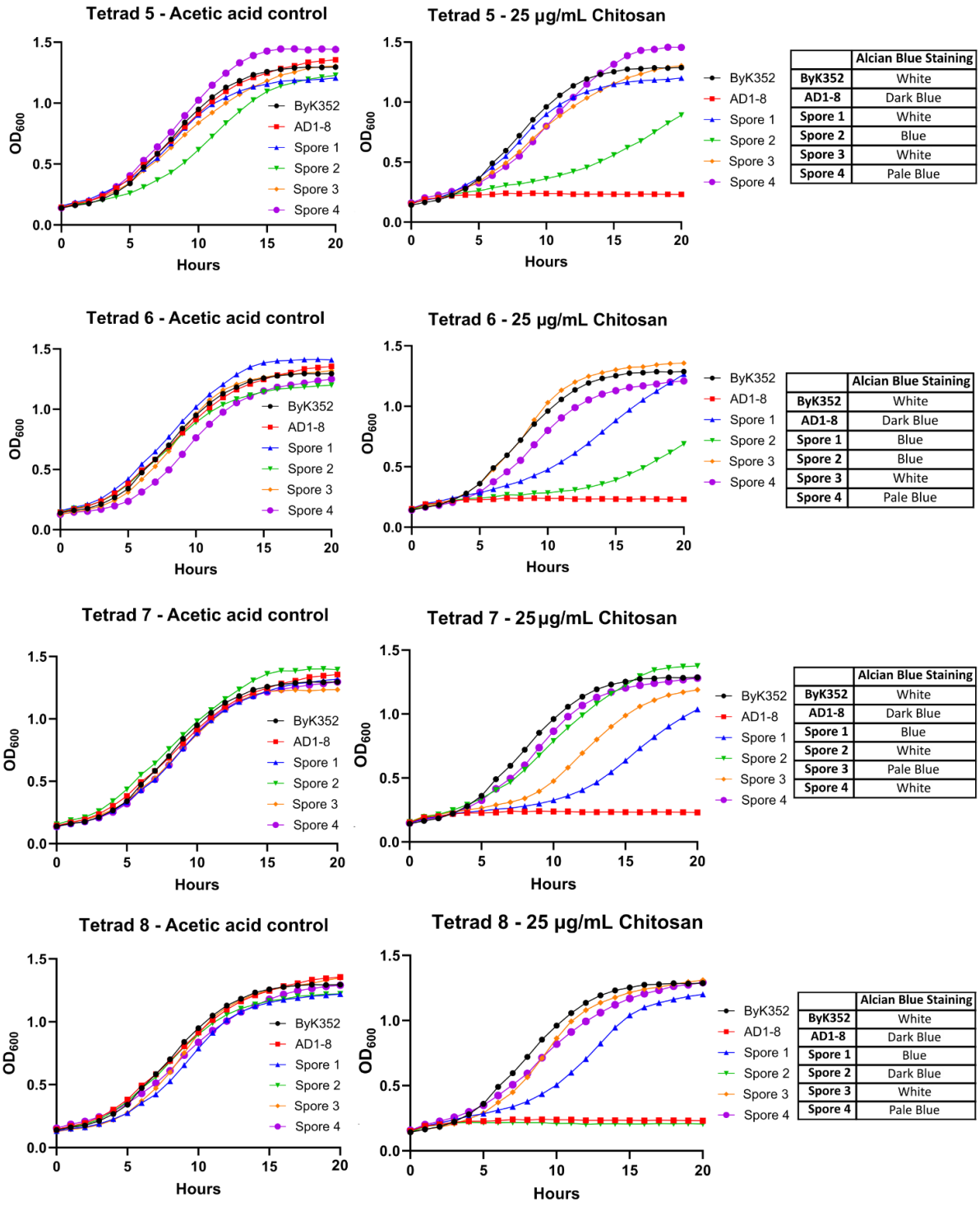

	Alcian Blue Staining
ByK352	White
AD1-8	Dark Blue
Spore 1	White
Spore 2	Blue
Spore 3	White
Spore 4	Pale Blue

	Alcian Blue Staining
ByK352	White
AD1-8	Dark Blue
Spore 1	Blue
Spore 2	Blue
Spore 3	White
Spore 4	Pale Blue

	Alcian Blue Staining
ByK352	White
AD1-8	Dark Blue
Spore 1	Blue
Spore 2	White
Spore 3	Pale Blue
Spore 4	White

	Alcian Blue Staining
ByK352	White
AD1-8	Dark Blue
Spore 1	Blue
Spore 2	Dark Blue
Spore 3	White
Spore 4	Pale Blue

Figure 7.8 – Chitosan resistance in ByK352 is a polygenic trait. Full figure legend is on next page.

Figure 7.8 – Chitosan resistance in ByK352 is a polygenic trait. Growth inhibition curves for progeny from eight separate tetrads treated with 25 µg/mL Chitosan or the corresponding acetic acid control (0.005% (v/v)). Tetrads were derived from AD1-8 x ByK352 diploid. Alcian blue staining results are summarised in the adjacent tables for progeny derived from each tetrad. Chitosan sensitivity tests and alcian blue staining were performed in SC 2% glucose medium. OD_{600} measurements were recorded using a Bioscreen C™ instrument.

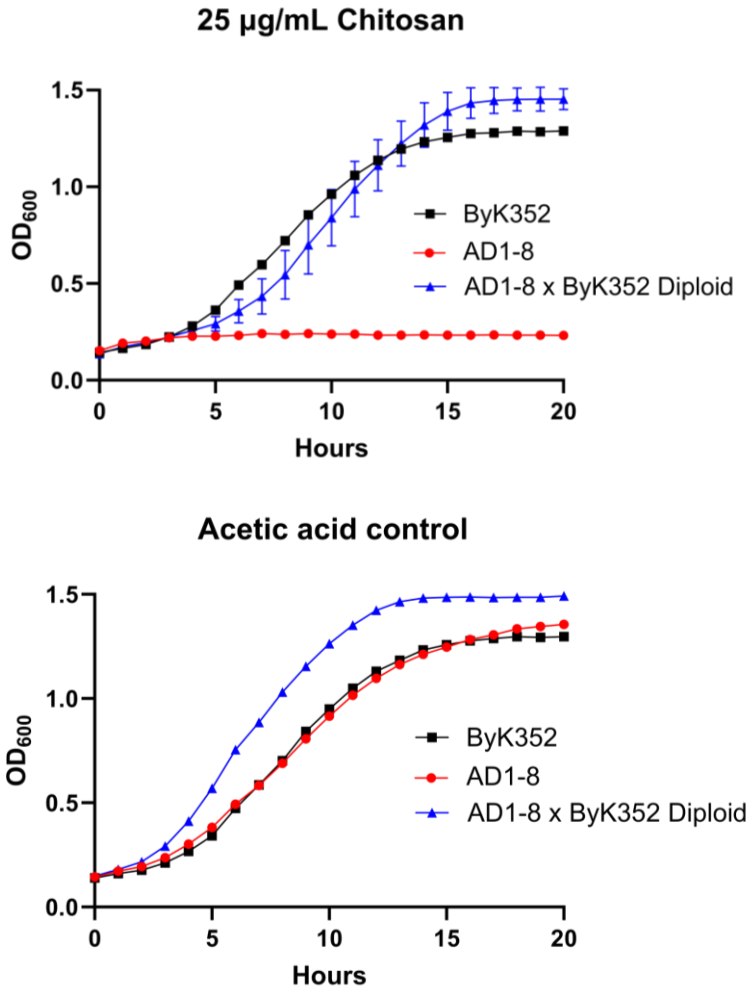

Figure 7.9 – The AD1-8 x ByK352 diploid was resistant to Chitosan. Growth inhibition curves for AD1-8, ByK352 and the AD1-8 x ByK352 diploid treated with **A)** 25 µg/mL Chitosan or **B)** the corresponding acetic acid control (0.005% (v/v)) in SC 2% glucose medium. OD_{600} measurements were recorded using a Bioscreen C™ instrument. Each data point is the mean OD_{600} measurement for three technical replicates. Error bars show standard deviation (SD). Error bars for some data points were too small to be displayed.

7.2.6. It remains unclear whether Chitosan binds to mannosylphosphate on the surface of *Botrytis cinerea*

Having established that Chitosan interacts with mannosylphosphate on the cell wall of *S. cerevisiae*, I assessed whether mannosylphosphate mediates Chitosan sensitivity in the fungal phytopathogen *Botrytis cinerea*. *B. cinerea* is one of the most destructive fungal phytopathogens, causing significant pre- and post-harvest yield losses in many economically important crops (Dean et al., 2012). Previous studies have shown that Chitosan can control *B. cinerea* infections on strawberries, tomato, cucumber and grapes (Romanazzi et al., 2013; Ben-Shalom et al., 2003; Munoz & Moret, 2010; Reglinski et al., 2010; De Vega et al., 2021). However, the cell wall components that bind Chitosan on the surface of *B. cinerea* have not been identified. Unveiling these components would improve our understanding of Chitosan's mode of action against this pathogen. For these reasons, Chitosan susceptibility was assessed in *B. cinerea* strains with deletions in putative homologs of *S. cerevisiae MNN4* (hereafter *ScMNN4*).

7.2.6.1. Bcin05p04770 and Bcin15p02200 are putative homologs of *Sc*Mnn4

The genes participating in mannosylphosphorylation in *B. cinerea* have not been characterised. As such, it was necessary to identify homologs of *Sc*Mnn4 in *B. cinerea*. This was achieved using the *Sc*Mnn4 protein sequence as a query in a BLASTp search against the *B. cinerea* B05.10 protein database on EnsemblFungi. Two proteins showing partial homology to *Sc*Mnn4 were identified: Bcin05p04770 and Bcin15p02200. Bcin05p04770 and Bcin15p02200 showed 19% and 24% identity to *Sc*Mnn4, respectively. A multiple sequence alignment revealed that Bcin05p04770 and

Bcin15p02200 were homologous to two main regions of *Sc*Mnn4 (**Figure 7.10**). By superimposing the AlphaFold2 models of *Sc*Mnn4, Bcin05p04770 and Bcin15p02200, these two homologous regions mapped to a beta sheet and adjacent alpha helices positioned at the core of all three proteins (**Figure 7.11**). Given that the *Sc*Mnn4 homolog could be Bcin05p04770 or Bcin15p02200, single mutants deleted in either *Bcin05g04770* or *Bcin15g02200*, and double mutants deleted in both of these genes were constructed.

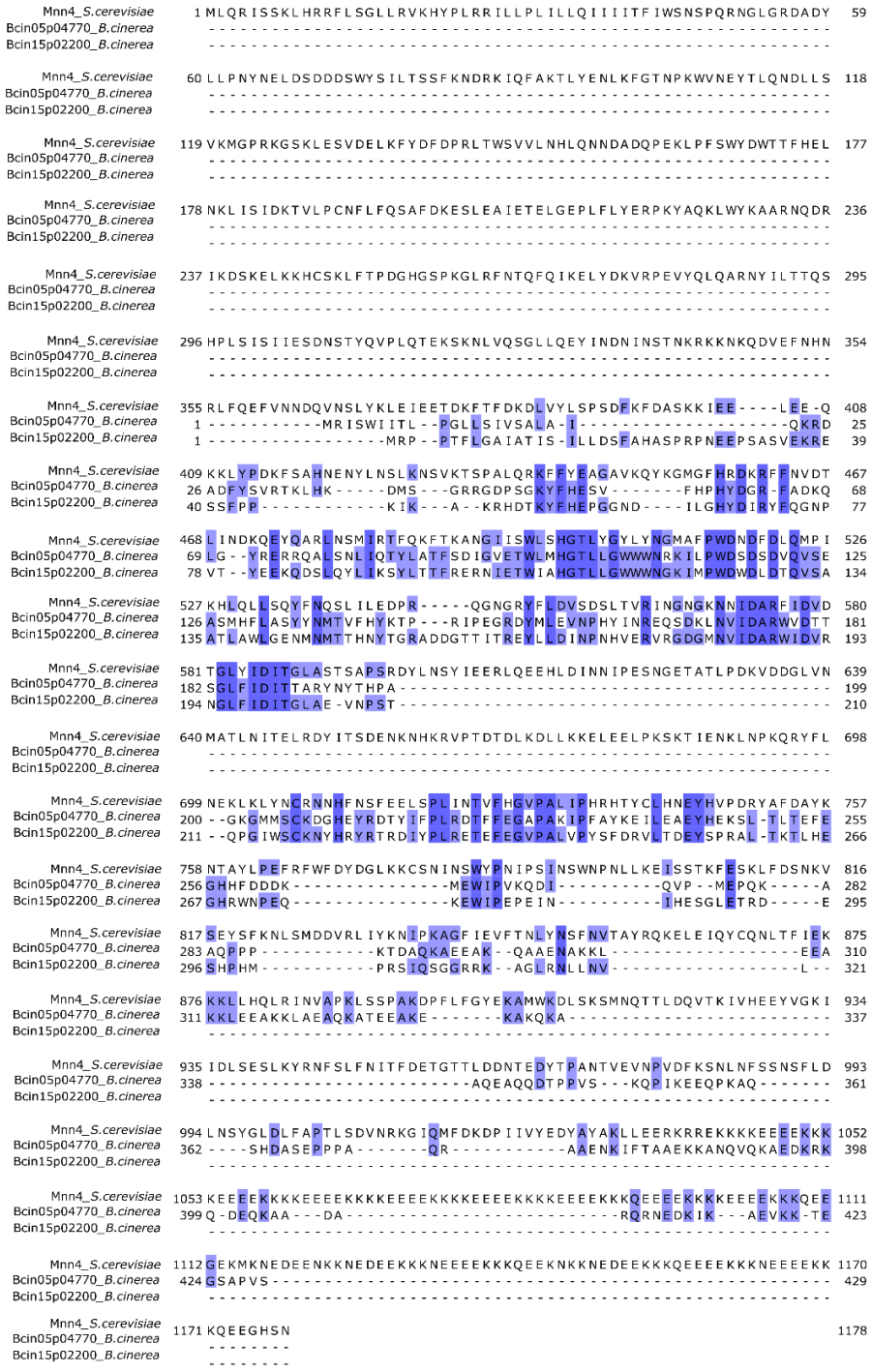

Figure 7.10 - Bcin05p04770 and Bcin15p02200 were homologous to two main regions of *Sc*Mnn4. Multiple sequence alignment of *Sc*Mnn4, Bcin05p04770 and Bcin15p02200 proteins using Clustal Omega. Sequence identity is indicated by blue highlighting, with darker blue indicating higher similarity. Alignment was visualised using Jalview (v 2.11.3.3).

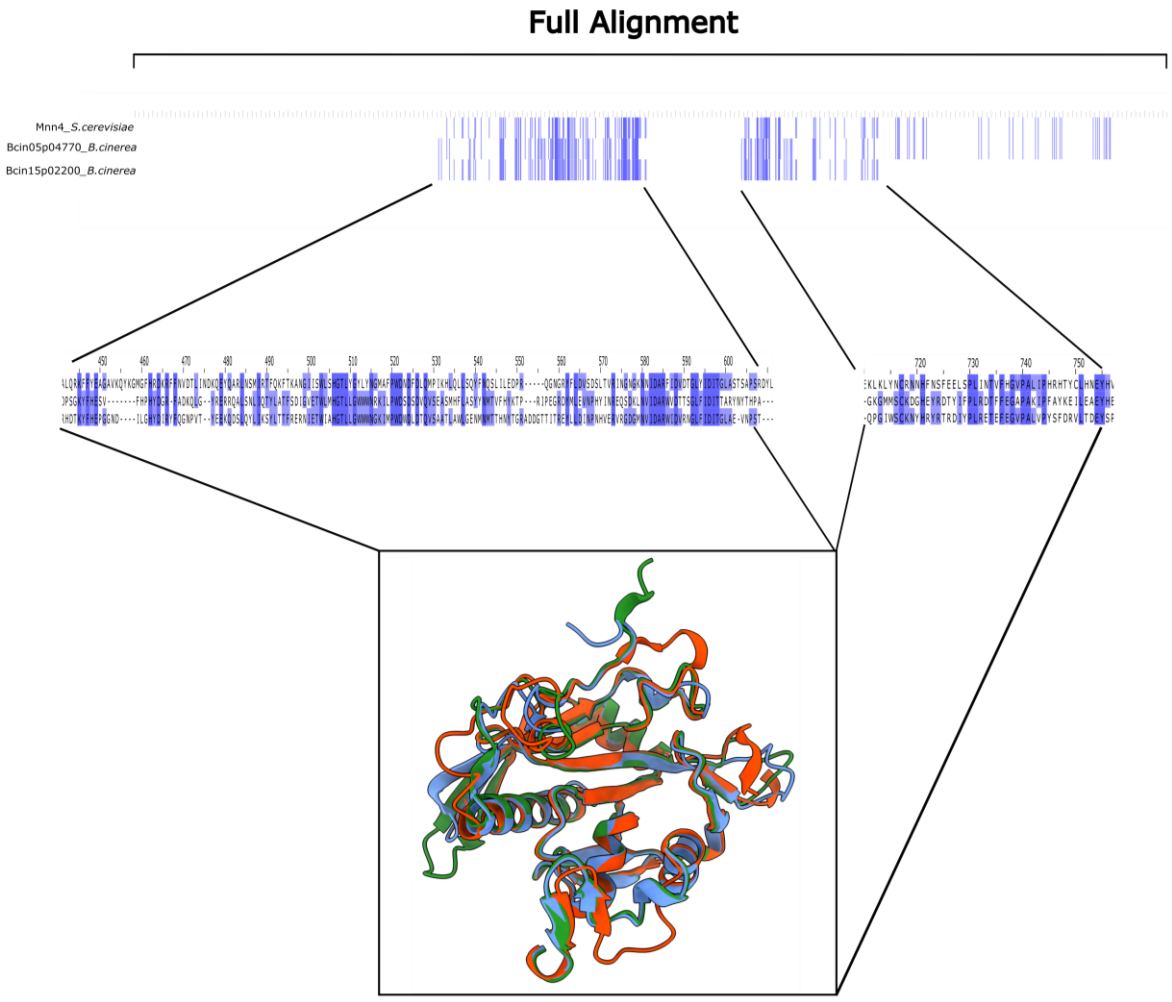

Figure 7.11 – The core of the ScMnn4, Bcin05p04770 and Bcin15p02200 proteins is conserved. Protein structure alignment was performed using the matchmaker command in ChimeraX (v.1.7.1) (Pettersen et al., 2021) for the AlphaFold2 models of *Sc*Mnn4 (orange) (UniProt Identifier P36044), Bcin05p04770 (green) (UniProt Identifier A0A384JHN4) and Bcin15p02200 (blue) (UniProt Identifier A0A384K4B3). The AlphaFold2 models were superimposed, and only the conserved beta sheet and alpha helices at the core of each protein are displayed.

7.2.6.2. Deletion of *Bcin15g02200* caused a slight reduction in Chitosan susceptibility

To determine whether *Bcin05g04770* or *Bcin15g02200* mediate Chitosan sensitivity in *B. cinerea*, single and double knock-out strains were challenged with Chitosan. For each strain, conidia were harvested from sporulating mycelium, washed and inoculated into medium containing serial dilutions of Chitosan or acetic acid, and growth was measured after 72 hours. This experiment was performed using the same Chitosan-acetic acid preparation as that in experiments with *S. cerevisiae*. Chitosan exhibited limited activity against all *B. cinerea* strains, with the IC_{50}'s ranging between 20-35 µg/mL (**Figure 7.12A**). Notably, the deletion of *Bcin15g02200* caused a slight reduction in Chitosan sensitivity. Indeed, the IC_{50} of Chitosan for *ΔBcin15g02200* and the double mutant strains was ~30 µg/mL, whereas the IC_{50} for the WT and *ΔBcin05g04770* strains was ~20 µg/mL (**Figure 7.12A**). This effect was not due to increased acetic acid tolerance in *ΔBcin15g02200* strains (**Figure 7.12B**). Thus, *Bcin15g02200* appears to contribute to Chitosan sensitivity in *B. cinerea*, although this effect is modest compared to that observed for *MNN4* in AD1-8.

A

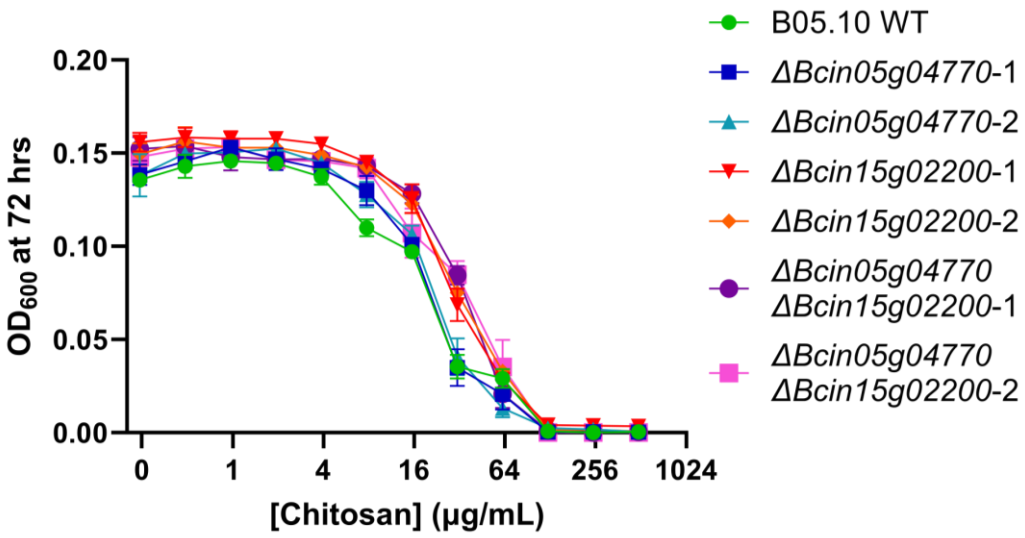

	B05.10 WT	*ΔBcin05g04770*		*ΔBcin15g02200*		*ΔBcin05g04770 ΔBcin15g02200*	
		1	2	1	2	1	2
Chitosan IC_{50} (µg/mL)	20.62	20.91	21.77	28.11	31.68	33.79	34.28
IC_{50} 95% confidence interval (µg/mL)	18.35-23.25	19.33-22.63	20.23-23.43	26.71-29.60	30.08-33.38	32.18-35.48	30.68-38.35

B

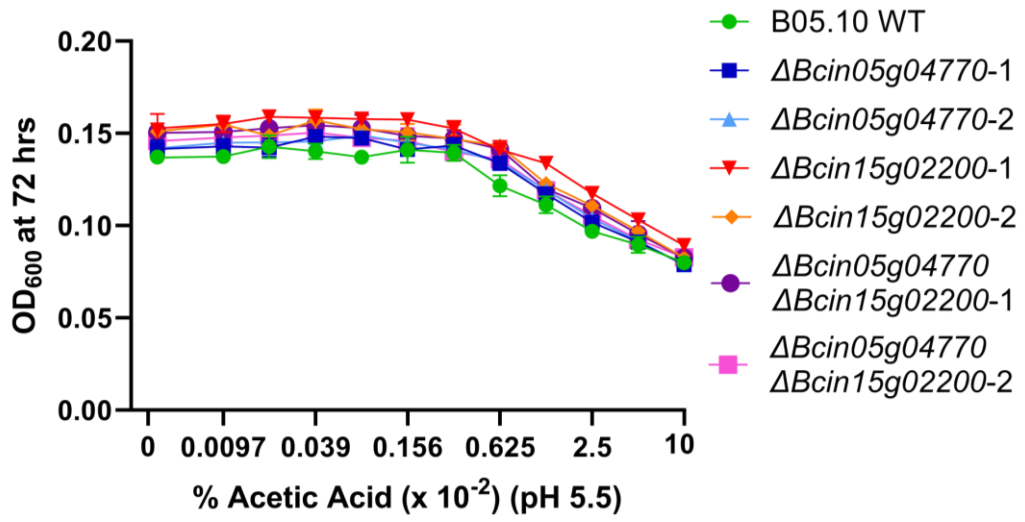

Figure 7.12 - The deletion of *Bcin15g02200* causes a slight reduction in Chitosan susceptibility after 72 hours of growth. Full figure legend is on next page.

Figure 7.12 - The deletion of *Bcin15g02200* causes a slight reduction in Chitosan susceptibility after 72 hours of growth. Growth inhibition curves of *Botrytis cinerea* WT and putative *MNN4* deletion mutants treated with (**A**) Chitosan or (**B**) acetic acid. Conidia from each strain were treated in GG medium at 20°C for 72 hours. Acetic acid was adjusted to pH 5.5 using NaOH to reflect the composition of the Chitosan stock solution. Two independent mutants of *ΔBcin05g04770*, *ΔBcin15g02200* and *ΔBcin05g04770 ΔBcin15g02200* were assessed. OD_{600} readings at 72 hours were normalised to the OD_{600} readings taken at 0 hours. OD_{600} readings are the mean for four technical replicates for each strain. Error bars show standard deviation. IC_{50} values were calculated in GraphPad Prism (v10.2) using the function: Dose-response-inhibition, log(inhibitor) vs. response – Variable slope (four parameters).

7.2.6.3. It was not clear whether putative *MNN4* homologs mediate Chitosan sensitivity in *Botrytis cinerea* over the first ten hours of growth

The slight decrease in Chitosan sensitivity in *ΔBcin15g02200* strains was observed after 72 hours of growth (**Figure 7.12A**). Over the course of 72 hours, the growth of the WT and *ΔBcin05g04770* strains might have caught up with the *ΔBcin15g02200* strains. This could occur if the *ΔBcin15g02200* strains reached saturation at an earlier time-point, in which case the relative differences in Chitosan sensitivity between strains would have been obscured. To assess whether more substantial differences in Chitosan sensitivity occur at an earlier time-point, conidia from each *B. cinerea* strain were germinated in GG medium containing 20 µg/mL Chitosan, and end-point images were taken after ten hours. Ten hours provided sufficient time for the conidia to germinate, whilst also ensuring that the germlings did not grow long enough to significantly overlap with each other (**Figure 7.13**), which would have complicated the quantification of their germ tube lengths. To facilitate this quantification further, the germlings were briefly treated with FM4-64 prior to imaging, which selectively stained the plasma membranes of the germlings without interfering with their cell walls (**Figure 7.14**). In total, the lengths of approximately 1,000 germlings were quantified for each strain in each treatment. Unexpectedly, the germlings for all the mutant strains were longer than the WT germlings in every treatment condition, including the untreated control (**Figure 7.15**). Consequently, it was very challenging to conclude from this experiment alone whether the *ΔBcin15g02200* deletion reduced Chitosan sensitivity during the first 10 hours of germination. Thus, it remains unclear whether Chitosan binds to mannosylphosphate on *B. cinerea*.

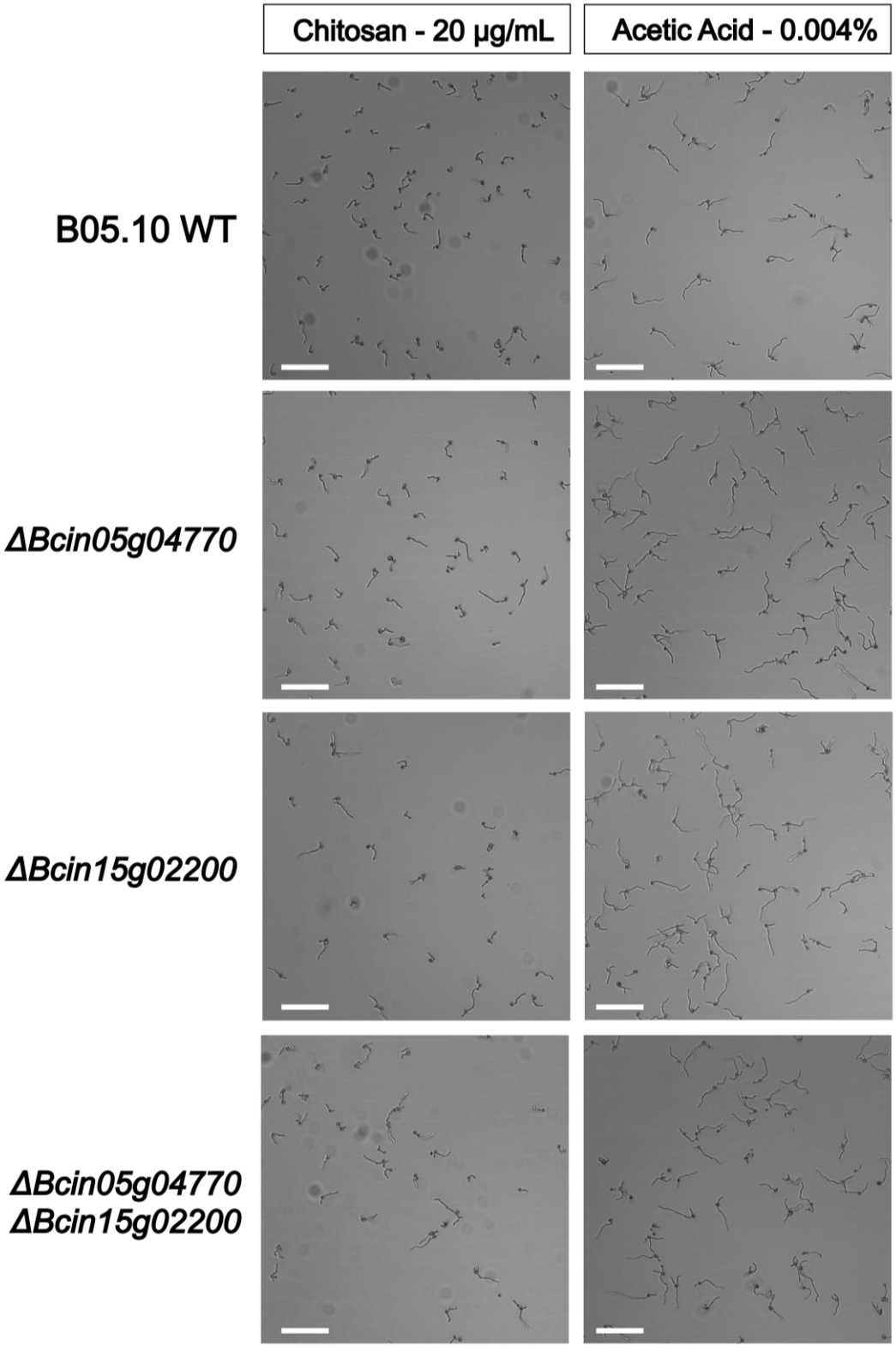

Figure 7.13 - Representative brightfield images of *Botrytis cinerea* germlings after 10 hours of growth with 20 µg/mL Chitosan or 0.004% (v/v) acetic acid. Full figure legend is on next page.

Figure 7.13 - Representative brightfield images of *Botrytis cinerea* germlings after 10 hours of growth in 20 µg/mL Chitosan or 0.004% (v/v) acetic acid. Treatments were initially applied to conidia in GG medium, which subsequently germinated. The conidia density was ~10,000/well to reduce overlapping of subsequent germ tubes. Acetic acid was adjusted to pH 5.5 using NaOH to reflect the composition of the Chitosan stock solution. All germlings were treated with 1.5 µM FM4-64 for 10 minutes prior to imaging. Scale bar = 50 µm.

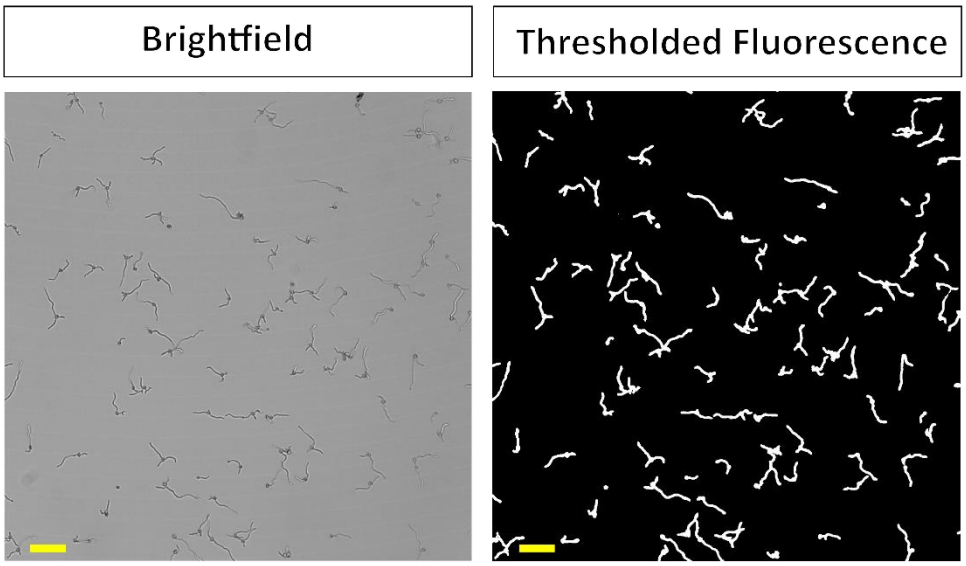

Figure 7.14 – Representative brightfield and corresponding thresholded fluorescence image of WT *Botrytis cinerea* germlings after 10 hours of treatment with 0.004% (v/v) acetic acid in GG medium. Germlings were treated with 1.5 µM FM4-64 for 10 minutes prior to imaging. Yellow scale bar = 50 µm.

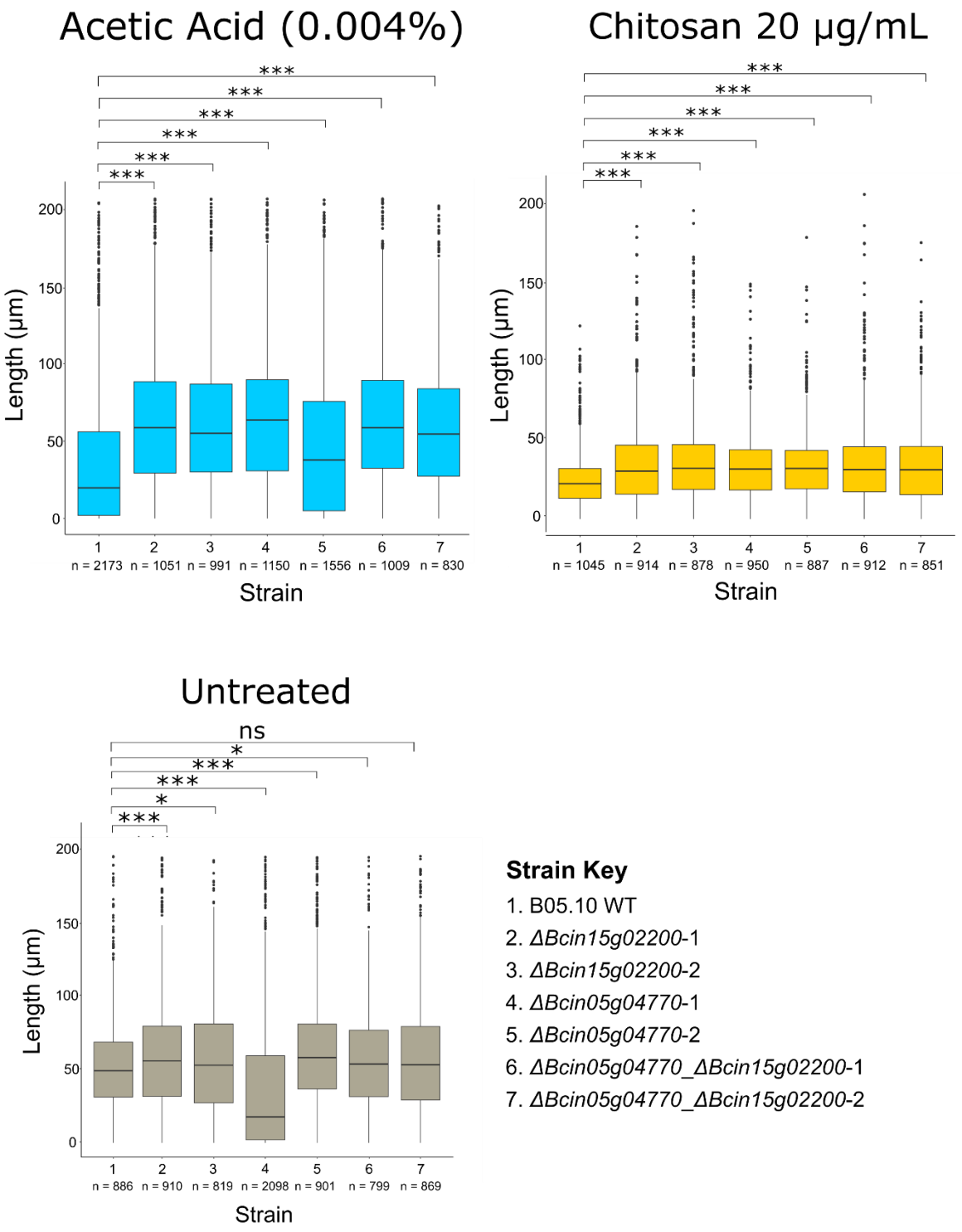

Figure 7.15 – Boxplots comparing germling lengths of WT, *ΔBcin15g02200* and *ΔBcin05g04770* strains of *Botrytis cinerea* after 10 hours of treatment with (A) 20 µg/mL Chitosan, (B) 0.004% acetic acid, or (C) an untreated control. Full figure legend is on next page.

Figure 7.15 – Boxplots comparing germling lengths of WT, *ΔBcin15g02200* and *ΔBcin05g04770* strains of *Botrytis cinerea* after 10 hours of treatment with (A) 20 µg/mL Chitosan, (B) 0.004% acetic acid, or (C) an untreated control. Germlings were grown in GG medium at 20°C for 10 hours. Acetic acid was adjusted to pH 5.5 using NaOH to reflect the composition of the Chitosan stock solution. The number of individual germlings quantified for each strain is indicated by n= below the respective boxplots. Statistical significance was calculated using the Kruskal-Wallis (non-parametric) test. * denotes $p < 0.05$ in comparison to WT. *** denotes $p < 0.001$ in comparison to WT. ns = not significant in comparison to WT.

7.3. Discussion

7.3.1. Chitosan electrostatically interacts with mannosylphosphate on the cell wall

This chapter discovers that Chitosan electrostatically interacts with mannosylphosphate groups on the cell wall of *S. cerevisiae*. Since mannosylphosphate confers a net negative charge to the yeast cell wall, this finding aligns with previous reports that negative charges on microbial cell surfaces are a critical determinant for Chitosan sensitivity. Indeed, Chitosan interacts with negatively charged teichoic acids on the surface of gram-positive bacteria (Raafat et al., 2008) and negatively charged lipopolysaccharide (LPS) on the outer membrane of gram-negative bacteria (Mellegard 2011; Naberezhnykh 2007; Davydova et al., 2000; Helander et al., 2001). Chitosan can additionally interact with negatively charged phospholipids on bacterial cell membranes (Liu et al., 2004). Regarding Chitosan's antifungal activity, it has been shown that Chitosan sensitivity in *Candida spp*. is directly correlated with the density of negative charges on their cell surfaces (Palmeira de Oliveira, 2011). However, the identity of the negatively charged components on fungal cell surfaces that bind Chitosan has remained unclear. Thus, by revealing that mannosylphosphate is a major target for Chitosan on the *S. cerevisiae* cell wall, this study advances our understanding of Chitosan's mode of action against fungi.

This study does not examine how growth is inhibited by Chitosan binding to mannosylphosphate. Previously, it was shown that Chitosan binding disrupts the cell wall integrity of *Candida albicans*, *Botrytis cinerea*, and *Rhizopus stolonifer*, altering cell

morphology and leading to the leakage of intracellular components (El Ghaouth, 1992; Tayel et al., 2010; Li et al., 2022). The permeabilization of the cell surface has also been widely observed in Chitosan-treated bacterial cells (Liu et al., 2004; Raafat et al., 2008; Chung & Chen, 2008). Thus, upon binding to cell wall mannosylphosphate, it seems likely that Chitosan inhibited the growth of AD1-8 by impairing the integrity of the cell wall.

7.3.2. SATAY in non-conventional strains of *S. cerevisiae* can unveil antifungal modes of action

The discovery that Chitosan interacts with cell wall mannosylphosphate was enabled by the ability to perform SATAY in a Chitosan-sensitive strain of *S. cerevisiae* called AD1-8 (Michel et al., 2017; Chen et al., 2022). AD1-8 is derived from the non-conventional laboratory strain US50-18C (Decottignies et al., 1998), and was found to exhibit Chitosan sensitivity because it possesses cell wall mannosylphosphate. In contrast, the S288C-derived strain ByK352 lacks sensitivity to Chitosan because it lacks cell wall mannosylphosphate. This finding therefore explains why previous studies utilising yeast deletion collections, which were constructed in S288C (Giaever et al., 2002; Winzeler et al., 1999), have not identified mannosylphosphate as the target of Chitosan (Galván Márquez et al., 2013; Jaime et al., 2012; Zakrzewska et al., 2007). This study therefore demonstrates the utility of performing SATAY in non-conventional strains for studying compounds without activity against conventional laboratory strains.

7.3.3. Multiple mutations are responsible for the lack of mannosylphosphate on the surface of S288C-derived strains

This study raises the question of why mannosylphosphate is scarcely present on the cell walls of S288C-derived strains, such as ByK352, despite harbouring wild-type copies of *MNN4* and *MNN6*. Since the AD1-8 x ByK352 diploid failed to bind alcian blue, the S288C-type mannan structure is dominant and must be underpinned by gain-of-function mutations. Moreover, it was observed that alcian blue staining was inherited in a complex polygenic fashion, meaning that the lack of mannosylphosphate on S288C is attributable to multiple genes. The identity of these genes was not revealed by this study. It is possible that S288C-derived strains harbour gain-of-function mutations that increase the activity of Mnn1. Mnn1 competes with the mannosylphosphate transferases Mnn4 and Mnn6 (Karson & Ballou, 1978) by adding terminal α1,3-linked mannose residues to the same acceptor sites (Raschke et al., 1973; Yip et al., 1994). Increased Mnn1 activity might therefore out-compete Mnn4/Mnn6 for available acceptor sites, decreasing cell wall mannosylphosphate levels. Besides mutations in Mnn1, it is not clear what other genes might harbour gain-of-function mutations that diminish mannosylphosphate levels in these strains. Indeed, mutations altering the cell-surface of S288C strains have been selected by decades of cultivation in laboratory environments (Liu et al., 1996). For example, certain traits such as flocculation, which leads to unwanted cellular aggregations (Stratford, 1992), have been deliberately lost (Mortimer & Johnston, 1986). Given that mannan chains are required for flocculation (Stratford, 1992), it is possible that yeast geneticists inadvertently selected for mutations in S288C that reduced the amount of cell wall mannosylphosphate.

7.3.4. It remains unclear whether Chitosan binds mannosylphosphate on the surface of *Botrytis cinerea*

From the analyses performed in this chapter, it remains unclear whether mannosylphosphate is important for Chitosan's activity against the fungal phytopathogen *Botrytis cinerea*. Although *B. cinerea* strains harbouring deletions in the putative *MNN4* homolog *Bcin15g02200* showed a slight reduction in Chitosan sensitivity after 72 hours of germination, it was very challenging to determine whether the *ΔBcin15g02200* germlings had reduced Chitosan sensitivity after 10 hours of germination. These findings contrast with the significant reduction in Chitosan sensitivity observed for *mnn4Δ* mutants of *S. cerevisiae*. There are multiple possible explanations for these contrasting results:

First, Bcin15p02200, and indeed Bcin05p04770, may not encode mannosylphosphate transferases. Although Bcin15p02200 and Bcin05p04770 share the highest homology with *Sc*Mnn4 in the *B. cinerea* proteome, they still only showed 24% and 19% identity to *Sc*Mnn4, respectively. If Bcin15p02200 is not a mannosylphosphate transferase, then the slight reduction in Chitosan sensitivity in *ΔBcin15g02200* strains might be caused by an alternative structural modification to the cell wall.

Second, the cell walls of *B. cinerea* might not possess mannosylphosphate in the first instance. Indeed, mannosylphosphorylation is not even a universal glycan modification in yeasts: *Schizosaccharomyces pombe* and *Kluyveromyces lactis* lack mannosylphosphate, whereas *Kloeckera brevis* and *Candida albicans* contain as much

mannosylphosphate as *S. cerevisiae* (Jigami et al., 1999). Given that *B. cinerea* is distantly related to *S. cerevisiae* and occupies a different ecological niche (Bi et al., 2023), it would not be surprising if their cell walls have different compositions and charges. The N-linked mannosylation pathway has not yet been characterised in *B. cinerea*, and very few reports have examined O-linked mannosylation in this species (Gonzalez et al., 2013). Although this study found that wild-type *B. cinerea* germlings failed to bind Alcian blue (data not shown), this does not necessarily indicate that mannosylphosphate is absent from *B. cinerea* cell walls, since alcian blue staining is dependent on both the amount and location of mannosylphosphate on the cell surface (Ballou et al., 1973). ε-poly-L-lysine, a polycation, might have otherwise revealed whether the *ΔBcin15p02200* or *ΔBcin05p04770* germlings had different negative charge densities on their surfaces relative to the wild-type germlings (Jiao et al., 2020).

Third, mannosylphosphate might be incorporated into the cell walls of *B. cinerea* during a specific growth stage that was not analysed in this study. In *S. cerevisiae*, mannosylphosphorylation occurs during stationary phase (Odani et al., 1997). If mannosylphosphate groups are only incorporated into the cell walls of mature mycelium of *B. cinerea*, then the experiments performed here did not evaluate the effects of mannosylphosphate on Chitosan sensitivity.

Fourth, mannosylphosphorylation in *B. cinerea* might be regulated by multiple redundant genes. If this situation occurs, then even if Bcin15p02200 and Bcin05p04770

are mannosylphosphate transferases, the *ΔBcin15g02200 ΔBcin05g04770* double mutants may still have contained mannosylphosphate at their cell walls.

Fifth, only one genetic background of *B. cinerea* (B05.10) (Büttner et al. 1994) was evaluated in this study. As observed in *S. cerevisiae*, it is possible that Chitosan sensitivity may vary between different genetic backgrounds, and these differences may be attributable to mannosylphosphate levels.

In summary, further work is required to establish whether Chitosan interacts with mannosylphosphate on the cell wall of *B. cinerea*. However, it would perhaps be more straightforward to assess whether Chitosan binds mannosylphosphate on fungal phytopathogens with better characterised N-linked mannosylation pathways and Chitosan sensitivities, such as *Ustilago maydis* or *Magnaporthe oryzae* (Liu et al., 2021).

Chapter 8 - General Discussion

8.1. Overview

This thesis aimed to apply SATAY to identify novel antifungal resistance mechanisms and the modes of action of several antifungal compounds. By addressing these knowledge gaps, this work can help guide strategies for optimising the use of these compounds and inform antifungal development pipelines. Additionally, this study further demonstrates that SATAY is a powerful tool for chemogenomic screening that can accelerate the discovery of antifungal resistance mechanisms and modes of action. The implications of the specific findings identified in this thesis are discussed in their respective chapters. In this chapter, the advantages and disadvantages of using SATAY for chemogenomic screening are considered, followed by a brief discussion of additional ways that SATAY could be applied for this purpose.

8.2. SATAY is a powerful approach for chemogenomic screening in *S. cerevisiae*

8.2.1. SATAY can identify a diverse array of antifungal resistance mechanisms

This thesis demonstrates that SATAY can identify a diverse array of antifungal resistance mechanisms. This is enabled by the fact that SATAY can systematically assess the fitness effects of thousands of loss- and gain-of-mutations in a single experiment. Transposons disrupting CDSs revealed metabolic and signal transduction pathways that engender antifungal susceptibility. For example, transposons disrupting sphingolipid biosynthesis,

N-linked mannosylation and the HOG signalling pathway conferred resistance to Caspofungin, Chitosan and Fludioxonil, respectively. Additionally, transposons interrupting CDSs unveiled cellular trafficking pathways that engender compound sensitivity. Indeed, transposons impairing intra-Golgi vesicle transport and endosome-to-Golgi retrograde vesicular transport reduced susceptibility to Chitosan and Myriocin, respectively. Furthermore, transposons mapping to CDSs can identify transporters responsible for antifungal import, as illustrated by the identification of Hol1 as the transporter of ATI-2307. Concurrently, transposons mapping to promoter regions can identify antifungal detoxification pathways involving drug efflux or drug metabolism. For instance, transposons in the promoter of the drug efflux pump gene *PDR5* conferred Prochloraz resistance, whilst promoter insertions for *SLI1* conferred Myriocin resistance, since Sli1 inactivates Myriocin by N-acetylation (Momoi et al., 2004). In addition, promoter insertions can reveal the direct targets of antifungal compounds, as illustrated by insertions in the promoter of *ERG11* conferring Prochloraz resistance. The ability to uncover both loss- and gain-of-function mutations conferring antifungal resistance means that SATAY can identify a wider range of resistance mechanisms than conventional chemogenomic approaches utilising yeast deletion collections, which are restricted to the analysis of loss-of-function mutations.

8.2.2. SATAY can be used to screen compounds that lack activity against conventional laboratory strains of *S. cerevisiae*

A significant advantage of SATAY is that it can be readily performed in different genetic backgrounds of *S. cerevisiae* (Michel et al., 2017; Chen et al., 2022). This is valuable

because conventional laboratory strains of *S. cerevisiae* lack sensitivity to several widely used antifungal compounds. This thesis provides three examples that demonstrate how SATAY can be utilised for the chemogenomic screening of such compounds.

First, SATAY can be performed in PDR-attenuated strains of *S. cerevisiae*. This is useful because many antifungal compounds are substrates of the PDR network (Kolaczkowski et al., 1998). This includes the agrochemical fungicide Prochloraz, which has limited activity against PDR-proficient strains. Upon treating a PDR-proficient transposon library with Prochloraz, transposons associated with PDR-dependent resistance were strongly selected, masking cellular responses relevant to Prochloraz's mode of action. However, by performing SATAY in a PDR-attenuated strain called 12geneΔ0HSR (Chinen et al., 2011), SATAY could identify PDR-independent mechanisms of Prochloraz resistance. This increases the specificity of chemogenomic profiles, and allows screens to be performed with lower concentrations.

Secondly, SATAY was performed in a strain called AD1-8, which is derived from the non-conventional strain US50-18C (Decottignies et al., 1998). This screen led to the discovery that Chitosan interacts with cell wall mannosylphosphate. In contrast to AD1-8, the cell walls of strains derived from the conventional laboratory strain S288C lacked mannosylphosphate, thereby explaining why Chitosan has minimal activity against these strains. Thus, this example demonstrates the utility of performing SATAY in non-conventional strains of *S. cerevisiae*. Indeed, conventional laboratory strains such as S288C have lost certain traits due to decades of selection in laboratory conditions, and

these traits might be required for antifungal susceptibility. SATAY therefore provides opportunities for screening compounds targeting processes lost from conventional laboratory strains. Other traits bred out of conventional laboratory strains include pseudo-hyphal growth (Gancedo et al., 2001) and complex biofilm production (Stovicek et al., 2010). Both yeast-to-hyphae transition (Talapko et al., 2021) and biofilm production (Nett et al., 2010) are known virulence factors in fungal pathogens. SATAY therefore provides an opportunity to examine these virulence factors in non-deficient, wild strains.

Thirdly, SATAY was performed in a strain heterologously expressing the group III HHK *DRK1* from *Blastomyces dermatitidis*. This allowed the chemogenomic screening of Fludioxonil and Iprodione. *S. cerevisiae* is otherwise insensitive to Fludioxonil and Iprodione (Motoyama et al., 2005) because it does not contain an endogenous group III HHK (Catlett et al., 2003). Performing such a screen with the yeast deletion collection would have been complex, requiring robotics to cross each of the ~5,000 deletion strains (Winzeler et al., 1999; Giaever et al., 2002) into the *sln1Δ BdDRK1* strain, and select for the sought-after meiotic progeny. Thus, SATAY can be readily applied to screen compounds that lack targets in *S. cerevisiae*. This creates many opportunities for chemogenomic screening. For example, SATAY could be used to screen the novel antifungal Olorofim, which is currently in phase III clinical trials for the treatment of invasive aspergillosis (ClinicalTrials.gov identifier: NCT05101187). Olorofim potently inhibits class II dihydroorotate dehydrogenase (DHODH) enzymes of the pyrimidine biosynthesis pathway in moulds (Oliver et al., 2016). *S. cerevisiae* only possesses a class

I DHODH (*ScURA1*), and therefore lacks sensitivity to Olorofim. However, *ScURA1* can functionally replace class II DHODHs (Bouwknegt et al., 2021). Given that *ScURA1* is essential on medium lacking uracil (Mary & Jones, 1992), a *ura1Δ* strain of *S. cerevisiae* heterologously expressing a class II DHODH may exhibit Olorofim sensitivity in uracil-deficient medium. Undertaking a SATAY screen in this strain could reveal new mechanisms of Olorofim resistance, potentially informing the future use of this novel compound. Moreover, SATAY screens performed with "humanised" yeast strains heterologously expressing human orthologs could potentially identify the determinants of sensitivity or resistance to anticancer agents (Matuo et al., 2012) or neuroprotective agents (Winderickx et al., 2014; Seynnaeve et al., 2018). Indeed, ~1,000 human disease genes can functionally complement their orthologs in *S. cerevisiae* (Heinicke et al., 2007). SATAY therefore has potential to improve our understanding of a wide range of pharmacological compounds.

8.2.3. Transposon libraries can be grown in non-fermentative conditions

In Chapter 5, a transposon library was grown under non-fermentative conditions in order to identify determinants of ATI-2307 susceptibility. ATI-2307 only inhibits *S. cerevisiae* under non-fermentative growth conditions (Shibata et al., 2012; Yamashita et al., 2019). This constituted the first study to treat a SATAY library in non-fermentative conditions. This possibility creates opportunities for screening other antifungals that inhibit mitochondrial respiration, including quinone outside inhibitors (QoIs) (Fernandez-Ortuno et al., 2008) and succinate dehydrogenase inhibitors (SDHIs) (Sierotzki & Scalliet,

2013). This is useful because compounds targeting mitochondrial respiration are among the most widely used agrochemical fungicides (Lamberth, 2022).

8.2.4. SATAY can be used to identify novel combination therapies

The SATAY screens performed in this thesis further demonstrate that cellular responses to antifungal compounds are complex and multifactorial. Indeed, antifungal resistance was frequently conferred by genes not directly associated with the target. This genetic buffering underscores the importance of identifying synergistic combinations of antifungals targeting compensatory pathways. For example, my SATAY screen with Caspofungin revealed that Caspofungin therapy might be enhanced by an inhibitor of long-chain base (LCB) synthesis, such as Myriocin. Consistently, Myriocin treatment was previously shown to increase the susceptibility of the fungal pathogen *Candida glabrata* to Caspofungin (Healey et al., 2012). Thus, SATAY has significant potential for identifying combination therapies.

Additionally, SATAY can reveal which antifungals should not be applied together, because compounds with substantially overlapping chemical-genetic profiles will be at risk of cross-resistance. For instance, SATAY revealed that the same genes engender susceptibility to Fludioxonil and Iprodione, and consistently, cross-resistance is frequently observed for these compounds in the fungal phytopathogen *Botrytis cinerea* (Fillinger et al., 2012; Zhou et al., 2020). At the same time, correlations between SATAY profiles could be used to infer the mode of action of novel compounds, as compounds with matching profiles likely target similar processes.

8.3. Limitations of using SATAY for chemogenomic screening

Although this thesis has highlighted the benefits of using SATAY for chemogenomic screening, there are a number of limitations with using SATAY for this purpose. These limitations can be categorised into technical challenges or inherent weaknesses.

8.3.1. Technical challenges with using SATAY for chemogenomic screening

Like all Tn-seq approaches, the quality of SATAY datasets depends on the density of transposon insertions across the genome i.e. the library complexity (van Opijnen & Levin, 2020). However, this complexity is inevitably reduced by challenging libraries with antifungal compounds. The stringency of compound treatments is critical for determining whether the same SATAY screen can identify transposons causing resistance and sensitivity. Significant reductions in library complexity (less than ~100,000 transposon insertions) preclude the identification of conditionally essential genes. Thus, the most optimal selection regime occurs when antifungals select for resistance without significantly reducing the library complexity. Concentrations close to the IC_{30} have the greatest likelihood of striking this balance (Michel et al., 2019). However, applying the correct level of selection can be challenging for potent compounds. For instance, the complexity of the Amphotericin B- and Caspofungin-treated libraries and the Prochloraz-treated 12geneΔ0HSR library were strongly reduced (< 60,000 transposon insertions) (**Chapter 3, Table 3.2**). Consequently, these libraries only revealed mutations conferring resistance. This problem could be mitigated by treating libraries with a range of antifungal concentrations before identifying the most optimally selected condition upon sequencing. Alternatively, a morbidostat (Toprak et al., 2012, 2013) could be used to

continuously monitor the growth rate of the library population, and automatically adjust the drug concentration accordingly. This would help to maintain a steady level of 30% growth inhibition.

8.3.2. Inherent limitations with using SATAY for chemogenomic screening

There are limitations with using *S. cerevisiae* to infer how antifungal resistance might emerge in fungal pathogens.

Firstly, *S. cerevisiae* lacks many morphological features and virulence factors found in fungal pathogens. Examples include hyphal growth, capsules, appressoria, melanin production, adhesion, and complex biofilms (Chandra et al., 2001; Demuyser & Van Dijck, 2019; Kaur & Nobile, 2023). These features may be important determinants of antifungal resistance and sensitivity in fungal pathogens. These effects might be very difficult to evaluate using laboratory strains of *S. cerevisiae*, although the possibility of performing SATAY in wild strains (Chen et al., 2022) that have retained some of these traits might mitigate this drawback.

Secondly, the mutations conferring antifungal resistance or susceptibility revealed using SATAY might not cause the same phenotypes in fungal pathogens. Indeed, the genomes of *S. cerevisiae* and fungal pathogens exhibit different degrees of functional redundancy. In *S. cerevisiae*, there is extensive redundancy between paralogs under standard laboratory conditions (Musso et al., 2008), owing to a recent whole-genome duplication event (Kellis et al., 2004). Thus, mutations conferring resistance in *S. cerevisiae* might be lethal in fungal pathogens that have less genomic redundancy. Meanwhile, many fungal

phytopathogens have larger genomes than *S. cerevisiae*, with more genes and more functional redundancy (Wang et al., 2023; Moller & Stukenbrok, 2017). As such, recessive loss-of-function mutations identified in haploid strains of *S. cerevisiae* might not manifest a phenotype when occurring in the orthologs of fungal phytopathogens, especially if they are diploid or polyploid. Moreover, there are differences in the genetic circuitries governing responses to drug-induced stresses in *S. cerevisiae* and fungal pathogens. For example, the circuitries downstream of Protein Kinase C (Pkc1), that mediate membrane stress responses elicited by azole treatments, have been considerably rewired between *S. cerevisiae* and *C. albicans*. Indeed, in response to Fluconazole, Pkc1 is required in *S. cerevisiae* for the activation of calcineurin, a key regulator of membrane stress responses, but in *C. albicans*, calcineurin regulates Fluconazole responses independently of Pkc1 (LaFayette et al., 2010). Nonetheless, the resistance mechanisms inferred in *S. cerevisiae* from the mutations identified using SATAY might be conserved even when the phenotype of these mutations may not be, due to different levels of redundancy or different genetic wiring.

Furthermore, SATAY has limited scope for examining the contribution of essential genes to antifungal susceptibility, since transposons disrupting the function of essential genes are lethal. This is notable because 19% of genes in *S. cerevisiae* are essential under standard laboratory conditions (Giaever et al., 2002). However, transposons within essential genes can tolerated if they are inserted upstream or downstream of essential domains (Michel et al., 2017). This is because the SATAY transposon contains promoter sequences (Yu et al., 2004), meaning that transposon insertions in the CDS can still

permit the expression of essential domains downstream. Moreover, transposons inserting into promoters can upregulate the expression of essential genes, which is useful for revealing antifungal drug targets (Michel et al., 2019). That being said, insertions mapping to promoters might not always generate meaningful increases in the activity of downstream genes. This might occur if the downstream gene is already highly expressed from a strong promoter, or if the protein product participates in a complex with a specific stoichiometry. These scenarios may limit the potential of SATAY for identifying some drug targets.

Finally, SATAY cannot identify target-site point mutations, because it specifically analyses mutations generated by transposon insertions. This is noteworthy because target-site point mutations are among the most prevalent mechanisms of antifungal resistance (Fisher et al., 2018; Robbins et al., 2017).

8.4. Additional applications of SATAY for chemogenomic screening

There are a couple of additional ways that SATAY could be applied for chemogenomic screening.

8.4.1. Fluorescence-based selection approaches

In this thesis, transposon mutants were distinguished by their abilities to survive and grow in the presence of antifungal compounds. In recent years, however, Tn-seq methods have separated mutants by phenotypes other than growth (Cain et al., 2020). For example, Tn-seq has been combined with fluorescence-activated cell sorting (FACS)

to separate transposon mutants based on fluorescence. This approach was applied to an ethidium bromide-treated *Acinetobacter baumannii* transposon library to identify genes encoding multidrug efflux pumps (Hassan et al., 2016), whereby mutants with high levels of fluorescence, and therefore a reduced ability to remove ethidium bromide, contained transposons in efflux pump genes. In a similar way, SATAY could be coupled to FACS to identify new drug efflux pumps in *S. cerevisiae*. Alternatively, transposon libraries could be treated with fluorescently-tagged compounds of interest to compare efflux rates through different pumps. FACS could also be employed to compare the amount of fluorescein-labelled Chitosan bound to the cell walls of different AD1-8 transposon mutants. This would allow the contributions of different mutations to fluorescein-labelled Chitosan binding to be compared more directly. More generally, SATAY could be engineered to measure the expression of fluorescent reporter genes, either affecting growth or cell fluorescence. Coupling SATAY to FACS could therefore unveil aspects of antifungal susceptibility that cannot be revealed through growth-based selection approaches alone.

8.4.2. Identifying conditionally essential genes in drug-resistant strains

Antifungal resistance is attributed to genetic mutations, which can be associated with fitness costs (Hawkins & Fraaije, 2018). SATAY could be used to uncover conditionally essential genes in drug-resistant strains (i.e. the “Achilles’ Heels”). Such genes could represent promising targets for the development of novel therapies for eliminating drug-resistant strains. For example, SATAY could be performed in multidrug-resistant strains bearing the *pdr1-3* gain-of-function mutation (F815S) in the transcription factor Pdr1

(Balzi et al., 1987). This mutation causes the overexpression of multiple ABC transporter-encoding genes (Carvajal et al., 1997). This screen would be relevant because similar gain-of-function point mutations occur in transcriptional activators of drug efflux pumps in fungal pathogens, such as *C. glabrata* (Tsai et al., 2006) and *B. cinerea* (Kretschmer et al., 2009), and it is unclear whether the overexpression of drug efflux pumps causes a fitness cost in fungi, either by increasing energy consumption or by the extrusion of useful metabolites. Additionally, SATAY could be performed in *S. cerevisiae* strains harbouring target-site mutations. This could include azole-resistant strains harbouring clinically-relevant point mutations in *ERG11* (Xiang et al., 2013). This would be interesting because target-site mutations reduce antifungal binding, resulting in potential trade-offs with the function of the original enzyme function (Cools et al., 2013; Hawkins et al., 2018).

8.5. Developing Tn-seq approaches in fungal phytopathogens is a worthwhile pursuit

By demonstrating the utility of SATAY for chemogenomic screening, this work sets a precedent for the development of analogous approaches in fungal pathogens. To date, Tn-seq has been applied in *C. glabrata* (Gale et al., 2020) and a stable haploid of *C. albicans* (Gao et al., 2018), but there are no published studies of Tn-seq in fungal phytopathogens. One fungal phytopathogen which could be suitable for Tn-seq is the corn smut fungus *Ustilago maydis* (Matei & Doehlemann, 2016). Indeed, *U. maydis* satisfies many of the requirements for Tn-seq: it is easily culturable in the laboratory, efficient transformation protocols are available (Bosch et al., 2016), and it possesses a small, well-annotated genome (Kamper et al., 2006). Moreover, there are haploid, yeast-

like laboratory strains of *U. maydis* available (Brachmann et al., 2001), which grow by budding, forming compact colonies on plates. The success of SATAY could be used to guide the development of Tn-seq in *U. maydis* and other fungal phytopathogens. Developing Tn-seq in fungal phytopathogens is a worthwhile pursuit, particularly because there are inherent limitations with using *S. cerevisiae* to explore how resistance may emerge in fungal phytopathogens (discussed in section 8.3.2). If successfully developed in fungal phytopathogens, Tn-seq would further hasten the discovery of novel modes of action and resistance mechanisms, facilitating efforts to tackle the increasing threat of antifungal resistance for global food security.

Appendix 1 – Primers used in this thesis

#	Primer Name	Sequence (5' to 3')
	Primers for gene deletions	
1	ADE2_Del_Fwd	GTATAAATTGGTGCGTAAAATCGTTGGATCTCTCTTCTAAcggatccccgggttaattaa
2	ADE2_Del_Rev	TATGTATGAAGTCCACATTTGATGTAATCATAACAAAGCCgaattcgagctcgtttaaac
3	SLN1_Del_Fwd	CACGTTGGGTATAATCTACTTTGTTTTGATTTAACAATACAAcggatccccgggttaattaa
4	SLN1_Del_Rev	CGCAAGCTTTTGATTTCTCTTACTATTCTTGGTTGTgaattcgagctcgtttaaac
5	HOL1_Del_Fwd	GTATCATATTACAATCTACAGGATATAACAAAACAGCTTCGCAACcggatccccgggttaattaa
6	HOL1_Del_Rev	GAAACTGTAATATTACCTAACCGGTATCCCACGTGTTTCACGAAGgaattcgagctcgtttaaac
7	SPE1_Del_Fwd	GTAGGTAAGATTTTTTGATTGTTCTACAACTTTTTCATAGTAATCcggatccccgggttaattaa
8	SPE1_Del_Rev	CACCCCCTCCGTCTCTCTTGCGAAAGTCGTGGTTAAATATATCCTgaattcgagctcgtttaaac
9	MNN4_Kan_Del_F2	CATTCCCCTAACCGCCGAACTCACCGCATCACAACGTCACTATTCcggatccccgggttaattaa
10	MNN4_Kan_Del_R2	AGGCTATAGAAATGAAGAGATTCATGAATTTTCAGTCAGGTTCgaattcgagctcgtttaaac
11	TPI1_Del_Fwd	CAATTTTTTGTTTGTATTCTTTTCTTGCTTAAATCTATAACTACAAcggatccccgggttaattaa
12	TPI1_Del_Rev	GCTTTCCGTAGTCATCAATTTATTTTACATAACACTAGATATAAAGgaattcgagctcgtttaaac
13	GLO1_Del_Fwd	TAAATAGGGAGAAAAAAAAATCGGAATAACATTTCCATGCCCGGATCCCCGGGTTAATTAA
14	GLO1_Del_Rev	TTAGTGTATGAAAAGTCAACAAGAATGGTCATTATTGTGAATTCGAGCTCGTTTAAAC
	Primers for amplifying *Candida albicans HOL1* for gap-repair cloning into pBK958	
15	C_albicans_HOL1_F	ACTATAGAAGAAAGTTTGCGAGTGTGAATCTTAAATTTTTAACAGatggcttttgatactactgt
16	C_albicans_HOL1_R	ACTTAATTCCTATCATCTACTAGATACAAGAAAGACGTCTCTGAAttatcccatcccttgagtca
	Primers used for *HOL1* separation-of-function mutation screening	
17	p[HOL1]_F	CTATTTCATGCTATTACTACCAAGTT
18	p[HOL1]_R	AGCTCTCCGCAACTAATGAG
19	HOL1_Seq_F1	CGCAACTTTTGCATTTCTAACG
20	HOL1_Seq_F2	GGTGCAACTGTCCCTGAGCGAC
21	HOL1_Seq_F3	GCAACTGCAATTATTGGGCCAGC
	Primers for introducing and checking point mutations in *BdDRK1*	
22	DRK1_H716A_GCA_Fwd	TGGCTAACATGTCTgcaGAAATTAGAACCCC
23	DRK1_H716A_GCA_Rev	GGGGTTCTAATTTCtgcAGACATGTTAGCCA
24	DRK1_H716Q_CAG_Fwd	TGGCTAACATGTCTcagGAAATTAGAACCCC
25	DRK1_H716Q_CAG_Rev	GGGGTTCTAATTTCctgAGACATGTTAGCCA
26	DRK1_D1140N_AAC_Fwd	ACGTCATTCTTATGaacGTTCAGATGCCAGT
27	DRK1_D1140N_AAC_Rev	ACTGGCATCTGAACgttCATAAGAATGACGT
28	Check_His_DRK1_Fwd	GATGGTGACTTCACCAAGT
29	Check_His_DRK1_Rev	GATGGTAAGCAAAGAATTGG
30	Check_Asp_DRK1_Fwd	CAATCACCACTGATCACAC
31	Check_Asp_DRK1_Rev	GTGGCACACTTCAAGATG

	Primers used for SATAY Library Amplification and Barcoding and Sequencing	
32	P5_MiniDs	AATGATACGGCGACCACCGAGATCTACtccgtcccgcaagttaaata
33	P7_indexD701	caagcagaagacggcatacgagatCGAGTAATacgaaaacgaacgggataaa*
34	P7_indexD702	caagcagaagacggcatacgagatTCTCCGGAacgaaaacgaacgggataaa*
35	P7_indexD703	caagcagaagacggcatacgagatAATGAGCGacgaaaacgaacgggataaa*
36	P7_indexD704	caagcagaagacggcatacgagatGGAATCTCacgaaaacgaacgggataaa*
37	P7_indexD705	caagcagaagacggcatacgagatTTCTGAATacgaaaacgaacgggataaa*
38	P7_indexD706	caagcagaagacggcatacgagatACGAATTCacgaaaacgaacgggataaa*
39	P7_indexD707	caagcagaagacggcatacgagatAGCTTCAGacgaaaacgaacgggataaa*
40	P7_indexD708	caagcagaagacggcatacgagatGCGCATTAacgaaaacgaacgggataaa*
41	P7_indexD709	caagcagaagacggcatacgagatCATAGCCGacgaaaacgaacgggataaa*
42	P7_indexD710	caagcagaagacggcatacgagatTTCGCGGAacgaaaacgaacgggataaa*
43	P7_indexD711	caagcagaagacggcatacgagatGCGCGAGAacgaaaacgaacgggataaa*
44	P7_indexD712	caagcagaagacggcatacgagatCTATCGCTacgaaaacgaacgggataaa*
45	P7_indexed_N701	caagcagaagacggcatacgagatTCGCCTTAacgaaaacgaacgggataaa*
46	P7_indexed_N702	caagcagaagacggcatacgagatCTAGTACGacgaaaacgaacgggataaa*
47	P7_indexed_N703	caagcagaagacggcatacgagatTTCTGCCTacgaaaacgaacgggataaa*
48	P7_indexed_N704	caagcagaagacggcatacgagatGCTCAGGAacgaaaacgaacgggataaa*
49	P7_indexed_N705	caagcagaagacggcatacgagatAGGAGTCCacgaaaacgaacgggataaa*
50	P7_indexed_N706	caagcagaagacggcatacgagatCATGCCTAacgaaaacgaacgggataaa*
51	P7_indexed_N707	caagcagaagacggcatacgagatGTAGAGAGacgaaaacgaacgggataaa*
52	P7_indexed_N710	caagcagaagacggcatacgagatCAGCCTCGacgaaaacgaacgggataaa*
53	P7_indexed_N711	caagcagaagacggcatacgagatTGCCTCTTacgaaaacgaacgggataaa*
54	P7_indexed_N712	caagcagaagacggcatacgagatTCCTCTACacgaaaacgaacgggataaa*
55	P7_indexed_N714	caagcagaagacggcatacgagatTCATGAGCacgaaaacgaacgggataaa*
56	P7_indexed_N715	caagcagaagacggcatacgagatCCTGAGATacgaaaacgaacgggataaa*
57	P7_indexed_N716	caagcagaagacggcatacgagatTAGCGAGTacgaaaacgaacgggataaa*
58	P7_indexed_N718	caagcagaagacggcatacgagatGTAGCTCCacgaaaacgaacgggataaa*
59	P7_indexed_N719	caagcagaagacggcatacgagatTACTACGCacgaaaacgaacgggataaa*
60	P7_indexed_N720	caagcagaagacggcatacgagatAGGCTCCGacgaaaacgaacgggataaa*
61	P7_indexed_N721	caagcagaagacggcatacgagatGCAGCGTAacgaaaacgaacgggataaa*
62	P7_indexed_N722	caagcagaagacggcatacgagatCTGCGCATacgaaaacgaacgggataaa*
63	P7_indexed_N723	caagcagaagacggcatacgagatGAGCGCTAacgaaaacgaacgggataaa*
64	P7_indexed_N724	caagcagaagacggcatacgagatCGCTCAGTacgaaaacgaacgggataaa*
65	P7_indexed_N726	caagcagaagacggcatacgagatGTCTTAGGacgaaaacgaacgggataaa*
66	P7_indexed_N727	caagcagaagacggcatacgagatACTGATCGacgaaaacgaacgggataaa*
67	P7_indexed_N728	caagcagaagacggcatacgagatTAGCTGCAacgaaaacgaacgggataaa*
68	P7_indexed_N729	caagcagaagacggcatacgagatGACGTCGAacgaaaacgaacgggataaa*
69	P7_Indexed_A701	caagcagaagacggcatacgagatGTCGTGATacgaaaacgaacgggataaa*
70	P7_Indexed_A702	caagcagaagacggcatacgagatACCACTGTacgaaaacgaacgggataaa*
71	P7_Indexed_A703	caagcagaagacggcatacgagatTGGATCTGacgaaaacgaacgggataaa*
72	P7_Indexed_A704	caagcagaagacggcatacgagatCCGTTTGTacgaaaacgaacgggataaa*

73	P7_Indexed_A705	caagcagaagacggcatacgagatTGCTGGGTacgaaaacgaacgggataaa*
74	P7_Indexed_A706	caagcagaagacggcatacgagatGAGGGGTTacgaaaacgaacgggataaa*
75	P7_Indexed_A707	caagcagaagacggcatacgagatAGGTTGGGacgaaaacgaacgggataaa*
76	P7_Indexed_A708	caagcagaagacggcatacgagatGTGTGGTGacgaaaacgaacgggataaa*
77	P7_Indexed_A709	caagcagaagacggcatacgagatTGGGTTTCacgaaaacgaacgggataaa*
78	P7_Indexed_A710	caagcagaagacggcatacgagatTGGTCACAacgaaaacgaacgggataaa*
79	688_minidsSEQ1210	TTTACCGACCGTTACCGACCGTTTTCATCCCTA
80	Custom_index1	GGTTTTCGATTACCGTATTTATCCCGTTCGTTTTCGT

*Oligonucleotide sequences © 2016 Illumina, Inc. All rights reserved. Derivative works created by Illumina customers are authorized for use with Illumina instruments and products only. All other uses are strictly prohibited

Primers used for colony PCR genotyping

81	KanMX_twd_5prime	CATGTTGGAATTTAATCGCGGCCTC
82	KanMX_twd_3prime	CTATGGAACTGCCTCGGTG
83	NAT +748 Fwd	CAATCGTATGTGAATGCTGG
84	NAT -249 Rev	GGATGTATGGGCTAAATGTAC
85	Sln1_Fwd_Geno_Nter	GGAGAAGATCTTATAGATCTATCATCCAATTATAATAAGCATAG
86	Sln1_Rev_Geno_Nter	CGTTACAGCCAGAATAATCAGTGAGCC
87	HIS3_Rev_Geno_Nter	GAGATAAACGCCTTGCGCTCCTGAACA
88	Drk1_Fwd_Geno_Nter	ATTTAAGTTAATAAACGGTC
89	Drk1_Rev_Geno_Nter	GATTTATAAGAATTGAATGGCAAAG
90	Drk1_Fwd_Geno_Cter	CCAGGTATGGATTCTCAAGCTAC
91	Drk1_Rev_Geno_Cter	CCTAGACTTCAGGTTGTCTAACTCC
92	HOL1_Geno_F_Nter	GCTATTACTACCAAGTTGAC
93	HOL1_Geno_R_Nter	GGTTGAGGGATTAGGACGAC
94	HOL1_Geno_F_Cter	CTACTATGGTAAGAGGATAAG
95	HOL1_Geno_R_Cter	GTGCCATTTCTTGGTACTGC
96	SPE1_Geno_F_Nter	CAGCACGGCTTTTGTTTCAAG
97	SPE1_Geno_R_Nter	CTTGACTTCTCCCAAATCGC
98	SPE1_Geno_F_Cter	CACATGTGATGGTTTGGATTG
99	SPE1_Geno_R_Cter	AATGGCGTACAGTGGTGGACAG
100	CaHOL1_F	CAAATAATACCATTCCTCACGAG
101	CaHOL1_R	GGTGGATTATAAAAATACGTGT
102	MNN4_Fwd_Cter	GCAGGAAGAAGGAGAAAAGATGAAG
103	MNN4_Rev_Cter	GAATTGTTTGCCACTTATCACTG
104	Tpi1_Geno_F_Cter	CATCAGAAAGTTCTTGGCTTCCAAG
105	Tpi1_Geno_R_Cter	CGAAATTTAAGTGGCTCAGAATGA
106	Glo1_Geno_F_Cter	GATCCAAACTTCCACTATCATAACG
107	Glo1_Geno_R_Cter	GATATTTGGCATGTATGCGTTGATG
108	IntgrtChckFwdSUP53	TCCTCGAGGAGAACTTCTAGTAT
109	IntgrtChckRevSUP53	TCGGGGCGAAAACTCTCAAG

Appendix 2 – Calculations of intracellular concentrations of ATI-2307, Pentamidine and Iminoctadine

All values shown are the average for three independent biological replicates.

Compound concentrations in cell lysates were determined using LC-MS, described in Chapter 5.

Appendix 2A – Calculations for intracellular concentration of ATI-2307

		Workings
[ATI-2307] in cell lysate as per calibration curve (µg/mL)	0.03	
To find the amount of ATI-2307 in cell lysate (µg)		
Weight of pellet (mg)	390	
Pellet volume comprised of yeast cells (µL) (assume 52% of pellet)	202.8	390*0.52
Volume of acetonitrile:water (80:20 (v/v)) added to pellet (µL)	1000	
Theoretical total volume of lysate (µL)	1202.8	202.8 + 1000
Amount of ATI-2307 in lysate (µg)	0.036	0.03*(1202.8/1000)
To find the [ATI-2307] inside *S. cerevisiae* cells (µg/mL)		
Amount of ATI-2307 in lysate (µg)	0.036	
Pellet volume comprised of yeast cells (µL) (assume 52% of pellet)	202.8	
[ATI-2307] inside *S. cerevisiae* cells (µg/mL)	0.178	0.036/(202.8/1000)

Appendix 2B – Calculations for intracellular concentration of Pentamidine

		Workings
[Pentamidine] in cell lysate as per calibration curve (µg/mL)**(1/10)**	0.841	
[Pentamidine] in cell lysate as per calibration curve (µg/mL)	8.41	0.841*10
To find the amount of Pentamidine in cell lysate (µg)		
Weight of pellet (mg)	713	
Pellet volume comprised of yeast cells (µL) (assume 52% of pellet)	370.76	713*0.52
Volume of acetonitrile:water (80:20 (v/v)) added to pellet (µL)	1833	
Theoretical total volume of lysate (µL)	2203.76	370.76 + 1833
Amount of Pentamidine in lysate (µg)	18.534	8.41*(2203.8/1000)
To find the [Pentamidine] inside *S. cerevisiae* cells (µg/mL)		
Amount of Pentamidine in lysate (µg)	18.534	
Pellet volume comprised of yeast cells (µL) (assume 52% of pellet)	370.76	
[Pentamidine] inside *S. cerevisiae* cells (µg/mL)	49.989	18.534/(370.76/1000)

Appendix 2C – Calculations for intracellular concentration of Iminoctadine

		Workings
[Iminoctadine] in cell lysate as per calibration curve (µg/mL)(1/10)	2.079	
[Iminoctadine] in cell lysate as per calibration curve (µg/mL)	20.79	2.079*10
To find the amount of Iminoctadine in cell lysate (µg)		
Weight of pellet (mg)	483.33	
Pellet volume comprised of yeast cells (µL) (assume 52% of pellet)	251.33	483.33*0.52
Volume of acetonitrile:water (80:20 (v/v)) added to pellet (µL)	1000	
Theoretical total volume of lysate (µL)	1251.33	1000 + 251.33
Amount of Iminoctadine in lysate (µg)	26.015	20.79*(1251.33/1000)
To find the [Iminoctadine] inside *S. cerevisiae* cells (µg/mL)		
Amount of Iminoctadine in lysate (µg)	26.015	
Pellet volume comprised of yeast cells (µL) (assume 52% of pellet)	251.33	
[Iminoctadine] inside *S. cerevisiae* cells (µg/mL)	103.51	26.015*(251.33/1000)

References

Abe, M., Nishida, I., Minemura, M., Qadota, H., Seyama, Y., Watanabe, T., & Ohya, Y. (2001). Yeast 1,3-β-Glucan Synthase Activity is Inhibited by Phytosphingosine Localized to the Endoplasmic Reticulum. *Journal of Biological Chemistry*, *276*(29), 26923–26930. https://doi.org/10.1074/jbc.M102179200

Abramson, J., Adler, J., Dunger, J., Evans, R., Green, T., Pritzel, A., Ronneberger, O., Willmore, L., Ballard, A. J., Bambrick, J., Bodenstein, S. W., Evans, D. A., Hung, C. C., O'Neill, M., Reiman, D., Tunyasuvunakool, K., Wu, Z., Žemgulytė, A., Arvaniti, E., … Jumper, J. M. (2024). Accurate structure prediction of biomolecular interactions with AlphaFold 3. *Nature*, *630*(8016), 493–500. https://doi.org/10.1038/s41586-024-07487-w

Ademe, M., & Girma, F. (2020). Candida auris: From multidrug resistance to pan-resistant strains. In *Infection and Drug Resistance* (Vol. 13, pp. 1287–1294). Dove Medical Press Ltd. https://doi.org/10.2147/IDR.S249864

Alburquenque, C., Bucarey, S. A., Neira-Carrillo, A., Urza, B., Hermosilla, G., & Tapia, C. V. (2010). Antifungal activity of low molecular weight chitosan against clinical isolates of Candida spp. *Medical Mycology*, *48*(8), 1018–1023. https://doi.org/10.3109/13693786.2010.486412

Alepuz, P. M., De Nadal, E., Zapater, M., Ammerer, G., & Posas, F. (2003). Osmostress-induced transcription by Hot1 depends on a Hog1-mediated recruitment of the RNA Pol II. *EMBO Journal*, *22*(10), 2433–2442. https://doi.org/10.1093/emboj/cdg243

Anderson, J. B. (2005). Evolution of antifungal-drug resistance: Mechanisms and pathogen fitness. *Nature Reviews Microbiology*, *3*(7), 547–556. https://doi.org/10.1038/nrmicro1179

Anderson, N. S., Mukherjee, I., Bentivoglio, C. M., & Barlowe, C. (2017). The golgin protein Coy1 functions in intra-Golgi retrograde transport and interacts with the COG complex and Golgi SNAREs. *Molecular Biology of the Cell*, *28*(20), 2686–2700. https://doi.org/10.1091/mbc.E17-03-0137

Anderson, T. M., Clay, M. C., Cioffi, A. G., Diaz, K. A., Hisao, G. S., Tuttle, M. D., Nieuwkoop, A. J., Comellas, G., Maryum, N., Wang, S., Uno, B. E., Wildeman, E. L., Gonen, T., Rienstra, C. M., & Burke, M. D. (2014). Amphotericin forms an extramembranous and fungicidal sterol sponge. *Nature Chemical Biology*, *10*(5), 400–406. https://doi.org/10.1038/nchembio.1496

Arendrup, M. C., & Patterson, T. F. (2017). Multidrug-resistant candida: Epidemiology, molecular mechanisms, and treatment. *Journal of Infectious Diseases*, *216*, S445–S451. https://doi.org/10.1093/infdis/jix131

Arthington, B. A., Bennett, L. G., Skatrud, P. L., Guynn, C. J., Barbuch, R. J., UIbright, C. E., & Bard, M. (1991). Cloning, disruption and sequence of the gene encoding yeast C-5 sterol desaturase. *Gene*, *102*(1), 39–44. https://doi.org/10.1016/0378-1119(91)90535-J

Avenot, H., Simoneau, P., Iacomi-Vasilescu, B., & Bataillé-Simoneau, N. (2005). Characterization of mutations in the two-component histidine kinase gene AbNIK1 from Alternaria brassicicola that confer high dicarboximide and phenylpyrrole resistance. *Current Genetics*, *47*(4), 234–243. https://doi.org/10.1007/s00294-005-0568-2

Balkan, C., Ercan, I., Isik, E., Akdeniz, S., Balcioglu, O., Kodedová, M., & Zimmermannová, O. (2019). Genomewide Elucidation of Drug Resistance Mechanisms for Systemically Used Antifungal Drugs Amphotericin B, Caspofungin, and Voriconazole in the Budding Yeast. *Antimicrobial Agents and Chemotherapy*, *63*(9), 1–11.

Ballou, C. E. (1990). Isolation, Characterization, and Properties of Saccharomyces Cerevisiae MNN Mutants with Nonconditional Protein Glycosylation Defects. *Methods in Enzymology*, *185*, 440–470. https://doi.org/10.1016/0076-6879(90)85038-P

Ballou, C. E., Kern, K. A., & Raschke, W. C. (1973). Genetic Control of Yeast Mannan Structure. *Journal of Biological Chemistry*, *248*(13), 4667–4670. https://doi.org/10.1016/s0021-9258(19)43715-0

Balzi, E., Chen, W., Ulaszewski, S., Capieaux, E., & Goffeau, A. (1987). The multidrug resistance gene PDR1 from Saccharomyces cerevisiae. *Journal of Biological Chemistry*, *262*(35), 16871–16879. https://doi.org/10.1016/s0021-9258(18)45464-6

Barbet, N. C., Schneider, U., Helliwell, S. B., Stansfield, I., Tuite, M. F., & Hall, M. N. (1996). TOR controls translation initiation and early G1 progression in yeast. *Molecular Biology of the Cell*, *7*(1), 25–42. https://doi.org/10.1091/mbc.7.1.25

Bari, V. K., Sharma, S., Alfatah, M., Mondal, A. K., & Ganesan, K. (2015). Plasma membrane proteolipid 3 protein modulates amphotericin B resistance through sphingolipid biosynthetic pathway. *Scientific Reports*, *5*. https://doi.org/10.1038/srep09685

Bartlett, D. W., Clough, J. M., Godwin, J. R., Hall, A. A., Hamer, M., & Parr-Dobrzanski, B. (2002). The strobilurin fungicides. In *Pest Management Science* (Vol. 58, Issue 7, pp. 649–662). John Wiley and Sons Ltd. https://doi.org/10.1002/ps.520

Bautista-Baños, S., Hernández-Lauzardo, A. N., Velázquez-Del Valle, M. G., Hernández-López, M., Ait Barka, E., Bosquez-Molina, E., & Wilson, C. L. (2006). Chitosan as a potential natural compound to control pre and postharvest diseases of horticultural commodities. *Crop Protection*, *25*(2), 108–118. https://doi.org/10.1016/j.cropro.2005.03.010

Bautista-Baños, S., Hernández-López, M., Bosquez-Molina, E., & Wilson, C. L. (2003). Effects of chitosan and plant extracts on growth of Colletotrichum gloeosporioides, anthracnose levels and quality of papaya fruit. *Crop Protection*, *22*(9), 1087–1092. https://doi.org/10.1016/S0261-2194(03)00117-0

Bebber, D. P., Ramotowski, M. A. T., & Gurr, S. J. (2013). Crop pests and pathogens move polewards in a warming world. *Nature Climate Change*, *3*(11), 985–988. https://doi.org/10.1038/nclimate1990

Becher, R., & Wirsel, S. G. R. (2012). Fungal cytochrome P450 sterol 14α-demethylase (CYP51) and azole resistance in plant and human pathogens. *Applied Microbiology and Biotechnology*, *95*, 825–840. https://doi.org/10.1007/s00253-012-4195-9

Beh, C. T., Cool, L., Phillips, J., & Rine, J. (2001). Overlapping functions of the yeast oxysterol-binding protein homologues. *Genetics*, *157*(3), 1117–1140. https://doi.org/10.1093/genetics/157.3.1117

Beh, C. T., & Rine, J. (2004). A role for yeast oxysterol-binding protein homologs in endocytosis and in the maintenance of intracellular sterol-lipid distribution. *Journal of Cell Science*, *117*(14), 2983–2996. https://doi.org/10.1242/jcs.01157

Benhamou, N. (1996). Elicitor-induced plant defence pathways. *Trends in Plant Science*, *1*(7), 233–240. https://doi.org/10.1016/1360-1385(96)86901-9

Ben-Shalom, N., Ardi, R., Pinto, R., Aki, C., & Fallik, E. (2003). Controlling gray mould caused by Botrytis cinerea in cucumber plants by means of chitosan. *Crop Protection*, *22*(2), 285–290. https://doi.org/10.1016/S0261-2194(02)00149-7

Berman, J., & Krysan, D. (2020). Drug resistance and tolerance in fungi. *Nature Reviews Microbiology*, *18*(6), 319–331. https://doi.org/10.1038/s41579-019-0322-2

Berninsone, P., Miret, J. J., & Hirschberg, C. B. (1994). The Golgi guanosine diphosphatase is required for transport of GDP- mannose into the lumen of Saccharomyces cerevisiae Golgi vesicles. *Journal of Biological Chemistry*, *269*(1), 207–211. https://doi.org/10.1016/s0021-9258(17)42335-0

Bersching, K., & Jacob, S. (2021). The molecular mechanism of fludioxonil action is different to osmotic stress sensing. *Journal of Fungi*, *7*(5). https://doi.org/10.3390/jof7050393

Bi, K., Liang, Y., Mengiste, T., & Sharon, A. (2023). Killing softly: a roadmap of Botrytis cinerea pathogenicity. *Trends in Plant Science*, *28*(2), 211–222. https://doi.org/10.1016/j.tplants.2022.08.024

Binda, M., Péli-Gulli, M. P., Bonfils, G., Panchaud, N., Urban, J., Sturgill, T. W., Loewith, R., & De Virgilio, C. (2009). The Vam6 GEF Controls TORC1 by Activating the EGO Complex. *Molecular Cell*, *35*(5), 563–573. https://doi.org/10.1016/j.molcel.2009.06.033

Bojsen, R., Regenberg, B., Gresham, D., & Folkesson, A. (2016). A common mechanism involving the TORC1 pathway can lead to amphotericin B-persistence in biofilm and planktonic Saccharomyces cerevisiae populations. *Scientific Reports*, *6*(1), 21874. https://doi.org/10.1038/srep21874

Bongomin, F., Gago, S., Oladele, R. O., & Denning, D. W. (2017). Global and multi-national prevalence of fungal diseases—estimate precision. *Journal of Fungi*, *3*(4). https://doi.org/10.3390/jof3040057

Borba, H. H. L., Steimbach, L. M., Riveros, B. S., Tonin, F. S., Ferreira, V. L., Bagatim, B. A. de Q., Balan, G., Pontarolo, R., & Wiens, A. (2018). Cost-effectiveness of amphotericin B formulations in the treatment of systemic fungal infections. *Mycoses*, *61*(10), 754–763. https://doi.org/10.1111/myc.12801

Bösch, K., Frantzeskakis, L., Vraneš, M., Kämper, J., Schipper, K., & Göhre, V. (2016). Genetic manipulation of the plant pathogen Ustilago maydis to study fungal biology and plant microbe interactions. *Journal of Visualized Experiments*, *2016*(115). https://doi.org/10.3791/54522

Bouwknegt, J., Koster, C. C., Vos, A. M., Ortiz-Merino, R. A., Wassink, M., Luttik, M. A. H., van den Broek, M., Hagedoorn, P. L., & Pronk, J. T. (2021). Class-II dihydroorotate dehydrogenases from three phylogenetically distant fungi support anaerobic pyrimidine biosynthesis. *Fungal Biology and Biotechnology*, *8*(1), 1–18. https://doi.org/10.1186/s40694-021-00117-4

Brachmann, A., Weinzierl, G., Kämper, J., & Kahmann, R. (2001). Identification of genes in the bW/bE regulatory cascade in Ustilago maydis. *Molecular Microbiology*, *42*(4), 1047–1063. https://doi.org/10.1046/j.1365-2958.2001.02699.x

Brandhorst, T. T., Kean, I. R. L., Lawry, S. M., Wiesner, D. L., & Klein, B. S. (2019). Phenylpyrrole fungicides act on triosephosphate isomerase to induce methylglyoxal stress and alter hybrid histidine kinase activity. *Scientific Reports*, *9*(1), 5047. https://doi.org/10.1038/s41598-019-41564-9

Brandhorst, T. T., & Klein, B. S. (2019). Uncertainty surrounding the mechanism and safety of the post-harvest fungicide fludioxonil. *Food and Chemical Toxicology*, *123*(August 2018), 561–565. https://doi.org/10.1016/j.fct.2018.11.037

Brauner, A., Fridman, O., Gefen, O., & Balaban, N. Q. (2016). Distinguishing between resistance, tolerance and persistence to antibiotic treatment. *Nature Reviews Microbiology*, *14*(5), 320–330. https://doi.org/10.1038/nrmicro.2016.34

Brent, K. J., & Hollomon, D. W. (2007). Fungicide resistance in crop pathogens: How can it be managed ? *FRAC Monograph*, *Second Edi*, 48.

Brown, G. D., Denning, D. W., Gow, N. A. R., Levitz, S. M., Netea, M. G., & White, T. C. (2012). Hidden killers: Human fungal infections. *Science Translational Medicine*, *4*(165), 1–10. https://doi.org/10.1126/scitranslmed.3004404

Bruinsma, P., Spelbrink, R. G., & Nothwehr, S. F. (2004). Retrograde transport of the mannosyltransferase Och1p to the early Golgi requires a component of the COG transport complex. *Journal of Biological Chemistry*, *279*(38), 39814–39823. https://doi.org/10.1074/jbc.M405500200

Buschart, A., Gremmer, K., El-Mowafy, M., van den Heuvel, J., Mueller, P. P., & Bilitewski, U. (2012). A novel functional assay for fungal histidine kinases group III reveals the role of HAMP domains for fungicide sensitivity. *Journal of Biotechnology*, *157*(1), 268–277. https://doi.org/10.1016/j.jbiotec.2011.09.017

Büttner, P., Koch, F., Voigt, K., Quidde, T., Risch, S., Blaich, R., Briickner, B., & Tudzynski, P. (1994). Variations in ploidy among isolates of Botrytis cinerea: implications for genetic and molecular analyses. In *Curr Genet* (Vol. 25).

Cain, A. K., Barquist, L., Goodman, A. L., Paulsen, I. T., Parkhill, J., & van Opijnen, T. (2020). A decade of advances in transposon-insertion sequencing. *Nature Reviews Genetics*, *21*(9), 526–540. https://doi.org/10.1038/s41576-020-0244-x

Cannon, R. D., Lamping, E., Holmes, A. R., Niimi, K., Baret, P. V., Keniya, M. V., Tanabe, K., Niimi, M., Goffeau, A., & Monk, B. C. (2009). Efflux-mediated antifungal drug resistance. *Clinical Microbiology Reviews*, *22*(2), 291–321. https://doi.org/10.1128/CMR.00051-08

Carvajal, E., Van Den Hazel, H. B., Cybularz-Kolaczkowska, A., Balzi, E., & Goffeau, A. (1997). Molecular and phenotypic: Characterization of yeast PDR1 mutants that show hyperactive transcription of various ABC multidrug transporter genes. *Molecular and General Genetics*, *256*(4), 406–415. https://doi.org/10.1007/s004380050584

Castagnolo, D., Schenone, S., & Botta, M. (2011). Guanylated diamines, triamines, and polyamines: Chemistry and biological properties. *Chemical Reviews*, *111*(9), 5247–5300. https://doi.org/10.1021/cr100423x

Catlett, N. L., Yoder, O. C., & Turgeon, B. G. (2003). Whole-Genome Analysis of Two-Component Signal Transduction Genes in Fungal Pathogens. *Eukaryotic Cell*, *2*(6), 1151–1161. https://doi.org/10.1128/EC.2.6.1151-1161.2003

Chaloner, T. M., Gurr, S. J., & Bebber, D. P. (2021). Plant pathogen infection risk tracks global crop yields under climate change. *Nature Climate Change*, *11*(8), 710–715. https://doi.org/10.1038/s41558-021-01104-8

Chaves, A. F. A., Navarro, M. V., Castilho, D. G., Calado, J. C. P., Conceição, P. M., & Batista, W. L. (2016). A conserved dimorphism-regulating histidine kinase controls the dimorphic switching in Paracoccidioides brasiliensis. *FEMS Yeast Research*, *16*(5). https://doi.org/10.1093/femsyr/fow047

Chen, P., Michel, A. H., & Zhang, J. (2022). Transposon insertional mutagenesis of diverse yeast strains suggests coordinated gene essentiality polymorphisms. *Nature Communications*, *13*(1490), 1–15. https://doi.org/10.1038/s41467-022-29228-1

Chinen, T., Ota, Y., Nagumo, Y., Masumoto, H., & Usui, T. (2011). Construction of multidrug-sensitive yeast with high sporulation efficiency. *Bioscience, Biotechnology and Biochemistry*, *75*(8), 1588–1593. https://doi.org/10.1271/bbb.110311

Chowdhary, A., Sharma, C., & Meis, J. F. (2017). Candida auris: A rapidly emerging cause of hospital-acquired multidrug-resistant fungal infections globally. In *PLoS Pathogens* (Vol. 13, Issue 5). Public Library of Science. https://doi.org/10.1371/journal.ppat.1006290

Christen, B., Abeliuk, E., Collier, J. M., Kalogeraki, V. S., Passarelli, B., Coller, J. A., Fero, M. J., McAdams, H. H., & Shapiro, L. (2011). The essential genome of a bacterium. *Molecular Systems Biology*, *7*(1). https://doi.org/10.1038/msb.2011.58

Chung, Y. C., & Chen, C. Y. (2008). Antibacterial characteristics and activity of acid-soluble chitosan. *Bioresource Technology*, *99*(8), 2806–2814. https://doi.org/10.1016/j.biortech.2007.06.044

Coe, K. A., Lee, W., Stone, M. C., Komazin-Meredith, G., Meredith, T. C., Grad, Y. H., & Walker, S. (2019). Multi-strain Tn-Seq reveals common daptomycin resistance determinants in Staphylococcus aureus. *PLoS Pathogens*, *15*(11). https://doi.org/10.1371/journal.ppat.1007862

Cokol, M., Chua, H. N., Tasan, M., Mutlu, B., Weinstein, Z. B., Suzuki, Y., Nergiz, M. E., Costanzo, M., Baryshnikova, A., Giaever, G., Nislow, C., Myers, C. L., Andrews, B. J.,

Boone, C., & Roth, F. P. (2011). Systematic exploration of synergistic drug pairs. *Molecular Systems Biology*, *7*. https://doi.org/10.1038/msb.2011.71

Compagno, C., Boschi, F., & Ranzi, B. M. (1996). Glycerol production in a triose phosphate isomerase deficient mutant of Saccharomyces cerevisiae. *Biotechnology Progress*, *12*(5), 591–595. https://doi.org/10.1021/bp960043c

Compagno, C., Brambilla, L., Capitanio, D., Boschi, F., Ranzi, B. M., & Porro, D. (2001). Alterations of the glucose metabolism in a triose phosphate isomerase-negative Saccharomyces cerevisiae mutant. *Yeast*, *18*(7), 663–670. https://doi.org/10.1002/yea.715

Conaway, R. C., & Conaway, J. W. (2009). The INO80 chromatin remodeling complex in transcription, replication and repair. *Trends in Biochemical Sciences*, *34*(2), 71–77. https://doi.org/10.1016/j.tibs.2008.10.010

Cools, H. J., Hawkins, N. J., & Fraaije, B. A. (2013). Constraints on the evolution of azole resistance in plant pathogenic fungi. *Plant Pathology*, *62*(S1), 36–42. https://doi.org/10.1111/ppa.12128

Coorey, N. V. C., Matthews, J. H., Bellows, D. S., & Atkinson, P. H. (2015). Pleiotropic drug-resistance attenuated genomic library improves elucidation of drug mechanisms. *Molecular BioSystems*, *11*(11), 3129–3136. https://doi.org/10.1039/c5mb00406c

Coradetti, S. T., Pinel, D., Geiselman, G. M., Ito, M., Mondo, S. J., Reilly, M. C., Cheng, Y.-F., Bauer, S., Grigoriev, I. V, Gladden, J. M., Simmons, B. A., Brem, R. B., Arkin, A. P., & Skerker, J. M. (2018). Functional genomics of lipid metabolism in the oleaginous yeast Rhodosporidium toruloides. *ELife*, *7*(e32110). https://doi.org/10.7554/eLife.32110.001

Coste, A., Selmecki, A., Forche, A., Diogo, D., Bougnoux, M. E., D'Enfert, C., Berman, J., & Sanglard, D. (2007). Genotypic evolution of azole resistance mechanisms in sequential Candida albicans isolates. *Eukaryotic Cell*, *6*(10), 1889–1904. https://doi.org/10.1128/EC.00151-07

Coste, A., Turner, V., Ischer, F., Morschhäuser, J., Forche, A., Selmecki, A., Berman, J., Bille, J., & Sanglard, D. (2006). A mutation in Tac1p, a transcription factor regulating CDR1 and CDR2, is coupled with loss of heterozygosity at chromosome 5 to mediate antifungal resistance in Candida albicans. *Genetics*, *172*(4), 2139–2156. https://doi.org/10.1534/genetics.105.054767

Cruz, C., Goldstein, A., Blankenship, J., Del Poeta, M., Davis, D., Cardenas, M., Perfect, J., McCusker, J., & Heitman, J. (2002). Calcineurin is essential for survival during membrane stress in Candida albicans. *The EMBO Journal*, *21*(4), 546–559.

Cui, J., Ren, B., Tong, Y., Dai, H., & Zhang, L. (2015). Synergistic combinations of antifungals and anti-virulence agents to fight against Candida albicans. *Virulence*, *6*(4), 362–371. https://doi.org/10.1080/21505594.2015.1039885

Daum, G., Tuller, G., Nemec, T., Hrastnik, C., Balliano, G., Cattel, L., Milla, P., Rocco, F., Conzelmann, A., Vionnet, C., Kelly, D. E., Kelly, S., Schweizer, E., Schüller, H. J., Hojad, U., Greiner, E., & Finger, K. (1999). Systematic analysis of yeast strains with possible defects in lipid metabolism. *Yeast*, *15*(7), 601–614. https://doi.org/10.1002/(SICI)1097-0061(199905)15:7<601::AID-YEA390>3.0.CO;2-N

Davydova, V. N., Yermak, I. M., & Solov'eva, T. (2000). Interaction of Bacterial Endotoxins with Chitosan. Effect of Endotoxin Structure, Chitosan Molecular Mass, and Ionic Strength of the Solution on the Formation of the Complex. In *Article in Biochemistry*. https://www.researchgate.net/publication/12280983

De Nadal, E., Zapater, M., Alepuz, P. M., Sumoy, L., Mas, G., & Posas, F. (2004). The MAPK Hog1 recruits Rpd3 histone deacetylase to activate osmoresponsive genes. *Nature*, *427*(6972), 370–374. https://doi.org/10.1038/nature02258

De Vega, D., Holden, N., Hedley, P. E., Morris, J., Luna, E., & Newton, A. (2021). Chitosan primes plant defence mechanisms against Botrytis cinerea, including expression of Avr9/Cf-9 rapidly elicited genes. *Plant Cell and Environment*, *44*(1), 290–303. https://doi.org/10.1111/pce.13921

Defosse, T. A., Sharma, A., Mondal, A. K., de Bernonville, T. D., Latgé, J. P., Calderone, R., Giglioli-Guivarc'h, N., Courdavault, V., Clastre, M., & Papon, N. (2015). Hybrid histidine kinases in pathogenic fungi. *Molecular Microbiology*, *95*(6), 914–924. https://doi.org/10.1111/mmi.12911

Demuyser, L., & Van Dijck, P. (2019). Can Saccharomyces cerevisiae keep up as a model system in fungal azole susceptibility research? *Drug Resistance Updates*, *42*(February), 22–34. https://doi.org/10.1016/j.drup.2019.02.002

de Nadal, E., & Posas, F. (2022). The HOG pathway and the regulation of osmoadaptive responses in yeast. *FEMS Yeast Research*, *22*(1), 1–7. https://doi.org/10.1093/femsyr/foac013

Denning, D. W. (2024). Global incidence and mortality of severe fungal disease. In *The Lancet Infectious Diseases*. Elsevier Ltd. https://doi.org/10.1016/S1473-3099(23)00692-8

Dephoure, N., Gould, K. L., Gygi, S. P., & Kellogg, D. R. (2013). Mapping and analysis of phosphorylation sites: A quick guide for cell biologists. In *Molecular Biology of the Cell* (Vol. 24, Issue 5, pp. 535–542). https://doi.org/10.1091/mbc.E12-09-0677

Deutschbauer, A. M., Jaramillo, D. F., Proctor, M., Kumm, J., Hillenmeyer, M. E., Davis, R. W., Nislow, C., & Giaever, G. (2005). Mechanisms of haploinsufficiency revealed by genome-wide profiling in yeast. *Genetics*, *169*(4), 1915–1925. https://doi.org/10.1534/genetics.104.036871

Dexter, J. P., Xu, P., Gunawardena, J., & McClean, M. N. (2015). Robust network structure of the Sln1-Ypd1-Ssk1 three-component phospho-relay prevents unintended activation of the HOG MAPK pathway in Saccharomyces cerevisiae. *BMC Systems Biology*, *9*(1), 1–15. https://doi.org/10.1186/s12918-015-0158-y

Dickson, R. C., Sumanasekera, C., & Lester, R. L. (2006). Functions and metabolism of sphingolipids in Saccharomyces cerevisiae. *Progress in Lipid Research*, 447–465. https://doi.org/10.1016/j.plipres.2006.03.004

Divon, H. H., & Fluhr, R. (2007). Nutrition acquisition strategies during fungal infection of plants. In *FEMS Microbiology Letters* (Vol. 266, Issue 1, pp. 65–74). https://doi.org/10.1111/j.1574-6968.2006.00504.x

Douglas, C. M., D'Ippolito, J. A., Shei, G. J., Meinz, M., Onishi, J., Marrinan, J. A., Li, W., Abruzzo, G. K., Flattery, A., Bartizal, K., Mitchell, A., & Kurtz, M. B. (1997). Identification of the FKS1 gene of Candida albicans as the essential target of 1,3-β-D-glucan synthase inhibitors. *Antimicrobial Agents and Chemotherapy*, *41*(11), 2471–2479. https://doi.org/10.1128/aac.41.11.2471

Douglas, C. M., Foor, F., Marrinan, J. A., Morin, N., Nielsen, J. B., Dahl, A. M., Mazur, P., Baginsky, W., Li, W., El-Sherbeini, M., Clemas, J. A., Mandala, S. M., Frommer, B. R., & Kurtz, M. B. (1994). The Saccharomyces cerevisiae FKS1 (ETG1) gene encodes an integral membrane protein which is a subunit of 1,3-β-D-glucan synthase. *Proceedings of the National Academy of Sciences of the United States of America*, *91*(26), 12907–12911. https://doi.org/10.1073/pnas.91.26.12907

Du, H., Bing, J., Hu, T., Ennis, C. L., Nobile, C. J., & Huang, G. (2020). Candida auris: Epidemiology, biology, antifungal resistance, and virulence. *PLoS Pathogens*, *16*(10). https://doi.org/10.1371/journal.ppat.1008921

Dubouloz, F., Deloche, O., Wanke, V., Cameroni, E., & De Virgilio, C. (2005). The TOR and EGO protein complexes orchestrate microautophagy in yeast. *Molecular Cell*, *19*(1), 15–26. https://doi.org/10.1016/j.molcel.2005.05.020

Duina, A. A., Miller, M. E., & Keeney, J. B. (2014). Budding yeast for budding geneticists: A primer on the Saccharomyces cerevisiae model system. *Genetics*, *197*(1), 33–48. https://doi.org/10.1534/genetics.114.163188

Dunkel, N., Blaß, J., Rogers, P. D., & Morschhäuser, J. (2008). Mutations in the multi-drug resistance regulator MRR1, followed by loss of heterozygosity, are the main cause of MDR1 overexpression in fluconazole-resistant Candida albicans strains. *Molecular Microbiology*, *69*(4), 827–840. https://doi.org/10.1111/j.1365-2958.2008.06309.x

Edskes, H. K., Mukhamedova, M., Edskes, B. K., & Wickner, R. B. (2018). Hermes transposon mutagenesis shows [URE3] prion pathology prevented by a ubiquitin-targeting protein: Evidence for carbon/nitrogen assimilation cross talk and a second function for Ure2p in Saccharomyces cerevisiae. *Genetics*, *209*(3), 789–800. https://doi.org/10.1534/genetics.118.300981

Eising, S., Esch, B., Wälte, M., Duarte, P. V., Walter, S., Ungermann, C., Bohnert, M., & Fröhlich, F. (2022). A lysosomal biogenesis map reveals the cargo spectrum of yeast vacuolar protein targeting pathways. *Journal of Cell Biology*, *221*(4). https://doi.org/10.1083/jcb.202107148

El Ghaouth, A., Arul, J., Asselin, A., & Benhamou, N. (1992). Antifungal activity of chitosan on post-harvest pathogens: induction of morphological and cytological alterations in Rhizopus stolonifer. *Mycological Research*, *96*(9), 769–779. https://doi.org/10.1016/S0953-7562(09)80447-4

El Yacoubi, B., Bailly, M., & De Crécy-Lagard, V. (2012). Biosynthesis and function of posttranscriptional modifications of transfer RNAs. *Annual Review of Genetics*, *46*, 69–95. https://doi.org/10.1146/annurev-genet-110711-155641

Enyenihi, A. H., & Saunders, W. S. (2003). Large-Scale Functional Genomic Analysis of Sporulation and Meiosis in Saccharomyces cerevisiae. *Genetics*, *163*, 47–54. http://www.genetics.org/supplemen-

Eraso, P., Mazón, M. J., & Portillo, F. (2006). Yeast protein kinase Ptk2 localizes at the plasma membrane and phosphorylates in vitro the C-terminal peptide of the H+-ATPase. *Biochimica et Biophysica Acta - Biomembranes*, *1758*(2), 164–170. https://doi.org/10.1016/j.bbamem.2006.01.010

Erez, O., & Kahana, C. (2001). Screening for Modulators of Spermine Tolerance Identifies Sky1, the SR Protein Kinase of Saccharomyces cerevisiae , as a Regulator of Polyamine Transport and Ion Homeostasis. *Molecular and Cellular Biology*, *21*(1), 175–184. https://doi.org/10.1128/mcb.21.1.175-184.2001

Fernández-Ortuño, D., Torés, J. A., De Vicente, A., & Pérez-García, A. (2008). Mechanisms of resistance to QoI fungicides in phytopathogenic fungi. In *International Microbiology* (Vol. 11, Issue 1, pp. 1–9). Sociedad Espanola de Microbiologia. https://doi.org/10.2436/20.1501.01.38

Fillinger, S., Ajouz, S., Nicot, P. C., Leroux, P., & Bardin, M. (2012). Functional and structural comparison of Pyrrolnitrin- and Iprodione-induced modifications in the class III histidine-kinase Bos1 of Botrytis cinerea. *PLoS ONE*, *7*(8), e42520. https://doi.org/10.1371/journal.pone.0042520

Fisher, M. C., Hawkins, N. J., Sanglard, D., & Gurr, S. J. (2018). Worldwide emergence of resistance to antifungal drugs challenges human health and food security. *Science*, *360*(6390), 739–742.

Fisher, M. C., Henk, D. A., Briggs, C. J., Brownstein, J. S., Madoff, L. C., Mccraw, S. L., & Gurr, S. J. (2012). Emerging fungal threats to animal , plant and ecosystem health. *Nature*. https://doi.org/10.1038/nature10947

Flowers, S. A., Barker, K. S., Berkow, E. L., Toner, G., Chadwick, S. G., Gygax, S. E., Morschhäuser, J., & Rogers, P. D. (2012). *Gain-of-Function Mutations in UPC2 Are a Frequent Cause of ERG11 Upregulation in Azole-Resistant Clinical Isolates of Candida albicans*. *11*(10), 1289–1299. https://doi.org/10.1128/EC.00215-12

Fones, H., & Gurr, S. (2015). The impact of Septoria tritici Blotch disease on wheat: An EU perspective. *Fungal Genetics and Biology*, *79*, 3–7. https://doi.org/10.1016/j.fgb.2015.04.004

Fones, H. N., Bebber, D. P., Chaloner, T. M., Kay, W. T., Steinberg, G., & Gurr, S. J. (2020). Threats to global food security from emerging fungal and oomycete crop pathogens. *Nature Food*, *1*(6), 332–342. https://doi.org/10.1038/s43016-020-0075-0

Fonzi, W. A. (1989). Biochemical and genetic characterization of the structure of yeast ornithine decarboxylase. *Biochemical and Biophysical Research Communications*, *162*(3), 1409–1416.

Forche, A., Alby, K., Schaefer, D., Johnson, A. D., Berman, J., & Bennett, R. J. (2008). The parasexual cycle in Candida albicans provides an alternative pathway to meiosis for the formation of recombinant strains. *PLoS Biology*, *6*(5), 1084–1097. https://doi.org/10.1371/journal.pbio.0060110

Forment, J., Mulet, J. M., Vicente, O., & Serrano, R. (2002). The yeast SR protein kinase Sky1p modulates salt tolerance, membrane potential and the Trk1,2 potassium transporter. *Biochimica et Biophysica Acta - Biomembranes*, *1565*(1), 36–40. https://doi.org/10.1016/S0005-2736(02)00503-5

Fouché, S., Badet, T., Oggenfuss, U., Plissonneau, C., Francisco, C. S., & Croll, D. (2020). Stress-Driven Transposable Element De-repression Dynamics and Virulence Evolution in a Fungal Pathogen. *Molecular Biology and Evolution*, *37*(1), 221–239. https://doi.org/10.1093/molbev/msz216

Fowler, D. M., & Fields, S. (2014). Deep mutational scanning: A new style of protein science. In *Nature Methods* (Vol. 11, Issue 8, pp. 801–807). Nature Publishing Group. https://doi.org/10.1038/nmeth.3027

Frenkel, O., Cadle-Davidson, L., Wilcox, W. F., & Milgroom, M. G. (2015). Mechanisms of resistance to an azole fungicide in the grapevine powdery mildew fungus, Erysiphe necator. *Phytopathology*, *105*(3), 370–377. https://doi.org/10.1094/PHYTO-07-14-0202-R

Fritz, R., Lanen, C., Colas, V., & Leroux, P. (1997). Inhibition of methionine biosynthesis in Botrytis cinerea by the anilinopyrimidine fungicide pyrimethanil. *Pesticide Science*, *49*(1), 40–46. https://doi.org/10.1002/(SICI)1096-9063(199701)49:1<40::AID-PS470>3.0.CO;2-Y

Fröhlich, F., Petit, C., Kory, N., Christiano, R., Hannibal-Bach, H. K., Graham, M., Liu, X., Ejsing, C. S., Farese, R. V., & Walther, T. C. (2015). The GARP complex is required for cellular sphingolipid homeostasis. *ELife*, *4*, e08712. https://doi.org/10.7554/eLife.08712

Furukawa, K., Randhawa, A., Kaur, H., Mondal, A. K., & Hohmann, S. (2012). Fungal fludioxonil sensitivity is diminished by a constitutively active form of the group III histidine kinase. *FEBS Letters*, *586*(16), 2417–2422. https://doi.org/10.1016/j.febslet.2012.05.057

Gaber, R. F., Styles, C. A., & Fink, G. R. (1988). TRK1 Encodes a Plasma Membrane Protein Required for High-Affinity Potassium Transport in Saccharomyces cerevisiae. *Molecular and Cellular Biology*. https://doi.org/10.1128/mcb.8.7.2848-2859.1988

Gale, A. N., Pavesic, M. W., Nickels, T. J., Xu, Z., Cormack, B. P., Cunningham, K. W., Gale, A. N., Pavesic, M. W., Nickels, T. J., Xu, Z., Cormack, B. P., Cunningham, K. W., Gale, A. N., Pavesic, M. W., Nickels, T. J., Xu, Z., Cormack, B. P., & Cunningham, K. W. (2023). Pdr1 functions as a sensor of cellular stresses in Candida glabrata. *MSphere*, *8*(4), e00254-23.

Gale, A. N., Sakhawala, R. M., Levitan, A., Sharan, R., Berman, J., Timp, W., & Cunningham, K. W. (2020). Identification of essential genes and fluconazole susceptibility genes in candida glabrata by profiling hermes transposon insertions. *G3: Genes, Genomes, Genetics*, *10*(10), 3859–3870. https://doi.org/10.1534/g3.120.401595

Galih Haribowo, A., Thomas Hannich, J., Michel, A. H., Megyeri, M., Schuldiner, M., Kornmann, B., & Riezman, H. (2019). Cytotoxicity of 1-deoxysphingolipid unraveled by genome-wide genetic screens and lipidomics in Saccharomyces cerevisiae.

Molecular Biology of the Cell, *30*(22), 2814–2826. https://doi.org/10.1091/mbc.E19-07-0364

Gallagher, L. A., Shendure, J., & Manoil, C. (2011). Genome-scale identification of resistance functions in Pseudomonas aeruginosa using Tn-seq. *MBio*, *2*(1). https://doi.org/10.1128/mBio.00315-10

Galocha, M., Costa, I. V., & Teixeira, M. C. (2020). Carrier-mediated drug uptake in fungal pathogens. *Genes*, *11*(11), 1324. https://doi.org/10.3390/genes11111324

Galván Márquez, I., Akuaku, J., Cruz, I., Cheetham, J., Golshani, A., & Smith, M. L. (2013). Disruption of protein synthesis as antifungal mode of action by chitosan. *International Journal of Food Microbiology*, *164*(1), 108–112. https://doi.org/10.1016/j.ijfoodmicro.2013.03.025

Gancedo, J. M. (2001). Control of pseudohyphae formation in Saccharomyces cerevisiae . *FEMS Microbiology Reviews*, *25*(1), 107–123. https://doi.org/10.1111/j.1574-6976.2001.tb00573.x

Gangadharan, S., Mularoni, L., Fain-Thornton, J., Wheelan, S. J., & Craig, N. L. (2010). DNA transposon Hermes inserts into DNA in nucleosome-free regions in vivo. *Proceedings of the National Academy of Sciences of the United States of America*, *107*(51), 21966–21972. https://doi.org/10.1073/pnas.1016382107

Gao, J., Wang, H., Li, Z., Wong, A., Wang, Y.-Z., Guo, Y., Lin, X., Zeng, G., Liu, H., Wang, Y., & Wang, J. (2018). Candida albicans gains azole resistance by altering sphingolipid composition. *Nature Communications*, *9*(1), 1–14. https://doi.org/10.1038/s41467-018-06944-1

Gao, X. D., Kaigorodov, V., & Jigami, Y. (1999). YND1, a homologue of GDA1, encodes membrane-bound apyrase required for Golgi N- and O-glycosylation in Saccharomyces cerevisiae. *Journal of Biological Chemistry*, *274*(30), 21450–21456. https://doi.org/10.1074/jbc.274.30.21450

Garcia, L. G. S., Guedes, G. M. de M., da Silva, M. L. Q., Castelo-Branco, D. S. C. M., Sidrim, J. J. C., Cordeiro, R. de A., Rocha, M. F. G., Vieira, R. S., & Brilhante, R. S. N. (2018). Effect of the molecular weight of chitosan on its antifungal activity against Candida spp. in planktonic cells and biofilm. *Carbohydrate Polymers*, *195*, 662–669. https://doi.org/10.1016/j.carbpol.2018.04.091

García, R., Botet, J., Rodríguez-Peña, J. M., Bermejo, C., Ribas, J. C., Revuelta, J. L., Nombela, C., & Arroyo, J. (2015). Genomic profiling of fungal cell wall-interfering compounds: Identification of a common gene signature. *BMC Genomics*, *16*(1), 1–20. https://doi.org/10.1186/s12864-015-1879-4

Gasmi, N., Jacques, P. E., Klimova, N., Guo, X., Ricciardi, A., Robert, F., & Turcotte, B. (2014). The switch from fermentation to respiration in Saccharomyces cerevisiae is regulated by the Ert1 transcriptional activator/repressor. *Genetics*, *198*(2), 547–560. https://doi.org/10.1534/genetics.114.168609

Gbelska, Y., Krijger, J. J., & Breunig, K. D. (2006). Evolution of gene families: The multidrug resistance transporter genes in five related yeast species. *FEMS Yeast Research*, *6*(3), 345–355. https://doi.org/10.1111/j.1567-1364.2006.00058.x

Geisinger, E., Vargas-Cuebas, G., Mortman, N. J., Syal, S., Dai, Y., Wainwright, E. L., Lazinski, D., Wood, S., Zhu, Z., Anthony, J., van Opijnen, T., & Isberg, R. R. (2019). The landscape of phenotypic and transcriptional responses to ciprofloxacin in acinetobacter baumannii: Acquired resistance alleles modulate drug-induced sos response and prophage replication. *MBio*, *10*(3). https://doi.org/10.1128/mBio.01127-19

Geva, Y., Crissman, J., Arakel, E. C., Gómez-Navarro, N., Chuartzman, S. G., Stahmer, K. R., Schwappach, B., Miller, E. A., & Schuldiner, M. (2017). Two novel effectors of trafficking and maturation of the yeast plasma membrane H+-ATPase. *Traffic*, *18*(10), 672–682. https://doi.org/10.1111/tra.12503

Giaever, G., Chu, A. M., Ni, L., Connelly, C., Riles, L., Véronneau, S., & Dow, S. (2002). Functional profiling of the Saccharomyces cerevisiae genome. *Nature*, *418*(6896), 387–391.

Giaever, G., Flaherty, P., Kumm, J., Proctor, M., Nislow, C., Jaramillo, D. F., Chu, A. M., Jordan, M. I., Arkin, A. P., & Davis, R. W. (2004). Chemogenomic profiling: Identifying the functional interactions of small molecules in yeast. *Proceedings of the National Academy of Sciences of the United States of America*, *101*(3), 793–798. https://doi.org/10.1073/pnas.0307490100

Giaever, G., Shoemaker, D. D., Jones, T. W., Liang, H., Winzeler, E. A., Astromoff, A., & Davis, R. W. (1999). Genomic profiling of drug sensitivities via induced haploinsufficiency. *Nature Genetics*, *21*(3), 278–283. https://doi.org/10.1038/6791

Gietz, R. D., & Schiestl, R. H. (2007). High-efficiency yeast transformation using the LiAc/SS carrier DNA/PEG method. *Nature Protocols*, *2*(1), 31–34. https://doi.org/10.1038/nprot.2007.13

Girgis, H. S., Liu, Y., Ryu, W. S., & Tavazoie, S. (2007). A comprehensive genetic characterization of bacterial motility. *PLoS Genetics*, *3*(9), 1644–1660. https://doi.org/10.1371/journal.pgen.0030154

Godfray, H. C. J., Mason-D'croz, D., & Robinson, S. (2016). Food system consequences of a fungal disease epidemic in a major crop. *Philosophical Transactions of the Royal Society B: Biological Sciences*, *371*(1709). https://doi.org/10.1098/rstb.2015.0467

González, M., Brito, N., Frías, M., & González, C. (2013). Botrytis cinerea Protein O-Mannosyltransferases Play Critical Roles in Morphogenesis, Growth, and Virulence. *PLoS ONE*, *8*(6). https://doi.org/10.1371/journal.pone.0065924

Goossens, A., de la Fuente, N., Forment, J., Serrano, R., & Portillo, F. (2000). Regulation of Yeast H + -ATPase by Protein Kinases Belonging to a Family Dedicated to Activation of Plasma Membrane Transporters. *Molecular and Cellular Biology*. https://doi.org/10.1128/mcb.20.20.7654-7661.2000

Goy, R. C., De Britto, D., & Assis, O. B. G. (2009). A review of the antimicrobial activity of chitosan. *Polimeros*, 241–247. https://doi.org/10.1590/S0104-14282009000300013

Grimmer, M. K., Bosch, F. Van Den, Powers, J., & Paveley, N. D. (2014). *Fungicide resistance risk assessment based on traits associated with the rate of pathogen evolution*. *March*. https://doi.org/10.1002/ps.3781

Guo, Y., Park, J. M., Cui, B., Humes, E., Gangadharan, S., Hung, S., FitzGerald, P. C., Hoe, K. L., Grewal, S. I. S., Craig, N. L., & Levin, H. L. (2013). Integration profiling of gene function with dense maps of transposon integration. *Genetics*, *195*(2), 599–609. https://doi.org/10.1534/genetics.113.152744

Hallstrom, T. C., & Moye-Rowley, W. S. (2000). Multiple signals from dysfunctional mitochondria activate the pleiotropic drug resistance pathway in Saccharomyces cerevisiae. *Journal of Biological Chemistry*, *275*(48), 37347–37356. https://doi.org/10.1074/jbc.M007338200

Haro-Reyes, T., Díaz-Peralta, L., Galván-Hernández, A., Rodríguez-López, A., Rodríguez-Fragoso, L., & Ortega-Blake, I. (2022). Polyene Antibiotics Physical Chemistry and Their Effect on Lipid Membranes; Impacting Biological Processes and Medical Applications. In *Membranes* (Vol. 12, Issue 7). MDPI. https://doi.org/10.3390/membranes12070681

Harrison, B. D., Hashemi, J., Bibi, M., Pulver, R., Bavli, D., Nahmias, Y., Wellington, M., Sapiro, G., & Berman, J. (2014). A Tetraploid Intermediate Precedes Aneuploid Formation in Yeasts Exposed to Fluconazole. *PLoS Biology*, *12*(3). https://doi.org/10.1371/journal.pbio.1001815

Hassan, K. A., Cain, A. K., Huang, T., Liu, Q., Elbourne, L. D. H., Boinett, C. J., Brzoska, A. J., Li, L., Ostrowski, M., Nhu, N. T. K., Nhu, T. D. H., Baker, S., Parkhill, J., & Paulsen, I. T. (2016). Fluorescence-based flow sorting in parallel with transposon insertion site

sequencing identifies multidrug efflux systems in acinetobacter baumannii. *MBio*, *7*(5). https://doi.org/10.1128/mBio.01200-16

Hawkins, N., & Fraaije, B. (2016). Predicting Resistance by Mutagenesis : Lessons from 45 Years of MBC Resistance. *Frontiers in Microbiology*, *7*, 1814. https://doi.org/10.3389/fmicb.2016.01814

Hawkins, N., & Fraaije, B. (2018). Fitness Penalties in the Evolution of Fungicide Resistance. *Annual Review of Phytopathology*, *56*, 339–360. https://doi.org/10.1146/annurev-phyto-080417-050012- 050012

Hawkins, N. J., & Fraaije, B. A. (2021). Contrasting levels of genetic predictability in the evolution of resistance to major classes of fungicides. *Molecular Ecology*, *August 2020*, 1–10. https://doi.org/10.1111/mec.15877

Healey, K. R., Katiyar, S. K., Raj, S., & Edlind, T. D. (2012). CRS-MIS in Candida glabrata: Sphingolipids modulate echinocandin-Fks interaction. *Molecular Microbiology*, *86*(2), 303–313. https://doi.org/10.1111/j.1365-2958.2012.08194.x

Heinicke, S., Livstone, M. S., Lu, C., Oughtred, R., Kang, F., Angiuoli, S. V., White, O., Botstein, D., & Dolinski, K. (2007). The Princeton Protein Orthology Database (P-POD): A comparative genomics analysis tool for biologists. *PLoS ONE*, *2*(8). https://doi.org/10.1371/journal.pone.0000766

Helander, I. M., Nurmiaho-Lassila, E. L., Ahvenainen, R., Rhoades, J., & Roller, S. (2001). Chitosan disrupts the barrier properties of the outer membrane of Gram-negative bacteria. *International Journal of Food Microbiology*, *71*(2–3), 235–244. https://doi.org/10.1016/S0168-1605(01)00609-2

Hillenmeyer, M. E., Fung, E., & Wildenhain, J. (2008). The chemical genomic portrait of yeast: Uncovering a phenotype for all genes. *Chemtracts*, *20*(12), 503–504. https://doi.org/10.1126/science.1150021.The

Ho, C. H., Magtanong, L., Barker, S. L., Gresham, D., Nishimura, S., Natarajan, P., Koh, J. L. Y., Porter, J., Gray, C. A., Andersen, R. J., Giaever, G., Nislow, C., Andrews, B., Botstein, D., Graham, T. R., Yoshida, M., & Boone, C. (2009). A molecular barcoded yeast ORF library enables mode-of-action analysis of bioactive compounds. *Nature Biotechnology*, *27*(4), 369–377. https://doi.org/10.1038/nbt.1534

Hoenigl, M., Sprute, R., Egger, M., Arastehfar, A., Cornely, O. A., Krause, R., Lass-Flörl, C., Prattes, J., Spec, A., Thompson, G. R., Wiederhold, N., & Jenks, J. D. (2021). The Antifungal Pipeline: Fosmanogepix, Ibrexafungerp, Olorofim, Opelconazole, and Rezafungin. *Drugs*, *81*(15), 1703–1729. https://doi.org/10.1007/s40265-021-01611-0

Hoepfner, D., Helliwell, S. B., Sadlish, H., Schuierer, S., Filipuzzi, I., Brachat, S., Bhullar, B., Plikat, U., Abraham, Y., Altorfer, M., Aust, T., Baeriswyl, L., Cerino, R., Chang, L., Estoppey, D., Eichenberger, J., Frederiksen, M., Hartmann, N., Hohendahl, A., … Movva, N. R. (2014). High-resolution chemical dissection of a model eukaryote reveals targets, pathways and gene functions. *Microbiological Research*, *169*(2–3), 107–120. https://doi.org/10.1016/j.micres.2013.11.004

Hohmann, S. (2002). Osmotic Stress Signaling and Osmoadaptation in Yeasts. *Microbiology and Molecular Biology Reviews*, *66*(2), 300–372. https://doi.org/10.1128/mmbr.66.2.300-372.2002

Holmes, K. J., Klass, D. M., Guiney, E. L., & Cyert, M. S. (2013). Whi3, an S. cerevisiae RNA-binding protein, is a component of stress granules that regulates levels of its target mRNAS. *PLoS ONE*, *8*(12). https://doi.org/10.1371/journal.pone.0084060

Holthuis, J. C. M., Nichols, B. J., Dhruvakumar, S., & Pelham, H. R. B. (1998). Two syntaxin homologues in the TGN/endosomal system of yeast. *EMBO Journal*. https://doi.org/10.1093/emboj/17.1.113

Hoon, S., St.Onge, R. P., Giaever, G., & Nislow, C. (2008). Yeast chemical genomics and drug discovery: an update. *Trends in Pharmacological Sciences*, *29*(10), 499–504. https://doi.org/10.1016/j.tips.2008.07.006

Horie, T., Tatebayashi, K., Yamada, R., & Saito, H. (2008). Phosphorylated Ssk1 Prevents Unphosphorylated Ssk1 from Activating the Ssk2 Mitogen-Activated Protein Kinase Kinase Kinase in the Yeast High-Osmolarity Glycerol Osmoregulatory Pathway. *Molecular and Cellular Biology*, *28*(17), 5172–5183. https://doi.org/10.1128/mcb.00589-08

Hossain, M. M., Sultana, F., Yesmin, L., Rubayet, M. T., Abdullah, H. M., Siddique, S. S., Bhuiyan, M. A. B., & Yamanaka, N. (2023). Understanding Phakopsora pachyrhizi in soybean: comprehensive insights, threats, and interventions from the Asian perspective. In *Frontiers in Microbiology* (Vol. 14). Frontiers Media SA. https://doi.org/10.3389/fmicb.2023.1304205

Hsu, J. W., Chang, L. C., Jang, L. T., Huang, C. F., & Lee, F. J. S. (2013). The N-Terminus of Vps74p Is Essential for the Retention of Glycosyltransferases in the Golgi but Not for the Modulation of Apical Polarized Growth in Saccharomyces cerevisiae. *PLoS ONE*, *8*(9), 1–16. https://doi.org/10.1371/journal.pone.0074715

Hu, M., & Chen, S. (2021). Non-target site mechanisms of fungicide resistance in crop pathogens: A review. *Microorganisms*, *9*(3), 1–19. https://doi.org/10.3390/microorganisms9030502

Hua, Z., Fatheddin, P., & Graham, T. R. (2002). An Essential Subfamily of Drs2p-related P-Type ATPases Is Required for Protein Trafficking between Golgi Complex and Endosomal/Vacuolar System. *Molecular Biology of the Cell*, *13*(9), 3162–3177. https://doi.org/10.1091/mbc.E02

Huang, B., Johansson, M. J. O., & Byström, A. S. (2005). An early step in wobble uridine tRNA modification requires the Elongator complex. *Rna*, *11*(4), 424–436. https://doi.org/10.1261/rna.7247705

Huang, X., Wang, A., Chen, Y., Sun, Q., Xu, L., Liu, F., Li, B., Pang, X., & Mu, W. (2022). Toxicological risks of SDHIs and QoIs to zebrafish (Danio rerio) and the corresponding poisoning mechanism. *Aquatic Toxicology*, *252*. https://doi.org/10.1016/j.aquatox.2022.106282

Huang, Z., Chen, K., Zhang, J., Li, Y., Wang, H., Cui, D., Tang, J., Liu, Y., Shi, X., Li, W., Liu, D., Chen, R., Sucgang, R. S., & Pan, X. (2013). A Functional Variomics Tool for Discovering Drug-Resistance Genes and Drug Targets. *Cell Reports*, *3*(2), 577–585. https://doi.org/10.1016/j.celrep.2013.01.019

Inoue', H., Nojima, H., & 0kayama, H. (1990). High efficiency transformation of Escherichia coli with plasmids (Competent cell; strain DH5; pBR322 vector; simple and efficient method (SEM); cDNA library; electroporation; frozen-stock; stability). In *Gene*.

Inoue, Y., & Kimura, A. (1996). Identification of the structural gene for glyoxalase I from Saccharomyces cerevisiae. *Journal of Biological Chemistry*, *271*(42), 25958–25965. https://doi.org/10.1074/jbc.271.42.25958

Islam, M. T., Croll, D., Gladieux, P., Soanes, D. M., Persoons, A., Bhattacharjee, P., Hossain, M. S., Gupta, D. R., Rahman, M. M., Mahboob, M. G., Cook, N., Salam, M. U., Surovy, M. Z., Sancho, V. B., Maciel, J. L. N., NhaniJúnior, A., Castroagudín, V. L., Reges, J. T. de A., Ceresini, P. C., … Kamoun, S. (2016). Emergence of wheat blast in Bangladesh was caused by a South American lineage of Magnaporthe oryzae. *BMC Biology*, *14*(1). https://doi.org/10.1186/s12915-016-0309-7

Jaime, M. D. L. A., Lopez-Llorca, L. V., Conesa, A., Lee, A. Y., Proctor, M., Heisler, L. E., Gebbia, M., Giaever, G., Westwood, J. T., & Nislow, C. (2012). Identification of yeast genes that confer resistance to chitosan oligosaccharide (COS) using chemogenomics. *BMC Genomics*, *13*(1). https://doi.org/10.1186/1471-2164-13-267

Janiak-Spens, F., Sparling, D. P., & West, A. H. (2000). Novel role for an HPt domain in stabilizing the phosphorylated state of a response regulator domain. *Journal of Bacteriology*, *182*(23), 6673–6678. https://doi.org/10.1128/JB.182.23.6673-6678.2000

Janke, C., Magiera, M. M., Rathfelder, N., Taxis, C., Reber, S., Maekawa, H., Moreno-Borchart, A., Doenges, G., Schwob, E., Schiebel, E., & Knop, M. (2004). A versatile toolbox for PCR-based tagging of yeast genes: New fluorescent proteins, more markers and promoter substitution cassettes. *Yeast*, *21*(11), 947–962. https://doi.org/10.1002/yea.1142

Jiao, W., Liu, X., Chen, Q., Du, Y., Li, Y., Yue, F., Dong, X., & Fu, M. (2020). Epsilon-poly-L-lysine (ε-PL) exhibits antifungal activity in vivo and in vitro against Botrytis cinerea and mechanism involved. *Postharvest Biology and Technology*, *168*. https://doi.org/10.1016/j.postharvbio.2020.111270

Jigami, Y., & Odani, T. (1999). Mannosylphosphate transfer to yeast mannan. *Biochimica et Biophysica Acta - General Subjects*, *1426*(2), 335–345. https://doi.org/10.1016/S0304-4165(98)00134-2

Jinna, S., & Finch, J. (2015). Spotlight on tavaborole for the treatment of onychomycosis. *Drug Design, Development and Therapy*, *9*, 6185–6190. https://doi.org/10.2147/DDDT.S81944

Johansson, M. J. O., Xu, F., & Byström, A. S. (2018). Elongator—a tRNA modifying complex that promotes efficient translational decoding. *Biochimica et Biophysica Acta - Gene Regulatory Mechanisms*, *1861*(4), 401–408. https://doi.org/10.1016/j.bbagrm.2017.11.006

Johansson, P., Wiltschi, B., Kumari, P., Kessler, B., Vonrhein, C., Vonck, J., Oesterhelt, D., & Grininger, M. (2008). Inhibition of the fungal fatty acid synthase type I multienzyme complex. *Proceedings of the National Academy of Sciences of the United States of America*, *105*(35), 12803–12808. https://doi.org/10.1073/pnas.0805827105

John Peter, A. T., Schie, S. N. S., Cheung, N. J., Michel, A. H., Peter, M., & Kornmann, B. (2022). Rewiring phospholipid biosynthesis reveals resilience to membrane perturbations and uncovers regulators of lipid homeostasis. *The EMBO Journal*, *41*(7), e109998. https://doi.org/10.15252/embj.2021109998

Johns, L. E., Goldman, G. H., Ries, L. N. A., & Brown, N. A. (2021). Nutrient sensing and acquisition in fungi: mechanisms promoting pathogenesis in plant and human hosts. In *Fungal Biology Reviews* (Vol. 36, pp. 1–14). Elsevier Ltd. https://doi.org/10.1016/j.fbr.2021.01.002

Johnson, M. E., Katiyar, S. K., & Edlind, T. D. (2011). New Fks hot spot for acquired echinocandin resistance in Saccharomyces cerevisiae and its contribution to intrinsic resistance of Scedosporium species. *Antimicrobial Agents and Chemotherapy*, *55*(8), 3774–3781. https://doi.org/10.1128/AAC.01811-10

Jordá, T., & Puig, S. (2020). Regulation of ergosterol biosynthesis in saccharomyces cerevisiae. *Genes*, *11*(7), 1–18. https://doi.org/10.3390/genes11070795

Jorgensen, J. R., Tei, R., Baskin, J. M., Michel, A. H., Kornmann, B., & Emr, S. D. (2020). ESCRT-III and ER–PM contacts maintain lipid homeostasis. *Molecular Biology of the Cell*, *31*(12), 1302–1313. https://doi.org/10.1091/MBC.E20-01-0061

Jumper, J., Evans, R., Pritzel, A., Green, T., Figurnov, M., Ronneberger, O., Tunyasuvunakool, K., Bates, R., Žídek, A., Potapenko, A., Bridgland, A., Meyer, C., Kohl, S. A. A., Ballard, A. J., Cowie, A., Romera-Paredes, B., Nikolov, S., Jain, R., Adler, J., … Hassabis, D. (2021). Highly accurate protein structure prediction with AlphaFold. *Nature*, *596*(7873), 583–589. https://doi.org/10.1038/s41586-021-03819-2

Kaida, D., Yashirod, H., Toh-E, A., & Kikuchi, Y. (2002). Yeast Whi2 and Psr1-phosphatase form a complex and regulate STRE-mediated gene expression. *Genes to Cells*, *7*(6), 543–552. https://doi.org/10.1046/j.1365-2443.2002.00538.x

Kalagiri, R., Stanfield, R. L., Meisenhelder, J., Clair, J. J. La, Fuhs, S. R., Wilson, I. A., & Hunter, T. (2021). Structural basis for differential recognition of phosphohistidine-containing peptides by 1-pHis and 3-pHis monoclonal antibodies. *PNAS*, *6*. https://doi.org/10.1073/pnas.2010644118/-/DCSupplemental

Kämper, J., Kahmann, R., Bölker, M., Ma, L. J., Brefort, T., Saville, B. J., Banuett, F., Kronstad, J. W., Gold, S. E., Müller, O., Perlin, M. H., Wösten, H. A. B., De Vries, R., Ruiz-Herrera, J., Reynaga-Peña, C. G., Snetselaar, K., McCann, M., Pérez-Martín, J., Feldbrügge, M., … Birren, B. W. (2006). Insights from the genome of the biotrophic fungal plant pathogen Ustilago maydis. *Nature*, *444*(7115), 97–101. https://doi.org/10.1038/nature05248

Kaouass, M., Audette, M., Ramotar, D., Verma, S., De Montigny, D., Gamache, I., Torossian, K., & Poulin, R. (1997). The STK2 Gene, Which Encodes a Putative Ser/Thr Protein Kinase, Is Required for High-Affinity Spermidine Transport in Saccharomyces cerevisiae. *Molecular and Cellular Biology*, *17*(6), 2994–3004. https://doi.org/10.1128/mcb.17.6.2994

Karlsborn, T., Tükenmez, H., Mahmud, A. K. M. F., Xu, F., Xu, H., & Byström, A. S. (2014). Elongator, a conserved complex required for wobble uridine modifications in Eukaryotes. *RNA Biology*, *11*(12), 1519–1528. https://doi.org/10.4161/15476286.2014.992276

Karson, E. M., & Ballou, C. E. (1978). Biosynthesis of yeast mannan. Properties of a mannosylphosphate transferase in Saccharomyces cerevisiae. *Journal of Biological Chemistry*, *253*(18), 6484–6492. https://doi.org/10.1016/s0021-9258(19)46958-5

Kato, U., Emoto, K., Fredriksson, C., Nakamura, H., Ohta, A., Kobayashi, T., Murakami-Murofushi, K., Kobayashi, T., & Umeda, M. (2002). A novel membrane protein, Ros3p, is required for phospholipid translocation across the plasma membrane in Saccharomyces cerevisiae. *Journal of Biological Chemistry*, *277*(40), 37855–37862. https://doi.org/10.1074/jbc.M205564200

Kaur, J., & Nobile, C. J. (2023). Antifungal drug-resistance mechanisms in Candida biofilms. *Current Opinion in Microbiology*, *71*, 102237. https://doi.org/10.1016/j.mib.2022.102237

Kayikci, Ö., & Nielsen, J. (2015). Glucose repression in Saccharomyces cerevisiae. *FEMS Yeast Research*, *15*(6), 1–8. https://doi.org/10.1093/femsyr/fov068

Ke, C. L., Deng, F. S., Chuang, C. Y., & Lin, C. H. (2021). Antimicrobial actions and applications of Chitosan. *Polymers*, *13*(6), 904. https://doi.org/10.3390/polym13060904

Kehrein, K., Schilling, R., Möller-Hergt, B. V., Wurm, C. A., Jakobs, S., Lamkemeyer, T., Langer, T., & Ott, M. (2015). Organization of Mitochondrial Gene Expression in Two Distinct Ribosome-Containing Assemblies. *Cell Reports*, *10*(6), 843–853. https://doi.org/10.1016/j.celrep.2015.01.012

Keighley, C., Garnham, & K., Harch, S. A. J., Robertson, & M., Chaw, & K., Teng, J. C., & Chen, -A. (2021). Candida auris: Diagnostic Challenges and Emerging Opportunities for the Clinical Microbiology Laboratory. *Current Fungal Infection Reports*, *15*, 116–126. https://doi.org/10.1007/s12281-021-00420-y/Published

Kellis, M., Birren, B. W., & Lander, E. S. (2004). *Proof and evolutionary analysis of ancient genome duplication in the yeast Saccharomyces cerevisiae*. http://www.broad.mit.edu/seq/YeastDuplication

Keon, J. P. R., White, G. A., & Hargreaves, J. A. (1991). Isolation, characterization and sequence of a gene conferring resistance to the systemic fungicide carboxin from the maize smut pathogen, Ustilago maydis. In *Curr Genet* (Vol. 19).

Kilani, J., & Fillinger, S. (2016). Phenylpyrroles: 30 years, two molecules and (nearly) no resistance. *Frontiers in Microbiology*, *7*. https://doi.org/10.3389/fmicb.2016.02014

Klopf, E., Paskova, L., Solé, C., Mas, G., Petryshyn, A., Posas, F., Wintersberger, U., Ammerer, G., & Schüller, C. (2009). Cooperation between the INO80 Complex and Histone Chaperones Determines Adaptation of Stress Gene Transcription in the Yeast Saccharomyces cerevisiae. *Molecular and Cellular Biology*. https://doi.org/10.1128/mcb.01858-08

Ko, C. H., Buckley, A. M., & Gaber, R. F. (1990). TRK2 is required for low affinity K+ transport in Saccharomyces cerevisiae. *Genetics*, *125*(2), 305. https://doi.org/10.1093/genetics/125.2.305

Kobayashi, S. D., & Nagiec, M. M. (2003). Ceramide/long-chain base phosphate rheostat in Saccharomyces cerevisiae: Regulation of ceramide synthesis by Elo3p and Cka2p. *Eukaryotic Cell*, *2*(2), 284–294. https://doi.org/10.1128/EC.2.2.284-294.2003

Kojima, K., Takano, Y., Yoshimi, A., Tanaka, C., Kikuchi, T., & Okuno, T. (2004). Fungicide activity through activation of a fungal signalling pathway. *Molecular Microbiology*, *53*(6), 1785–1796. https://doi.org/10.1111/j.1365-2958.2004.04244.x

Kolaczkowski, M., Kolaczkowska, A., Luczynski, J., Witek, S., & Goffeau, A. (1998). In vivo characterization of the drug resistance profile of the major ABC transporters and other components of the yeast pleiotropic drug resistance network. *Microbial Drug Resistance*, *4*(3), 143–158. https://doi.org/10.1089/mdr.1998.4.143

Kretschmer, M., Leroch, M., Mosbach, A., Walker, A. S., Fillinger, S., Mernke, D., Schoonbeek, H. J., Pradier, J. M., Leroux, P., De Waard, M. A., & Hahn, M. (2009). Fungicide-driven evolution and molecular basis of multidrug resistance in field populations of the grey mould fungus Botrytis cinerea. *PLoS Pathogens*, *5*(12). https://doi.org/10.1371/journal.ppat.1000696

Krutyhołowa, R., Hammermeister, A., Zabel, R., Abdel-Fattah, W., Reinhardt-Tews, A., Helm, M., Stark, M. J. R., Breunig, K. D., Schaffrath, R., & Glatt, S. (2019). Kti12, a PSTK-like tRNA dependent ATPase essential for tRNA modification by Elongator. *Nucleic Acids Research*, *47*(9), 4814–4830. https://doi.org/10.1093/nar/gkz190

Kuge, S., Jones, N., & Nomoto, A. (1997). Regulation of yAP-1 nuclear localization in response to oxidative stress. *EMBO Journal*. https://doi.org/10.1093/emboj/16.7.1710

Kuhn, N. J., Ward, S., & Leong, W. S. (1991). Submicromolar manganese dependence of Golgi vesicular galactosyltransferase (lactose synthetase). *European Journal of Biochemistry*, *195*(1), 243–250. https://doi.org/10.1111/j.1432-1033.1991.tb15700.x

Lacey, E. (1990). Mode of action of benzimidazoles. *Parasitology Today*, *6*(4), 112–115.

Lafayette, S. L., Collins, C., Zaas, A. K., Schell, W. A., Betancourt-Quiroz, M., Leslie Gunatilaka, A. A., Perfect, J. R., & Cowen, L. E. (2010). PKC signaling regulates drug resistance of the fungal pathogen candida albicans via circuitry comprised of mkc1, calcineurin, and hsp90. *PLoS Pathogens*, *6*(8), 79–80. https://doi.org/10.1371/journal.ppat.1001069

Lamberth, C. (2022). Latest Research Trends in Agrochemical Fungicides: Any Learnings for Pharmaceutical Antifungals? *ACS Medicinal Chemistry Letters*, *13*(6), 895–903. https://doi.org/10.1021/acsmedchemlett.2c00113

Lanthaler, K., Bilsland, E., Dobson, P. D., Moss, H. J., Pir, P., Kell, D. B., & Oliver, S. G. (2011). Genome-wide assessment of the carriers involved in the cellular uptake of drugs: A model system in yeast. *BMC Biology*, *9*, 1–14. https://doi.org/10.1186/1741-7007-9-70

Lawry, S. M., Tebbets, B., Kean, I., Stewart, D., Hetelle, J., & Klein, B. S. (2017). Fludioxonil Induces Drk1, a Fungal Group III Hybrid Histidine Kinase, To Dephosphorylate Its Downstream Target, Ypd1. *Antimicrobial Agents and Chemotherapy*, *61*(2), 10–1128.

Lazarow, K., Du, M. L., Weimer, R., & Kunze, R. (2012). A hyperactive transposase of the maize transposable element Activator (Ac). *Genetics*, *191*(3), 747–756. https://doi.org/10.1534/genetics.112.139642

Lecointe, F., Simos, G., Sauer, A., Hurt, E. C., Motorin, Y., & Grosjean, H. (1998). Characterization of yeast protein Deg1 as pseudouridine synthase (Pus3) catalyzing the formation of Ψ38 and Ψ39 in tRNA anticodon loop. *Journal of Biological Chemistry*, *273*(3), 1316–1323. https://doi.org/10.1074/jbc.273.3.1316

Lee, A. Y., St.Onge, R. P., Proctor, M. J., Wallace, I. M., Nile, A. H., Spagnuolo, P. A., Jitkova, Y., Gronda, M., Wu, Y., Kim, M. K., Cheung-Ong, K., Torres, N. P., Spear, E. D., Han, M. K. L., Schlecht, U., Suresh, S., Duby, G., Heisler, L. E., Surendra, A., … Giaever, G. (2014). Mapping the cellular response to small molecules using chemogenomic fitness signatures. *Science*, *344*(6186), 208–212. https://doi.org/10.1126/science.1255771

Lee, Y., Robbins, N., & Cowen, L. E. (2023). Molecular mechanisms governing antifungal drug resistance. *Npj Antimicrobials and Resistance*, *1*(1), 1–5. https://doi.org/10.1038/s44259-023-00007-2

Leidel, S., Pedrioli, P. G. A., Bucher, T., Brost, R., Costanzo, M., Schmidt, A., Aebersold, R., Boone, C., Hofmann, K., & Peter, M. (2009). Ubiquitin-related modifier Urm1 acts as a sulphur carrier in thiolation of eukaryotic transfer RNA. *Nature*, *458*(7235), 228–232. https://doi.org/10.1038/nature07643

Lesage, G., Sdicu, A. M., Ménard, P., Shapiro, J., Hussein, S., & Bussey, H. (2004). Analysis of β-1,3-glucan assembly in Saccharomyces cerevisiae using a synthetic interaction network and altered sensitivity to caspofungin. *Genetics*, *167*(1), 35–49. https://doi.org/10.1534/genetics.167.1.35

Letscher-Bru, V., & Herbrecht, R. (2003). Caspofungin: The first representative of a new antifungal class. *Journal of Antimicrobial Chemotherapy*, *51*(3), 513–521. https://doi.org/10.1093/jac/dkg117

Li, J., Zhang, J. M., Li, X., Suo, F., Zhang, M. J., Hou, W., Han, J., & Du, L. L. (2011). A piggyBac transposon-based mutagenesis system for the fission yeast Schizosaccharomyces pombe. *Nucleic Acids Research*, *39*(6). https://doi.org/10.1093/nar/gkq1358

Li, R., Zhu, L., Liu, D., Wang, W., Zhang, C., Jiao, S., Wei, J., Ren, L., Zhang, Y., Gou, X., Yuan, X., Du, Y., & Wang, Z. A. (2022). High molecular weight chitosan oligosaccharide exhibited antifungal activity by misleading cell wall organization via targeting PHR transglucosidases. *Carbohydrate Polymers*, *285*, 119253. https://doi.org/10.1016/j.carbpol.2022.119253

Liu, C., Talbot, N. J., & Chen, X. L. (2021). Protein glycosylation during infection by plant pathogenic fungi. In *New Phytologist* (Vol. 230, Issue 4, pp. 1329–1335). Blackwell Publishing Ltd. https://doi.org/10.1111/nph.17207

Liu, H., Du, Y., Wang, X., & Sun, L. (2004). Chitosan kills bacteria through cell membrane damage. *International Journal of Food Microbiology*, *95*(2), 147–155. https://doi.org/10.1016/j.ijfoodmicro.2004.01.022

Liu, H., Stylest, C. A., Finkt, G. R., & Rudolph, A. A. (1996). *Saccharomyces cerevisiae S288C Has a Mutation in FL08, a Gene Required for Filamentous Growth*.

Loewith, R., & Hall, M. N. (2011). Target of rapamycin (TOR) in nutrient signaling and growth control. *Genetics*, *189*(4), 1177–1201. https://doi.org/10.1534/genetics.111.133363

Longtine, M. S., McKenzie, A., Demarini, D. J., Shah, N. G., Wach, A., Brachat, A., Philippsen, P., & Pringle, J. R. (1998). Additional modules for versatile and economical PCR-based gene deletion and modification in Saccharomyces cerevisiae. *Yeast*, *14*(10), 953–961. https://doi.org/10.1002/(SICI)1097-0061(199807)14:10<953::AID-YEA293>3.0.CO;2-U

Lorrain, C., Gonçalves dos Santos, K. C., Germain, H., Hecker, A., & Duplessis, S. (2019). Advances in understanding obligate biotrophy in rust fungi. In *New Phytologist* (Vol. 222, Issue 3, pp. 1190–1206). Blackwell Publishing Ltd. https://doi.org/10.1111/nph.15641

Lu, J. M. Y., Deschenes, R. J., & Fassler, J. S. (2003). Saccharomyces cerevisiae Histidine Phosphotransferase Ypd1p Shuttles between the Nucleus and Cytoplasm for SLN1-Dependent Phosphorylation of Ssk1p and Skn7p. *Eukaryotic Cell*, *2*(6), 1304–1314. https://doi.org/10.1128/EC.2.6.1304-1314.2003

Lucas, J. A., Hawkins, N. J., & Fraaije, B. A. (2015). The Evolution of Fungicide Resistance. In *Advances in Applied Microbiology* (Vol. 90). Elsevier Ltd. https://doi.org/10.1016/bs.aambs.2014.09.001

Luk, E. E. C., & Culotta, V. C. (2001). Manganese Superoxide Dismutase in Saccharomyces cerevisiae Acquires Its Metal Co-factor through a Pathway Involving the Nramp Metal Transporter, Smf2p. *Journal of Biological Chemistry*, *276*(50), 47556–47562. https://doi.org/10.1074/jbc.M108923200

Ma, Z., Garrido-Maestu, A., & Jeong, K. C. (2017). Application, mode of action, and in vivo activity of chitosan and its micro- and nanoparticles as antimicrobial agents: A review. *Carbohydrate Polymers*, *176*, 257–265. https://doi.org/10.1016/j.carbpol.2017.08.082

Madrid, R., Gómez, M. J., Ramos, J., & Rodríguez-Navarro, A. (1998). Ectopic potassium uptake in trk1 trk2 mutants of Saccharomyces cerevisiae correlates with a highly hyperpolarized membrane potential. *Journal of Biological Chemistry*, *273*(24), 14838–14844. https://doi.org/10.1074/jbc.273.24.14838

Maeda, T., Wurgler-Murphy, S. M., & Saito, H. (1994). A two-component system that regulates an osmosensing MAP kinase cascade in yeast. *Nature*, *369*(6477), 242–245. https://doi.org/10.1038/369242a0

Majumdar, S., Ghatak, J., Mukherji, S., Bhattacharjee, H., & Bhaduri, A. (2004). UDPgalactose 4-epimerase from Saccharomyces cerevisiae: A bifunctional enzyme with aldose 1-epimerase activity. *European Journal of Biochemistry*, *271*(4), 753–759. https://doi.org/10.1111/j.1432-1033.2003.03974.x

Malina, C., Larsson, C., & Nielsen, J. (2018). Yeast mitochondria: An overview of mitochondrial biology and the potential of mitochondrial systems biology. In *FEMS Yeast Research* (Vol. 18, Issue 5). Oxford University Press. https://doi.org/10.1093/femsyr/foy040

Marcireau, C., Guilloton, M., & Karst, F. (1990). In vivo effects of fenpropimorph on the yeast Saccharomyces cerevisiae and determination of the molecular basis of the antifungal property. *Antimicrobial Agents and Chemotherapy*, *34*(6), 989–993. https://doi.org/10.1128/AAC.34.6.989

Marichal, P., Vanden Bossche, H., Odds, F. C., Nobels, G., Warnock, D. W., Timmerman, V., Van Broeckhoven, C., Fay, S., & Mose-Larsen, P. (1997). *Molecular Biological Characterization of an Azole-Resistant Candida glabrata Isolate* (Vol. 41, Issue 10).

Markovich, S., Yekutiel, A., Shalit, I., Shadkchan, Y., & Osherov, N. (2004). Genomic approach to identification of mutations affecting caspofungin susceptibility in

Saccharomyces cerevisiae. *Antimicrobial Agents and Chemotherapy*, *48*(10), 3871–3876. https://doi.org/10.1128/AAC.48.10.3871-3876.2004

Martel, C. M., Parker, J. E., Bader, O., Weig, M., Gross, U., Warrilow, A. G. S., Kelly, D. E., & Kelly, S. L. (2010). A clinical isolate of Candida albicans with mutations in ERG11 (encoding sterol 14α-demethylase) and ERG5 (encoding C22 desaturase) is cross resistant to azoles and amphotericin B. *Antimicrobial Agents and Chemotherapy*, *54*(9), 3578–3583. https://doi.org/10.1128/AAC.00303-10

Martinez, L. R., Mihu, M. R., Han, G., Frases, S., Cordero, R. J. B., Casadevall, A., Friedman, A. J., Friedman, J. M., & Nosanchuk, J. D. (2010). The use of chitosan to damage Cryptococcus neoformans biofilms. *Biomaterials*, *31*(4), 669–679. https://doi.org/10.1016/j.biomaterials.2009.09.087

Mary, I., & Jones, E. (1992). Orotidylate Decarboxylase of Yeast and Man. In *CURRENT TOPICS IN CELLULAR REGULATION* (Vol. 33).

Mas, G., De Nadal, E., Dechant, R., De La Concepción, M. L. R., Logie, C., Jimeno-González, S., Chávez, S., Ammerer, G., & Posas, F. (2009). Recruitment of a chromatin remodelling complex by the Hog1 MAP kinase to stress genes. *EMBO Journal*, *28*(4), 326–336. https://doi.org/10.1038/emboj.2008.299

Matei, A., & Doehlemann, G. (2016). Cell biology of corn smut disease — Ustilago maydis as a model for biotrophic interactions. In *Current Opinion in Microbiology* (Vol. 34, pp. 60–66). Elsevier Ltd. https://doi.org/10.1016/j.mib.2016.07.020

Matuo, R., Sousa, F. G., Soares, D. G., Bonatto, D., Saffi, J., Escargueil, A. E., Larsen, A. K., & Henriques, J. A. P. (2012). Saccharomyces cerevisiae as a model system to study the response to anticancer agents. In *Cancer Chemotherapy and Pharmacology* (Vol. 70, Issue 4, pp. 491–502). https://doi.org/10.1007/s00280-012-1937-4

Mazur, P., Morin, N., Baginsky, W., el-Sherbeini, M., Clemas, J. A., Nielsen, J. B., & Foor, F. (1995). Differential Expression and Function of Two Homologous Subunits of Yeast 1,3-β-D-Glucan Synthase. *Molecular and Cellular Biology*, *15*(10), 5671–5681. https://doi.org/10.1128/mcb.15.10.5671

Meena, N., Kaur, H., & Mondal, A. K. (2010). Interactions among HAMP domain repeats act as an osmosensing molecular switch in group III hybrid histidine kinases from fungi. *Journal of Biological Chemistry*, *285*(16), 12121–12132. https://doi.org/10.1074/jbc.M109.075721

Mellado, E., Garcia-Effron, G., Alcázar-Fuoli, L., Melchers, W. J. G., Verweij, P. E., Cuenca-Estrella, M., & Rodriguez-Tudela, J. L. (2007). A new Aspergillus fumigatus resistance mechanism conferring in vitro cross-resistance to azole antifungals involves a

combination of cyp51A alterations. *Antimicrobial Agents and Chemotherapy*, *51*(6), 1897–1904. https://doi.org/10.1128/AAC.01092-06

Mellegård, H., Strand, S. P., Christensen, B. E., Granum, P. E., & Hardy, S. P. (2011). Antibacterial activity of chemically defined chitosans: Influence of molecular weight, degree of acetylation and test organism. *International Journal of Food Microbiology*, *148*(1), 48–54. https://doi.org/10.1016/j.ijfoodmicro.2011.04.023

Meyers, S., Schauer, W., Balzi, E., Wagner, M., Goffeau, A., & Golin, J. (1992). Interaction of the yeast pleiotropic drug resistance genes PDR1 and PDR5. *Current Genetics*, *21*(6), 431–436. https://doi.org/10.1007/BF00351651

Michel, A., Hatakeyama, R., Kimmig, P., Arter, M., Peter, M., Joao, M., De Virgilio, C., & Kornmann, B. (2017). Functional mapping of yeast genomes by saturated transposition. *Elife*, *6*, e23570. https://doi.org/10.7554/eLife.23570

Michel, A., & Kornmann, B. (2022). SAturated Transposon Analysis in Yeast (SATAY) for Deep Functional Mapping of Yeast Genomes. In *Yeast Functional Genomics* (Vol. 2477). Springer US. https://doi.org/10.1163/ej.9789004172067.i-752.59

Michel, A., Schie, S. Van, Mosbach, A., Scalliet, G., & Kornmann, B. (2019). Exploiting Homologous Recombination Increases SATAY Efficiency for Loss- And Gain-of-Function Screening. *BioRxiv*, 866483. https://doi.org/10.1101/866483

Mielich, K., Shtifman-Segal, E., Golz, J. C., Zeng, G., Wang, Y., Berman, J., & Kunze, R. (2018). Maize transposable elements Ac/Ds as insertion mutagenesis tools in Candida albicans. *G3: Genes, Genomes, Genetics*, *8*(4), 1139–1145. https://doi.org/10.1534/g3.117.300388

Mitsuyama, J., Nomura, N., Hashimoto, K., Yamada, E., Nishikawa, H., Kaeriyama, M., Kimura, A., Todo, Y., & Narita, H. (2008). In vitro and in vivo antifungal activities of T-2307, a novel arylamidine. *Antimicrobial Agents and Chemotherapy*, *52*(4), 1318–1324. https://doi.org/10.1128/AAC.01159-07

Miyake, Y., Kozutsumi, Y., Nakamura, S., Fujita, T., & Kawasaki, T. (1995). Serine palmitoyltransferase is the primary target of a sphingosine-like immunosuppressant, ISP-1/myriocin. In *Biochemical and Biophysical Research Communications* (Vol. 211, Issue 2, pp. 396–403). https://doi.org/10.1006/bbrc.1995.1827

Molefi, M., Chofle, A. A., Molloy, S. F., Kalluvya, S., Changalucha, J. M., Cainelli, F., Leeme, T., Lekwape, N., Goldberg, D. W., Haverkamp, M., Bisson, G. P., Perfect, J. R., Letang, E., Fenner, L., Meintjes, G., Burton, R., Makadzange, T., Ndhlovu, C. E., Hope, W., … Jarvis, J. N. (2015). AMBITION-cm: Intermittent high dose AmBisome on a high dose fluconazole backbone for cryptococcal meningitis induction therapy in sub-Saharan

Africa: Study protocol for a randomized controlled trial. *Trials*, *16*(1). https://doi.org/10.1186/s13063-015-0799-6

Möller, M., & Stukenbrock, E. H. (2017). Evolution and genome architecture in fungal plant pathogens. *Nature Reviews Microbiology*, *15*(12), 756–771. https://doi.org/10.1038/nrmicro.2017.76

Momoi, M., Tanoue, D., Sun, Y., Takematsu, H., Suzuki, Y., Suzuki, M., Suzuki, A., Fujita, T., & Kozutsumi, Y. (2004). SLI1 (YGR212W) is a major gene conferring resistance to the sphingolipid biosynthesis inhibitor ISP-1, and encodes an ISP-1 N-acetyltransferase in yeast. *Biochemical Journal*, *381*(1), 321–328. https://doi.org/10.1042/BJ20040108

Morio, F., Loge, C., Besse, B., Hennequin, C., & Le Pape, P. (2010). Screening for amino acid substitutions in the Candida albicans Erg11 protein of azole-susceptible and azole-resistant clinical isolates: new substitutions and a review of the literature. *Diagnostic Microbiology and Infectious Disease*, *66*(4), 373–384. https://doi.org/10.1016/j.diagmicrobio.2009.11.006

Mortimer, R. K., & Johnston, J. R. (1986). Genealogy of principal strains of the yeast genetic stock center. *Genetics*, *113*(1), 35–43. https://doi.org/10.1093/genetics/113.1.35

Mosbach, A., Edel, D., Farmer, A. D., Widdison, S., Barchietto, T., Dietrich, R. A., Corran, A., & Scalliet, G. (2017). Anilinopyrimidine resistance in Botrytis cinerea is linked to mitochondrial function. *Frontiers in Microbiology*, *8*(NOV). https://doi.org/10.3389/fmicb.2017.02361

Motoyama, T., Ohira, T., Kadokura, K., Ichiishi, A., Fujimura, M., Yamaguchi, I., & Kudo, T. (2005). An Os-1 family histidine kinase from a filamentous fungus confers fungicide-sensitivity to yeast. *Current Genetics*, *47*, 298–306. https://doi.org/10.1007/s00294-005-0572-6

Mukherjee, P. K., Chandra, J., Kuhn, D. M., & Ghannoum, M. A. (2003). Mechanism of fluconazole resistance in Candida albicans biofilms: Phase-specific role of efflux pumps and membrane sterols. *Infection and Immunity*, *71*(8), 4333–4340. https://doi.org/10.1128/IAI.71.8.4333-4340.2003

Mulet, J. M., Leube, M. P., Kron, S. J., Rios, G., Fink, G. R., & Serrano, R. (1999). A Novel Mechanism of Ion Homeostasis and Salt Tolerance in Yeast: the Hal4 and Hal5 Protein Kinases Modulate the Trk1-Trk2 Potassium Transporter. *Molecular and Cellular Biology*, *19*(5), 3328–3337. https://doi.org/10.1128/mcb.19.5.3328

Muñoz, Z., & Moret, A. (2010). Sensitivity of Botrytis cinerea to chitosan and acibenzolar-S-methyl. *Pest Management Science*, *66*(9), 974–979. https://doi.org/10.1002/ps.1969

Munro, S. (2001). *What can yeast tell us about N-linked glycosylation in the Golgi apparatus? 498*, 223–227.

Murray, J. L., Kwon, T., Marcotte, E. M., & Whiteley, M. (2015). Intrinsic antimicrobial resistance determinants in the superbug pseudomonas aeruginosa. *MBio*, *6*(6). https://doi.org/10.1128/mBio.01603-15

Musso, G., Costanzo, M., Huangfu, M. Q., Smith, A. M., Paw, J., San Luis, B. J., Boone, C., Giaever, G., Nislow, C., Emili, A., & Zhang, Z. (2008). The extensive and condition-dependent nature of epistasis among whole-genome duplicates in yeast. *Genome Research*, *18*(7), 1092–1099. https://doi.org/10.1101/gr.076174.108

Muzzarelli, R. A. A., Boudrant, J., Meyer, D., Manno, N., Demarchis, M., & Paoletti, M. G. (2012). Current views on fungal chitin/chitosan, human chitinases, food preservation, glucans, pectins and inulin: A tribute to Henri Braconnot, precursor of the carbohydrate polymers science, on the chitin bicentennial. *Carbohydrate Polymers*, *87*(2), 995–1012. https://doi.org/10.1016/j.carbpol.2011.09.063

Myer, V. E., & Young, R. A. (1998). RNA polymerase II holoenzymes and subcomplexes. *Journal of Biological Chemistry*, *273*(43), 27757–27760. https://doi.org/10.1074/jbc.273.43.27757

Naberezhnykh, G. A., Gorbach, V. I., Likhatskaya, G. N., Davidova, V. N., & Solov'eva, T. F. (2008). Interaction of chitosans and their N-acylated derivatives with lipopolysaccharide of gram-negative bacteria. *Biochemistry (Moscow)*, *73*(4), 432–441. https://doi.org/10.1134/S0006297908040081

Nadal-Ribelles, M., Conde, N., Flores, O., González-Vallinas, J., Eyras, E., Orozco, M., de Nadal, E., & Posas, F. (2012). Hog1 bypasses stress-mediated down-regulation of transcription by RNA polymerase II redistribution and chromatin remodeling. *Genome Biology*, *13*, 1–11. https://doi.org/10.1186/gb-2012-13-11-r106

Navarre, C., & Goffeau, A. (2000). Membrane hyperpolarization and salt sensitivity induced by deletion of PMP3, a highly conserved small protein of yeast plasma membrane. *EMBO Journal*, *19*(11), 2515–2524. https://doi.org/10.1093/emboj/19.11.2515

Neoh, C. F., Slavin, M., Chen, S. C. A., Stewart, K., & Kong, D. C. M. (2014). Echinocandins in the treatment of candidaemia and invasive candidiasis: Clinical and economic perspectives. In *International Journal of Antimicrobial Agents* (Vol. 43, Issue 3, pp. 207–214). Elsevier B.V. https://doi.org/10.1016/j.ijantimicag.2013.08.010

Nett, J. E., Crawford, K., Marchillo, K., & Andes, D. R. (2010). Role of Fks1p and matrix glucan in Candida albicans biofilm resistance to an echinocandin, pyrimidine, and

polyene. *Antimicrobial Agents and Chemotherapy*, *54*(8), 3505–3508. https://doi.org/10.1128/AAC.00227-10

Nickels, T., Gale, A., Harrington, A., Timp, W., & Cunningham, K. (2024). Tn-seq of the Candida glabrata reference strain CBS138 reveals epigenetic plasticity, structural variation, and intrinsic mechanisms of resistance to micafungin. *BioRxiv*.

Nikko, Elina, and Hugh RB Pelham. "Arrestin-mediated endocytosis of yeast plasma membrane transporters." Traffic 10.12 (2009): 1856-1867.

Niimi, K., Maki, K., Ikeda, F., Holmes, A. R., Lamping, E., Niimi, M., Monk, B. C., & Cannon, R. D. (2006). Overexpression of Candida albicans CDR1, CDR2, or MDR1 does not produce significant changes in echinocandin susceptibility. *Antimicrobial Agents and Chemotherapy*, *50*(4), 1148–1155. https://doi.org/10.1128/AAC.50.4.1148-1155.2006

Niimi, M., Niimi, K., Takano, Y., Holmes, A. R., Fischer, F. J., Uehara, Y., & Cannon, R. D. (2004). Regulated overexpression of CDR1 in Candida albicans confers multidrug resistance. *Journal of Antimicrobial Chemotherapy*, *54*(6), 999–1006. https://doi.org/10.1093/jac/dkh456

Nishikawa, H., Fukuda, Y., Mitsuyama, J., Tashiro, M., Tanaka, A., Takazono, T., Saijo, T., Yamamoto, K., Nakamura, S., Imamura, Y., Miyazaki, T., Kakeya, H., Yamamoto, Y., Yanagihara, K., Mukae, H., Kohno, S., & Izumikawa, K. (2017). In vitro and in vivo antifungal activities of T-2307, a novel arylamidine, against Cryptococcus gattii: An emerging fungal pathogen. *Journal of Antimicrobial Chemotherapy*, *72*(6), 1709–1713. https://doi.org/10.1093/jac/dkx020

Nishikawa, H., Sakagami, T., Yamada, E., Fukuda, Y., Hayakawa, H., Nomura, N., Mitsuyama, J., Miyazaki, T., Mukae, H., & Kohno, S. (2016). T-2307, a novel arylamidine, is transported into Candida albicans by a high-affinity spermine and spermidine carrier regulated by Agp2. *Journal of Antimicrobial Chemotherapy*, *71*(7), 1845–1855. https://doi.org/10.1093/jac/dkw095

Nishikawa, H., Yamada, E., Shibata, T., Uchihashi, S., Fan, H., Hayakawa, H., Nomura, N., & Mitsuyama, J. (2010). Uptake of T-2307, a novel arylamidine, in Candida albicans. *Journal of Antimicrobial Chemotherapy*, *65*(8), 1681–1687. https://doi.org/10.1093/jac/dkq177

Ochiai, N., Fujimura, M., Oshima, M., Motoyama, T., Ichiishi, A., Yamada-Okabe, H., & Yamaguchi, I. (2002). Effects of Iprodione and Fludioxonil on Glycerol Synthesis and Hyphal Development in Candida albicans. In *Biosci. Biotechnol. Biochem* (Vol. 66, Issue 10). https://academic.oup.com/bbb/article/66/10/2209/5944805

Odani, T., Shimma, Y. I., Tanaka, A., & Jigami, Y. (1996). Cloning and analysis of the MNN4 gene required for phosphorylation of N-linked oligosaccharides in Saccharomyces cerevisiae. *Glycobiology*, *6*(8), 805–810. https://doi.org/10.1093/glycob/6.8.805

Odani, T., Shimma, Y. I., Wang, X. H., & Jigami, Y. (1997). Mannosylphosphate transfer to cell wall mannan is regulated by the transcriptional level of the MNN4 gene in Saccharomyces cerevisiae. *FEBS Letters*, *420*(2–3), 186–190. https://doi.org/10.1016/S0014-5793(97)01513-5

O'Donoghue, L., & Smolenski, A. (2022). Analysis of protein phosphorylation using Phos-tag gels. *Journal of Proteomics*, *259*. https://doi.org/10.1016/j.jprot.2022.104558

Oh, C. S., Toke, D. A., Mandala, S., & Martin, C. E. (1997). ELO2 and ELO3, homologues of the Saccharomyces cerevisiae ELO1 gene, function in fatty acid elongation and are required for sphingolipid formation. *Journal of Biological Chemistry*, *272*(28), 17376–17384. https://doi.org/10.1074/jbc.272.28.17376

Oliver, J. D., Sibley, G. E. M., Beckmann, N., Dobb, K. S., Slater, M. J., McEntee, L., Du Pré, S., Livermore, J., Bromley, M. J., Wiederhold, N. P., Hope, W. W., Kennedy, A. J., Law, D., & Birch, M. (2016). F901318 represents a novel class of antifungal drug that inhibits dihydroorotate dehydrogenase. *Proceedings of the National Academy of Sciences of the United States of America*, *113*(45), 12809–12814. https://doi.org/10.1073/pnas.1608304113

Omrane, S., Audéon, C., Ignace, A., Duplaix, C., Aouini, L., Kema, G., Walker, A.-S., & Fillinger, S. (2017). Plasticity of the MFS1 Promoter Leads to Multidrug Resistance in the Wheat Pathogen Zymoseptoria tritici . *MSphere*, *2*(5), 1–18. https://doi.org/10.1128/msphere.00393-17

Onyewu, C., Blankenship, J. R., Del Poeta, M., & Heitman, J. (2003). Ergosterol biosynthesis inhibitors become fungicidal when combined with calcineurin inhibitors against Candida albicans, Candida glabrata, and Candida krusei. *Antimicrobial Agents and Chemotherapy*, *47*(3), 956–964. https://doi.org/10.1128/AAC.47.3.956-964.2003

Orlean, P. (2012). Architecture and biosynthesis of the Saccharomyces cerevisiae cell wall. *Genetics*, *192*(3), 775–818. https://doi.org/10.1534/genetics.112.144485

Oskouian, B., & Saba, J. D. (1999). YAP1 confers resistance to the fatty acid synthase inhibitor cerulenin through the transporter Flr1p in Saccharomyces cerevisiae. *Molecular and General Genetics MGG*, *261*, 346–353. https://doi.org/10.1007/s004380050975

Osumi, M. (1998). The ultrastructure of yeast: Cell wall structure and formation. *Micron*, *29*(2–3), 207–233. https://doi.org/10.1016/S0968-4328(97)00072-3

Ota, I. M., & Varshavsky, A. (1993). A yeast protein similar to bacterial two-component regulators. *Science*, *262*(5133), 566–569. https://doi.org/10.1126/science.8211183

Ottilie, S., Luth, M. R., Hellemann, E., Goldgof, G. M., Vigil, E., Kumar, P., Cheung, A. L., Song, M., Godinez-Macias, K. P., Carolino, K., Yang, J., Lopez, G., Abraham, M., Tarsio, M., LeBlanc, E., Whitesell, L., Schenken, J., Gunawan, F., Patel, R., … Winzeler, E. A. (2022). Adaptive laboratory evolution in S. cerevisiae highlights role of transcription factors in fungal xenobiotic resistance. *Communications Biology*, *5*(1). https://doi.org/10.1038/s42003-022-03076-7

Palma-Guerrero, J., Lopez-Jimenez, J. A., Pérez-Berná, A. J., Huang, I. C., Jansson, H. B., Salinas, J., Villalaín, J., Read, N. D., & Lopez-Llorca, L. V. (2010). Membrane fluidity determines sensitivity of filamentous fungi to chitosan. *Molecular Microbiology*, *75*(4), 1021–1032. https://doi.org/10.1111/j.1365-2958.2009.07039.x

Palmeira-de-Oliveira, A., Passarinha, L. A., Gaspar, C., Palmeira-de-Oliveira, R., Sarmento, B., Martinez-de-Oliveira, J., Pina-Vaz, C., Rodrigues, A. G., & Queiroz, J. A. (2011). The relationship between Candida species charge density and chitosan activity evaluated by ion-exchange chromatography. *Journal of Chromatography B*, *879*(31), 3749–3751. https://doi.org/10.1016/j.jchromb.2011.07.034

Pappas, P. G., Kauffman, C. A., Andes, D., Benjamin, D. K., Calandra, T. F., Edwards, J. E., Filler, S. G., Fisher, J. F., Kullberg, B. J., Ostrosky-Zeichner, L., Reboli, A. C., Rex, J. H., Walsh, T. J., & Sobel, J. D. (2009). Clinical practice guidelines for the management of candidiasis: 2009 Update by the Infectious Diseases Society of America. *Clinical Infectious Diseases*, *48*(5), 503. https://doi.org/10.1086/596757

Parsons, A. B., Brost, R. L., Ding, H., Li, Z., Zhang, C., Sheikh, B., Brown, G. W., Kane, P. M., Hughes, T. R., & Boone, C. (2004). Integration of chemical-genetic and genetic interaction data links bioactive compounds to cellular target pathways. *Nature Biotechnology*, *22*(1), 62–69. https://doi.org/10.1038/nbt919

Parsons, A. B., Lopez, A., Givoni, I. E., Williams, D. E., Gray, C. A., Porter, J., Chua, G., Sopko, R., Brost, R. L., Ho, C. H., Wang, J., Ketela, T., Brenner, C., Brill, J. A., Fernandez, G. E., Lorenz, T. C., Payne, G. S., Ishihara, S., Ohya, Y., … Boone, C. (2006). Exploring the Mode-of-Action of Bioactive Compounds by Chemical-Genetic Profiling in Yeast. *Cell*, *126*(3), 611–625. https://doi.org/10.1016/j.cell.2006.06.040

Patterson, K., Yu, J., Landberg, J., Chang, I., Shavarebi, F., Bilanchone, V., & Sandmeyer, S. (2018). Functional genomics for the oleaginous yeast Yarrowia lipolytica. *Metabolic Engineering*, *48*, 184–196. https://doi.org/10.1016/j.ymben.2018.05.008

Pavesic, M. W., Gale, A. N., Nickels, T. J., Harrington, A. A., Bussey, M., & Cunningham, K. W. (2024). Calcineurin-dependent contributions to fitness in the opportunistic pathogen Candida glabrata . *MSphere*, *9*(1). https://doi.org/10.1128/msphere.00554-23

Péli-Gulli, M. P., Sardu, A., Panchaud, N., Raucci, S., & De Virgilio, C. (2015). Amino Acids Stimulate TORC1 through Lst4-Lst7, a GTPase-Activating Protein Complex for the Rag Family GTPase Gtr2. *Cell Reports*, *13*(1), 1–7. https://doi.org/10.1016/j.celrep.2015.08.059

Pérez-Valle, J., Jenkins, H., Merchan, S., Montiel, V., Ramos, J., Sharma, S., Serrano, R., & Yenush, L. (2007). Key Role for Intracellular K + and Protein Kinases Sat4/Hal4 and Hal5 in the Plasma Membrane Stabilization of Yeast Nutrient Transporters. *Molecular and Cellular Biology*, *27*(16), 5725–5736. https://doi.org/10.1128/mcb.01375-06

Perfect, J. R. (2017). The antifungal pipeline: A reality check. *Nature Reviews Drug Discovery*, *16*(9), 603–616. https://doi.org/10.1038/nrd.2017.46

Perlin, D. S., Rautemaa-Richardson, R., & Alastruey-Izquierdo, A. (2017). The global problem of antifungal resistance: prevalence, mechanisms, and management. *The Lancet Infectious Diseases*, *17*(12), e383–e392. https://doi.org/10.1016/S1473-3099(17)30316-X

Pettersen, E. F., Goddard, T. D., Huang, C. C., Meng, E. C., Couch, G. S., Croll, T. I., Morris, J. H., & Ferrin, T. E. (2021). UCSF ChimeraX: Structure visualization for researchers, educators, and developers. *Protein Science*, *30*(1), 70–82. https://doi.org/10.1002/pro.3943

Pfaller, M. A. (2012). Antifungal drug resistance: Mechanisms, epidemiology, and consequences for treatment. *American Journal of Medicine*, *125*(1 SUPPL.). https://doi.org/10.1016/j.amjmed.2011.11.001

Posas, F., Chamber, J. R., Heyman, J. A., Hoeffler, J. P., De Nadal, E., & Ariño, J. (2000). The transcriptional response of yeast to saline stress. *Journal of Biological Chemistry*, *275*(23), 17249–17255. https://doi.org/10.1074/jbc.M910016199

Posas, F., Wurgler-Murphy, S. M., Maeda, T., Witten, E. A., Thai, T. C., & Saito, H. (1996). Yeast HOG1 MAP kinase cascade is regulated by a multistep phosphorelay mechanism in the SLN1-YPD1-SSK1 “two-component” osmosensor. *Cell*, *86*(6), 865–875. https://doi.org/10.1016/S0092-8674(00)80162-2

Posteraro, B., Sanguinetti, M., Sanglard, D., La Sorda, M., Boccia, S., Romano, L., Morace, G., & Fadda, G. (2003). Identification and characterization of a Cryptococcus neoformans ATP binding cassette (ABC) transporter-encoding gene, CnAFR1, involved

in the resistance to fluconazole. *Molecular Microbiology*, *47*(2), 357–371. https://doi.org/10.1046/j.1365-2958.2003.03281.x

Price, C. L., Parker, J. E., Warrilow, A. G., Kelly, D. E., & Kelly, S. L. (2015). Azole fungicides - understanding resistance mechanisms in agricultural fungal pathogens. *Pest Management Science*, *71*(8), 1054–1058. https://doi.org/10.1002/ps.4029

Proft, M., & Struhl, K. (2002). Hog1 kinase converts the Sko1-Cyc8-Tup1 repressor complex into an activator that recruits SAGA and SWI/SNF in response to osmotic stress. *Molecular Cell*, *9*(6), 1307–1317. https://doi.org/10.1016/S1097-2765(02)00557-9

Puumala, E., Fallah, S., Robbins, N., & Cowen, L. E. (2024). Advancements and challenges in antifungal therapeutic development. *Clinical Microbiology Reviews*, *37*(1), e00142-23. https://doi.org/10.1128/cmr.00142-23

Raafat, D., Von Bargen, K., Haas, A., & Sahl, H. G. (2008). Insights into the mode of action of chitosan as an antibacterial compound. *Applied and Environmental Microbiology*, *74*(12), 3764–3773. https://doi.org/10.1128/AEM.00453-08

Raffi, F., Corelli, F., & Botta, M. (2007). Efficient synthesis of iminoctadine, a potent antifungal agent and polyamine oxidase inhibitor (PAO). *Synthesis*, *19*, 3013–3016. https://doi.org/10.1055/s-2007-983898

Ramage, G., Rajendran, R., Sherry, L., & Williams, C. (2012). Fungal biofilm resistance. In *International Journal of Microbiology*. https://doi.org/10.1155/2012/528521

Randhawa, A., Chawla, S., & Mondal, A. K. (2016). Functional dissection of HAMP domains in NIK1 ortholog from pathogenic yeast Candida lusitaniae. *Gene*, *577*(2), 251–257. https://doi.org/10.1016/j.gene.2015.12.002

Randhawa, A., Kundu, D., Sharma, A., Prasad, R., & Mondal, A. K. (2019). Overexpression of the CORVET complex alleviates the fungicidal effects of fludioxonil on the yeast Saccharomyces cerevisiae expressing hybrid histidine kinase 3. *Journal of Biological Chemistry*, *294*(2), 461–475. https://doi.org/10.1074/jbc.RA118.004736

Raschke, W. C., Kern, K. A., Antalis, C., & Ballou, C. E. (1973). Genetic Control of Yeast Mannan Structure. *Journal of Biological Chemistry*, *248*(13), 4660–4666. https://doi.org/10.1016/s0021-9258(19)43714-9

Ravikumar, A., Arrieta, A., & Liu, C. C. (2014). An orthogonal DNA replication system in yeast. *Nature Chemical Biology*, *10*(3), 175–177. https://doi.org/10.1038/nchembio.1439

Ravikumar, A., Arzumanyan, G. A., Obadi, M. K. A., Javanpour, A. A., & Liu, C. C. (2018). Scalable, Continuous Evolution of Genes at Mutation Rates above Genomic Error Thresholds. *Cell*, *175*(7), 1946-1957.e13. https://doi.org/10.1016/j.cell.2018.10.021

Regelmann, J., Schü Le, T., Josupeit, F. S., Horak, J., Rose, M., Entian, K.-D., Thumm, M., & Wolf, D. H. (2003). Catabolite Degradation of Fructose-1,6-bisphosphatase in the Yeast Saccharomyces cerevisiae: A Genome-wide Screen Identifies Eight Novel GID Genes and Indicates the Existence of Two Degradation Pathways. *Molecular Biology of the Cell*, *14*, 1652–1663. https://doi.org/10.1091/mbc.E02-08

Reglinski, T., Elmer, P. A. G., Taylor, J. T., Wood, P. N., & Hoyte, S. M. (2010). Inhibition of Botrytis cinerea growth and suppression of botrytis bunch rot in grapes using chitosan. *Plant Pathology*, *59*(5), 882–890. https://doi.org/10.1111/j.1365-3059.2010.02312.x

Ren, W., Shao, W., Han, X., Zhou, M., & Chen, C. (2016). Molecular and biochemical characterization of laboratory and field mutants of botrytis cinerea resistant to fludioxonil. *Plant Disease*, *100*(7), 1414–1423. https://doi.org/10.1094/PDIS-11-15-1290-RE

Robbins, N., Caplan, T., & Cowen, L. E. (2017). Molecular Evolution of Antifungal Drug Resistance. *Annual Review of Microbiology*, *71*(1), 753–775. https://doi.org/10.1146/annurev-micro-030117-020345

Robbins, N., & Cowen, L. E. (2022). Antifungal discovery. *Current Opinion in Microbiology*, *69*, 102198. https://doi.org/10.1016/j.mib.2022.102198

Robbins, N., Uppuluri, P., Nett, J., Rajendran, R., Ramage, G., Lopez-Ribot, J. L., Andes, D., & Cowen, L. E. (2011). Hsp90 governs dispersion and drug resistance of fungal biofilms. *PLoS Pathogens*, *7*(9). https://doi.org/10.1371/journal.ppat.1002257

Rock, F. L., Mao, W., Yaremchuk, A., Tukalo, M., Crépin, T., Zhou, H., Zhang, Y. K., Hernandez, V., Akama, T., Baker, S. J., Plattner, J. J., Shapiro, L., Martinis, S. A., Benkovic, S. J., Cusack, S., & Alley, M. R. K. (2007). An antifungal agent inhibits an aminoacyl-tRNA synthetase by trapping tRNA in the editing site. *Science*, *316*(5832), 1759–1761. https://doi.org/10.1126/science.1142189

Rodrigues, M. L. (2018). The Multifunctional Fungal Ergosterol. *MBio*, *9*(5).

Roemer, T., Davies, J., Giaever, G., & Nislow, C. (2012). Bugs, drugs and chemical genomics. In *Nature Chemical Biology* (Vol. 8, Issue 1, pp. 46–56). Nature Publishing Group. https://doi.org/10.1038/nchembio.744

Rogers, B., Decottignies, A., Kolaczkowski, M., Carvajal, E., Balzi, E., & Goffeau, A. (2001). The pleitropic drug ABC transporters from Saccharomyces cerevisiae. *Journal of Molecular Microbiology and Biotechnology*, *3*(2), 207–214.

Romanazzi, G., Feliziani, E., Santini, M., & Landi, L. (2013). Effectiveness of postharvest treatment with chitosan and other resistance inducers in the control of storage decay of strawberry. *Postharvest Biology and Technology*, *75*, 24–27. https://doi.org/10.1016/j.postharvbio.2012.07.007

Ross, R. L., & Santiago-Tirado, F. H. (2024). Advanced genetic techniques in fungal pathogen research. *MSphere*, *9*(4), e00643-23. https://doi.org/10.1128/msphere.00643-23

Ryu, H., Park, H., Suh, D. S., Jung, G. H., Park, K., & Lee, B. D. (2014). Biological control of Colletotrichum panacicola on Panax ginseng by bacillus subtilis HK-CSM-1. *Journal of Ginseng Research*, *38*(3), 215–219. https://doi.org/10.1016/j.jgr.2014.05.001

Sá-Correia, I., dos Santos, S. C., Teixeira, M. C., Cabrito, T. R., & Mira, N. P. (2009). Drug:H+ antiporters in chemical stress response in yeast. *Trends in Microbiology*, *17*(1), 22–31. https://doi.org/10.1016/j.tim.2008.09.007

Sanchez, M. R., Payen, C., Cheong, F., Hovde, B. T., Bissonnette, S., Arkin, A. P., Skerker, J. M., Brem, R. B., Caudy, A. A., & Dunham, M. J. (2019). Transposon insertional mutagenesis in Saccharomyces uvarum reveals trans-acting effects influencing species-dependent essential genes. *Genome Research*, *29*(3), 396–406. https://doi.org/10.1101/gr.232330.117

Sang, H., Hulvey, J. P., Green, R., Xu, H., Im, J., Chang, T., & Jung, G. (2018). *A Xenobiotic Detoxification Pathway through Transcriptional Regulation in Filamentous Fungi*. https://doi.org/10

Sanglard, D., Ischer, F., Monod, M., & Billel, J. (1997). Cloning of Candida albicans genes conferring resistance to azole antifungal agents: characterization of CDR2, a new multidrug ABC transporter gene. In *Microbiology* (Vol. 143).

Sanglard, D., Kuchler, K., Ischer, F., Pagani, J.-L., Monod, M., & Bille, A. J. (1995). Mechanisms of Resistance to Azole Antifungal Agents in Candida albicans Isolates from AIDS Patients Involve Specific Multidrug Transporters. In *ANTIMICROBIAL AGENTS AND CHEMOTHERAPY* (Vol. 39, Issue 11). https://journals.asm.org/journal/aac

Sardana, R., Highland, C. M., Straight, B. E., Chavez, C. F., Fromme, J. C., & Emr, S. D. (2021). Golgi membrane protein erd1 is essential for recycling a subset of golgi glycosyltransferases. *ELife*, *10*(e70774). https://doi.org/10.7554/eLife.70774

Satish, S., Cristina Jiménez-Ortigosa, Y. Z., Lee, M. H., Dolgov, E., Krüger, T., Park, S., Denning, D. W., Kniemeyer, O., Brakhage, A. A., & Perlin, D. S. (2019). *Stress-Induced Changes in the Lipid Microenvironment of ᴺʟ- (1,3)-D-Glucan Synthase Cause Clinically Important Echinocandin Resistance in Aspergillus fumigatus*. *June*, 1–15.

Schmitz, K. R., Liu, J., Li, S., Setty, T. G., Wood, C. S., Burd, C. G., & Ferguson, K. M. (2008). Golgi Localization of Glycosyltransferases Requires a Vps74p Oligomer. *Developmental Cell*, *14*(4), 523–534. https://doi.org/10.1016/j.devcel.2008.02.016

Schork, S. M., Bee, G., Thumm, M., & Wolf, D. H. (1994). Catabolite inactivation of fructose-1,6-bisphosphatase in yeast is mediated by the proteasome. *FEBS Letters*, *349*(2), 270–274. https://doi.org/10.1016/0014-5793(94)00668-7

Schule, T., Rose, M., Entian, K.-D., Thumm, M., & Wolf, D. (2000). Ubc8p-functions-in-catabolite-degradation-of-fructose-1-6-bisphosphatase-in-yeast. *The EMBO Journal*, *19*(10), 2161–2167.

Schwarz, P., Dromer, F., Lortholary, O., & Dannaoui, E. (2006). Efficacy of amphotericin B in combination with flucytosine against flucytosine-susceptible or flucytosine-resistant isolates of Cryptococcus neoformans during disseminated murine cryptococcosis. *Antimicrobial Agents and Chemotherapy*, *50*(1), 113–120. https://doi.org/10.1128/AAC.50.1.113-120.2006

Seaman, M. N. J., Marcusson, E. G., Cereghino, J. L., & Emr, S. D. (1997). Endosome to Golgi retrieval of the vacuolar protein sorting receptor, Vps10p, requires the function of the VPS29, VPS30, and VPS35 gene products. *Journal of Cell Biology*, *137*(1), 79–92. https://doi.org/10.1083/jcb.137.1.79

Seaman, M. N. J., McCaffery, J. M., & Emr, S. D. (1998). A membrane coat complex essential for endosome-to-Golgi retrograde transport in yeast. *Journal of Cell Biology*, *142*(3), 665–681. https://doi.org/10.1083/jcb.142.3.665

Sedivy, J. M., & Fraenkelt, D. G. (1985). Fructose Bisphosphatase of Saccharomyces cerevisiae Cloning, Disruption and Regulation of the FBPI Structural Gene. In *J. Mol. Biol* (Vol. 186).

Segal, E. S., Gritsenko, V., Levitan, A., Yadav, B., Dror, N., Steenwyk, J. L., Silberberg, Y., Mielich, K., Rokas, A., Gow, N. A. R., Kunze, R., Sharan, R., & Berman, J. (2018). Gene Essentiality Analyzed by In Vivo Transposon Mutagenesis and Machine Learning in a Stable Haploid Isolate of Candida albicans. *MBio*, *9*(5), 1–21.

Selmecki, A., Forche, A., & Berman, J. (2006). Aneuploidy and Isochromosome Formation in Drug-Resistant Candida albicans. *Science*, *313*(5785), 367–369. https://doi.org/10.1126/science.1130164

Selmecki, A., Gerami-Nejad, M., Paulson, C., Forche, A., & Berman, J. (2008). An isochromosome confers drug resistance in vivo by amplification of two genes, ERG11 and TAC1. *Molecular Microbiology*, *68*(3), 624–641. https://doi.org/10.1111/j.1365-2958.2008.06176.x

Serbyn, N., Bagdiul, I., Noireterre, A., Michel, A. H., Suhandynata, R. T., Zhou, H., Kornmann, B., & Stutz, F. (2021). SUMO orchestrates multiple alternative DNA-protein crosslink repair pathways. *Cell Reports*, *37*(8). https://doi.org/10.1016/j.celrep.2021.110034

Serbyn, N., Noireterre, A., Bagdiul, I., Loewith, R., & Δ, Δ. (2020). *The Aspartic Protease Ddi1 Contributes to DNA- Protein Crosslink Repair in Yeast Article The Aspartic Protease Ddi1 Contributes to DNA-Protein Crosslink Repair in Yeast*. 1066–1079. https://doi.org/10.1016/j.molcel.2019.12.007

Serrano, R., Kielland-Brandt, M. C., & Fink, G. R. (1986). Yeast plasma membrane ATPase is essential for growth and has homology with (Na+ + K+), K+- and Ca2+-ATPases. *Nature*, *319*(6055), 689–693. https://doi.org/10.1038/319689a0

Seynnaeve, D., Del Vecchio, M., Fruhmann, G., Verelst, J., Cools, M., Beckers, J., Mulvihill, D. P., Winderickx, J., & Franssens, V. (2018). Recent insights on Alzheimer's disease originating from yeast models. In *International Journal of Molecular Sciences* (Vol. 19, Issue 7). MDPI AG. https://doi.org/10.3390/ijms19071947

Sharathchandra, R. G. S., Raj, S. N., Shetty, N. P., Amruthesh, K. N., & Shetty, H. S. (2004). A Chitosan formulation Elexa^{TM} induces downy mildew disease resistance and growth promotion in pearl millet. *Crop Protection*, *23*(10), 881–888. https://doi.org/10.1016/j.cropro.2003.12.008

Shematek, E. M., Braatz, J. A., & Cabib, E. (1980). Biosynthesis of the yeast cell wall: I. Preparation and properties of β-(1→3)glucan synthetase. *Journal of Biological Chemistry*, *255*(3), 888–894. https://doi.org/10.1016/S0021-9258(19)86117-3

Shibata, T., Takahashi, T., Yamada, E., Kimura, A., Nishikawa, H., Hayakawa, H., Nomura, N., & Mitsuyama, J. (2012). T-2307 causes collapse of mitochondrial membrane potential in yeast. *Antimicrobial Agents and Chemotherapy*, *56*(11), 5892–5897. https://doi.org/10.1128/AAC.05954-11

Shih, P. Y., Liao, Y. T., Tseng, Y. K., Deng, F. S., & Lin, C. H. (2019). A potential antifungal effect of chitosan against candida albicansis mediated via the inhibition of SAGA complex component expression and the subsequent alteration of cell surface integrity. *Frontiers in Microbiology*, *10*(602). https://doi.org/10.3389/fmicb.2019.00602

Sierotzki, H., & Scalliet, G. (2013). A Review of Current Knowledge of Resistance Aspects for the Next-Generation Succinate Dehydrogenase Inhibitor Fungicides. *Phytopathology*, *103*(9), 880–887.

Sikorski, R., & Hieter, P. (1983). A System of Shuttle Vectors and Yeast Host Strains Designed for Efficient Manipulation of DNA in Saccharomyces ceratisiae. *Medical Mycology*, *21*(4), 271–286. https://doi.org/10.1080/00362178385380431

Sikorski, R. S., & Hieter, P. (1989). A System of Shuttle Vectors and Yeast Host Strains Designed for Efficient Manipulation of DNA in Saccharomyces cerevisiae. *Genetics*, *122*(1), 19–27.

Singh, S. D., Robbins, N., Zaas, A. K., Schell, W. A., Perfect, J. R., & Cowen, L. E. (2009). Hsp90 governs echinocandin resistance in the pathogenic yeast Candida albicans via calcineurin. *PLoS Pathogens*, *5*(7). https://doi.org/10.1371/journal.ppat.1000532

Skaggs, B. A., Alexander, J. F., Pierson, C. A., Schweitzer, K. S., Chun, K. T., Koegel, C., Barbuch, R., & Bard, M. (1996). Cloning and characterization of the Saccharomyces cerevisiae C-22 sterol desaturase gene, encoding a second cytochrome P-450 involved in ergosterol biosynthesis. *Gene*, *169*(1), 105–109. https://doi.org/10.1016/0378-1119(95)00770-9

Slaven, J. W., Anderson, M. J., Sanglard, D., Dixon, G. K., Bille, J., Roberts, I. S., & Denning, D. W. (2002). *Increased expression of a novel Aspergillus fumigatus ABC transporter gene, atrF, in the presence of itraconazole in an itraconazole resistant clinical isolate*. www.academicpress.com

Smith, R. D., & Lupashin, V. V. (2008). Role of the conserved oligomeric Golgi (COG) complex in protein glycosylation. *Carbohydrate Research*, *343*(12), 2024–2031. https://doi.org/10.1016/j.carres.2008.01.034

Smith, Jeffrey S., Robert J. Lefkowitz, and Sudarshan Rajagopal. "Biased signalling: from simple switches to allosteric microprocessors." *Nature reviews Drug discovery* 17.4 (2018): 243-260.

Soontorngun, N., Larochelle, M., Drouin, S., Robert, F., & Turcotte, B. (2007). Regulation of Gluconeogenesis in Saccharomyces cerevisiae Is Mediated by Activator and Repressor Functions of Rds2 . *Molecular and Cellular Biology*, *27*(22), 7895–7905. https://doi.org/10.1128/mcb.01055-07

Sopko, R., Huang, D., Preston, N., Chua, G., Papp, B., Kafadar, K., Snyder, M., Oliver, S. G., Cyert, M., Hughes, T. R., Boone, C., & Andrews, B. (2006). Mapping pathways and phenotypes by systematic gene overexpression. *Molecular Cell*, *21*(3), 319–330. https://doi.org/10.1016/j.molcel.2005.12.011

Stathopoulos, A. M., & Cyert, M. S. (1997). Calcineurin acts through factor to regulate gene expression in yeast. *Genes & Development*, 3432–3444.

Steinberg, G., & Gurr, S. J. (2020). Fungi, fungicide discovery and global food security. *Fungal Genetics and Biology*, *144*, 103476. https://doi.org/10.1016/j.fgb.2020.103476

Šťovíček, V., Váchová, L., Kuthan, M., & Palková, Z. (2010). General factors important for the formation of structured biofilm-like yeast colonies. *Fungal Genetics and Biology*, *47*(12), 1012–1022. https://doi.org/10.1016/j.fgb.2010.08.005

Stratford, M. (1992). Yeast flocculation: Reconciliation of physiological and genetic viewpoints. *Yeast*, *8*(1), 25–38. https://doi.org/10.1002/yea.320080103

Strom, N. B., & Bushley, K. E. (2016). Two genomes are better than one: History, genetics, and biotechnological applications of fungal heterokaryons. *Fungal Biology and Biotechnology*, *3*(1), 1–14. https://doi.org/10.1186/s40694-016-0022-x

Stukenbrock, E., & Gurr, S. (2022). Address the growing urgency of fungal disease in crops.

Suwunnakorn, S., Wakabayashi, H., Kordalewska, M., Perlin, D. S., & Rustchenko, E. (2018). FKS2 and FKS3 genes of opportunistic human pathogen Candida albicans influence echinocandin susceptibility. *Antimicrobial Agents and Chemotherapy*, *62*(4), 1–12. https://doi.org/10.1128/AAC.02299-17

Suzuki, Y., Onge, R. P. S., Mani, R., King, O. D., Heilbut, A., Labunskyy, V. M., Chen, W., Pham, L., Zhang, L. V., Tong, A. H. Y., Nislow, C., Giaever, G., Gladyshev, V. N., Vidal, M., Schow, P., Lehär, J., & Roth, F. P. (2011). Knocking out multigene redundancies via cycles of sexual assortment and fluorescence selection. *Nature Methods*, *8*(2), 159–164. https://doi.org/10.1038/nmeth.1550

Taipale, M., Jarosz, D. F., & Lindquist, S. (2010). HSP90 at the hub of protein homeostasis: Emerging mechanistic insights. In *Nature Reviews Molecular Cell Biology* (Vol. 11, Issue 7, pp. 515–528). https://doi.org/10.1038/nrm2918

Talapko, J., Juzbašić, M., Matijević, T., Pustijanac, E., Bekić, S., Kotris, I., & Škrlec, I. (2021). Candida albicans-the virulence factors and clinical manifestations of infection. *Journal of Fungi*, *7*(2), 1–19. https://doi.org/10.3390/jof7020079

Talbot, N. J. (2003). On the Trail of a Cereal Killer: Exploring the Biology of Magnaporthe grisea. In *Annual Review of Microbiology* (Vol. 57, pp. 177–202). https://doi.org/10.1146/annurev.micro.57.030502.090957

Tanaka, C., & Izumitsu, K. (2010). Two-Component Signaling System in Filamentous Fungi and the Mode of Action of Dicarboximide and Phenylpyrrole Fungicides. *Fungicides*. https://doi.org/10.5772/13774

Tayel, A. A., Moussa, S., El-Tras, W. F., Knittel, D., Opwis, K., & Schollmeyer, E. (2010). Anticandidal action of fungal chitosan against Candida albicans. *International Journal of Biological Macromolecules*, *47*(4), 454–457. https://doi.org/10.1016/j.ijbiomac.2010.06.011

Teng, X., Dayhoff-Brannigan, M., Cheng, W. C., Gilbert, C. E., Sing, C. N., Diny, N. L., Wheelan, S. J., Dunham, M. J., Boeke, J. D., Pineda, F. J., & Hardwick, J. M. (2013). Genome-wide consequences of deleting any single gene. *Molecular Cell*, *52*(4), 485–494. https://doi.org/10.1016/j.molcel.2013.09.026

Tillman, R. W., Siegel, M. R., & Long, J. W. (1973). Mechanism of action and fate of the fungicide chlorothalonil (2,4,5,6-tetrachloroisophthalonitrile) in biological systems. *Pesticide Biochemistry and Physiology*, *3*(2), 160–167. https://doi.org/10.1016/0048-3575(73)90100-4

Tkacz, J. S., & Lampen, J. O. (1975). Tunicamycin inhibition of polyisoprenyl N-acetylglucosaminyl pyrophosphate formation in calf-liver microsomes. *Biochemical and Biophysical Research Communications*, *65*(1), 248–257.

Todd, R. T., & Selmecki, A. (2020). Expandable and reversible copy number amplification drives rapid adaptation to antifungal drugs. *ELife*, *9*, 1–33. https://doi.org/10.7554/eLife.58349

Toprak, E., Veres, A., Michel, J. B., Chait, R., Hartl, D. L., & Kishony, R. (2012). Evolutionary paths to antibiotic resistance under dynamically sustained drug selection. *Nature Genetics*, *44*(1), 101–105. https://doi.org/10.1038/ng.1034

Toprak, E., Veres, A., Yildiz, S., Pedraza, J. M., Chait, R., Paulsson, J., & Kishony, R. (2013). Building a morbidostat: an automated continuous-culture device for studying bacterial drug resistance under dynamically sustained drug inhibition. *Nature Protocols*, *8*(3), 555–567. https://doi.org/10.1038/nprot.nprot.2013.021

Tsai, G. J., & Su, W. H. (1999). Antibacterial activity of shrimp chitosan against Escherichia coli. *Journal of Food Protection*, *62*(3), 239–243. https://doi.org/10.4315/0362-028X-62.3.239

Tsai, H. F., Krol, A. A., Sarti, K. E., & Bennett, J. E. (2006). Candida glabrata PDR1, a transcriptional regulator of a pleiotropic drug resistance network, mediates azole resistance in clinical isolates and petite mutants. *Antimicrobial Agents and*

Chemotherapy, *50*(4), 1384–1392. https://doi.org/10.1128/AAC.50.4.1384-1392.2006

van Dijk, M., Morley, T., Rau, M. L., & Saghai, Y. (2021). A meta-analysis of projected global food demand and population at risk of hunger for the period 2010–2050. *Nature Food*, *2*(7), 494–501. https://doi.org/10.1038/s43016-021-00322-9

van Opijnen, T., Bodi, K. L., & Camilli, A. (2009). Tn-seq: High-throughput parallel sequencing for fitness and genetic interaction studies in microorganisms. *Nature Methods*, *6*(10), 767–772. https://doi.org/10.1038/nmeth.1377

Van Opijnen, T., & Camilli, A. (2012). A fine scale phenotype-genotype virulence map of a bacterial pathogen. *Genome Research*, *22*(12), 2541–2551. https://doi.org/10.1101/gr.137430.112

Van Opijnen, T., & Levin, H. L. (2020). Transposon Insertion Sequencing, a Global Measure of Gene Function. *Annual Review of Genetics*, *54*, 337–365. https://doi.org/10.1146/annurev-genet-112618-043838

Vande Zande, P., Zhou, X., & Selmecki, A. (2023). The Dynamic Fungal Genome: Polyploidy, Aneuploidy and Copy Number Variation in Response to Stress. *Annual Review of Microbiology*, *40*(77), 341–361. https://doi.org/10.1146/annurev-micro-041320

Vindu, A., Shin, B. S., Choi, K., Christenson, E. T., Ivanov, I. P., Cao, C., Banerjee, A., & Dever, T. E. (2021). Translational autoregulation of the S. cerevisiae high-affinity polyamine transporter Hol1. *Molecular Cell*, *81*(19), 3904–3918. https://doi.org/10.1016/j.molcel.2021.07.020

Walker, L. A., Gow, N. A. R., & Munro, C. A. (2010). Fungal echinocandin resistance. *Fungal Genetics and Biology*, *47*(2), 117–126. https://doi.org/10.1016/j.fgb.2009.09.003

Wang, B., Abubakar, Y. S., & Wang, Z. (2023). Special Issue “Genomics of Fungal Plant Pathogens.” In *Journal of Fungi* (Vol. 9, Issue 7). Multidisciplinary Digital Publishing Institute (MDPI). https://doi.org/10.3390/jof9070713

Wang, X. H., Nakayama, K. I., Shimma, Y. I., Tanaka, A., & Jigami, Y. (1997). MNN6, a member of the KRE2/MNT1 family, is the gene for mannosylphosphate transfer in Saccharomyces cerevisiae. *Journal of Biological Chemistry*, *272*(29), 18117–18124. https://doi.org/10.1074/jbc.272.29.18117

Weil, C. F., & Kunze, R. (2000). Transposition of maize Ac/Ds transposable elements in the yeast Saccharomyces cerevisiae. *Nature Genetics*, *26*(2), 187–190. https://doi.org/10.1038/82827

Whitney, P. A., & Morris, D. R. (1978). Polyamine auxotrophs of Saccharomyces cerevisiae. *Journal of Bacteriology*, *134*(1), 214–220. https://doi.org/10.1128/jb.134.1.214-220.1978

Wiederhold, N. P. (2021). Review of T-2307, an investigational agent that causes collapse of fungal mitochondrial membrane potential. *Journal of Fungi*, *7*(2), 1–9. https://doi.org/10.3390/jof7020130

Wiederhold, N. P., Najvar, L. K., Fothergill, A. W., Bocanegra, R., Olivo, M., McCarthy, D. I., Fukuda, Y., Mitsuyama, J., & Patterson, T. F. (2016). The novel arylamidine T-2307 demonstrates in vitro and in vivo activity against echinocandin-resistant Candida glabrata. *Journal of Antimicrobial Chemotherapy*, *71*(3), 692–695. https://doi.org/10.1093/jac/dkv398

Wiederhold, N. P., Najvar, L. K., Fothergill, A. W., Bocanegra, R., Olivo, M., McCarthy, D. I., Kirkpatrick, W. R., Fukuda, Y., Mitsuyama, J., & Pattersona, T. F. (2015). The novel arylamidine T-2307 maintains in vitro and in vivo activity against echinocandin-resistant Candida albicans. *Antimicrobial Agents and Chemotherapy*, *59*(2), 1341–1343. https://doi.org/10.1128/AAC.04228-14

Winderickx, J., Delay, C., De Vos, A., Klinger, H., Pellens, K., Vanhelmont, T., Van Leuven, F., & Zabrocki, P. (2008). Protein folding diseases and neurodegeneration: Lessons learned from yeast. In *Biochimica et Biophysica Acta - Molecular Cell Research* (Vol. 1783, Issue 7, pp. 1381–1395). Elsevier. https://doi.org/10.1016/j.bbamcr.2008.01.020

Winzeler et al., E. (1999). Functional characterization of the S. cerevisiae genome by gene deletion and parallel analysis. *Science*, *285*(5429), 901–906.

Woodage, T., Basrai, M., Baxevanis, A., Hieter, P., & Collins, F. (1997). Characterization of the CHD family of proteins. *Proceedings of the National Academy of Sciences of the United States of America*, *94*(21), 11472–11477.

World Health Organisation. (2022). *WHO fungal priority pathogens list to guide research, development and public health action*.

Xiang, M. J., Liu, J. Y., Ni, P. H., Wang, S., Shi, C., Wei, B., Ni, Y. X., & Ge, H. L. (2013). Erg11 mutations associated with azole resistance in clinical isolates of Candida albicans. *FEMS Yeast Research*, *13*(4), 386–393. https://doi.org/10.1111/1567-1364.12042

Xu, F., Byström, A. S., & Johansson, M. J. O. (2020). SSD1 modifies phenotypes of Elongator mutants. *Current Genetics*, *66*(3), 481–485. https://doi.org/10.1007/s00294-019-01048-9

Xu, Z., Wei, W., Gagneur, J., Perocchi, F., Clauder-Münster, S., Camblong, J., Guffanti, E., Stutz, F., Huber, W., & Steinmetz, L. M. (2009). Bidirectional promoters generate pervasive transcription in yeast. *Nature*, *457*(7232), 1033–1037. https://doi.org/10.1038/nature07728

Xue, A., Robbins, N., & Cowen, L. E. (2021). Advances in fungal chemical genomics for the discovery of new antifungal agents. *Annals of the New York Academy of Sciences*, *1496*(1), 5–22. https://doi.org/10.1111/nyas.14484

Yamashita, K., Miyazaki, T., Fukuda, Y., Mitsuyama, J., Saijo, T., Shimamura, S., Yamamoto, K., Imamura, Y., Izumikawa, K., Yanagihara, K., Kohno, S., & Mukaeb, H. (2019). The novel arylamidine T-2307 selectively disrupts yeast mitochondrial function by inhibiting respiratory chain complexes. *Antimicrobial Agents and Chemotherapy*, *63*(8), 10–1128. https://doi.org/10.1128/AAC.00374-19

Yan, N. (2015). Structural Biology of the Major Facilitator Superfamily Transporters. *Annual Review of Biophysics*, *44*, 257–283. https://doi.org/10.1146/annurev-biophys-060414-033901

Yanicostas, C., & Soussi-yanicostas, N. (2021). Sdhi fungicide toxicity and associated adverse outcome pathways: What can zebrafish tell us? In *International Journal of Molecular Sciences* (Vol. 22, Issue 22). MDPI. https://doi.org/10.3390/ijms222212362

Yin, X. (2023). *Binding Mode and Molecular Mechanism of the Two-Component Histidine Kinase Bos1 of Botrytis cinerea to Fludioxonil and Iprodione*. *X*(X), 1–10.

Yip, C. L., Welch, S. K., Klebl, F., Gilbert, T., Seidel, P., Grant, F. J., O'Hara, P. J., & MacKay, V. L. (1994). Cloning and analysis of the Saccharomyces cerevisiae MNN9 and MNN1 genes required for complex glycosylation of secreted proteins. *Proceedings of the National Academy of Sciences of the United States of America*, *91*(7), 2723–2727. https://doi.org/10.1073/pnas.91.7.2723

Yoshida, J., Akagi, K., Misawa, R., Kokubu, C., Takeda, J., & Horie, K. (2017). Chromatin states shape insertion profiles of the piggyBac, Tol2 and Sleeping Beauty transposons and murine leukemia virus. *Scientific Reports*, *7*. https://doi.org/10.1038/srep43613

Yoshimi, A., Kojima, K., Takano, Y., & Tanaka, C. (2005). Group III histidine kinase is a positive regulator of Hog1-type mitogen-activated protein kinase in filamentous fungi. *Eukaryotic Cell*, *4*(11), 1820–1828. https://doi.org/10.1128/EC.4.11.1820-1828.2005

Yu, C. J., & Lee, F. J. S. (2017). Multiple activities of Arl1 GTPase in the trans-Golgi network. *Journal of Cell Science*, *130*(10), 1691–1699. https://doi.org/10.1242/jcs.201319

Yu, J., Marshall, K., Yamaguchi, M., Haber, J. E., & Weil, C. F. (2004). Microhomology-Dependent End Joining and Repair of Transposon-Induced DNA Hairpins by Host Factors in Saccharomyces cerevisiae. *Molecular and Cellular Biology*, *24*(3), 1351–1364. https://doi.org/10.1128/mcb.24.3.1351-1364.2004

Zakrzewska, A., Boorsma, A., Brul, S., Hellingwerf, K. J., & Klis, F. M. (2005). Transcriptional response of Saccharomyces cerevisiae to the plasma membrane-perturbing compound chitosan. *Eukaryotic Cell*, *4*(4), 703–715. https://doi.org/10.1128/EC.4.4.703-715.2005

Zakrzewska, A., Boorsma, A., Delneri, D., Brul, S., Oliver, S. G., & Klis, F. M. (2007). Cellular processes and pathways that protect Saccharomyces cerevisiae cells against the plasma membrane-perturbing compound chitosan. *Eukaryotic Cell*, *6*(4), 600–608. https://doi.org/10.1128/EC.00355-06

Zapater, M., Sohrmann, M., Peter, M., Posas, F., & de Nadal, E. (2007). Selective Requirement for SAGA in Hog1-Mediated Gene Expression Depending on the Severity of the External Osmostress Conditions. *Molecular and Cellular Biology*. https://doi.org/10.1128/mcb.00089-07

Zhang, K., Fu, Y., Long, C., & Zhu, F. (2024). Iminoctadine tris (albesilate) resistance in Geotrichum citri-aurantii and its management. *Crop Protection*, *175*. https://doi.org/10.1016/j.cropro.2023.106475

Zhang, X., & Moye-Rowley, W. S. (2001). Saccharomyces cerevisiae Multidrug Resistance Gene Expression Inversely Correlates with the Status of the F0 Component of the Mitochondrial ATPase. *Journal of Biological Chemistry*, *276*(51), 47844–47852. https://doi.org/10.1074/jbc.M106285200

Zhang, Y., Lamm, R., Pillonel, C., Lam, S., & Xu, J. R. (2002). Osmoregulation and fungicide resistance: The Neurospora crassa os-2 gene encodes a HOG1 mitogen-activated protein kinase homologue. *Applied and Environmental Microbiology*, *68*(2), 532–538. https://doi.org/10.1128/AEM.68.2.532-538.2002

Zhao, J., Wang, Y., Liu, Q., Lu, X., Tian, Z., & Long, C. A. (2023). Investigation of specific molecular marker and EC50 values of guazatine for Geotrichum citri-aurantii on citrus in China. *Scientia Horticulturae*, *310*. https://doi.org/10.1016/j.scienta.2022.111772

Zhou, F., Li, D. X., Hu, H. Y., Song, Y. L., Fan, Y. C., Guan, Y. Y., Song, P. W., Wei, Q. C., Yan, H. F., & Li, C. W. (2020). Biological characteristics and molecular mechanisms of fludioxonil resistance in fusarium graminearum in China. *Plant Disease*, *104*(9), 2426–2433. https://doi.org/10.1094/PDIS-01-20-0079-RE

Zhu, J., Gong, R., Zhu, Q., He, Q., Xu, N., Xu, Y., Cai, M., Zhou, X., Zhang, Y., & Zhou, M. (2018). Genome-wide determination of gene essentiality by transposon insertion sequencing in yeast pichia pastoris. *Scientific Reports*, *8*(1), 10223. https://doi.org/10.1038/s41598-018-28217-z

Zhu, J., Zhang, L., Ma, D., Gao, Y., Mu, W., & Liu, F. (2019). A bioactivity and biochemical analysis of iminoctadine tris (albesilate) as a fungicide against Corynespora cassiicola. *Pesticide Biochemistry and Physiology*, *158*(April), 121–127. https://doi.org/10.1016/j.pestbp.2019.04.016

Zlotnik, H., Pilar Fernandez, M., Bowers, B., & Cabib, E. (1984). Saccharomyces cerevisiae mannoproteins form an external cell wall layer that determines wall porosity. *Journal of Bacteriology*, *159*(3), 1018–1026. https://doi.org/10.1128/jb.159.3.1018-1026.1984